A Study of Spin-Liquids in the Kitaev-Hubbard and Kitaev-Heisenberg Models

By

P.V. Sriluckshmy

PHYS10200904003

The Institute of Mathematical Sciences, Chennai

A thesis submitted to the

Board of Studies in Physical Sciences

In partial fulfillment of requirements

For the Degree of

DOCTOR OF PHILOSOPHY

of

HOMI BHABHA NATIONAL INSTITUTE

August 2016

Homi Bhabha National Institute

Recommendations of the Viva Voce Board

As members of the Viva Voce Board, we certify that we have read the dissertation prepared by P.V. Srilucksshmy entitled “A study of Spin-Liquids in the Kitaev-Hubbard and Kitaev-Heisenberg Models” and recommend that it maybe accepted as fulfilling the dissertation requirement for the Degree of Doctor of Philosophy.

____ Date:

Chair -

____ Date:

Guide/Convener -

____ Date:

Member 1 -

____ Date:

Member 2 -

____ Date:

Member 3 -

Final approval and acceptance of this dissertation is contingent upon the candidate’s submission of the final copies of the dissertation to HBNI.

I hereby certify that I have read this dissertation prepared under my direction and recommend that it may be accepted as fulfilling the dissertation requirement.

Date:

Place: Guide

STATEMENT BY AUTHOR

P.V. Srilucksshmy

DECLARATION

I, hereby declare that the investigation presented in the thesis has been carried out by me. The work is original and has not been submitted earlier as a whole or in part for a degree / diploma at this or any other Institution / University.

P.V. Srilucksmy

List of Publications arising from the thesis

This thesis is based on the following publications:

- **Published**

  1. S. R. Hassan, **P. V. Sriluckshmy**, Sandeep K. Goyal, R. Shankar and David Senechal, "Stable Algebraic Spin Liquid in a Hubbard model", Phys. Rev. Lett. 110, 037201 (2013).
  2. **P.V. Sriluckshmy**, Archana Mishra, S. R. Hassan and R. Shankar, "Topological transitions in a model with Particle-Hole symmetry, Pancharatnam-Berry Curvature and Dirac Points", Phys. Rev. B 89, 045105 (2014).
  3. Satyendra Nath Gupta, **P.V. Sriluckshmy**, Kavita Mehlawat, Ashiwini Balodhi,Dileep K Mishra, D.V.S. Muthu, S.R. Hassan,Yogesh Singh, T.V. Ramakrishnan and A.K. Sood, "Raman Signatures of strong Kitaev Exchange Correlations in $(Na_{1-x}Li_x)_2IrO_3$: Experiments and Theory", Euro. Phys. Lett. 114, 47004(2016)

- **Sent for Publication**

  1. Satyendra Nath Gupta, **P.V. Sriluckshmy**, Kavita Mehlawat, Ashiwini Balodhi,Dileep K Mishra, D.V.S. Muthu, S.R. Hassan,Yogesh Singh, T.V. Ramakrishnan and A.K. Sood, "Spin Liquid like Raman Signatures in hyperkagome $Na_4Ir_3O_8$", sent for publication to Phys. Rev. B

List of corrections and changes as suggested by the Thesis and Viva Voce Examiners

Publication list has been updated.

Chapter 2: A Brief History of Kitaev Model

- Page 12, Para 1: It happens to be one of the ~~few~~ models in $2D$ whose exact solution is known.
- Section 2.1: Added explanation of σ^{α} and $\boldsymbol{\tau}$.

Chapters 4,5,7: Corrected typos

Chapter 9: Raman Response for Honeycomb Sodium Iridate

- Added a conclusion at the end, summarising the results.

Chapter 10: Raman Response for Hyperkagome Sodium Iridate

- Section 10.2: Text added for the explanation of mean field theory.
- Section 10.3: Added text to summarize the calculations.
- Section 10.2,10.3: Updated Figures.
- Added a conclusion at the end, summarising the results.

The corrections and changes suggested by the Thesis and Viva Voce Examiners have been incorporated in the thesis.

Guide

DEDICATIONS

To my mom, the reason for who I am today.

ACKNOWLEDGEMENTS

“ It’s Impossible", said Pride.

“ It’s Risky", said Experience.

“ It’s Pointless", said Reason.

“ Give it a try", whispered the Heart.

-Unknown

My deepest gratitude for all the help and support to all who have contributed in making this possible!

My thesis advisor Prof. S. R. Hassan has been a father figure to me during my PhD life. He has instilled the spirit of adventure in regard to research and has inspired me to pursue condensed matter physics. I will always cherish the discussions I have had with him both academic and non-academic. Without his guidance and persistent help none of this would ever be possible.

Special thanks to Prof. R. Shankar from whom I learnt the most important lesson in research – to never give up. Our discussions have always been stimulating and rewarding but above all, lots of fun. I would like to thank Prof. G. Baskaran, Prof. Andre Marie Tremblay, Prof. Ajay K. Sood and Prof. T.V. Ramakrishnan with whom I have had some of the most insightful discussions. I would also like to thank Prof. Ronojoy Adhikari, Prof. Mukul Laad and Dr. R. Ganesh who have given me motivation, support and help whenever and wherever I needed them.

I am grateful to my dear friends who have constantly supported me in all my work and made my graduate student life bearable and fun. It would be incomplete if I didn't name a few of my friends: Dr. Sandeep K Goyal from whom I learnt a lot regarding coding and research attitude in general which he taught in his own special way. Dr. Somdeb Ghose who has been at the receiving end of many of my frustrations during PhD. He has also proof-read many of my papers and this thesis. Dr. Rajeev Singh who has always been a motivation for me to do good work. They have been at my constant beck and call despite their own problems. Abhrajit Laskar, Madhushree Basu, Soumyajit Pramanick, Archana Mishra, Dibyakrupa Sahoo,Satyendra Nath Gupta, Subhadeep Roy, Ankita C., Padmavathy Vasudevan, Arya S. are some of the wonderful friends I made. Thank you to all my old friends who stuck by me through all the tough decisions I had to take.

I would like to thank the administration and the library staff for making my stay at the Institute pleasant and enjoyable.

Last but not the least, I would like to thank my mom for her great support and continuous care throughout my life.

Contents

Synopsis

The advent of high-temperature superconductors almost thirty years back has led to a profusion of theoretical models for analyzing the phenomenon. The spin liquid–a phase of matter defined by a pure Mott insulator with no magnetic order–is one such model. Subsequently, spin liquids have evolved in a path separate from high-Tc superconductors after the discovery of a number of materials which demonstrated behaviour that classified them as spin liquids. In modern hard condensed matter physics, both theoretical and experimental, spin liquids have carved out a niche of their own. As of now, around 180 different types of spin liquids have been classified based on symmetry properties[1]. Out of these, a certain Z2 type spin liquid–called the Kitaev spin liquid[2]–has gained a lot of interest due to the exact solvability of the ground state. Its stability, however, has been an issue as perturbations to the Kitaev model destabilize the spin liquid phase and allow for long-range order to set in[3, 4]. In this thesis, I try to address some aspects of this question.

Experimental detection of spin liquids presents another set of challenges for the condensed matter community in recent years. In this thesis, I try and find a phenomenon that can act as a signature of Kitaev spin liquids in materials as well as in optical lattices. For example, I ask if it might be possible to use a Hubbard model–the typical model of Mott insulators–to stabilize a Kitaev spin liquid in optical lattices, an exercise which necessitates a search for special properties of said model. The advantage of working with optical lattices–namely, the freedom to tweak tuning parameters–disappears when we take this question to domain of actual materials. Since iridates have recently been shown to possess Kitaev-like correlations using Raman response as an experimental probe, we analyze theoretical models of iridates and study Raman responses in depth.

Stable Algebraic Spin Liquid in a Hubbard model

A Hubbard model with spin-dependent hopping on a honeycomb lattice, first proposed by Duan et al [5], was shown to have properties similar to a Kitaev spin model for large onsite interactions and strong spin-dependant hopping. We call this the Kitaev-Hubbard (KHUB) model. The KHUB model was at the primary target of our investigations. When we mapped out its phase diagram using numerical techniques such as the Cluster Perturbation Theory (CPT) and the Variational Cluster Approximation (VCA) method, we detected three distinct phases; a Semi-Metallic phase where magnetic order is absent and the charge gap is zero, an Anti-ferromagnetic Insulator phase with anti-ferromagnetic order and non-zero charge gap, and a new phase where magnetic order is absent but the charge gap is non-zero. This new phase is the Spin Liquid phase.

Since spin liquids are generally susceptible to perturbations, their stability needs to be ensured. In our model, time-reversal symmetry for the Mott phase is sufficient to ensure stability. Using the method of Perturbative Canonical Unitary Transformations (PCUT), I computed the effective spin model in the large U limit and found that it contains an even number of spin operators. Based on this, and using the particle-hole symmetry operator, we proved that the effective spin model will be time reversal symmetric upto all orders of perturbation theory. Then using perturbation theory we also computed the long-wavelength spin-spin correlations and found that they decay as power law. This established the fact that the spin liquid phase in the KHUB model is actually an Algebraic Spin Liquid phase.

We used the Majorana mean field theory of the corresponding fourth order effective spin Hamiltonian to show that no spontaneous time reversal symmetry breaking occurs in the KHUB model. Since this proves the absence of a chiral spin liquid phase we established that there is no transition from an ASL to a possible chiral spin liquid phase, thus ensuring the stability of the ASL phase.

Experimental detection of Kitaev spin liquids using Raman Response

At low temperatures, sodium iridates of the form Na_2IrO_3 exhibit long-range zig-zag magnetic order, while at high temperatures the same compounds behave like spin liquids. The low energy states of the Ir^{4+} ions in these compounds form pseudo spin-half moments that live on the honeycomb lattice[6]. The high spin-orbit coupling present in these compounds could lead to Kitaev-like correlations. An exact theoretical model that would fit all its properties has not been forthcoming. Experimentally, it has been shown that the Raman response of this compound contains a broad band, an observation which is at odds with how compounds having magnetic order behave.

The Raman response is a two-photon process where the incoming photon gets inelastically scattered from the system and the outgoing photon is collected and analyzed. The polarization dependence of Raman scattering experiments provides information about the underlying magnetic states in the system. Unfortunately, the compounds in question seemed to show very weak polarization dependence. This necessitated a theoretical approach.

Many variants of the Kitaev-Heisenberg model have been utilized to describe the iridates in question. Using Majorana mean field decoupling of one such model on a honeycomb lattice, we studied the energetically favourable states at zero temperature, concentrating our analysis near the spin liquid-zigzag boundary. By computing the Raman Response for the model at zero temperature in a region of parameter space where zig-zag magnetic order exists with short range correlations, we found that the Raman response contains a broad band, which is a signature of the short range correlations of the nearby spin liquid phase. We also found that the Raman intensity is weakly dependent on the polarization direction. Thus our theoretical results confirmed the experimental findings qualitatively and also agreed well, quantitatively.

Alternatively, in sodium iridates of the form $Na_4Ir_3O_8$, the Ir planes form a hyper-kagome lattice[7]. Unlike Na_2IrO_3, this compound is yet to provide any experimental evidence regarding magnetic ordering. Although a number of theoretical models that exhibit quantum spin liquid behaviour have been used to describe the compound, the dearth of supporting experimental evidence has rendered such exercises nearly useless. Nevertheless, experiments conducted recently have detected a broad Raman band in these class of compounds as well. Thus, taking a hint from the technique we employed to analyze Na_2IrO_3 iridates, we once again turn to the Kitaev-Heisenberg model. The Majorana mean field decoupling of the hyper-kagome lattice is quite unlike its honeycomb counterpart, in that the gauge sector is gap-less and the spinon sector has a Fermi surface instead of a Dirac point. The lack of evidence of ordering led us to focus on the spin-liquid regimes in the Kitaev-Heisenberg parameter space. Our theoretical Raman response results for $Na_4Ir_3O_8$, which once again tally well with experiments.

List of Figures

Chapter 1

Introduction

Two Roads diverged in a wood,

and I took the one less traveled by,

And that has made all the

difference.

Robert Frost

To the famous song by Metallica, *"Nothing Else Matters"*, I add *"..., except Matter"*.

Condensed matter theory, one of the pillars of modern day physics, deals with the various phases of matter. Using the underlying symmetry of matter, Landau [14] proposed a theory of phase transition that has been highly successful in explaining the behaviour of many such phases; the classic solid-liquid transition, the superfluidity of He, superconductivity in metals, and various magnetic orders are some such examples. Among the various fascinating fields that condensed matter has to offer, strongly correlated fermionic systems, a hotbed of frenetic activity on the theoretical and experimental sides of cutting-edge physics research, offers up many strange and exotic phenomena that Landau's formalism fails to explain. The physics of spin liquids is one such example, and requires an understanding of topology of the collective excitations. The study of spin liquids is currently in the spotlight due to its importance in explaining the physics of high-T_c superconductors. The popularity of spin liquids has gained a further boost very recently with the advent of various organic and inorganic salts, and is now one of the leading fields of study in condensed matter physics.

Anderson [15] was the first to look at a spin liquid as a Mott phase lacking local magnetic order. Its relevance to the physics of high-T_c superconductors[16, 17] led to the development of a gauge theory of spin liquids [18, 17] analogous to quantum electrodynamics (QED). Within this framework, spinons are the counterparts of QED electrons, while the emergent excitation particles called visons are the counterparts of photons. Attempts at understanding the emergence of fermionic quasi-particles in spin systems in analogy with the anyonic quasi-particles in fractional quantum Hall systems has led to a general theory of quantum/topological order in spin liquids [1].

Spin liquids are purely quantum phenomena that do not have a classical parallel. Frustration in magnetic interactions and quantum fluctuations tend to prevent magnetic ordering. Wen [1] has tabulated around 180 different types of spin liquids using theoretical techniques. His classification is based on the symmetry properties of these phases. Experimental evidence for a spin liquid ground state has been seen, for instance, in the quasi-two dimensional organic material κ-(BEDT-TTF)$_2$Cu$_2$(CN)$_3$ (dmit salts) [19] where hyperfine nuclear magnetic resonance (HNMR) studies show no evidence for long range magnetic order down to $32mK$ inspite of the large anti-ferromagnetic interactions $O(100K)$ present. There is a veritable glut of models as well as materials for example :

- $ZnCu_3(OH)_6Cl_2$ Herbertsmithite Kagome lattice [20]: Neutron scattering experiments on single-crystal samples show that the spin excitations form a continuum which is a signature of fractional quantum numbers.

- $Ba_3CuSb_2O_9$ triangular compounds [21] : Apart from showing no magnetic order down to $0.2K$, the magnetic specific heat revealed a linear-T dependence below $1.4K$. This suggests that a Fermi surface forms at finite temperatures which fits well with the predicted signatures of a spin liquid ground state.

- $BaCu_3V_2O_8(OH)_2$ Vesignieite Kagome structure [22]: Magnetic Susceptibility shows no long range order nor a spin gap down to $2K$. A broad peak observed at a finite temperature indicates a gapless spin liquid.

- $Na_4Ir_3O_8$ three-dimensional Hyper-Kagome lattice [10]: Magnetization and magnetic specific heat C_m showed the absence of long range magnetic ordering down to $2K$. The large C_m is independent of the applied magnetic field.

that are proposed to show spin liquid behaviour.

Kitaev [23] constructed an exactly solvable anisotropic spin-$1/2$ model on a honeycomb lattice that exhibits the important properties of a spin liquid. The frustration arises here from the anisotropic interactions and not the geometry. The Kitaev model can be expressed as a model of two gapless Majorana-Dirac fermions (spinons) interacting with Z_2 gauge fields (visons). A remarkable feature of the model is that the magnetic flux associated with every plaquette is conserved leading to the visons being static. Consequently, while multi-spin operators that conserve flux have algebraic correlations, those which do not–this includes the single spin operators—are extremely short ranged [24]. Tikhonov *et. al*[3] showed that spin-spin correlations become algebraic when a single-spin operator is added to the Hamiltonian. The class of perturbations that can induce algebraic spin-spin correlations were classified by Mandal *et. al.* [25] who showed that Ising and Heisenberg perturbations—which have been studied earlier [25, 26, 27]—do not induce power law correlations.

Algebraic spin liquids (ASL) a special class of spin liquids that can be realized in perturbed Kitaev models. Spinons in ASLs are gapless and Dirac-like, and spin-correlations decay as a power law. ASLs have primarily been studied in frustrated spin-1/2 Heisenberg anti-ferromagnets [28, 29, 30] and have recently been realized in an interacting fermion model, the Kitaev-Hubbard model [31]. In addition to demonstrating power law decay for spin correlations, the ASL shows similar behaviour for a host of other local order parameters as well. This makes it intrinsically susceptible to any one of them ordering and inducing a spinon gap, which makes the ASL immediately unstable. Thus, any realization of this phase must be accompanied by a mechanism for ensuring its stability. The stability of the ASL in the Kitaev model is due to time reversal (TR) symmetry : the two Majorana-Dirac fermions combine to form a *single* Dirac fermion with an energy spectrum that cannot have a gap without breaking TR-symmetry. Thus perturbations must preserve this symmetry in order to ensure a stable ASL phase. In the model due to Tikhonov *et al.* [3], single-spin perturbations break TR-symmetry and thus there is a possibility of a spinon gap developing at higher orders in perturbation theory. An exactly solvable spin-3/2 model with algebraic spin correlations has also been constructed [32].

The prevalence of ASLs in the Kitaev-Hubbard model is one aspect of the studies considered in this thesis. The Kitaev-Hubbard is an interacting fermion model proposed to realize the Kitaev model in optical lattice systems [5]. A second aspect is to find real-world systems that can realize the Kitaev model. Of the various materials that seem to show effects of the spin liquid phases, we shall concentrate our study on iridates and in particular sodium iridates: Na_2IrO_3 with honeycomb planes and $Na_4Ir_3O_8$ with hyper-kagome structure.

Sodium Iridates were proposed to be avenues where Kitaev like interactions might be realized because the strong spin-orbit coupling in these 5d-materials would lead to orbital dependent anisotropic exchanges which could mimic the Kitaev couplings [33]. It was realized that in addition to the Kitaev-like interactions the real materials would have direct- and super-exchange Heisenberg like spin couplings as well. Both these compounds have been modelled by the Kitaev-Heisenberg model. The Na_2IrO_3 compound shows zigzag magnetic order at low temperatures whereas the $Na_4Ir_3O_8$ has not shown any magnetic order till date. Although a recent ultrafast optical study on $\mathrm{Na_2IrO_3}$ has claimed to see signatures of a spin liquid state in the confinement-deconfinement transition of spin and charge excitations across T_N [34], smoking gun evidence of the Kitaev spin-liquid or of dominant Kitaev interactions has been missing. The current experimentally constrained estimates of various exchange parameters are obtained either by comparing theoretical results with magnetic measurements of the Curie-Weiss scale [35], or from a fitting of the available low energy inelastic neutron scattering data [36]. Ideally inelastic scattering measurements giving the full momentum and energy resolved magnetic dispersion spectrum are needed to settle these issues. Carrying out inelastic neutron scattering measurements is problematic because of the strong absorption by iridium. Inelastic Raman scattering can also give information about magnetic energy scales. Infact the first estimate of the magnetic exchange interaction for $\mathrm{La_2CuO_4}$ were obtained from the position of the two-magnon peak in Raman scattering [37]. Raman spectroscopy experimental studies show a broad Raman band for both these compounds. We shall model these compounds using the Kitaev-Heisenberg model, theoretically study the Raman intensity and compare the theoretical predictions with the experimental results.

Chapter-wise summary of the thesis:

- The Kitaev spin liquid is one of the cornerstones of this thesis, and we will get introduced to it in detail in Chapter 2.
- In Chapter 3 we will discuss the Kitaev-Hubbard model, which, as mentioned previously, is a realization of the Kitaev model on the optical lattice.
- We will describe the non-interacting limit of the model in detail and discuss some of its important topological properties like merging-emerging of Dirac Points and Chern numbers in Chapter 4.
- Having concluded a review of the model in these two chapters, I shall then turn to my describing the interacting limit of my work on this model. In Chapter 5, I shall describe the numerical techniques that we have used to study the phase diagram of the Kitaev-Hubbard model at half-filling and discuss the results obtained which includes the presence of a spin liquid phase.
- In Chapter 6 we probe the nature of the spin liquid phase using perturbative continuous unitary transformations, discuss its stability issues and analytically compute the spin-spin correlation function thereby showing that the phase is a stable ASL. Then we eliminate the possibility of spontaneous time reversal symmetry breaking which destabilizes the ASL phase into

other spin liquid phases. With that we conclude the first part of my work.

- Chapter 7 begins the second part of my work. Here I will give a brief introduction to the Iridate materials.

- In chapter 8, I will describe briefly Raman spectroscopy which I shall calculate using the Kitaev-Heisenberg model for the two iridates separately in Chapter 9 and 10.

- Finally I will conclude my thesis in Chapter 11.

Chapter 2

A Brief History of Kitaev Model

जाती ना पुछो साधु की, पूछ्
लीजिए न्यान्।
मोल् करो तलवार् का पड़ा रहन्
दो म्यान् ॥

Kabir Das

It was Kitaev who first studied a frustrated spin model on the honeycomb lattice [2]. His objective was to apply such a model to problems in quantum information theory. The toric code model is a limit of the Kitaev model that is used for fault tolerance and gate operations. Using the Majorana fermion representation and the Jordan-Wigner transformation, Kitaev found the ground state of this model. It happens to be one of the models in $2D$ whose exact solution is known. The exact solvability of the model combined with the knowledge of its ground state makes it a suitable model for us to study. The underlying symmetry is the Z_2 symmetry and each of the Z_2 components take values ± 1 giving us a four-fold degenerate ground state. It took a few years for the condensed matter community to realize the importance of this model and label the ground state to be a Z_2 spin liquid.

We cannot hope to cover all the work and the vast literature on the Kitaev model in these few pages. However, we will give a brief description of the properties of the Kitaev model which will come in handy further down the line. We shall begin with the Majorana representation and then move on to the ground state of the model in this representation. We shall derive a long wavelength Hamiltonian for the model and study how time reversal symmetry manifests itself in the spin-spin correlation of this system.

2.1 Ground State of the Kitaev Model

The spin-1/2 Hamiltonian for the Kitaev model on the honeycomb lattice, as shown in Fig:(2.1), is given by

$$\mathcal{H} = J \sum_{\langle ij \rangle \alpha} S_i^\alpha S_j^\alpha, \tag{2.1}$$

where $S^\alpha = \sigma^\alpha$ (the Pauli matrices), with the basis vectors

$$\mathbf{e}_1 = \frac{1}{2}\hat{x} + \frac{\sqrt{3}}{2}\hat{y} \tag{2.2}$$

$$\mathbf{e}_2 = -\frac{1}{2}\hat{x} + \frac{\sqrt{3}}{2}\hat{y}. \tag{2.3}$$

This model is highly frustrated as the spins at each site need to satisfy each of the spin orientations from its nearest representation and quantum mechanically the spin operators do not commute. Thus the ground state is one in which the spins are disordered and hence degeneracy of the ground state is also expected. A suitable representation to study such a system is the Majorana fermion representation

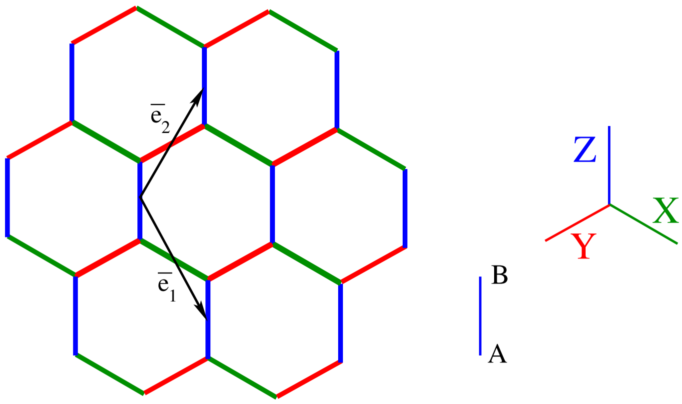

Figure 2.1: The honeycomb lattice and its basis with the two sub-lattices. The colors represent the three types of links X, Y and Z on it.

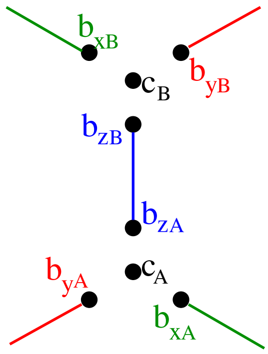

Figure 2.2: The representation of Majorana fermions on the honeycomb lattice.

of the spin operators which is given as

$$\sigma_i^\alpha = ic_i b_i^\alpha, \qquad \{c_i, c_j\} = 2\delta_{ij} \qquad \{b_i^\alpha, b_j^\beta\} = 2\delta_{\alpha\beta}\delta_{ij}, \qquad \{c_i, b_j^\alpha\} = 0 \tag{2.4}$$

See Fig:(2.2) for the representation. Since the Hilbert space is extended due to such a representation, the physical subspace is defined by the constraint

$$c_i b_i^x b_i^y b_i^z |\psi\rangle_{\rm phys} = |\psi\rangle_{\rm phys}. \tag{2.5}$$

Therefore the Kitaev model can now be written as

$$\mathcal{H} = -iJ \sum_{\langle ij\rangle\alpha} c_i u_{\langle ij\rangle\alpha} c_j, \tag{2.6}$$

where $u_{\langle ij\rangle\alpha} = ib_i^\alpha b_j^\alpha$. These are conserved quantities of the system since they commute with the Hamiltonian i.e. $[\mathcal{H}, u_{\langle ij\rangle\alpha}] = 0$. Thus the b fermions are static and have the property $u^2_{\langle ij\rangle\alpha} = 1$. Therefore it can take values ± 1 thereby giving it a Z_2 gauge symmetry. The Hamiltonian, when all of $ib_i^\alpha b_j^\alpha = 1$, reduces to nearest-neighbour hopping of c fermions on a honeycomb lattice which in momentum basis given by

$$c_{i\alpha} = \frac{1}{N} \sum_k e^{i\mathbf{k}\cdot\mathbf{r}} c_{k\alpha}, \tag{2.7}$$

with α corresponding to the sub-lattice index and $c^\dagger_{k\alpha} = c_{-k\alpha}$, is

$$\mathcal{H} = \sum_{k\in HBZ} \left(c^\dagger_{kA},\ c^\dagger_{kB}\right) \begin{pmatrix} 0 & if \\ if^* & 0 \end{pmatrix} \begin{pmatrix} c_{kA} \\ c_{kB} \end{pmatrix}, \tag{2.8}$$

where $f = J(1 + e^{ik_1} + e^{ik_2})$, k_1 and k_2 point along the X and Y bond respectively and HBZ is half-Brillouin zone. Eq:(2.8) is similar to real fermions hopping in Graphene, that is in the tight binding model. Graphene has low-energy Dirac quasi-particles about two points in the Brillouin zone : $\mathbf{K}$ and $\mathbf{K}'$. However, since the c fermions are Majorana fermions, the excitations exist only over half the Brillouin zone which forces the low-energy modes to constitute a single Dirac quasi-particle. The continuum theory about the Dirac point is derived by introducing slowly varying fields $\psi_l(\mathbf{r})$ such that

$$c_{\mathbf{r}l} = \frac{1}{2}\left(e^{i\mathbf{K}\cdot\mathbf{r}}\psi_l(\mathbf{r}) + e^{-i\mathbf{K}\cdot\mathbf{r}}\psi_l^\dagger(\mathbf{r})\right). \tag{2.9}$$

Substituting equation (2.9) in equation and expanding about the Dirac point we find the following continuum Hamiltonian

$$\mathcal{H} = \frac{\sqrt{3}J}{2}\int d^2x\, \psi^{\dagger}(x)\, i\, (\boldsymbol{\tau}\cdot\boldsymbol{\nabla})\, \psi(x). \tag{2.10}$$

It can be seen that the low energy continuum theory is that of a single Dirac fermion. The Green's function for the above Hamiltonian is a solution to the equation

$$i\left(\partial_t - \frac{\sqrt{3}J}{2}\boldsymbol{\tau}\cdot\boldsymbol{\nabla}\right)G(R,t) = \delta(R-R')\delta(t-t') \tag{2.11}$$

and thus the Green's function in operator form can be written as

$$G_{lm}(\mathbf{r},t) = \langle T\left(\psi_l(\mathbf{r},t)\psi_m^{\dagger}(0,0)\right)\rangle. \tag{2.12}$$

We can thus write

$$G_{lm} = (\boldsymbol{\tau}\cdot\mathbf{r} - J_p t\mathbb{I})_{lm}\frac{J_p^2}{4\pi}\frac{1}{(\mathbf{r}^2 - J_p^2t^2)^{\frac{3}{2}}} \tag{2.13}$$

where $\boldsymbol{\tau} = (\tau_x, \tau_y)$ are the Pauli matrices in the sublattice indices and $J_p = \dfrac{\sqrt{3}J}{2}$.

Apart from the single particle propagators calculated above, quantities like the spin-spin correlation have been calculated and have been found to be extremely short-ranged thanks to the Z_2 gauge fields. The spin-spin correlations exist only upto nearest neighbours and are zero beyond that. For instance, on the x link only $x-x$ correlation exists and so on [24].

$$S_{ij}^{ab}(t) = \langle S_i^a(t)S_j^b(0)\rangle = g_{<ij>a}(t)\delta_{a,b}. \tag{2.14}$$

But the correlation functions are susceptible to change under perturbations. On adding a single-spin perturbation which acts like a magnetic field [3] the correlations decay as a power-law.

$$H_p = H_K + \sum_i \mathbf{h}_i \cdot \mathbf{S}_i. \tag{2.15}$$

This term breaks time-reversal symmetry. This opens up a gap and imparts mass to the Dirac fermion. In $2+1$ dimensions, the breaking of time-reversal symmetry corresponds to adding a mass term and hence opening up a gap in the system. The short range nature is unaffected by the addition of an anisotropic Heisenberg term [4] since it is time-reversal invariant.

$$H_p = H_K + \sum_{<ij>} J^{\alpha} \mathbf{S}_i^{\alpha} \mathbf{S}_i^{\alpha}. \tag{2.16}$$

It is thus apparent from this that preserving time-reversal symmetry while simultaneously introducing power-law correlations is tricky business. In the next chapter we shall discuss the Kitaev-Hubbard model, a model proposed to realize the Kitaev model in optical lattice systems, in which power-law correlations exist and time-reversal symmetry is preserved.

Chapter 3

The Kitaev-Hubbard Model

Nobody owns the world. So feel free to explore it.

Erghie Cabaltica

In 2003, Duan *et al.*[5] added an anisotropic spin-dependent hopping term to the classic Hubbard model that leads to a high degree of frustration in the effective spin model giving a Kitaev model. We call this modified model the Kitaev-Hubbard model, and write its Hamiltonian as

$$H = \sum_{\langle ij \rangle_\alpha} \left\{ c_i^\dagger \left(\frac{t + t' \sigma_\alpha}{2} \right) c_j + \text{H.c} \right\} + U \sum_i n_{i\uparrow} n_{i\downarrow} \tag{3.1}$$

where $c_{i\sigma}$ annihilates a fermion of spin projection $\sigma = \uparrow, \downarrow$ at site i (the spin index is implicit in the first term), σ_α ($\alpha = x, y, z$) are the Pauli matrices, $n_\sigma \equiv c_\sigma^\dagger c_\sigma$ is the number of fermions of spin σ at site i, and $\langle ij \rangle_\alpha$ denotes the nearest-neighbor pairs in the three hopping directions of the lattice (see Fig. 3.1). In general, the spin-dependent term breaks time reversal symmetry although the complete model is itself particle-hole symmetric.

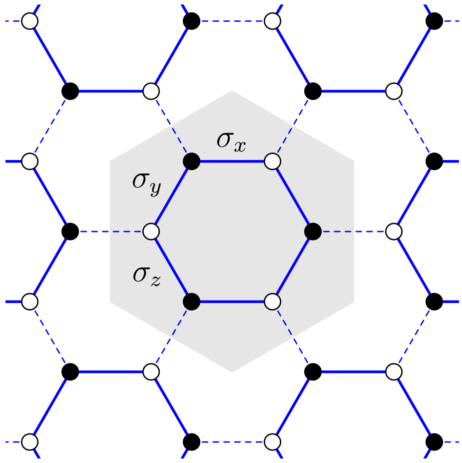

Figure 3.1: The honeycomb lattice with the two sub-lattices marked by white and black dots. The six-site cluster used in this work is shown as the shaded area. The σ_i label the different spin-dependent hopping directions (blue solid lines), whereas the inter-cluster bonds are shown as dashed lines.

3.1 Analysis of Experimental Realization of KHUB model

As described earlier, the Kitaev-Hubbard model, which I shall henceforth abbreviate as KHUB, is a model on the honeycomb lattice with spin-dependent hopping. This can be experimentally realized in a number of ways [38]. For example, three intersecting laser beams at an angle of 120° to each other will form an optical honeycomb lattice [5, 38]. In this section, we systematically derive the spin-dependent hopping on the honeycomb lattice using the method suggested by Duan *et. al.* [5] which is different from that discussed earlier [39].

Most fermionic optical lattice experiments are performed using ^{40}K atoms [8]. In the absence of external magnetic field the $^2S_{1/2}$ and the $^2P_{1/2}$ levels of potassium each split into two hyperfine levels. Two of the hyperfine energy levels of $^2S_{1/2}$ are much lower in energy compared to levels of $^2P_{1/2}$. FIG. (3.2) is a schematic of the three level system formed by the low levels of ${}^2S_{1/2}$ and a level of ${}^2P_{1/2}$.

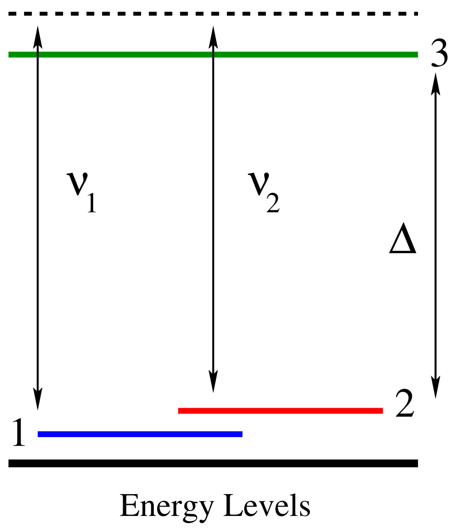

Figure 3.2: Schematic of the effective hyperfine energy levels of ${}^{40}K$. The gap Δ is orders of magnitude larger in energy compared to the lower energy levels [8].

The lower two energy levels 1, 2 are separated from the third 3 by a gap $\Delta \approx 0.3eV$ which is orders of magnitude larger[8] than the hopping parameter $\approx 10^{-13}eV$ seen in typical optical lattice experiments [39]. Two blue de-tuned laser beams L_1 and L_2 excite virtual transitions between the first and the third $(1 \rightarrow 3)$ and the second and the third $(2 \rightarrow 3)$ levels respectively. Since these virtual transitions are fast compared to the hopping of the atoms, a local microscopic Hamiltonian can be written as

$$\mathcal{H} = \int d^2x \sum_{i=1}^{2} \epsilon_i C_i^\dagger(\mathbf{x}) C_i(\mathbf{x}) + \Delta C_3^\dagger(\mathbf{x}) C_3(\mathbf{x}) + \sum_{i=1}^{2} g_i C_3^\dagger(\mathbf{x}) a_i(\mathbf{x}, \tau) C_i(\mathbf{x}) + h.c. \tag{3.2}$$

Here ϵ_i represents the energies of 1 and 2. C_i is the atomic creation operator for the i-th energy level at $\mathbf{x}$. The last two terms in the above expression arise due to the interaction of the atom with the laser beams. The wavelengths of the laser beams is such that it only causes transitions from the energy levels 1 and 2 to the energy level 3. Here g_1 and g_2 represent the strength of these transitions respectively and $a_i(\mathbf{x}, \tau)$ represents the electromagnetic field. The effective two-level system can be obtained by integrating out the third energy level. The action S in the path integral formalism for the three level system can be written as

$$S = -\int d\tau \left(\sum_{i=1}^{3} C_i^\dagger(\mathbf{x}) \partial_\tau C_i(\mathbf{x}) + \mathcal{H} \right). \tag{3.3}$$

Integrating the third energy level we obtain the effective action of the two-level system as

$$S_e = -\int d\tau d\tau' \int d^2x \sum_{i,j=1}^{2} C_i^\dagger(\mathbf{x}, \tau) G_{ij}(\mathbf{x}, \tau, \tau') C_j(\mathbf{x}, \tau') \tag{3.4}$$

where the matrix G is given as

$$G_{ij}(\mathbf{x}, \tau, \tau') = \partial_\tau \delta_{ij} + \epsilon_i(\mathbf{x}) \delta_{ij} + g_i g_j a_i^*(\mathbf{x}, \tau) \langle \tau | \frac{1}{\partial_\tau + \Delta} | \tau' \rangle a_j(\mathbf{x}, \tau') \tag{3.5}$$

Since the beams are monochromatic, the electromagnetic fields can be written as $a_i(\mathbf{x}, \tau) = e^{i\nu_i \tau} b_i(\mathbf{x})$, where ν_i is the frequency of transition from the i-th, $i = 1, 2$, energy level to the third energy level. This is clearly seen in FIG.(3.2). Thus the effective new G matrix is given by

$$G_{ij}(\mathbf{x}, \tau, \tau') = \partial_\tau \delta_{ij} + \epsilon_i(\mathbf{x}) \delta_{ij} + \frac{g_i g_j}{\Delta} b_i^*(\mathbf{x}) b_j(\mathbf{x}). \tag{3.6}$$

The two low lying energy levels can be represented by pseudo-spin indices σ and effective potential seen by the pseudo-spins is given as

$$V_s^{\sigma\sigma'}(\mathbf{x}) = g_\sigma g_{\sigma'} b_\sigma^*(\mathbf{x}) b_{\sigma'}(\mathbf{x}). \tag{3.7}$$

When N laser beams of varying intensities and directed along the wave-vectors $\mathbf{k}_n$ are incident on this effective two-level atom, the field can be written as

$$b_\sigma(\mathbf{x}) = \sum_n a_{n\sigma} \sin(\mathbf{k}_n \cdot \mathbf{x}) \tag{3.8}$$

with the condition $\langle a^*_{n\sigma} a_{n'\sigma'} \rangle = \delta_{nn'} \langle a^*_{n\sigma} a_{n\sigma'} \rangle$. This implies that the fields arising due to different laser beams are independent. The effective potential which depends on the spin becomes

$$V_s^{\sigma\sigma'}(\mathbf{x}) = g_\sigma g_{\sigma'} \sum_n \sin^2(\mathbf{k}_n \cdot \mathbf{x}) a'^*_{n\sigma} a'_{n\sigma'}. \tag{3.9}$$

Thus the spin dependent potential can be varied by tuning the laser beams L_1 and L_2.

The spin-dependent potential on the honeycomb lattice can be generated by tuning three lasers with different strengths oriented along the three directions X, Y and Z, at an angle of 120° relative to one another [5, 38], FIG.(2.1). The L_1 laser beam is sufficient to generate a spin dependent coupling on the Z link, $a_{Z\downarrow} = 0$. The lasers L_1 and L_2 directed along X and Y with a relative phase difference are required to generate the couplings along these directions. Thus we have $g_\uparrow a_{X\uparrow} = g_\downarrow a_{X\downarrow}$ and $g_\uparrow a_{Y\uparrow} = i g_\downarrow a_{Y\downarrow}$ respectively for the X and Y directions. We now write the potential as a sum of spin-independent and spin-dependent parts,

$$V_s(\mathbf{x}) = V(\mathbf{x})\mathbb{I} + \mathbf{B}(\mathbf{x}) \cdot \boldsymbol{\sigma} \tag{3.10}$$

where $\mathbf{B}(\mathbf{x})$ is the effective space dependent magnetic field generated by the laser beams. Its individual components can be written as

$$B_x(\mathbf{x}) = g_\uparrow^2 |a'_{x\uparrow}|^2 \sin^2(\mathbf{k}_X \cdot \mathbf{x}) \tag{3.11}$$

$$B_y(\mathbf{x}) = g_\uparrow^2 |a'_{y\uparrow}|^2 \sin^2(\mathbf{k}_Y \cdot \mathbf{x}) \tag{3.12}$$

$$B_z(\mathbf{x}) = \frac{1}{2} g_\uparrow^2 |a'_{z\uparrow}|^2 \sin^2(\mathbf{k}_Z \cdot \mathbf{x}) \tag{3.13}$$

where $\mathbf{k}_{X,Y,Z}$ is the wave-vector along X, Y and Z respectively. The spin independent potential $V(\mathbf{x})$ can be written as

$$V(\mathbf{x}) = g_\uparrow^2 |a'_{x\uparrow}|^2 \sin^2(\mathbf{k}_X \cdot \mathbf{x}) + g_\uparrow^2 |a'_{y\uparrow}|^2 \sin^2(\mathbf{k}_Y \cdot \mathbf{x}) + \frac{1}{2} g_\uparrow^2 |a'_{z\uparrow}|^2 \sin^2(\mathbf{k}_Z \cdot \mathbf{x}). \tag{3.14}$$

This shows that the spin-independent part V cannot be tuned individually as it is coupled to $\mathbf{B}(\mathbf{x})$. So we add an additional spin-independent potential $V_h^{\sigma\sigma'}(\mathbf{x})$ which can be tuned without affecting the spin-dependent part. Now the wave-function of the atom in the spin-dependent honeycomb lattice potential follows the time-independent Schrödinger equation of the form

$$\left(\frac{p^2}{2M} \delta_{\sigma\sigma'} + V^{\sigma\sigma'}(\mathbf{x}) \right) \psi_{\sigma'}(\mathbf{x}) = E \psi_\sigma(\mathbf{x}) \tag{3.15}$$

where $V^{\sigma\sigma'}(\mathbf{x}) = V_h^{\sigma\sigma'}(\mathbf{x}) + V_s^{\sigma\sigma'}(\mathbf{x})$ is the total potential. The wave-function of the atoms can be expanded in terms of atomic orbitals $\phi_\alpha(\mathbf{x} - \mathbf{x}_i)$ which are localized in the α^{th} sub-lattice of the i-th triangular Bravais lattice, that is

$$\psi_{\sigma'}(\mathbf{x}) = \sum_{i\alpha} d_{i\alpha}^{\sigma'} \phi_\alpha^{\sigma'}(\mathbf{x} - \mathbf{x}_i). \tag{3.16}$$

This allows us to compute the hopping parameter as

$$t^{\sigma'\sigma}_{i\alpha j\beta} = \int d^2x\, \phi^{*\sigma}_{\beta}(\mathbf{x}-\mathbf{x}_j)\left(\frac{p^2}{2M} + V^{\sigma\sigma'}(\mathbf{x})\right)\phi^{\sigma'}_{\alpha}(\mathbf{x}-\mathbf{x}_i). \tag{3.17}$$

The hopping part of the Hamiltonian Eq.(3.1), is applicable when the nearest neighbours provide the dominant contributions. Thus we need $i = j \pm 1$ for the X and Y links and $i = j$ for the Z link with $\alpha \neq \beta$. Once we obtain the spin-dependent hopping the onsite interactions between the atoms in the optical lattice systems can be created by Feshbach resonance[38].

3.2 Properties of the KHUB model

Over the past few years, the KHUB model has been studied extensively using both analytical and numerical means. We discuss a few of the findings.

At $t' = 0$, the model reduces to the simple spin- and TR-invariant, nearest-neighbor Hubbard model[40, 41, 42]. The term proportional to t' is a spin-dependent hopping term and breaks TR symmetry, $SU(2)$ spin symmetry and the three-fold spatial rotation symmetry of the $t' = 0$ model. It is however invariant under a spatial rotation of $2\pi/3$ combined with a spin rotation of $2\pi/3$ about the (111) spin axis. At $t' = t$, the one-body part of the Hamiltonian is a combination of the projection operators $\frac{1}{2}(1 + \sigma_\alpha)$. Thus, only those electrons that are spin-polarized in the α^{th} direction can hop along the α bonds. At this value of t', the effective low-energy spin model, at half-filling and large U, is the Kitaev honeycomb model.[43, 44]

At $U = 0$, the non-interacting limit, the model exhibits nontrivial properties [45, 46] such as topological Lifshitz transitions and non-zero Chern numbers which we discuss in detailed in the next chapter.

Chapter 4

Life without interactions of the Kitaev-Hubbard model

Solitary trees, if they grow at all,

grow strong.

Winston Churchill

In this chapter we investigate the non-interacting limit of the Kitaev-Hubbard model[31, 45, 46] (KHUB) presented by the Hamiltonian,

$$\mathcal{H} = \sum_{\langle ij\rangle^{\alpha}} \left\{ C_i^{\dagger} \frac{(tI + t'\sigma^{\alpha})}{2} C_j + h.c. \right\} + U \sum_i n_{i\uparrow} n_{i\downarrow} \tag{4.1}$$

There are topological transitions in this regime corresponding to creation and merging of Dirac Points (DP) which occur at $t'/t = 0, 1/\sqrt{3}, \sqrt{3}$. It has been shown that these features persist even at non-zero values of U [42]. We study, in detail, the topology of the phases and the transition between them. We point out possible experimental signals of the topological features.

4.1 Discrete symmetries and the Pancharatnam-Berry (PB) curvature

As mentioned earlier, topological phases of insulators have been classified according to the presence or absence of certain discrete symmetries [47, 48, 49], namely time reversal symmetry (TRS), charge conjugation symmetry (CCS) and their composition which we call particle-hole symmetry (PHS). In this section, these symmetries are briefly reviewed and the constraints that are imposed on the Pancharatnam Berry (PB) curvatures are examined for number-conserving, non-interacting, 2-dimensional fermionic systems. The Hamiltonian for such systems can be written as

$$H = \int \frac{d^2k}{(2\pi)^2} C_a^\dagger(k) h_{ab}(k) C_b(k) \tag{4.2}$$

where k goes over the Brillouin zone of a 2-dimensional Bravais lattice, $h = h^\dagger$ is the single-particle Hamiltonian and $a, b = 1, \ldots, N_B$ label the sub-lattice and spin indices. The single-particle Hamiltonian of KHUB in Eq.(4.1), has $N_B = 4$ corresponding to two sub-lattice and two spin orbitals in every unit cell. Setting $t = 1$, it can be written as

$$h_{KHUB}(k, t') = \alpha^\dagger \otimes \Sigma(k, t') + \alpha \otimes \Sigma^\dagger(k, t') \tag{4.3}$$

where α and Σ are 2×2 matrices in the sub-lattice and spin space respectively.

$$\alpha = \begin{pmatrix} 0 & 0 \\ 1 & 0 \end{pmatrix} \tag{4.4}$$

$$\Sigma(k, t') = P^z + P^x e^{ik_1} + P^y e^{-ik_2} \tag{4.5}$$

where $k_1 = \frac{1}{2}k_x - \frac{\sqrt{3}}{2}k_y$, $k_2 = \frac{1}{2}k_x + \frac{\sqrt{3}}{2}k_y$, $k_x = \mathbf{k}\cdot\mathbf{x}$, $k_y = \mathbf{k}\cdot\mathbf{y}$ and $P^\alpha = \frac{1}{2}(I + t'\sigma^\alpha)$. The single-particle spectrum is completely determined in terms of the spectrum of the positive semi-definite matrix

$$\Sigma^\dagger\Sigma = f^* f + \frac{3}{4}(t')^2 + \frac{t'}{2}\mathbf{B}\cdot\boldsymbol{\sigma} \tag{4.6}$$

where

$$\begin{aligned} f &= \frac{1}{2}(1 + \mathrm{e}^{ik_1} + \mathrm{e}^{-ik_2}) \\ B_1 &= 1 - t' \sin k_1 + \cos k_2 + \cos k_3 \\ B_2 &= 1 + \cos k_1 - t' \sin k_2 + \cos k_3 \\ B_3 &= 1 + \cos k_1 + \cos k_2 - t' \sin k_3 \end{aligned} \tag{4.7}$$

If $\phi^\pm(\mathbf{k})$ are the eigenvectors of $\mathbf{B}(\mathbf{k})\cdot\boldsymbol{\sigma}$, with eigenvalues $\pm|\mathbf{B}(\mathbf{k})|$, then they are also the eigenvectors of $\Sigma^\dagger(\mathbf{k})\Sigma(\mathbf{k})$ with eigenvalues,

$$\epsilon_\pm^2(\mathbf{k}) = f^* f + \frac{3}{4}(t')^2 \pm \frac{t'}{2}|\mathbf{B}(\mathbf{k})| \tag{4.8}$$

The four-component vectors

$$\Phi^{\pm\pm}(\mathbf{k}) = \frac{1}{\sqrt{2}}\begin{pmatrix} \phi^\pm(\mathbf{k}) \\ \pm e^{i\chi(\mathbf{k})}\phi^\pm(-\mathbf{k}) \end{pmatrix} \tag{4.9}$$

are then the eigenvectors of the single-particle Hamiltonian defined by Eq. (4.3) with eigenvalues $\pm\epsilon_\pm(\mathbf{k})$. $\chi(\mathbf{k})$ is a phase factor which we will discuss later. Fig:(4.1) shows the band structure at $t' = 1$.

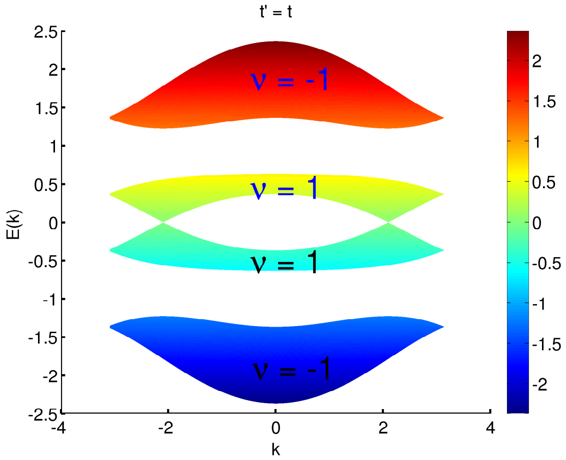

Figure 4.1: The non-interacting bands at $t' = 1$ showing the chern number ν of the individual bands.

If we denote the spectrum as,

$$h(k)u^n(k) = \epsilon^n(k)u^n(k), \quad n = 1, \ldots, N_B. \tag{4.10}$$

In terms of these single particle eigen-functions, the PB vector potential, $\mathcal{A}_i^n(k)$ and curvature, $\mathcal{B}^n(k)$ are given by

$$\mathcal{A}_i^n(k) = -i(u^n(k))^\dagger \frac{\partial u^n(k)}{\partial k_i} \tag{4.11}$$

$$\mathcal{B}^n(k) = \epsilon_{ij}\partial_i \mathcal{A}_j^n(k). \tag{4.12}$$

From the PB curvature, the Chern number

$$\nu_n = \frac{1}{2\pi}\int \frac{d^2k}{4\pi^2}\mathcal{B}^n(k). \tag{4.13}$$

can be computed. Now we discuss effect of the discrete symmetries on the energy bands and the PB curvature, one by one.

Time-reversal symmetry (TRS)

The time-reversal transformation replaces particles (holes) with momentum k by particles (holes) with momentum $-k$. It is an anti-unitary transformation in the many-body Hilbert space which we denote by $\mathcal{T}$,

$$\mathcal{T}^{-1}C_a(k)\mathcal{T} = \tau_{ab}C_b(-k), \ \ \mathcal{T}^{-1}\mathcal{T} = I, \ \ \mathcal{T}^{-1}i\mathcal{T} = -i \tag{4.14}$$

All transition amplitudes are invariant under this transformation if there is a unitary matrix τ with $\tau^2 = \pm 1$ such that,

$$\tau^{\dagger}h^{*}(-k)\tau = h(k) \tag{4.15}$$

Under the time-reversal transformation, $\mathcal{B}^n(k) = -\mathcal{B}^n(-k)$. Thus if it is a symmetry, then the Chern numbers, ν^n are all 0.

The KHUB satisfies the condition

$$h^{*}_{KHUB}(-k, t') = \sigma^{y}h(k, -t')\sigma^{y}. \tag{4.16}$$

Thus for time-reversal symmetry to hold the condition in Eq.(4.15) needs to be satisfied for finite t', implying that the matrix $\sigma^{y}\tau$ has to anti-commute with all the three Pauli matrices. Since such a matrix does not exist for any t', the model in general is not TRS. But at two special points, $t' = 0$ with $\tau = \sigma^{y}$ and $t' = \infty$ with $\tau = \beta \otimes \sigma^{y}$, where β anti-commutes with α and $\alpha^{\dagger}$ the model preserves TRS.

Charge conjugation symmetry (CCS)

The charge-conjugation transformation replaces particles with momentum k by holes with momentum k and vice-versa. It is unitary transformation in the many-body Hilbert space that we denote by C,

$$C^{-1}C_a(k)C = \gamma_{ab}C_b^{\dagger}(-k), \;\; C^{\dagger}C = I, \;\; C^{\dagger}iC = i. \tag{4.17}$$

All transition amplitudes are invariant under this transformation if there is a unitary matrix γ with $\gamma^2 = \pm 1$ such that,

$$\gamma^{\dagger}h^{*}(-k)\gamma = -h(k). \tag{4.18}$$

If the system has CCS, then all the single particle energies come in pairs with $\epsilon^{\bar{n}}(k) = -\epsilon^{n}(k)$ and $\mathcal{B}^{\bar{n}}(k) = -\mathcal{B}^{n}(-k)$. $\bar{n}$ corresponds to the band index with negative of the energy of n. The positive and negative energy bands have opposite Chern numbers. From Eq.(4.16) it follows that the KHUB has CCS only at $t' = 0$ with $\gamma = \beta \otimes \sigma^{y}$ and at $t = 0$ with $\gamma = \sigma^{y}$.

Particle-hole symmetry (PHS)

The particle-hole transformation which we denote as $\mathcal{P}$ is the composition $\mathcal{T}C$. It replaces particles with momentum k by holes with momentum $-k$ and vice-versa. Note that the nomenclature is not uniform in the literature. For example Schnyder *et. al.* [47] refer to what we call CCS as the particle-hole symmetry and what we call PHS by "chiral" or "sub-lattice" symmetry.

The particle hole symmetry is anti-unitary in the many-body Hilbert space

$$\mathcal{P}^{-1}C_a(k)\mathcal{P} = \tau_{ab}\gamma_{bc}C_c^\dagger(k), \;\; \mathcal{P}^{-1}\mathcal{P} = I, \;\; \mathcal{P}^{-1}i\mathcal{P} = -i. \tag{4.19}$$

All transition amplitudes are invariant under the particle-hole transformation defined above if

$$\gamma^\dagger\tau^\dagger h(k)\tau\gamma = -h(k). \tag{4.20}$$

The KHUB has PHS with $\tau\gamma = \beta$ at all values of t'. This symmetry is very common in condensed matter systems. It occurs in all bipartite lattices where the fermion hopping is only from one sub-lattice to the other. PHS implies that all the single particle levels come in pairs with $\epsilon^{\bar{n}}(k) = -\epsilon^n(k)$ and $\mathcal{B}^{\bar{n}}(k) = \mathcal{B}^n(k)$. The sum of the PB curvature over the positive and negative energy bands are equal to zero individually as we shall show below. We can write

$$\sum_{\epsilon^n(k)} \mathcal{B}^n(k) = \sum_{\epsilon^n(k)<0} \mathcal{B}^n(k) + \sum_{\epsilon^n(k)>0} \mathcal{B}^n(k) = 0 \tag{4.21}$$

and using the particle hole symmetry property we get

$$\sum_{\epsilon^n(k)<0} \mathcal{B}^n(k) = \sum_{\epsilon^n(k)>0} \mathcal{B}^n(k) \tag{4.22}$$

and thus we have

$$\sum_{\epsilon^n(k)<0} \mathcal{B}^n(k) = 0 = \sum_{\epsilon^n(k)>0} \mathcal{B}^n(k). \tag{4.23}$$

Thus the total PB curvature vanishes for insulators with PHS at half-filling. Hatsugai [50] has shown that in such systems, namely gaped systems invariant under an anti-unitary transformation, it is possible to define local topologically protected quantities.

4.2 Topology of bands with DP and PHS

In this section, we consider the case when the highest negative energy band and the lowest positive energy band touch at N_D DPs, where N_D is an even integer. We denote the DPs by $\mathbf{K}_n,\ n = 1, \ldots N_D$. We will show that for systems with PHS at half filling the PB curvature is given by,

$$\mathcal{B}(k) = \sum_{n=1}^{N_D} p_n \pi \delta^2(\mathbf{k} - \mathbf{K}_n) \tag{4.24}$$

where p_n is the PB flux passing through $\mathbf{K}_n$. Consequently, the Zak phases[51, 52, 53], Φ_Z defined as

$$\Phi_Z = \int_C \mathcal{A}_i(k) dk^i \tag{4.25}$$

are topological invariants. These quantities are independent of the contour C, provided it does not cross a DP. They are completely determined by the position and indices of the DPs. DPs lead to non-dispersive edge modes and we will show that the wave-vectors of these edge modes are determined by the Zak phases of the loops that wind around the Brillouin zone.

PHS implies that in the basis where β is diagonal, the single-particle Hamiltonian is of the form,

$$\beta = \begin{pmatrix} I & 0 \\ 0 & -I \end{pmatrix}, \quad h(k) = \begin{pmatrix} 0 & \Sigma(k) \\ \Sigma^\dagger(k) & 0 \end{pmatrix}. \tag{4.26}$$

In general the two blocks defined above can have different dimensions, say N and M, for example a bipartite lattice with different number of A and B lattice sites. However if $N \neq M$, there will be $|N - M|$ zero eigenvalues at every k, i.e. $|N - M|$ flat bands. While this may have interesting effects, we concentrate on the $N = M$ case so that we have an even number of bands, $N_B = 2N$. It is then convenient to replace the index $a = 1, \ldots, N_B$ by a pair (r, σ), $r = A, B$, $\sigma = 1, \ldots, N$.

Using the fact that every matrix admits a singular value decomposition, we express Σ as,

$$\Sigma = U_A \epsilon U_B^\dagger \tag{4.27}$$

where $U_{A(B)}$ are unitary matrices and ϵ is a diagonal matrix, $\epsilon_{nm} = \epsilon^n \delta_{nm}$, $\epsilon^n \geq 0$, $n, m = 1, \ldots, N$. The eigenvalues of the Hamiltonian are then $\pm\epsilon^n$, the eigenvectors being,

$$u^{\pm n} = \begin{pmatrix} U^A|n\rangle \\ \pm U^B|n\rangle \end{pmatrix}, \quad h|n\rangle = \epsilon^n|n\rangle. \tag{4.28}$$

We can write $U_{A(B)} = e^{i\Omega_{A(B)}}\widetilde{U}_{A(B)}$, where $\widetilde{U}_{A(B)}$ are $SU(N)$ matrices with unit determinant. The PB vector potential and curvature summed over all the negative energy bands can be computed to be,

$$\mathcal{A}_i(k) = \frac{1}{2}\partial_i\left(\Omega_A(k) - \Omega_B(k)\right), \tag{4.29}$$

$$\mathcal{B}(k) = \frac{1}{2}\left(\partial_1\partial_2 - \partial_2\partial_1\right)\left(\Omega_A(k) - \Omega_B(k)\right). \tag{4.30}$$

Thus $\mathcal{B}(k)$ can be non-zero only at points where $\Omega(k) = \Omega_A(k) - \Omega_B(k)$ has a vortex type singularity. From Eq.(4.27), we see that $N\Omega$ is the phase of $\det\Sigma$. Since the matrix elements of Σ are smooth functions of k, Ω can be multi-valued only at points where $\det\Sigma = 0$. These are precisely the DPs. Thus we have proved Eq.(4.24) showing that the PB curvature for systems with PHS at half filling is that of a set of vortices at the DPs. We also see that $\det\Sigma(k)$ contains complete information of the topology of the system. The zeros of the determinant are the positions, $\mathbf{K}_n$, of the vortices. PB flux passing through $\mathbf{K}_n$ is $W_n\pi/N$, where W_n is the winding number of the phase of $\det\Sigma(k)$ around it. We discuss the topological properties discussed above in the context of the KHUB in the following sections.

4.2.1 Topology of KHUB with PBC

We now apply the above developed formalism to the non-interacting Hamiltonian KHUB which has PHS. It exhibits nontrivial properties [45] such as topological Lifshitz transitions and non-zero Chern numbers which we discuss in detail here, with t fixed at unity.

The first and the second band of the four band Hamiltonian overlap in the range $0 \leq t' < 0.717$ beyond which there is a non-zero gap between the bands at all k. The model also features multiple DPs whose number changes as a function of the spin-dependent hopping parameter t'. The transition points are seen at $t' = 0$, $1/\sqrt{3}$ and $\sqrt{3}$ (FIG.(4.2)). The location of the DPs can be determined from the

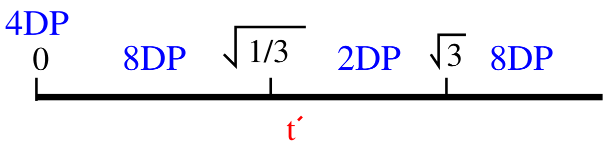

Figure 4.2: Number of DPs as a function of t'.

energy spectra as the values at which the eigenvalues $\epsilon(k)$ vanishes. At the DPs the wave-functions of the two sub-lattices decouple and we get

$$\Sigma(k, t')\psi_B = 0 \tag{4.31}$$

We look for solutions in the $k_1 = k_2 = q$ direction, which imposes the condition on q to be

$$\pm t' \sqrt{1 + 2\cos(2q)} = 1 + 2\cos q. \tag{4.32}$$

This condition is satisfied by $(q, q) = \pm\mathbf{K}_g = \pm(2\pi/3, 2\pi/3)$ for all t'. At $t' = 0$, the Graphene limit, doubly degenerate DPs are located at $\mathbf{K}_g$ and $-\mathbf{K}_g$ summing up to a total of 4 DPs. With increasing t', this condition is satisfied by another value of $q \in (0, \pi)$. Thus for $0 < t' < 1/\sqrt{3}$ there are a total of 8 DPs located at $\pm\mathbf{K}$ given by

$$\mathbf{K} = (2\pi/3, 2\pi/3), (q, q), (q, 2\pi - 2q), (2\pi - 2q, q) \tag{4.33}$$

where the last two are related to (q, q) through the underlying honeycomb lattice symmetry. At $t' = 1/\sqrt{3}$, six of these DPs merge in pairs at (π, π), $(0, \pi)$ and $(\pi, 0)$, leaving only those at $\pm\mathbf{K}_g$. For $t' \in (1/\sqrt{3}, \sqrt{3})$, there are only 2DPs. At $t' = \sqrt{3}$, six DPs emerge from $(0, 0)$ and move away from each other in the Brillouin Zone with increasing t'. FIG.(4.3) shows the DPs for various t' [54]. The merging and emerging of the DPs, previously discussed in other systems in [55, 56, 57, 58, 59], is a topological Lifshitz transition [55, 56]. Lifshitz transition refers to the transition where there is a change in the Fermi surface without any symmetry breaking.

In order to examine the Lifshitz transitions, we employ either the density of states or the thermodynamic consequences of the Fermi velocity, depending upon the transition point in question. The density of states does not change behaviour for the transition at $t' = 0$. The Fermi velocity, which varies linearly with t' for $t' > 0$ and is thus expected to vanish at $t' = 0$, remains non-zero and finite at that value. This should reflect in many of the thermodynamic properties of the system, and thus it can be used as a probe for this Lifshitz transition.

The energy dispersion relation of the system for $t' \in [0, 1/\sqrt{3})$ close to each of the DP is linear and is given by

$$\epsilon = \sqrt{a(t')q_1^2 + b(t')q_2^2} \tag{4.34}$$

where q_1 and q_2 are small deviations away from the DP and $a(t')$ and $b(t')$ are constants dependent on t'. The density of states $\rho(\omega)$ thus varies linearly with the energy ω for all t' except for the values at which the DPs merge and emerge. At $t' = 1/\sqrt{3}$, its behaviour changes sharply, with the dominant contribution varying as the square root of the energy. This is because, the dispersion relation takes the form

$$\epsilon = \sqrt{a(t')q_1^2 + b(t')q_2^4} \tag{4.35}$$

at (π, π), $(0, \pi)$ and $(\pi, 0)$ merging points for $t' = 1/\sqrt{3}$. On the other hand around the $(0, 0)$ emerging point for $t' = \sqrt{3}$, the dispersion relation takes the form

$$\epsilon = \sqrt{a(t')q_1^4 + b(t')q_2^4}. \tag{4.36}$$

thereby giving a constant and a linear contribution to the density of states. Very close to $\omega = 0$, however the constant term dominates. This sharp change in the density of states at $t' = 1/\sqrt{3}$ and $t' = \sqrt{3}$ as can be seen from Fig:(4.4) which probes the Lifshitz transitions.

Information about the DPs as well as the PB curvature of the system, as shown earlier, can be obtained from the phase of $\det \Sigma(k_1, k_2)$. In FIG.(4.5), we plot this for various values of t'. For $t' = 0.5$, there are eight distinct points around which the phase changes discontinuously by a value of $\pm 2\pi$ corresponding to the DPs. On the other hand, there are only two such points at $t' = 1$.

At the DPs, as shown earlier the PB curvature $\mathscr{B}$ is singular. Applying a small staggered mass term to induce a gap at the DPs we compute the PB curvature of the second band at two t' values, shown in FIG.(4.6). The PB curvature of the second band shows a peak at the DPs. Using the PB curvature $\mathcal{B}$ obtain the Chern numbers, $\nu_n = -1$ for $n = 1, 4$ and $\nu_n = 1$ for $n = 2, 3$. At half-filling, the total Chern number given by $\nu = \nu_1 + \nu_2$ vanishes, implying that the Hall conductance also vanishes [31, 45]. Remarkably, even though the Chern number for the lowest and the highest bands are both equal to -1, the $\mathcal{B}^n(k)$ for these bands is not negative for all values of k. This surprising result is true for the other bands as well with the signs flipped appropriately. FIG.(4.7) shows the PB phase as a function of filling for the lowest band, clearly depicting this behaviour. Thus the non-interacting KHUB with PBC shows intriguing topological character.

4.2.2 Topology of KHUB with OBC

The properties of the KHUB that were discussed till now are for PBC. We study the edge states in this model in a cylindrical geometry with zig-zag edges along $\hat{e}_1$ direction. There are zero energy edge states between the second and the third band and chiral edge states between the bottom two and the upper two bands. The number and the location of the zero-energy edge states in the quasi-momentum direction k change as a function of t' which can be determined using the Zak phase [51, 52, 53] around a closed contour. There have been proposals to probe these phases in optical lattices [60].

At the Graphene limit, $t' = 0$, there are $2\pi/3$ continuous zero-energy edge states for each of the two spin species for $k \in (2\pi/3, 4\pi/3)$, making a total of $4\pi/3$ states. Here the Zak phase is $+1$ for $k \in (2\pi/3, 4\pi/3)$, and 0 elsewhere. For values of $0 < t' < 1/\sqrt{3}$ between these two limits the edge states are not continuous, Fig:(4.8). The doubly-degenerate edge states in $k \in (2\pi/3, q) \cup (2\pi - q, 4\pi/3)$ shift to $k \in (2\pi - 2k, 2\pi/3) \cup (4\pi/3, 2k)$, respectively, forming unique states and thus preserving the total number. On the other hand, for $1/\sqrt{3} < t' < \sqrt{3}$, there are unique continuous edge states for $k \in (-2\pi/3, 2\pi/3)$. Beyond $t' = \sqrt{3}$ again patches of zero-energy edge states occur.

The edge states carry current due to the breaking of time-reversal symmetry in the model. Using the Heisenberg equation of motion for the density operator and the density-current continuity equation, we can compute a general expression for the charge current between two sites on each of the X, Y and Z links. From the current along the Z link

$$J^Z(i_1, i_2; i_1, i_2) = i \sum_{\mu\sigma} a^\dagger_{i_1,i_2,\sigma} P^z_{\sigma,\mu} b_{i_1,i_2,\mu} - h.c., \tag{4.37}$$

the average charge current for cylindrical geometry can be computed

$$J^Z(i_1; i_1) = \sum_{i_2} J^Z(i_1, i_2; i_1, i_2) \tag{4.38}$$

$$= i \sum_{k_2} \sum_{\mu\sigma} a^\dagger_{i_1,k_2,\sigma} P^z_{\sigma,\mu} b_{i_1,k_2,\mu} - h.c. \tag{4.39}$$

Similarly the average current on the Z link can also be calculated. Using these expressions, we find that the total average charge current explicitly involves the time-reversal breaking spin-dependent strength t'. Thus the existence of non-zero currents at the two edges of the system in FIG.(4.9) can be attributed to a non-zero t'. At $t' = 0$ there is no current at the edges, as expected. As $t' > 0$ a non-zero edge current appears and is initially negative at the left edge and positive at the right edge. However, by $t' = 1$ the signs of the currents on the two edges have flipped. The sign of the edge current also depends on which states are filled for $t' > 0.717$. Since the chiral edge states have an opposite and larger contribution than those in the bulk, the edge current flips sign at quarter filling when the former begins to fill, as shown in FIG.(4.10).

These rich topological properties of the model motivates the study of realizing the model and the properties in optical lattice experiments.

4.3 Experimental Realization

We now discuss methods of probing the DPs using Bloch-Zener oscillations. Recently an experimental method to probe the DPs using Bloch-Zener oscillations [61, 62] was suggested by Tarruell *et al.* [63], whereas a detailed method of numerically simulating such oscillations was discussed by Uehlinger *et al.* [64]. Here we probe the DPs in our model using Bloch-Zener oscillations.

At time $T = 0$, the tight binding Kitaev-Hubbard Hamiltonian with a staggered potential and in the presence of a harmonic trap is given by

$$\begin{aligned}\mathcal{H}_0 = &-\sum_{<ij>} C^{\dagger}_{i\mu}\frac{(tI + t'\sigma^{\alpha})_{\mu\nu}}{2}C_{j\nu} + \frac{W}{2}\sum_{i\in A} n_i \\ &-\frac{W}{2}\sum_{i\in B} n_i + \sum_i(\gamma_x x_i^2 + \gamma_y y_i^2)n_i \end{aligned} \tag{4.40}$$

Here W is the strength of the staggered onsite potential, γ_x and γ_y are the strengths of the harmonic trap in the $\hat{e}_1$ and $\hat{e}_2$ directions, while x_i and y_i represent the spatial coordinates of the i^{th} lattice site which are measured in terms of the lattice parameter a.

We calculate the n-particle many body ground state $|\psi(0)\rangle$ for this Hamiltonian and evolve it using the total Hamiltonian $\mathcal{H} = \mathcal{H}_0 + \mathcal{H}_{int}$. Here the interaction term is that of an external force field of magnitude F (Electric field) along $\hat{f}$ on the lattice, and is given by

$$\mathcal{H}_{int} = F \sum_i \hat{f} \cdot \hat{r}_i \tag{4.41}$$

where $\hat{r} = (x, y)$ is the position vector of the lattice site. The Schrödinger evolution is

$$|\psi(\tau)\rangle = e^{-i\mathcal{H}\tau}|\psi(0)\rangle \tag{4.42}$$

where τ is measured in terms of the Bloch oscillation time period $T_B = 2\pi/F$. We choose 2×120^2 lattice sites in order to prevent the cloud from ever hitting the boundary. At every time step we measure the projection of the Fourier-transformed many-body density matrix on to the density matrix of the single-particle bands in the presence of the staggered potential,

$$P_n(k_1, k_2, \tau) = |\langle\chi_n|k_1, k_2\rangle\langle k_1, k_2|\psi(\tau)\rangle|^2. \tag{4.43}$$

Here $|\chi_n\rangle$ is the single-particle eigen-state of the n-th band of the non-interacting Hamiltonian with staggered mass. It is possible to project the density matrix because we have assumed that the trap potential varies slowly so that the single-particle bands do not change in the presence of the trap.

We also compute probability amplitude per particle

$$P_n(\tau) = \frac{1}{N} \int \frac{d^2k}{4\pi^2} P_n(k_1, k_2, \tau) \tag{4.44}$$

where N is the number of particles in the system. The quasi-momentum distribution of the particles clearly shows a sudden reduction in the density when a DP is encountered which gives us a method of probing them in experiments.

We study the quasi-momentum distribution for $t' = t$ and $t' = 0.5t$. In FIG.(4.11) the quasi-momentum probability amplitude (in the orthogonal coordinates (k_x, k_y)) of 187 particles in the second band for various instances during one Bloch oscillation is plotted. The parameters are $t/h = 589$Hz, $t' = t$, $F/h = 80$Hz, $\gamma_{x,y}/h = [0.01, 0.01]$Hz, $W/h = 2$Hz and $\hat{f} = \hat{e}_1 + \hat{e}_2$. The probability amplitude $P_n(k_x, k_y, \tau = 0)$ initially localized around the origin, moves along the k_x direction and encounters a DP at location $(-4\pi/3, 0)$ at time $\tau = 0.27T_B$. On further evolution the DPs at $(4\pi/3, 0)$ is probed finally returning to the center of the Brillouin zone after one oscillation. There is a transfer of particles to the higher bands close to the DPs as seen in FIG.(4.13) where we have plotted $P_l(\tau) = P_1(\tau) + P_2(\tau)$ and $P_u(\tau) = P_3(\tau) + P_4(\tau)$. The two peaks in the figure corresponds to the DPs seen from the quasi-momentum distribution. The inset shows the probabilities for individual bands, with transitions occurring between each of the successive bands.

In contrast with the above situation, we show in FIG.(4.12) the Bloch-Zener oscillation of 256 particles at $t' = 0.5t$ keeping the rest of the parameters unchanged. At this t' and in this direction the system has four DPs, all of which are probed at different times by the cloud. There is a transfer of amplitude when the state passes through each of the four DPs [54].

In FIG.(4.13) we plot $P_l(\tau)$ and $P_u(\tau)$ for $t' = 0.5t$. The lower band only shows two peaks even though this system has four DPs. This is because we have been unable to resolve the transfer at each of the four DPs to high accuracy which is obtained only when there is a reasonable fraction of the cloud in the second band at time $\tau = 0$. This requires a large number of particles in the cloud, increasing its width in momentum space. This decreases the resolution of the DPs, and can only be circumvented by increasing the size of the system, which is limited by currently available computational power to us.

No DPs are encountered when we apply the force field in the $\hat{e}_1 = \frac{1}{2}\hat{x} - \frac{\sqrt{3}}{2}\hat{y}$ direction or the $\hat{e}_2 = \frac{1}{2}\hat{x} + \frac{\sqrt{3}}{2}\hat{y}$ direction. The quasi-momentum distribution for the second band corresponds to the second Brillouin zone in the momentum distribution obtained in optical lattice experiments. Thus from the above discussion, we see that the DPs can be probed in such experiments.

4.4 Conclusions

To summarize, we have analyzed the non-interacting limit of the Kitaev-Hubbard model on the honeycomb lattice with spin-dependent hopping that breaks time-reversal symmetry but preserves the particle-hole (chiral/sub-lattice) symmetry. The model has DPs and is a semi-metal at half filling. We have shown that the particle-hole symmetry implies that the total PB curvature vanishes everywhere on the Brillioun zone at half filling. Consequently, the generalized Zak phases are topological invariants that are wholly determined by the positions and chiralities of the DPs. We show that all this information about the topology is contained in the determinant of a matrix $\Sigma(k)$ defined in Eq.(4.5). We also numerically show that the structure of the non-dispersive edge states are determined by these topological invariants.

Multiple DPs exist in this model and as the strength of the spin-dependent hopping parameter, t', is varied, topological Lifshitz transitions occur where the DPs are created and merge. At $t' = 0$, the model is same as Graphene and there are 4 DPs. As soon as t' changes from zero, there is a transition from 4 to 8 DPs. As

t' increases the DPs migrate over the Brillioun zone and pairwise merge at (0π), $(\pi, 0)$ and (π, π), resulting in a transition 2 DPs at $t' = 1/\sqrt{3}$. At $t' > \sqrt{3}$, there is again a transition to 8 DPs which now emerge from $(0, 0)$. The signal of these transitions can be seen in the density of states and in the edge state structure. The effect of broken time reversal symmetry of this model can be seen from the existence of the charge currents at the edges of the system. We observe that the edge currents change sign near the transitions.

Finally, we have examined experimental signals of the topological features of the model realized in cold atom systems. We have shown that Bloch-Zener oscillations in our system probes the location of the DPs and can hence be used to observe the creation, migration and the merging process.

This concludes my work on the non-interacting KHUB. Next we study the KHUB with interactions. Later in the thesis, we will show using the Variational Cluster Approximation (VCA) [65] and Cluster Perturbation Theory (CPT) [66] methods, both of which I will describe in detail in later chapters, we have delineated a region on the $U - t'$ plane where the staggered magnetization vanishes and the spectral gap is nonzero. As this region includes the $t = t'$ line above a certain critical U, we surmise that it constitutes an algebraic spin liquid phase. Such phases will perform a central role in this thesis, and I shall describe these too in a later chapter.

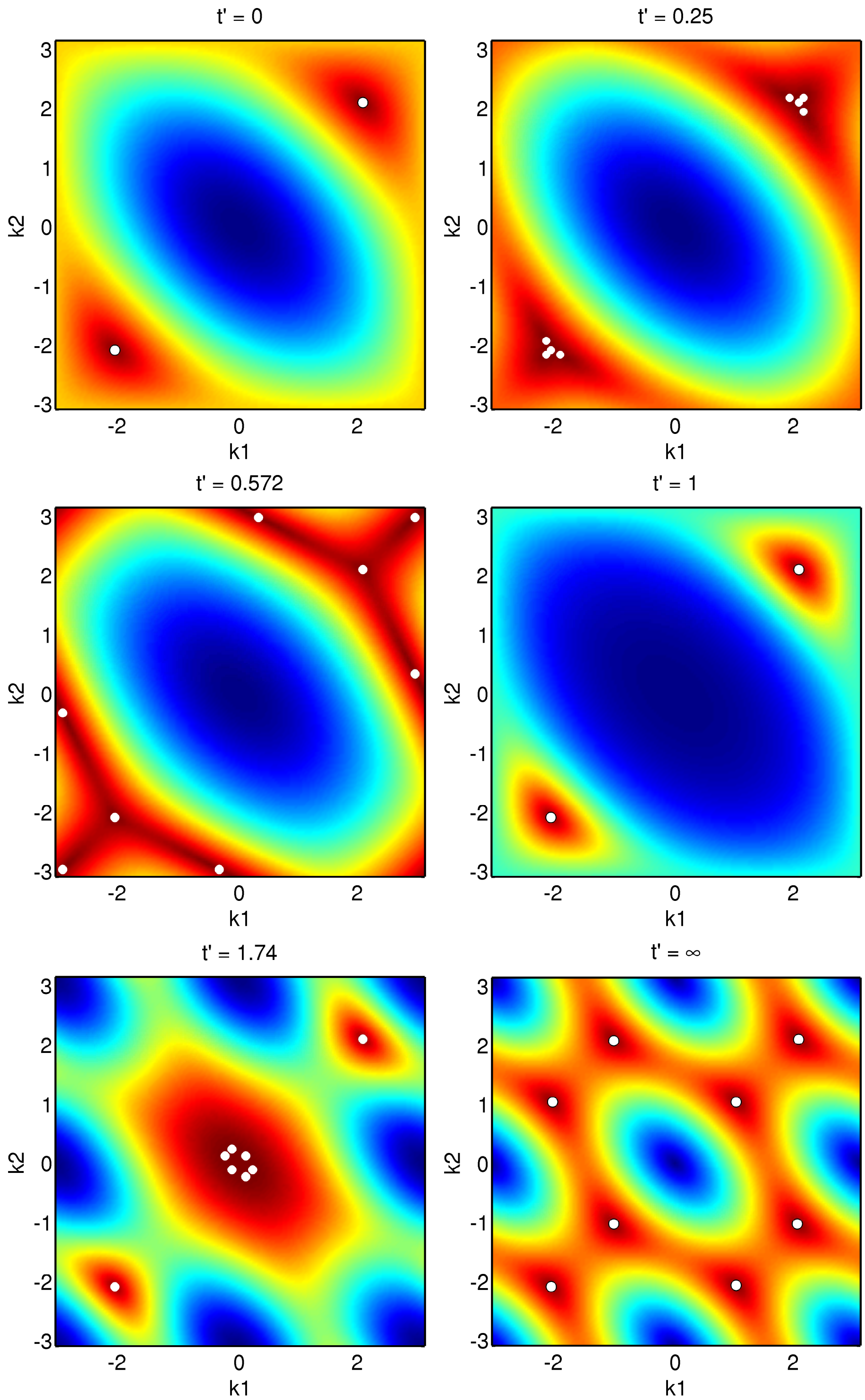

Figure 4.3: Pseudo color plots of the energy of the second band showing the DPs in the Brillouin zone for various t'.

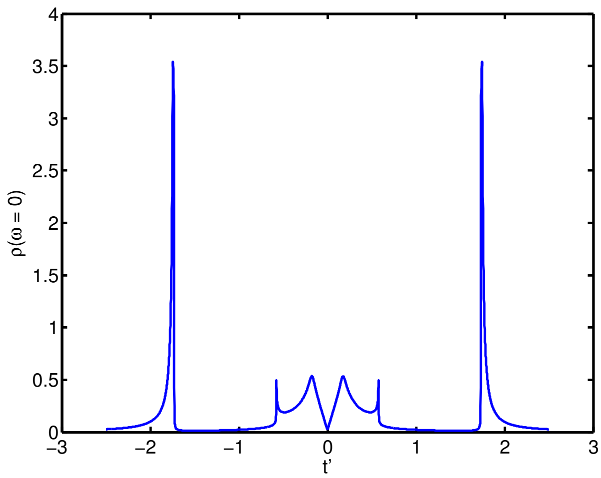

Figure 4.4: Density of states around $\omega = 0$ as a function of t'.

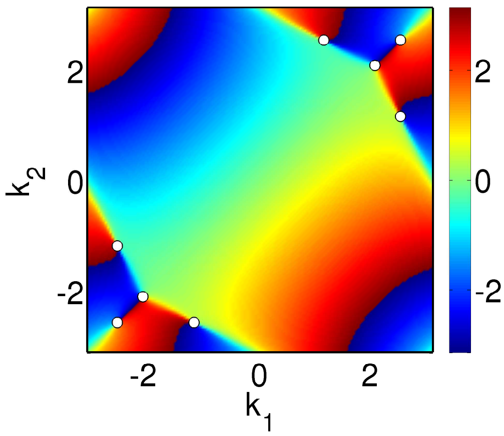

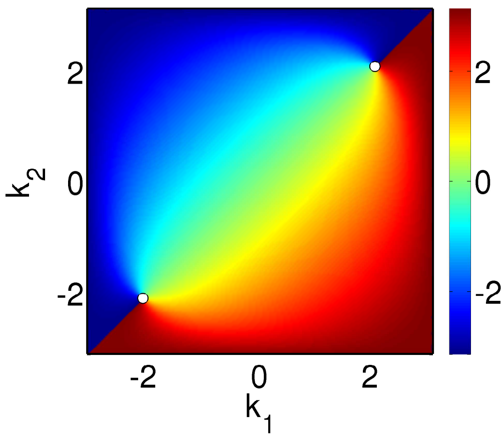

Figure 4.5: The phase of the determinant as a function of (k_1, k_2) for $t' = 0.5$ and $t' = 1$. The phase changes discontinuously at the white dots which represents the location of the DPs.

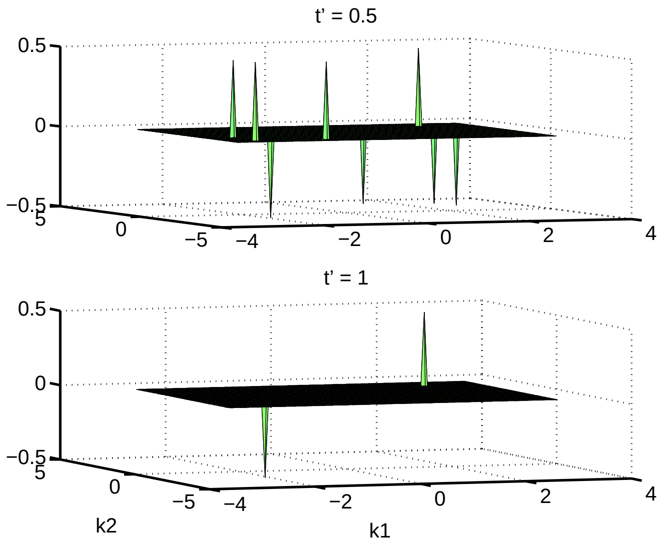

Figure 4.6: PB Curvature as a function of k_1 and k_2 for two different t' values for the second band. The peaks correspond to the location of the DPs. As we change the t' the number of DPs in the system changes.

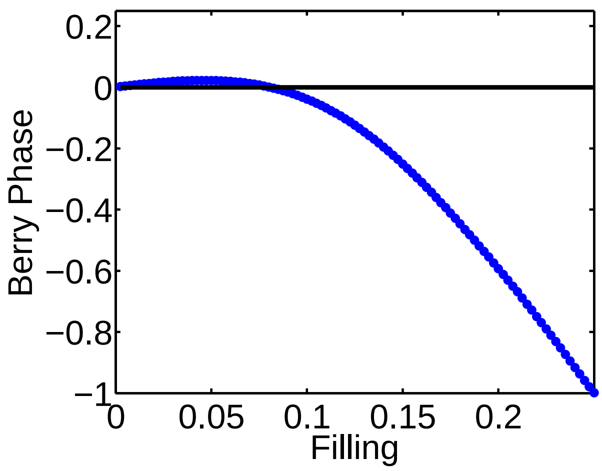

Figure 4.7: PB phase as a function of filling for $t' = 1$. The PB phase is not negative for all values of the filling. For some values it is positive reflecting that the PB curvature of the band takes both positive and negative values.

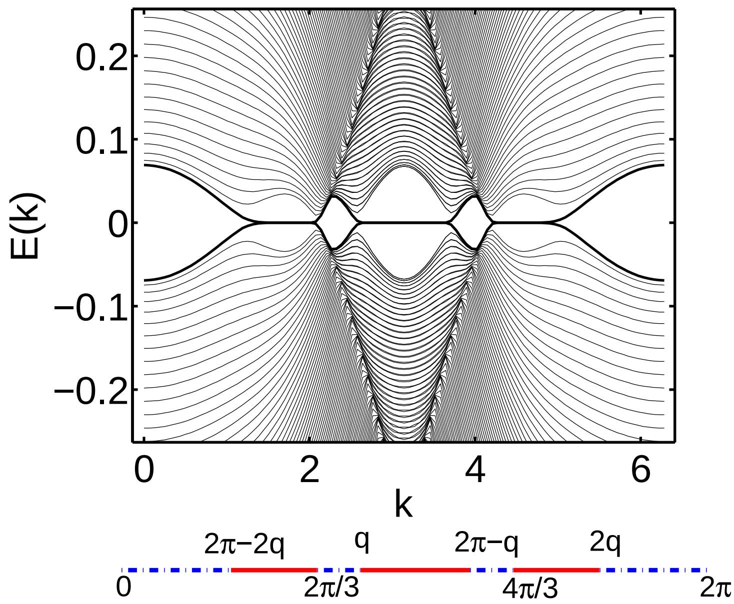

Figure 4.8: The figure on the top panel is the zoomed spectrum for the energy of the KHUB with OBC showing the zero energy edge states. On the red solid lines of the figure in the bottom panel, the Zak phase is +1 whose correspondence to the existence of the edge states in the figure on the top panel can be seen.

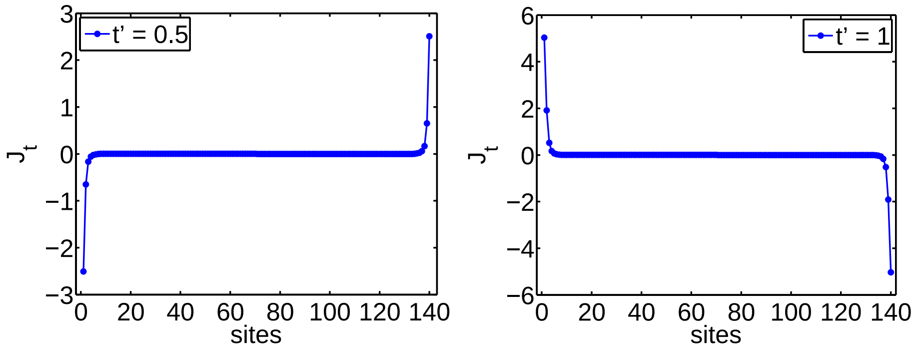

Figure 4.9: The total average charge current at $t' = 0.5t$ and $t' = t$. The current at the edges changes sign as a function of t'.

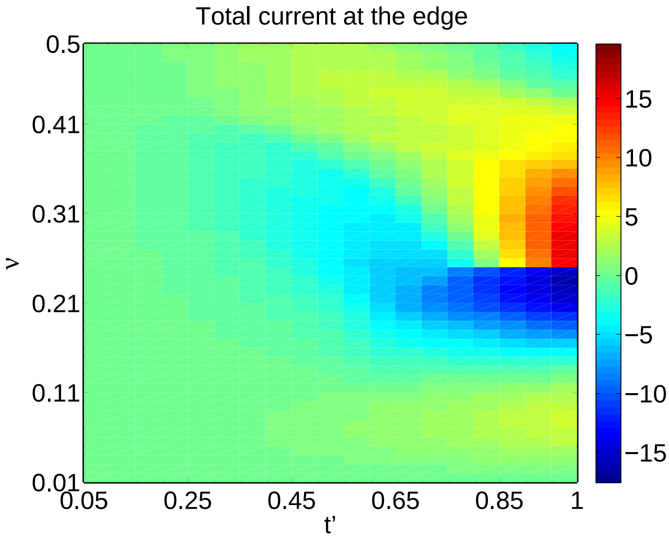

Figure 4.10: The total average charge current for an open tube of circumference $L = 140$ with zig-zag edges for various t'. Note that the sign of the edge current changes as a function for filling beyond the merging of the DPs at $t' = 1/\sqrt{3}$.

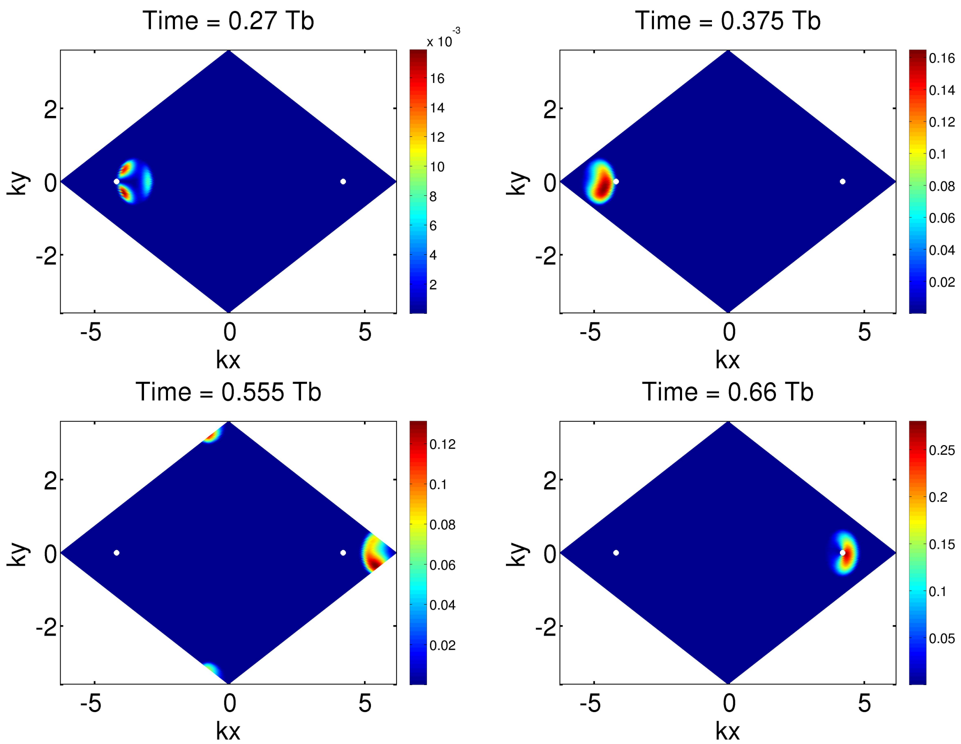

Figure 4.11: The quasi momentum distribution of the second band for Bloch-Zener oscillations as a function of (k_x, k_y) at $t' = t$ resulting from a force acting along the $\hat{e}_1 + \hat{e}_2 = \hat{x}$ direction. Total number of particles considered is 187.

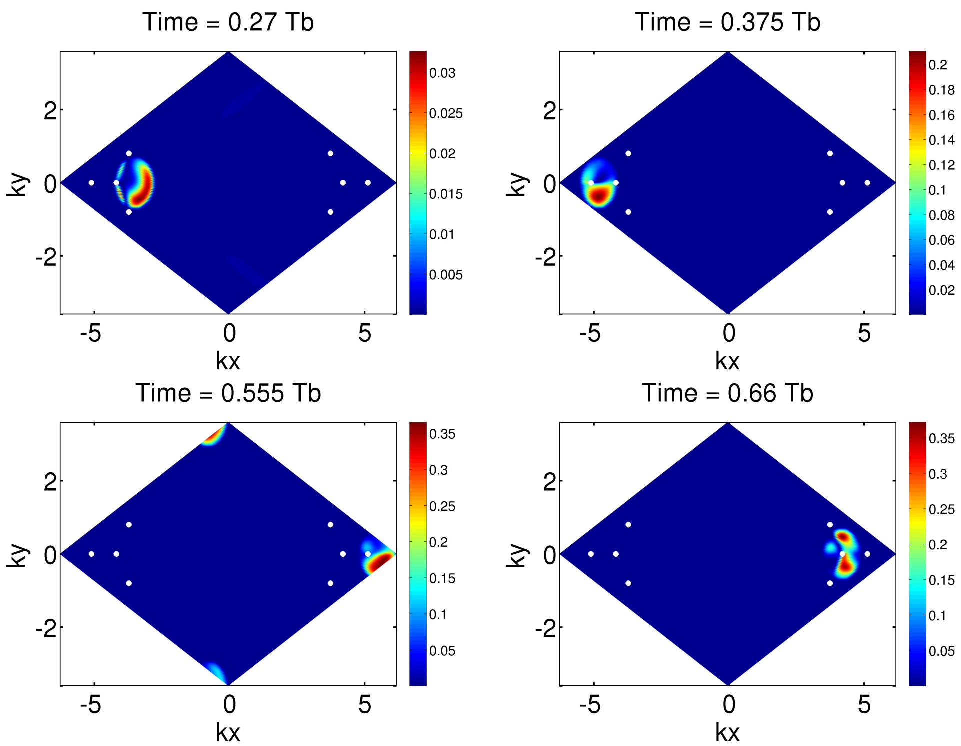

Figure 4.12: The quasi-momentum distribution of the second band for Bloch-Zener oscillations as a function of (k_x, k_y) at $t' = 0.5t$ resulting from a force acting along the $\hat{e}_1 + \hat{e}_2 = \hat{x}$ direction. Total number of particles considered is 256.

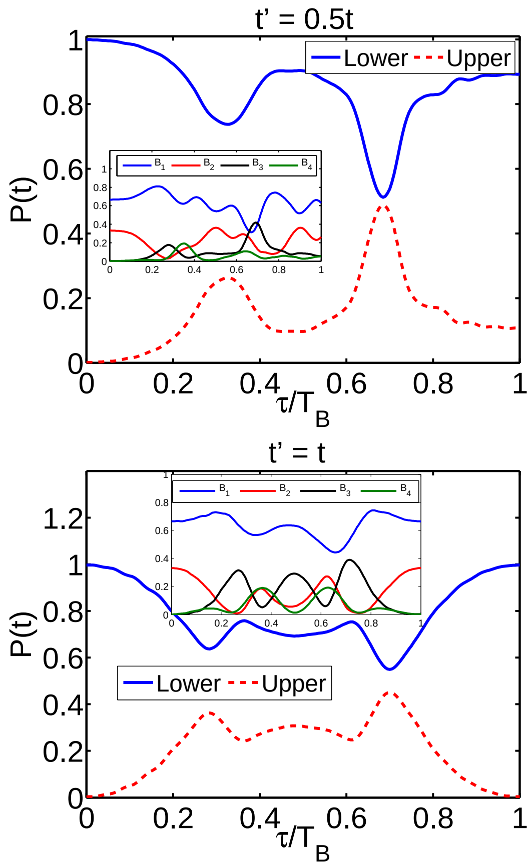

Figure 4.13: $P_l(\tau)$ is plotted in blue and $P_u(\tau)$ is plotted in red for the parameters in FIG.(4.12). In the inset we have the individual amplitudes for all the bands.

Chapter 5

Numerical Technique - CPT and VCA

Every Interaction is an opportunity to learn

Unknown

We have described the Kitaev-Hubbard model in the previous chapter. In this chapter, we shall try and go deeper into the model. Our investigations will be aided by two efficient numerical techniques which will enable us to plot out the phase diagram of the model in good detail.

5.1 Cluster Perturbation theory and the Variational Cluster Approximation

Cluster Perturbation Theory (CPT) is an approximation scheme–within Hubbard-like models–for the one-electron Green's function $\mathbf{G}(\omega)$ [66, 67, 68]. In the scheme, the infinite lattice γ is converted into a finite super-lattice Γ with several identical clusters, each comprising L sites. Fig:(3.1) illustrates the cluster used in this work. The lattice is now effectively a collection of clusters, and hopping terms are now labelled as being intra-cluster and inter-cluster. The lattice Hamiltonian H can then be broken up into two parts : H_c, which contains the hopping terms within clusters, and H_T, which contains the hopping terms between clusters. Thus $H = H_c + H_T$. Let $\mathbf{T}$ be the matrix of inter-cluster hopping terms and $\mathbf{G}^c(\omega)$ the exact Green's function of the cluster. Because of the periodicity of the super-lattice, $\mathbf{T}$ can be expressed as a function of the reduced wave-vector $\tilde{\mathbf{k}}$ and as a matrix in site indices within the cluster: $T_{ab}(\tilde{\mathbf{k}})$. Likewise, $\mathbf{G}^c$ is a matrix in cluster site indices only, since all clusters are identical: $G^c_{ab}(\omega)$. Thus, in what follows, hopping matrices and Green's functions will be $\tilde{\mathbf{k}}$-dependent matrices of order L, which, as mentioned previously, is the number of sites within each cluster. The fundamental result of CPT for the system's one-electron Green's function is

$$\mathbf{G}^{-1}(\tilde{\mathbf{k}}, \omega) = \mathbf{G}^{c-1}(\omega) - \mathbf{T}(\tilde{\mathbf{k}}). \tag{5.1}$$

However, in order for this to be numerically computable, the cluster must be small enough. Also, in practice, $\mathbf{G}^c(\omega)$ is calculated numerically using the Lanczos method.

Breaking up the infinite lattice, that is, tiling it has consequences, the most serious and immediate being the loss of translational invariance. CPT has a ready prescription for restoring this, and, according to that, the modified periodization can be written as

$$G(\mathbf{k},\omega) = \frac{1}{L}\sum_{a,b} \mathrm{e}^{-i(\mathbf{k})\cdot(\mathbf{r}_a-\mathbf{r}_b)} G_{ab}(\mathbf{k},\omega) \tag{5.2}$$

where $\mathbf{k}$ now belongs to the Brillouin zone of the original lattice and the sum is carried over cluster sites. Remarkably, this formula is exact in both the strong ($t \to 0$) and the weak ($U \to 0$) coupling limits. This is one of the strengths of this method.

The computation of the approximate interacting Green's function directly leads to the spectral function $A(\mathbf{k},\omega) = -2\,\mathrm{Im}\,G(\mathbf{k},\omega)$ which then allows the density of states $N(\omega)$ to be calculated via numerical integration of $A(\mathbf{k},\omega)$ over wave-vectors. This also makes it possible to assess the possibility of and investigate the existence of a spectral gap. Numerically, the evaluation of $N(\omega)$ is carried out keeping the frequency complex with a small imaginary part η which serves to broaden the spectral peaks. By plugging in a few values of η and then extrapolating to $\eta \to 0$, it is possible to detect if a spectral gap exists at the Fermi level. This is a powerful tool since it allows us to distinguish between a metal and a Mott insulator.

On the other hand, this entire extrapolation scheme can be avoided if the value of wave-vector at which the gap first opens up is known beforehand. This happens at $t' = 0$, at the Dirac points. We can then estimate the gap much more reliably by simply looking up the Lehmann representation[69] of the CPT Green's function, which can be calculated when the cluster Green's function is computed using the band Lanczos method.

The Variational Cluster Approximation (VCA) is an extension of CPT in which parameters of the cluster Hamiltonian H_c may be treated variationally, according to Potthoff's Self-Energy Functional Theory (SFT) [65, 70]. In particular, it allows the emergence of spontaneously broken symmetries and provides an approximate value for the system's grand potential Ω. For the case at hand, a single variational parameter is used. This is the strength M_c of a staggered magnetization field that is added to the cluster Hamiltonian :

$$H_M = M \sum_{\alpha} m_\alpha c_\alpha^\dagger c_\alpha \tag{5.3}$$

where the symbol m_α is $+1$ for spin-up orbitals on the A sub-lattice and spin-down orbitals on the B sub-lattice, and -1 otherwise.

Technically, VCA proceeds by minimizing the following quantity:

$$\Omega(M_c) = \Omega_c(M_c) - \int \frac{\mathrm{d}\omega}{\pi} \frac{\mathrm{d}^2 k}{(2\pi)^2} \sum_{\tilde{\mathbf{k}}} \ln\det\left[\mathbf{1} - \mathbf{T}(\tilde{\mathbf{k}})\mathbf{G}(\tilde{\mathbf{k}}, i\omega)\right] \tag{5.4}$$

where $\Omega_c(M_c)$ is the grand potential of the individual cluster and is obtained in the exact diagonalization process. The integral over frequencies is carried over the positive imaginary axis. At the optimal value M_c^*, $\Omega(M_c^*)$ is the best estimate of the system's grand potential. At this value of M_c, the order parameter M is calculated:

$$M = \int \frac{\mathrm{d}^2 \tilde{k}}{(2\pi)^2} \int \frac{\mathrm{d}\omega}{2\pi} m_\alpha G_{\alpha\alpha}(\tilde{\mathbf{k}}, i\omega) \tag{5.5}$$

where $G_{\alpha\alpha}$ are the diagonal elements of the CPT Green's function (5.1).

Much like mean-field theory, VCA provides estimates of order parameters. Nevertheless, it boasts of several advantages over mean-field theory. For instance, in VCA, the Hamiltonian remains fully interacting with no need for factorization of the interaction. Additionally, spatial correlations are treated exactly within the

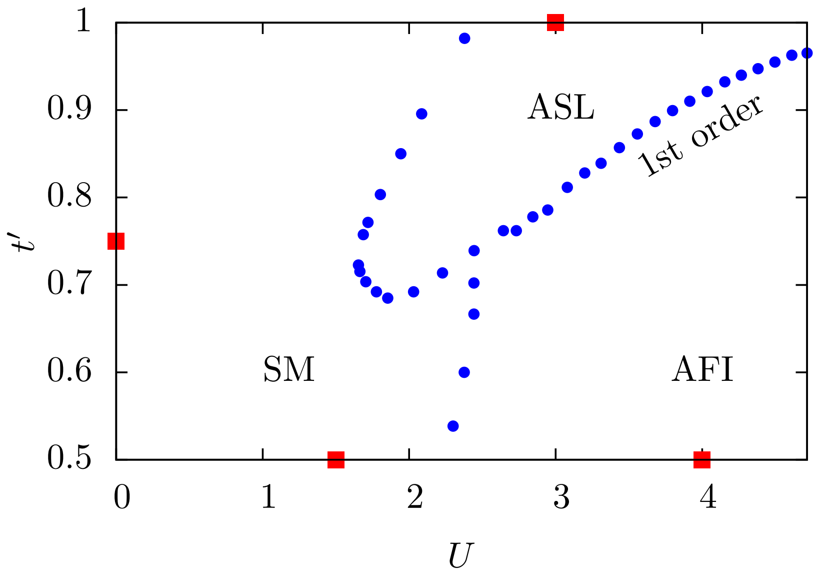

Figure 5.1: The phase diagram of the Kitaev-Hubbard model at half-filling, showing the phases. The transition from the AFI to the ASL phase is discontinuous. The red squares correspond to the parameter values at which the spectral graphs have been plotted in Fig. 5.3.

cluster in VCA.

We have used both VCA and CPT in the work presented in this thesis. The former has been used to delineate the phase boundary of the anti-ferromagnetic phase, where the latter was used to monitor the closure of the gap, which ultimately led to the transition between the spin-liquid and semi-metal phases.

5.2 Results using CPT and VCA

CPT and VCA allow us to map the spectral gap of the model on to the $t' - U$ plane, and to calculate the extent of the Néel phase. VCA also allows us to find out whether or not the transitions out of the Néel phase are continuous. However, the same cannot be done for the Mott transitions to the spin-liquid phases for

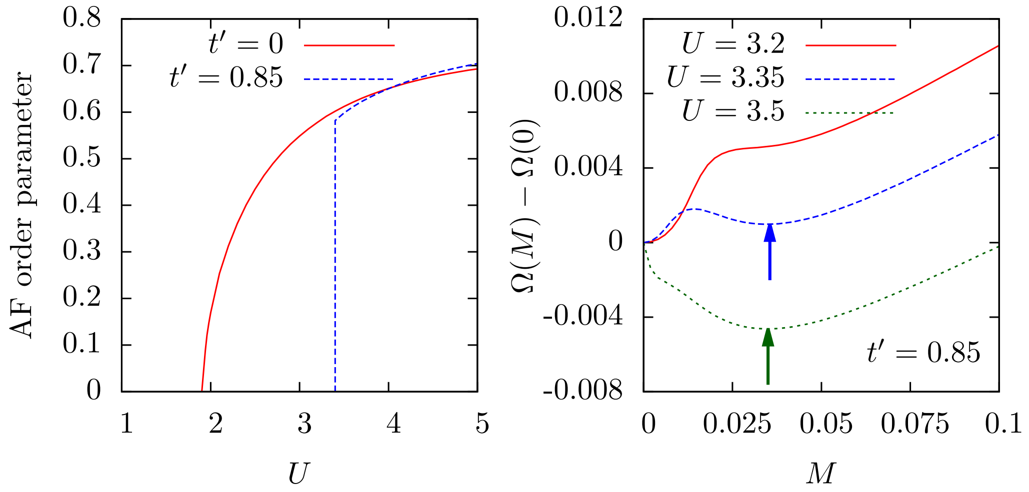

Figure 5.2: Left panel: AF order parameter computed in VCA for $t' = 0.85$ and $t' = 0$ as a function of U. The transition is discontinuous in the first case, and continuous at $t' = 0$. Right panel: profile of the Potthoff functional as a function of Weiss field M for three values of U across the transition at $t' = 0.85$, demonstrating the first-order character of the magnetic transition there. Arrows indicate the positions of the minima, associated with magnetic solutions, metastable in one case ($U = 3.35$) and stable in another ($U = 3.5$).

which a cluster dynamical mean field technique would be required[42].

The phase diagram of the Kitaev-Hubbard model from $t' = 1$ to $t' = 0.5$ is summarized in Fig. 5.1, where we have set $t = 1$. At low U there is a TR-breaking semi-metallic phase (SM), characterized by gap-less charged, spin-1/2 fermionic quasi-particles. This nonmagnetic phase exists in the region $1 > t' > 0.5$ and $U \lesssim 2.4$. When $U \approx 2.4$ and $t' = 1$, a spectral gap opens up, signature of a Mott transition from the SM to the Algebraic Spin Liquid (ASL) phase, which extends to $U \to \infty$. In the ASL phase there is no magnetic order. Between $U \gtrsim 1.5$ and $U \lesssim 2.4$ and with steadily decreasing t', the system starts off in the SM phase, then makes a transition into the ASL phase and finally re-enters the SM phase until $t' = 0.5$. For $U > 2.4$, decreasing t' destabilizes the ASL phase and brings about a transition to the antiferromagnetic (Néel) phase (AFI-antiferromagnetic insulator) which also has a spectral gap.

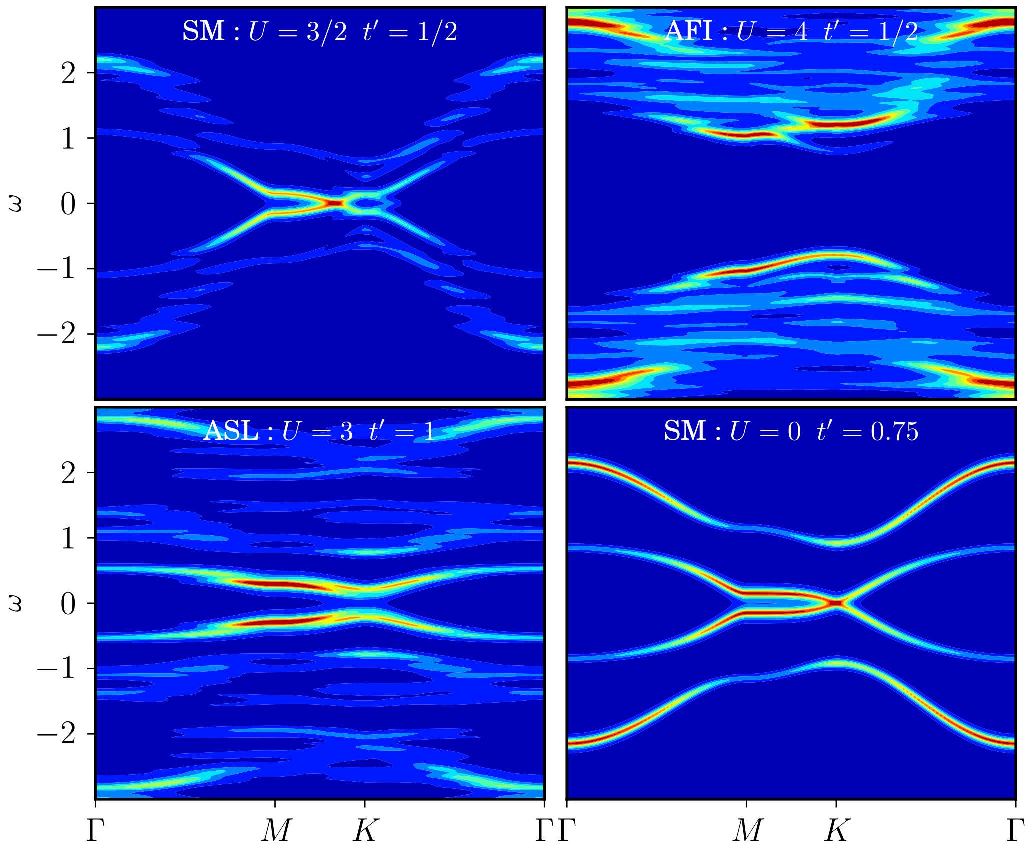

Figure 5.3: Spectral functions of the Kitaev-Hubbard model, computed using CPT, as a function of energy (ω, y-axis) and momentum (k, x-axis) for the four sets of parameter values marked by the squares in Fig. 5.1, red indicating maximum value and blue indicating minimum values. The spectrum is gapless only for the SM. Γ, M and K represent the high symmetry points of the Brillouin zone.

The ASL phase is bounded by the AFI and SM phases and is hence not connected to the possible short-ranged spin liquid at $t' = 0$[40, 41, 42]. The SM and AFI phases do not have quasi-particles with fractional quantum numbers or statistics. Thus the ASL is topologically distinct from the SM and the AFI and we expect the transitions between them to be discontinuous, as illustrated for instance in Fig. 5.2.

Spectral functions illustrating each of the three phases and computed with CPT are shown in Fig. 5.3. It is intriguing that the single particle bands of opposite Chern numbers remain gapped in the same range of t' as the existence of the ASL. This seems to indicate that geometric phase effects may play an important role in this model.

CPT and VCA were only able to detect the fact that there is a Spin-Liquid phase in the KHUB model. To show that it is truly Algebraic in nature, let us now proceed to the large-U, analytic treatment of the model on the $t' = 1$ line in the next chapter.

Chapter 6

Establishing a Stable Algebraic Spin Liquid

The secret of change is to focus all your energy not on fighting the old, but on building the new.

Socrates

In this chapter, our primary goal is to systematically establish the spin liquid phase found in the previous chapter using CPT and VCA to be an algebraic spin liquid. To do that we begin by finding an effective Hamiltonian of a Hubbard model that represents the system at half-filling and in the large onsite interaction, U, limit. At half-filling, the number of sites in the lattice is the same as the number of fermions in the system. In this limit, the hopping strengths, t and t', behave as perturbation terms, the charge degrees of freedom are gapped out and the spin degrees of freedom dominate the physics. The effective Hamiltonian can thus be represented by a spin Hamiltonian. We shall now explain the general procedure to obtain an effective Hamiltonian using the Perturbative Continuous Unitary Transformation (PCUT). Then we move on to talk about the stability of the spin liquid using time reversal symmetry and finally compute the spin-spin correlation which decays as power law. This will help us successfully achieve our goal. We end with the mean field of the spin model to eliminate the possibility of spontaneous time-reversal symmetry breaking.

6.1 Perturbative Continuous Unitary Transformation(PCUT)

We shall begin by breaking the Hubbard model into two parts. The first shall comprise the unperturbed Hamiltonian, the term that survives in the large U limit.

$$\mathcal{H}_0 = U \sum_i n_{i\uparrow} n_{i\downarrow}. \tag{6.1}$$

The solutions to this are known exactly; the eigenfunctions are the fock states for fermionic systems. At half-filling, the ground state will have a homogeneous fermion distribution, with each site getting one fermion to reckon with, and double occupancy will necessarily not occur. If N is the number of lattice sites, then there will be 2^N such states, which differ in the spin configurations, having zero energy. The second part is the perturbation or the kinetic energy part $\mathcal{H}_k$, and this represents the hopping Hamiltonian, where a single fermion hops to neighbouring site on the lattice. This can be further subdivided into three parts T_1, T^0 and $T_1^\dagger = T_{-1}$. The first of these increase the number of doubly occupied sites by 1, the second one keeps the number of doubly occupied sites fixed while the third term decreases the number of doubly occupied sites by 1. We have

$$T_1 = \sum_{\langle ij\rangle_\alpha} n_{i\bar{\sigma}} c^{\dagger}_{i\sigma} P^{\alpha}_{\sigma\sigma'} c_{j\sigma'} h_{j\bar{\sigma}'} \tag{6.2}$$

$$T^0 = \sum_{\langle ij\rangle_\alpha} h_{i\bar{\sigma}} c^{\dagger}_{i\sigma} P^{\alpha}_{\sigma\sigma'} c_{j\sigma'} h_{j\bar{\sigma}'} + \sum_{\langle ij\rangle_\alpha} n_{i\bar{\sigma}} c^{\dagger}_{i\sigma} P^{\alpha}_{\sigma\sigma'} c_{j\sigma'} n_{j\bar{\sigma}'} \tag{6.3}$$

where n_i represents the total number operator at site i and $n_i + h_i = 1$. The T operators follow the following commutation relations with the unperturbed Hamiltonian

$$[\mathcal{H}_0, T^0] = 0 \tag{6.4}$$

$$[\mathcal{H}_0, T_1] = UT \tag{6.5}$$

$$[\mathcal{H}_0, T_1^{\dagger}] = -UT^{\dagger}. \tag{6.6}$$

Thus only the T_0 operator commutes with $\mathcal{H}_0$. The Hamiltonian can now be written as

$$\mathcal{H} = \mathcal{H}_0 + T_0 + T_1 + T_1^{\dagger}. \tag{6.7}$$

Following Chernyshev *et al.*[71], we block-diagonalize the Hamiltonian order-by-order in t/U. Physically this implies that we allow for virtual hoppings of that order. The $(k+1)^{th}$ order Hamiltonian is written as

$$\mathcal{H}^{(k+1)} = e^{S^{(k)}} e^{S^{(k-1)}} e^{S^{(k-2)}} \cdots H \cdots e^{-S^{(k-2)}} e^{-S^{(k-1)}} e^{-S^{(k)}}. \tag{6.8}$$

We shall use Baker-Campbell-Hausdorff formula and retain terms upto a fixed order in t/U. $S^{(k)}$ is chosen so as to eliminate the off-block diagonal (OBD) terms of order $\left(\frac{t}{U}\right)^k$ that survive in the Hamiltonian after performing the canonical transformation at order $k-1$. By construction, $S^{(k)}$ does not contain terms that preserve the number of doubly occupied sites. $S^{(k)}$ has to satisfy the equation

$$[S^{(k)}, \mathcal{H}_0] = -\mathcal{H}^k_{\mathrm{OBD}} \tag{6.9}$$

where $\mathcal{H}^{(k)}_{\mathrm{OBD}}$ is the OBD part of $\mathcal{H}^{(k)}$. The effective spin Hamiltonian at half-filling, $H^{(k)}$, is obtained by projecting $\mathcal{H}^{(k)}$ onto the singly occupied subspace.

Let us compute the S operator for a simplest Hubbard model. The off-diagonal block part of the Hamiltonian, $\mathcal{H} = T_{-1} + T_0 + T_1 + \mathcal{H}_0$ is $T_{-1} + T_1$ since we have seen earlier that T_0 commutes with $\mathcal{H}_0$. We can thus easily compute

$$S^{(1)} = \frac{1}{U}(T_1 - T_{-1}). \tag{6.10}$$

The effective Hamiltonians display the following property : the sum of the indices of the T operators, that is the individual terms, must vanish whereas the S operator will contain all terms that are non-zero. At the n^{th} order the effective Hamiltonian will contain n products of T operators. It is thus possible to estimate which terms for the effective Hamiltonian do not vanish, and this leaves only the coefficients to be determined.

6.1.1 Analytic calculations of PCUT

Since the half-filling ground state is unreachable in a single virtual hop starting from itself, the first-order effective Hamiltonian vanishes in the half-filling subspace. However, since a fermion can move to a neighbouring site and hop back to its own site in a pair of virtual hops, thereby creating an intermediate doubly occupied state. Thus, in perturbation theory, the next leading order in the second order effective Hamiltonian can be written as:

$$H^{(2)} = -\frac{1}{U}T^{\dagger}T. \tag{6.11}$$

It is clear from the fact that we are working on the honeycomb lattice, it would require an even number of hops to take the system from a ground state to another in the degenerate ground state space, since an odd number of hops would necessarily result in at least one doubly occupied site. This eliminates the odd effective Hamiltonians from the half-filling sector. The analytic expression for the fourth-order effective Hamiltonian is thus

$$H^{(4)} = \frac{1}{U^3}(T^{\dagger}TT^{\dagger}T - T^{\dagger}T_0T_0T - \frac{1}{2}T^{\dagger}T^{\dagger}TT). \tag{6.12}$$

Analytical study of the model beyond this is a difficult task to pursue. This is where numerics enters the scene. It is simple to show that

$$S^{(k)} = \sum_{i\neq j}\frac{1}{U(i-j)}P_i\mathcal{H}^{(k)}P_j \tag{6.13}$$

where P_m represent the projector on the Hilbert subspace containing m doubly occupied sites. Thus we have $P_m^2 = P_m$ and $\sum_{m=0}^{\infty}P_m = 1$. It is possible to confirm whether the effective Hamiltonians calculated above can be obtained from the Eq:(6.13). The action of the T matrices for many body states on two sites connected by a z link is

$$T^z|\uparrow,\downarrow\rangle = \frac{1}{2}(t+t_z)|0,\uparrow\downarrow\rangle + \frac{1}{2}(t-t_z)|\uparrow\downarrow,0\rangle \tag{6.14}$$

$$T^z|\downarrow,\uparrow\rangle = -\frac{1}{2}(t-t_z)|0,\uparrow\downarrow\rangle - \frac{1}{2}(t+t_z)|\uparrow\downarrow,0\rangle \tag{6.15}$$

$$T^{z\dagger}|0,\uparrow\downarrow\rangle = \frac{1}{2}(t+t_z)|\uparrow,\downarrow\rangle - \frac{1}{2}(t-t_z)|\downarrow,\uparrow\rangle \tag{6.16}$$

$$T^{z\dagger}|\uparrow\downarrow,0\rangle = \frac{1}{2}(t-t_z)|\uparrow,\downarrow\rangle - \frac{1}{2}(t+t_z)|\downarrow,\uparrow\rangle \tag{6.17}$$

with the action of the T_0 operators

$$T_0^z|0,\uparrow\rangle = \frac{1}{2}(t+t_z)|\uparrow,0\rangle \tag{6.18}$$

$$T_0^z|\uparrow,0\rangle = \frac{1}{2}(t+t_z)|0,\uparrow\rangle \tag{6.19}$$

$$T_0^z|0,\downarrow\rangle = \frac{1}{2}(t-t_z)|\downarrow,0\rangle \tag{6.20}$$

$$T_0^z|\downarrow,0\rangle = \frac{1}{2}(t+t_z)|0,\downarrow\rangle \tag{6.21}$$

$$T_0^z|\uparrow\downarrow,\uparrow\rangle = -\frac{1}{2}(t-t_z)|\uparrow,\uparrow\downarrow\rangle \tag{6.22}$$

$$T_0^z|\uparrow\downarrow,\downarrow\rangle = -\frac{1}{2}(t+t_z)|\downarrow,\uparrow\downarrow\rangle \tag{6.23}$$

$$T_0^z|\uparrow,\uparrow\downarrow\rangle = -\frac{1}{2}(t-t_z)|\uparrow\downarrow,\uparrow\rangle \tag{6.24}$$

$$T_0^z|\downarrow,\uparrow\downarrow\rangle = -\frac{1}{2}(t+t_z)|\uparrow\downarrow,\downarrow\rangle. \tag{6.25}$$

The corresponding operators for the T operators connecting two sites on the x link is given as

$$T^x|\uparrow,\downarrow\rangle = \frac{1}{2}t\{|0,\uparrow\downarrow\rangle + |\uparrow\downarrow,0\rangle\} \tag{6.26}$$
$$T^x|\downarrow,\uparrow\rangle = -\frac{1}{2}t\{|0,\uparrow\downarrow\rangle + |\uparrow\downarrow,0\rangle\} \tag{6.27}$$
$$T^x|\uparrow,\uparrow\rangle = \frac{1}{2}t_x\{|0,\uparrow\downarrow\rangle - |\uparrow\downarrow,0\rangle\} \tag{6.28}$$
$$T^x|\downarrow,\downarrow\rangle = -\frac{1}{2}t_x\{|0,\uparrow\downarrow\rangle - |\uparrow\downarrow,0\rangle\} \tag{6.29}$$

$$T^{x\dagger}|\uparrow\downarrow,0\rangle = \frac{1}{2}t\{|\uparrow,\downarrow\rangle - |\downarrow,\uparrow\rangle\} + \frac{1}{2}t_x\{|\uparrow,\uparrow\rangle - |\downarrow,\downarrow\rangle\} \tag{6.30}$$
$$T^{x\dagger}|0,\uparrow\downarrow\rangle = \frac{1}{2}t\{|\uparrow,\downarrow\rangle - |\downarrow,\uparrow\rangle\} - \frac{1}{2}t_x\{|\uparrow,\uparrow\rangle - |\downarrow,\downarrow\rangle\} \tag{6.31}$$

$$T_0^x|\uparrow,0\rangle = \frac{1}{2}t|0,\uparrow\rangle + \frac{1}{2}t_x|0,\downarrow\rangle \tag{6.32}$$
$$T_0^x|0,\uparrow\rangle = \frac{1}{2}t|\uparrow,0\rangle + \frac{1}{2}t_x|\downarrow,0\rangle \tag{6.33}$$
$$T_0^x|\downarrow,0\rangle = \frac{1}{2}t|0,\downarrow\rangle + \frac{1}{2}t_x|0,\uparrow\rangle \tag{6.34}$$
$$T_0^x|0,\downarrow\rangle = \frac{1}{2}t|\downarrow,0\rangle + \frac{1}{2}t_x|\uparrow,0\rangle \tag{6.35}$$
$$T_0^x|\uparrow,\uparrow\downarrow\rangle = -\frac{1}{2}t|\uparrow\downarrow,\uparrow\rangle + \frac{1}{2}t_x|\uparrow\downarrow,\downarrow\rangle \tag{6.36}$$
$$T_0^x|\downarrow,\uparrow\downarrow\rangle = \frac{1}{2}t_x|\uparrow\downarrow,\uparrow\rangle - \frac{1}{2}t|\uparrow\downarrow,\downarrow\rangle \tag{6.37}$$
$$T_0^x|\uparrow\downarrow,\uparrow\rangle = -\frac{1}{2}t|\uparrow,\uparrow\downarrow\rangle + \frac{1}{2}t_x|\downarrow,\uparrow\downarrow\rangle \tag{6.38}$$
$$T_0^x|\uparrow\downarrow,\downarrow\rangle = -\frac{1}{2}t|\downarrow,\uparrow\downarrow\rangle + \frac{1}{2}t_x|\uparrow,\uparrow\downarrow\rangle \tag{6.39}$$

One can similarly compute the operations for two sites on the y link.

6.1.2 Results from PCUT

Using the expression that we obtained above, we shall now compute the effective spin Hamiltonian for the Kitaev-Hubbard model. Thus we can write the operator form of the Hamiltonian for two sites on the z link as

$$H_z^{(2)} = -T_z^\dagger T_z = -\frac{1}{2}(t^2 + t_z^2)| \uparrow, \downarrow\rangle\langle\uparrow, \downarrow | - \frac{1}{2}(t^2 + t_z^2)| \downarrow, \uparrow\rangle\langle\downarrow, \uparrow | \tag{6.40}$$

$$+ \frac{1}{2}(t^2 - t_z^2)| \uparrow, \downarrow\rangle\langle\downarrow, \uparrow | + \frac{1}{2}(t^2 - t_z^2)| \downarrow, \uparrow\rangle\langle\uparrow, \downarrow |. \tag{6.41}$$

Now we convert the above Hamiltonian into spin Hamiltonian using the following transformations

$$| \uparrow\rangle\langle\uparrow | = \frac{\sigma^0 + \sigma^z}{2} \tag{6.42}$$

$$| \downarrow\rangle\langle\downarrow | = \frac{\sigma^0 - \sigma^z}{2} \tag{6.43}$$

$$| \uparrow\rangle\langle\downarrow | = \frac{\sigma^x + i\sigma^y}{2} \tag{6.44}$$

$$| \downarrow\rangle\langle\uparrow | = \frac{\sigma^x - i\sigma^y}{2}. \tag{6.45}$$

Now substituting we get

$$H_z^{(2)} = -\frac{1}{2}(t^2 + t_z^2)\frac{\sigma_1^0 + \sigma_1^z}{2}\frac{\sigma_2^0 - \sigma_2^z}{2} - \frac{1}{2}(t^2 + t_z^2)\frac{\sigma_1^0 - \sigma_1^z}{2}\frac{\sigma_2^0 + \sigma_2^z}{2} \tag{6.46}$$

$$+ \frac{1}{2}(t^2 - t_z^2)\frac{\sigma_1^x + i\sigma_1^y}{2}\frac{\sigma_2^x - i\sigma_2^y}{2} + \frac{1}{2}(t^2 - t_z^2)\frac{\sigma_1^x - i\sigma_1^y}{2}\frac{\sigma_2^x + i\sigma_2^y}{2} \tag{6.47}$$

$$= -\frac{1}{4}(t^2 + t_z^2)\sigma_1^0\sigma_2^0 + \frac{1}{4}(t^2 + t_z^2)\sigma_1^z\sigma_2^z \tag{6.48}$$

$$+ \frac{1}{4}(t^2 - t_z^2)\sigma_1^x\sigma_2^x + \frac{1}{4}(t^2 - t_z^2)\sigma_1^y\sigma_2^y \tag{6.49}$$

$$= (t^2 + t_z^2)S_1^z S_2^z + (t^2 - t_z^2)S_1^x S_2^x + (t^2 - t_z^2)S_1^y S_2^y \tag{6.50}$$

$$= (t^2 - t_z^2)\mathbf{S}_1.\mathbf{S}_2 + 2t_z^2 S_1^z S_2^z. \tag{6.51}$$

Computation of the effective Hamiltonian for two sites are sufficient to determine the expression for the second order effective spin Hamiltonian for the full lattice which is given as

$$\mathcal{H}_{eff} = \frac{1}{U}\sum_{\langle ij^{\alpha}\rangle}(t^2 - t_\alpha^2)\mathbf{S}_i \cdot \mathbf{S}_j + 2t_\alpha^2 S_i^\alpha S_j^\alpha. \tag{6.52}$$

Some of the expressions needed are given in Appendix (A.1). The above Hamiltonian is a form of the Kitaev-Heisenberg model. As discussed in the Kitaev model preliminaries, this perturbation does not affect the nature of the spin-spin correlation function. It is imperative that we compute the next leading order correction—the fourth order effective Hamiltonian—in order to understand the system better. The above expression for the full lattice is given by

$$H^{(4)} = \frac{1}{U^3}\sum_{\langle ij\rangle_\alpha;\beta\neq\alpha}\left[(t_\alpha^4 - t^4)\mathbf{S}_i.\mathbf{S}_j - 2t_\alpha^4 S_i^\alpha S_j^\alpha - 2t^2 t_\alpha t_\beta(S_i^\alpha S_j^\beta + S_i^\beta S_j^\alpha)\right] \tag{6.53}$$

$$+ \frac{1}{4U^3}\sum_{\langle\langle ij\rangle\rangle_{\alpha\beta};\gamma\neq\alpha\neq\beta}\Big[(t^2 + t_\alpha^2)(t^2 - t_\beta^2)S_i^\alpha S_j^\alpha + (t^2 - t_\alpha^2)(t^2 + t_\beta^2)S_i^\beta S_j^\beta \tag{6.54}$$

$$+ (t^2 - t_\alpha^2)(t^2 - t_\beta^2)S_i^\gamma S_j^\gamma + 12t^2 t^\alpha t^\beta S_i^\alpha S_j^\beta\Big]. \tag{6.55}$$

We show in the Appendix (A.2) the systematic calculation for a three-site open chain. Remarkably, like the second order effective Hamiltonian, we find that this Hamiltonian also preserves time-reversal symmetry, and thus a gap-less Dirac point still exists upto this order in perturbation theory. The obvious follow-up question concerns the behaviour of the system for the higher-order terms which we solve for numerically. Here's the Algorithm for the code.

1. The first step is to generate the matrices for a fixed number of sites N and a prescription for the connecting links namely x, y or z.

2. Since the T matrices are distinguished based on the number of doubly occupied sites, the many body states are generated in blocks of fixed number of doubly occupied sites at half filling. We start with the least first which is no doubly occupied sites: 2^N such states.

3. Now we generate the T matrices in the above generated many body sector in sparse matrix form. T_0 will be block diagonal and T will connect a block with n doubly occupied sites with $n + 1$ block.

4. The interacting Hamiltonian which is the U term will be diagonal in the above basis. The diagonal term of each block of n doubly occupied sites will be nU.

5. Now we present a code snippet.

```
%----------------------------------
% CODE SNIPPET
%----------------------------------
% dim represents the total number os states at half
% filling
dim = factorial(2*N)/(factorial(N))^2;
% H at the end of the code will represent the M^th order
% effective hamiltonian
H = cell(M+1,1);
H{1} = H0; % zeroth order in tw
H{2} = (T + T0 + T');% first order in tw
for i = 3:M+1
    H{i} = sparse(1,1);
end
```

6. Generate projector matrices $P\{i\}$, $i = 1, 2 \cdots N/2 + 1$, representing the projection onto $i - 1$ number of doubly occupied sites.

```
%=========================================================
% Perturbation theory begins ...
for k = 1:M
H = correctedH(H,M,P,N,dim,k+1);
end
%---------------------------------------------------------
% This function will generate the corrected hamiltonian
% given the exact hamiltonian and the effective hamiltonian
% for Mth order and N lattice sites
%---------------------------------------------------------
function Hpp = correctedH(H,M,P,N,dim,m)
Hpp = H;

S = sparse(dim,dim);
for ii = 1:(floor(N/2)+1)
    for jj = 1:(floor(N/2)+1)
    if ii ~= jj
    S = S +(1/(ii-jj))*P{ii}*Hpp{m}*P{jj}';
    end
    end
end

Hp = cell(M+1,1);
```

```
for i = 1:M+1
Hp{i} = sparse(dim,dim);
end

for k = 1:M+1
    for i = 1:M+1
            if i+m-1<M+2
            Hp{i+m-1} = Hp{i+m-1}+(1/k)*com(S,H{i});
            end
    end
    H = Hp;
    for i = 2:M+1
        Hpp{i} = Hpp{i} + Hp{i};
        Hp{i} = sparse(dim,dim);
    end
    Hp{1} = sparse(dim,dim);
end

end

function C = com(A,B)
C = A*B-B*A;
end
%==========================================================
```

7. Each of the $H\{i\}$ is now projected onto the 2^N states of singly occupied states and converted to spin Hamiltonian.

The major task of the code is to write the matrices in sparse form including the symmetries of the system and projection onto the spin Hamiltonian. In Appendix (A.3) we have computed the sixth order effective Hamiltonian computed on a six site plaquette cluster. We find no odd spin terms. We have gone till 14 sites upto 10th order and find no odd spin terms. If all the symmetries of the Hamiltonian can be used then one can go till 21 sites for triangular lattice for example[72]. Based on this observation we now outline the general proof to show that the system is time reversal symmetric in the entire Mott phase.

6.2 Time reversal symmetry of the KHUB model

The purpose of this section is to outline the derivation of the effective spin-Hamiltonian and prove that it is time-reversal (TR) invariant in the Mott phase. This ensures that the system remains gap-less upto all orders of perturbation theory.

6.2.1 Particle-Hole Symmetry and Time reversal symmetries

The Hamiltonian (3.1) is symmetric under particle-hole (C) transformation:

$$U_C \, c^{\dagger}_{i\sigma} \, U^{\dagger}_C = \eta_i c_{i\sigma} \tag{6.56}$$

where η_i is $+1$ on sub-lattice A and -1 on sub-lattice B. The unitary operator U_C can be explicitly written as

$$U_C = \prod_i e^{i\pi S^y_i} e^{i\pi G^y_i} \tag{6.57}$$

where S_i^a are the spin operators acting on the singly occupied states and G_i^a are the pseudo-spin operators acting on the empty and doubly occupied states. These are defined as

$$G_i^z = \frac{1}{2}\left(n_{\uparrow i} + n_{\downarrow i} - 1\right) \qquad G_i^+ = c_\uparrow^\dagger c_\downarrow^\dagger = (G_i^-)^\dagger . \tag{6.58}$$

Every term in the Hamiltonian, $\mathcal{H}_0$ and T_s, is C-invariant:

$$U_C H U_C^\dagger = H, \qquad U_C T_s U_C^\dagger = T_s . \tag{6.59}$$

It then follows from equations (6.13) and (6.8) that every term of H^k is C-invariant, for all k.

The time reversal operator is

$$U_T\, c_{i\sigma}^\dagger\, U_T^\dagger = i\sigma^y_{\sigma\sigma'} c_{i\sigma'} \qquad\qquad U_T = \prod_j e^{i\pi S^y_j}\mathcal{K} \tag{6.60}$$

where $\mathcal{K}$ is the complex conjugation operator. Any state $|\mathrm{hf}\rangle$ in the singly occupied subspace satisfies the condition $G_i^a|\mathrm{hf}\rangle = 0$. It then follows that

$$U_C U_T|\mathrm{hf}\rangle = \mathcal{K}|\mathrm{hf}\rangle . \tag{6.61}$$

6.2.2 Time reversal symmetry of $H^{(k)}$

We show the TR symmetry of $H^{(k)}$ by explicitly proving the equality of the matrix elements of $H^{(k)}$ and $U_T H^{(k)} U_T^\dagger$ in a real basis. Specifically, we can choose the simultaneous eigenstates of S_i^z,

$$S_i^z|\{\sigma_i\}\rangle = \frac{1}{2}\sigma_i|\{\sigma_i\}\rangle. \tag{6.62}$$

We can always choose S_i^z to be real and hence we have $\mathcal{K}|\{\sigma_i\}\rangle = |\{\sigma_i\}\rangle$. It then follows that,

$$\begin{aligned}\langle\{\sigma_i\}|U_T H^{(k)} U_T^\dagger|\{\sigma_i\}'\rangle &= \langle\{\sigma_i\}|U_T^\dagger U_C^\dagger U_C H^{(k)} U_C^\dagger U_C U_T|\{\sigma_i\}'\rangle \\ &= \langle\{\sigma_i\}|\mathcal{K} H^{(k)} \mathcal{K}|\{\sigma_i\}'\rangle \\ &= \langle\{\sigma_i\}|H^{(k)}|\{\sigma_i\}'\rangle. \end{aligned} \tag{6.63}$$

Thus the effective spin Hamiltonian is TR-symmetric. This implies that it does not contain any odd-spin terms. If this emergent symmetry in the Mott phase is not spontaneously broken then the spinons remain gapless.

6.3 Spin Spin Correlation

According to Saptarshi *et al* [25], the condition for the existence of a spin-spin correlation function which has a power law decay is

$$[\Sigma^\alpha, H_p] \neq 0 \tag{6.64}$$

where H_p contains all terms barring the Kitaev term and $\Sigma^\alpha = \Pi_i^\alpha \sigma_i^\alpha$. We checked this condition for the new terms and find that the above constraint is satisfied giving us an indication that at least one of the spin-spin correlations is algebraic in nature. The exponent of the power law is yet to be determined for which we now outline the computation of the spin-spin correlation function. We write the

Hamiltonian as $H = \mathcal{H}_0 + \mathcal{H}_p$ where $\mathcal{H}_0 = J\sum_{\langle ij\rangle_\alpha} S_i^\alpha S_j^\alpha$ and

$$\mathcal{H}_p = \sum_{\substack{\langle ij\rangle_\alpha \\ \alpha\neq\beta}} \delta_1 S_i^\beta S_j^\beta + \gamma_1\left[S_i^\alpha S_j^\beta + S_j^\alpha S_i^\beta\right] + \sum_{\langle\langle ij\rangle\rangle_{\alpha\beta}}\left[\delta_2 \mathbf{S}_i.\mathbf{S}_j + \delta_3(S_i^\alpha S_j^\alpha + S_i^\beta S_j^\beta) + \gamma_2 S_i^\alpha S_j^\beta\right] \tag{6.65}$$

with the expression for the coefficients as

$$J = \left(\frac{1+t'^2}{U} - \frac{1+t'^4}{U^2}\right) \qquad \gamma_1 = -\frac{2t'^2}{U^3} \qquad \gamma_2 = \frac{3t'^2}{U^3} \tag{6.66}$$
$$\delta_1 = \frac{t'^4-1}{U^3} \qquad \delta_2 = \frac{(1-t'^2)^2}{4U^3} \qquad \delta_3 = \frac{t'^2-t'^4}{2U^3}.$$

The Kitaev Hamiltonian $\mathcal{H}_0$ is now the unperturbed Hamiltonian while $\mathcal{H}_p$ acts as a perturbation. We want to compute the correlation function

$$g(\mathbf{r},t) = \left\langle T\left(S_{\mathbf{r}l}^\alpha(t) S_{\mathbf{0}m}^\beta(0)\right)\right\rangle. \tag{6.67}$$

where $\mathbf{r} = r_1\mathbf{e}_1 + r_2\mathbf{e}_2$, $\mathbf{e}_1$ and $\mathbf{e}_2$ are basis vectors as shown in Fig.((6.1)) and

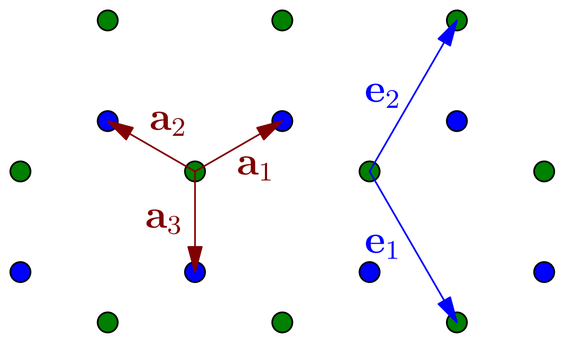

Figure 6.1: Basis vector used. Green (Blue) represents sub-lattice A (B).

l, m are the sub-lattice indices. To leading order, this is the spin-spin correlation function of the Kitaev model. The Kitaev model has a 6-spin conserved operator associated with every plaquette, W_p which can take values ± 1 and can be interpreted as a Z_2 flux [73]. The ground state is in the flux-free sector ($W_p = 1\ \forall p$) as shown in Fig:(6.2). The spin operators at site $\mathbf{r}$ create a pair of flux tubes in two of the plaquettes that the site belongs to. Since the time evolution does not change the flux configuration, the spin-spin correlation (6.67) is zero except when $\mathbf{r}$ and $\mathbf{0}$ are nearest neighbors [25] .

The second-order perturbation term is

$$g^{(2)} = \frac{(-i)^2}{2} \int d\tau_1 \int d\tau_2 \left\langle T \left(S^{\alpha}_{\mathbf{r}l}(t) \mathcal{H}_p(\tau_1) \mathcal{H}_p(\tau_2) S^{\beta}_{0m}(0) \right) \right\rangle . \tag{6.68}$$

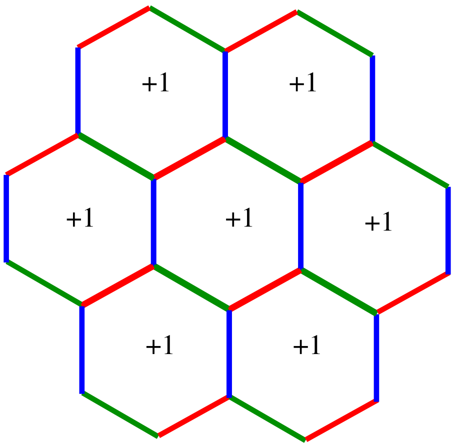

Figure 6.2: The honeycomb lattice with the fluxes in each of the plaquette representing the ground state configuration of the pure Kitaev Model.

The time evolution is governed by $\mathcal{H}_0$. This term will be non-zero only if there are terms in $\mathcal{H}_p$ such that the product of the four operators in (6.68) do not change the flux configuration of the ground state [25]. We find that such terms do exist in $\mathcal{H}_p$. We concentrate on the correlation function $\langle S^z_{r_1,r_2,A} S^z_{0,0,A} \rangle$. The following terms combine with $S^z_{r_1,r_2,A}$ to produce flux-free configurations when acting on the ground state,

$$\gamma_2 S^x_{r_1-1,r_2,B} S^y_{r_1-1,r_2+1,B}; \quad \gamma_2 S^y_{r_1+1,r_2-1,A} S^x_{r_1+1,r_2,A}; \quad \gamma_1 S^x_{r_1,r_2,A} S^y_{r_1-1,r_2+1,B}$$
$$\gamma_1 S^y_{r_1,r_2,A} S^x_{r_1-1,r_2,B}; \quad \gamma_1 S^y_{r_1,r_2,B} S^x_{r_1+1,r_2,A}; \quad \gamma_1 S^x_{r_1,r_2,B} S^y_{r_1+1,r_2-1,A}. \tag{6.69}$$

The action of $S^z_{r_1,r_2,A}$ on the ground state is to change the sign of the fluxes in the plaquettes adjacent to the z bond of site r_1, r_2 as shown in Fig:(6.3) which is made flux-free by the application of any one of the 6 terms of Eq:(6.69). For example the effect of $S^x_{r_1-1,r_2,B} S^y_{r_1-1,r_2+1,B}$ is shown in Fig:(6.4).

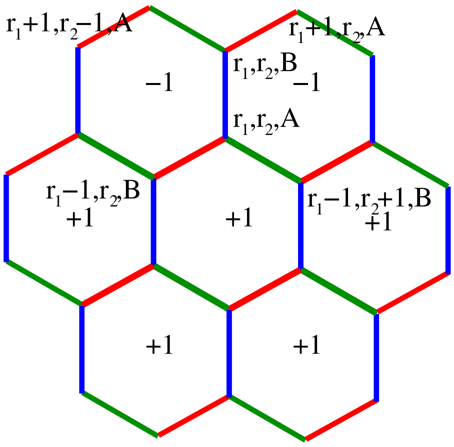

Figure 6.3: The honeycomb lattice with the unconserved fluxes, obtained by the action of $S^z_{r_1,r_2,A}$ on the ground state of the Kitaev model.

Thus the terms in Eq:(6.69) and the terms with $(r_1, r_2) \to (0, 0)$ which combine with $S^z_{0,0,A}$ give 36 possibly non-zero contributions to $g^{(2)}$.

The problem now is to compute the resulting 6-spin correlation functions in the Kitaev model. We do this in the Majorana fermion representation as we have discussed in our introductory chapter. The correlation function in equation (6.68) thus factorizes into propagators of the c_i operators. Since the spin operators create two units of flux on adjoining plaquettes, the Majorana fermion propagators are in the background of an even number of fluxes at a few points.

To compute the asymptotic form or the propagators, we can derive the continuum theory of the low-energy modes in the flux-free background. We can then compute the correlation function in equation (6.68) to obtain the following expression:

$$\begin{aligned}\langle S^z_{\mathbf{r}l}(t) S^z_{0l}(0)\rangle = &(-0.56\cos(2\mathbf{K}\cdot\mathbf{r})\gamma_1^2 + 1.13\gamma_1\gamma_2 + 1.69\gamma_2^2\epsilon)\det G \\ &+ (0.28\gamma_1^2 + 0.07\gamma_2^2 + 0.84\gamma_1\gamma_2\epsilon + 0.63\gamma_2^2\epsilon^2 - 0.28\gamma_1\gamma_2 - 0.42\gamma_2^2\epsilon)(\mathrm{Tr}G)^2 \\ &+ 0.28\gamma_1^2\mathrm{Tr}(\tau_x G\tau_x G) + (0.56\gamma_1^2 - 0.28\gamma_1\gamma_2 + 0.84\gamma_1\gamma_2\epsilon)\mathrm{Tr}(G\tau_x G)\end{aligned} \tag{6.70}$$

where l represents the sub-lattice index (A or B), α represents the three types of bonds x, y, z and ϵ is the energy density of the Kitaev model. We can obtain the $\langle S^x_{\mathbf{r}l}(t)S^x_{0l}(0)\rangle$ and $\langle S^y_{\mathbf{r}l}(t)S^y_{0l}(0)\rangle$ from the above correlation function by using the following property: a $2\pi/3$ rotation about a sub-lattice A point takes x link to y link, y link to z and z link to x, in a cycle. The direction is reversed for sub-lattice B.

Using equation (6.70) and (2.13), we find that the long-wavelength correlation function falls off as $1/r^4$. This exponent is the same as the one computed single-spin perturbations studied in Ref. [3] and can be motivated by simple dimensional counting. This proves the existence of the ASL in the Kitaev-Hubbard model. Although the pre-factor is extremely small for large U ($\sim 1/U^6$), this is the leading behavior at long distances. Therefore the effect of the perturbation cannot be neglected for any value of U, however large. Indeed, we can expect the strength

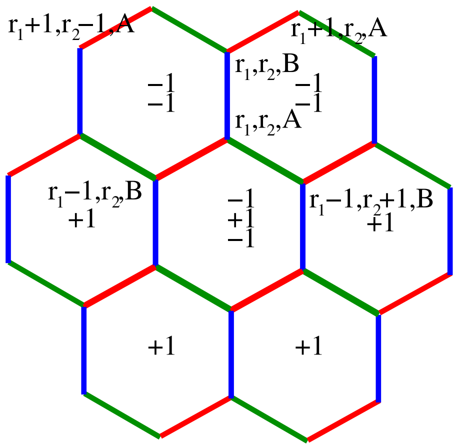

Figure 6.4: The honeycomb lattice with the conserved fluxes, obtained by the action of $S^z_{r_1,r_2,A}$ and $S^x_{r_1-1,r_2,B}S^y_{r_1-1,r_2+1,B}$ on the ground state of the Kitaev model.

of these correlations to grow as U decreases. Thus, at large U, the leading order contribution to the spin susceptibility is independent of U as in the Kitaev model, whereas the next order contribution goes as $(t/U)^6$. The U dependence of the spin susceptibility will hence be of the form $\chi = a + b(t/U)^6$, where a and b are constants independent of U. Experimental methods for measuring the spin susceptibility in cold atom systems have recently been developed [74]. The value of $(t/U)^6$, for the lowest values of (t/U) that the ASL exists ranges from 0.08 – 0.005, depending on t'. Thus susceptibility measurements as a function of U, with an accuracy of about 1%, can provide evidence for the existence of the ASL in this model.

6.4 Mean Field Theory of the effective spin model

As we have seen before, the Algebraic Spin Liquid (ASL) phase that we detected in the Kitaev-Hubbard model is susceptible to the opening up of a spontaneous spinon gap. Using a Majorana mean field theory we eliminate the possibility of a violation of spontaneous time-reversal symmetry.

Consider the fourth order effective spin Hamiltonian given in equation (6.65). This is of the form,

$$H_{\text{eff}} = \sum_{\langle ij \rangle_a} \Gamma^a_{bc} \sigma^b_i \sigma^c_j + \sum_{\langle\langle ij \rangle\rangle_{ab}} \Delta^{ab}_{cd} \sigma^c_i \sigma^d_j \tag{6.71}$$

where,

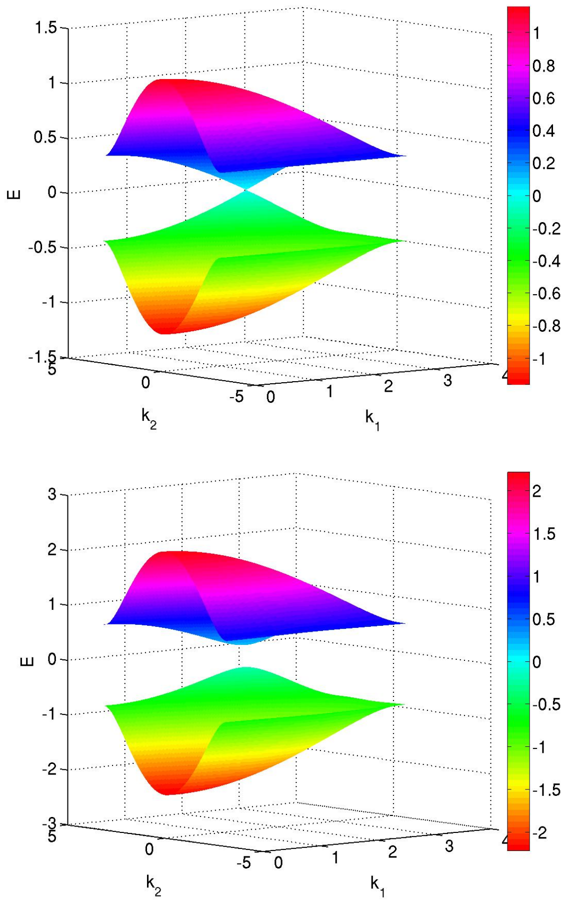

Figure 6.5: Spinon dispersion relation at $U = 2$ and $U = 1.4$ respectively.

$$\Gamma^x = \begin{pmatrix} \frac{t^2+t'^2}{U} - \frac{t^4+t'^4}{U^3} & -\frac{2t^2t'^2}{U^3} & -\frac{2t^2t'^2}{U^3} \\ -\frac{2t^2t'^2}{U^3} & \frac{t^2-t'^2}{U} - \frac{t^4-t'^4}{U^3} & 0 \\ -\frac{2t^2t'^2}{U^3} & 0 & \frac{t^2-t'^2}{U} - \frac{t^4-t'^4}{U^3} \end{pmatrix} \tag{6.72}$$

$$\Gamma^y = \begin{pmatrix} \frac{t^2-t'^2}{U} - \frac{t^4-t'^4}{U^3} & -\frac{2t^2t'^2}{U^3} & 0 \\ -\frac{2t^2t'^2}{U^3} & \frac{t^2+t'^2}{U} - \frac{t^4+t'^4}{U^3} & -\frac{2t^2t'^2}{U^3} \\ 0 & -\frac{2t^2t'^2}{U^3} & \frac{t^2-t'^2}{U} - \frac{t^4-t'^4}{U^3} \end{pmatrix} \tag{6.73}$$

$$\Gamma^z = \begin{pmatrix} \frac{t^2-t'^2}{U} - \frac{t^4-t'^4}{U^3} & 0 & -\frac{2t^2t'^2}{U^3} \\ 0 & \frac{t^2-t'^2}{U} - \frac{t^4-t'^4}{U^3} & -\frac{2t^2t'^2}{U^3} \\ -\frac{2t^2t'^2}{U^3} & -\frac{2t^2t'^2}{U^3} & \frac{t^2+t'^2}{U} - \frac{t^4+t'^4}{U^3} \end{pmatrix} \tag{6.74}$$

$$\Delta^{xy} = \begin{pmatrix} \frac{t^4-t'^4}{4U^3} & \frac{3t^2t'^2}{U^3} & 0 \\ 0 & \frac{t^4-t'^4}{4U^3} & 0 \\ 0 & 0 & \frac{(t^2-t'^2)^2}{4U^3} \end{pmatrix} \tag{6.75}$$

$$\Delta^{yz} = \begin{pmatrix} \frac{(t^2-t'^2)^2}{4U^3} & 0 & 0 \\ 0 & \frac{t^4-t'^4}{4U^3} & \frac{3t^2t'^2}{U^3} \\ 0 & 0 & \frac{t^4-t'^4}{4U^3} \end{pmatrix} \tag{6.76}$$

$$\Delta^{zx} = \begin{pmatrix} \frac{t^4-t'^4}{4U^3} & 0 & 0 \\ 0 & \frac{(t^2-t'^2)^2}{4U^3} & 0 \\ \frac{3t^2t'^2}{U^3} & 0 & \frac{t^4-t'^4}{4U^3} \end{pmatrix} \tag{6.77}$$

and $\Delta^{xy} = (\Delta^{yx})^T$, $\Delta^{yz} = (\Delta^{zy})^T$ and $\Delta^{zx} = (\Delta^{xz})^T$. The Hamiltonian is then,

$$
\begin{aligned}
H_{\text{eff}} \;=\; & \sum_{i_1,i_2}\Big(\Gamma^x_{ab}\sigma^a_{i_1,i_2,1}\sigma^b_{i_1-1,i_2,2} + \Gamma^y_{ab}\sigma^a_{i_1,i_2,1}\sigma^b_{i_1,i_2+1,2} + \Gamma^z_{ab}\sigma^a_{i_1,i_2,1}\sigma^b_{i_1,i_2,2} \\
& +\Delta^{xy}_{ab}\sigma^a_{i_1,i_2,1}\sigma^b_{i_1-1,i_2-1,1} + \Delta^{yx}_{ab}\sigma^a_{i_1,i_2,1}\sigma^b_{i_1+1,i_2+1,1} \\
& +\Delta^{xy}_{ab}\sigma^a_{i_1,i_2,2}\sigma^b_{i_1+1,i_2+1,2} + \Delta^{yx}_{ab}\sigma^a_{i_1,i_2,2}\sigma^b_{i_1-1,i_2-1,2} \\
& +\Delta^{yz}_{ab}\sigma^a_{i_1,i_2,1}\sigma^b_{i_1,i_2+1,1} + \Delta^{zy}_{ab}\sigma^a_{i_1,i_2,1}\sigma^b_{i_1,i_2-1,1} \\
& +\Delta^{yz}_{ab}\sigma^a_{i_1,i_2,2}\sigma^b_{i_1,i_2-1,2} + \Delta^{zy}_{ab}\sigma^a_{i_1,i_2,2}\sigma^b_{i_1,i_2+1,2} \\
& +\Delta^{zx}_{ab}\sigma^a_{i_1,i_2,1}\sigma^b_{i_1+1,i_2,1} + \Delta^{xz}_{ab}\sigma^a_{i_1,i_2,1}\sigma^b_{i_1-1,i_2,1} \\
& +\Delta^{zx}_{ab}\sigma^a_{i_1,i_2,2}\sigma^b_{i_1-1,i_2,2} + \Delta^{xz}_{ab}\sigma^a_{i_1,i_2,2}\sigma^b_{i_1+1,i_2,2}\Big). \qquad (6.78)
\end{aligned}
$$

To investigate the instability of the ASL, we perform a mean-field treatment of the Hamiltonian in the Majorana fermionic representation (2.4). The decoupling of the spinon and gauge field sectors is represented by

$$
\sigma^\alpha_i\sigma^\beta_j = -ic_ic_j\; ib^\alpha_i b^\beta_j \approx -ic_ic_jB^{\alpha\beta}_{ij} - iC_{ij}b^\alpha_i b^\beta_j + C_{ij}B^{\alpha\beta}_{ij} \qquad (6.79)
$$

where we allow for only short range Majorana correlations. Substituting in equation (6.71), we get the mean field Hamiltonian,

$$
\begin{aligned}
H_{MF} \;=\; & -\sum_{\langle ij\rangle_a}\Big(\Gamma^a_{bc}B^{bc}_{ij}\; ic_ic_j + \Gamma^a_{bc}C_{ij}\; ib^b_i b^c_j\Big) \\
& -\sum_{\langle\langle ij\rangle\rangle_{ab}}\Big(\Delta^{ab}_{cd}B^{cd}_{ij}\; ic_ic_j + \Delta^{ab}_{cd}C_{ij}\; ib^c_i b^d_j\Big). \qquad (6.80)
\end{aligned}
$$

We assume that the ground state is translationally invariant, isotropic and denote,

$$C_{i_1,i_2,1\ i_1-1,i_2,2} = C_{i_1,i_2,1\ i_1,i_2+1,2} = C_{i_1,i_2,1\ i_1,i_2,2} = \epsilon \tag{6.81}$$

$$B^{xx}_{i_1,i_2,1\ i_1-1,i_2,2} = B^{yy}_{i_1,i_2,1\ i_1,i_2+1,2} = B^{zz}_{i_1,i_2,1\ i_1,i_2,2} = \eta \tag{6.82}$$

$$B^{xy}_{i_1,i_2,1\ i_1-1,i_2,2} = B_{xxy}; \qquad B^{yx}_{i_1,i_2,1\ i_1-1,i_2,2} = B_{xyx} \tag{6.83}$$

$$B^{xz}_{i_1,i_2,1\ i_1-1,i_2,2} = B_{xxz}; \qquad B^{zx}_{i_1,i_2,1\ i_1-1,i_2,2} = B_{xzx} \tag{6.84}$$

$$B^{yx}_{i_1,i_2,1\ i_1,i_2+1,2} = B_{yyx}; \qquad B^{xy}_{i_1,i_2,1\ i_1,i_2+1,2} = B_{yxy} \tag{6.85}$$

$$B^{yz}_{i_1,i_2,1\ i_1,i_2+1,2} = B_{yyz}; \qquad B^{zy}_{i_1,i_2,1\ i_1,i_2+1,2} = B_{yzy} \tag{6.86}$$

$$B^{xz}_{i_1,i_2,1\ i_1,i_2,2} = B_{zxz}; \qquad B^{zx}_{i_1,i_2,1\ i_1,i_2,2} = B_{zzx} \tag{6.87}$$

$$B^{yz}_{i_1,i_2,1\ i_1,i_2,2} = B_{zyz}; \qquad B^{zy}_{i_1,i_2,1\ i_1,i_2,2} = B_{zzy} \tag{6.88}$$

$$C_{i_1,i_2,1\ i_1-1,i_2-1,1} = C_{i_1,i_2,1\ i_1+1,i_2,1} = C_{i_1,i_2,1\ i_1,i_2+1,1} = \mu_1 \tag{6.89}$$

$$C_{i_1,i_2,2\ i_1+1,i_2+1,2} = C_{i_1,i_2,2\ i_1-1,i_2,2} = C_{i_1,i_2,2\ i_1,i_2-1,2} = \mu_2 \tag{6.90}$$

$$B^{xy}_{i_1,i_2,1\ i_1-1,i_2-1,1} = B^{yz}_{i_1,i_2,1\ i_1+1,i_2,1} = B^{zx}_{i_1,i_2,1\ i_1,i_2+1,1} = b_1 \tag{6.91}$$

$$B^{xy}_{i_1,i_2,2\ i_1+1,i_2+1,2} = B^{yz}_{i_1,i_2,2\ i_1-1,i_2,2} = B^{zx}_{i_1,i_2,2\ i_1,i_2-1,2} = b_2. \tag{6.92}$$

The mean field Hamiltonian at $t' = 1$ is

$$H_{MF} = H^b_{MF} + H^c_{MF} \tag{6.93}$$

$$H^b_{MF} = \frac{1}{4}\sum_{k\in HBZ} \begin{pmatrix} (b^\alpha_{\mathbf{k}1})^\dagger & (b^\alpha_{\mathbf{k}2})^\dagger \end{pmatrix} \begin{pmatrix} iV_{\alpha\beta,1}(\mathbf{k}) & iU_{\alpha\beta}(\mathbf{k}) \\ -iU^*_{\alpha\beta}(\mathbf{k}) & iV_{\alpha\beta,2}(\mathbf{k}) \end{pmatrix} \begin{pmatrix} b^\beta_{\mathbf{k}1} \\ b^\beta_{\mathbf{k}2} \end{pmatrix} \tag{6.94}$$

$$U(\mathbf{k}) = \epsilon \begin{pmatrix} Je^{-ik_1} & \gamma_1(e^{-ik_1} + e^{ik_2}) & \gamma_1(e^{-ik_1} + 1) \\ \gamma_1(e^{-ik_1} + e^{ik_2}) & Je^{ik_2} & \gamma_1(e^{ik_2} + 1) \\ \gamma_1(e^{-ik_1} + 1) & \gamma_1(e^{ik_2} + 1) & J \end{pmatrix} \tag{6.95}$$

$$V_{\alpha\beta,1} = \mu_1\gamma_2 \begin{pmatrix} 0 & e^{ik_3} & -e^{-ik_1} \\ -e^{-ik_3} & 0 & e^{ik_2} \\ e^{ik_1} & -e^{-ik_2} & 0 \end{pmatrix} \quad V_{\alpha\beta,2} = \mu_2\gamma_2 \begin{pmatrix} 0 & -e^{-ik_3} & -e^{-ik_1} \\ e^{ik_3} & 0 & -e^{-ik_2} \\ e^{ik_1} & e^{ik_2} & 0 \end{pmatrix} \tag{6.96}$$

$$H^c_{MF} = \frac{1}{4}\sum_{\mathbf{k}\in HBZ} \begin{pmatrix} c^\dagger_{\mathbf{k}1} & c^\dagger_{\mathbf{k}2} \end{pmatrix} \begin{pmatrix} iv_1(\mathbf{k}) & iu(\mathbf{k}) \\ -iu^*(\mathbf{k}) & iv_2(\mathbf{k}) \end{pmatrix} \begin{pmatrix} c_{\mathbf{k}1} \\ c_{\mathbf{k}2} \end{pmatrix} \tag{6.97}$$

$$u(\mathbf{k}) = \sum_\alpha e^{-i\mathbf{k}\cdot\mathbf{e}_\alpha}\left(J\eta + \gamma_1 \sum_{\beta\neq\alpha} B^{\alpha\beta}_\alpha\right) \tag{6.98}$$

$$v_1(\mathbf{k}) = 2ib_1\gamma_2 \sum_\alpha \sin(\mathbf{k}\cdot\mathbf{e}_\alpha) \qquad v_2(\mathbf{k}) = -2ib_2\gamma_2 \sum_\alpha \sin(\mathbf{k}\cdot\mathbf{e}_\alpha) \tag{6.99}$$

where $k_i = \mathbf{k}\cdot\mathbf{e}_i$

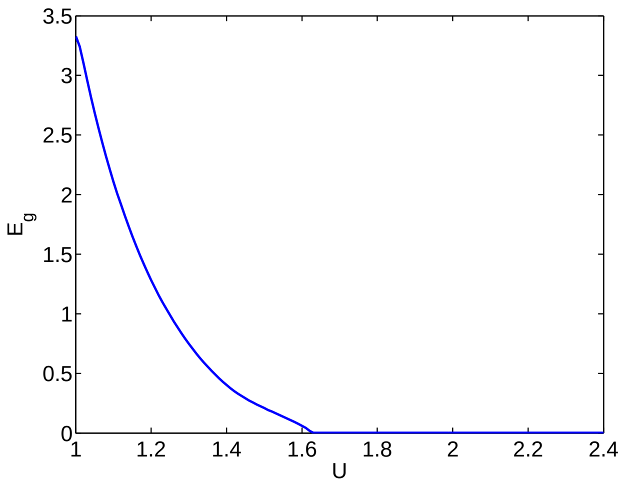

Figure 6.6: Spinon gap, E_g as a function of U.

Both the nearest-neighbour and the next-to-nearest neighbour terms in the Hamiltonian (6.65) results in closing the gap in the spinon sector. While the former occurs at the Dirac points (see Fig: 6.5), the latter leads to a collapse of the gap at $(0, 0)$ and (π, π). For large values of U the nearest-neighbour term dominates; for smaller values of U, on the other hand, the next-nearest neighbour term comes into play and the Dirac points shift to $(0, 0)$ and (π, π). Numerically we find that the spinon sector is gapless for $U \geq 1.6$ Fig:(6.6). We have checked that this remains true for $1 < t' < 0.5$. VCA indicates a Mott transition at $U = 2.4$. This shows the absence of the CSL phase in the presence of higher order perturbative terms and indicates that the ASL phase continues till the Mott transition.

6.5 Conclusion

In the conclusion to the first part of the thesis, we have shown that the Kitaev-Hubbard model which is a Hubbard model, with spin-dependant hopping on the honeycomb lattice, shows a Mott transition from a semi-metallic phase to an algebraic spin-liquid phase. The former breaks time-reversal symmetry whereas the latter preserves it. The ASL is stabilized by this TR symmetry. We have proved the TR invariance in the Mott phase to all orders in t/U using particle-hole symmetry. At intermediate U the ASL phase occurs for a wide range of t' which narrows down as U is increased. The model also features a first order transition from an ASL phase to an AFI phase. We computed the spin-spin correlation function and find a power law behaviour. Using a Majorana mean field technique we eliminate the possibility of a spontaneous time reversal symmetry. Concrete schemes to realize this model have been proposed[43, 75], and experimental methods to probe the semi-metal at low U[76] and the ASL at large U[74] exist. This demonstration of the existence of the ASL might help better understand the physics of the pseudo-gap phase of the underdoped high temperature superconductors [77, 29, 30].

Chapter 7

Introduction to Iridate Materials

The woods are lovely, dark and deep,
But I have promises to keep,
And miles to go before I sleep,
And miles to go before I sleep.

Robert Frost

In this chapter we familiarize ourselves with the Iridates. The strong spin orbit coupling present in these compounds makes them interesting subjects to realize perturbed Kitaev models.

7.1 The IrO_3-type Iridates

The $A_2\mathrm{IrO}_3$ (A = Na, Li) family of iridates have a structure that is made up of layers containing only A atoms alternating with AIr_2O_6 layers stacked along the c axis as shown in Fig:(7.1)[9]. A Kitaev-Heisenberg (KH) model for $A_2\mathrm{IrO}_3$ was

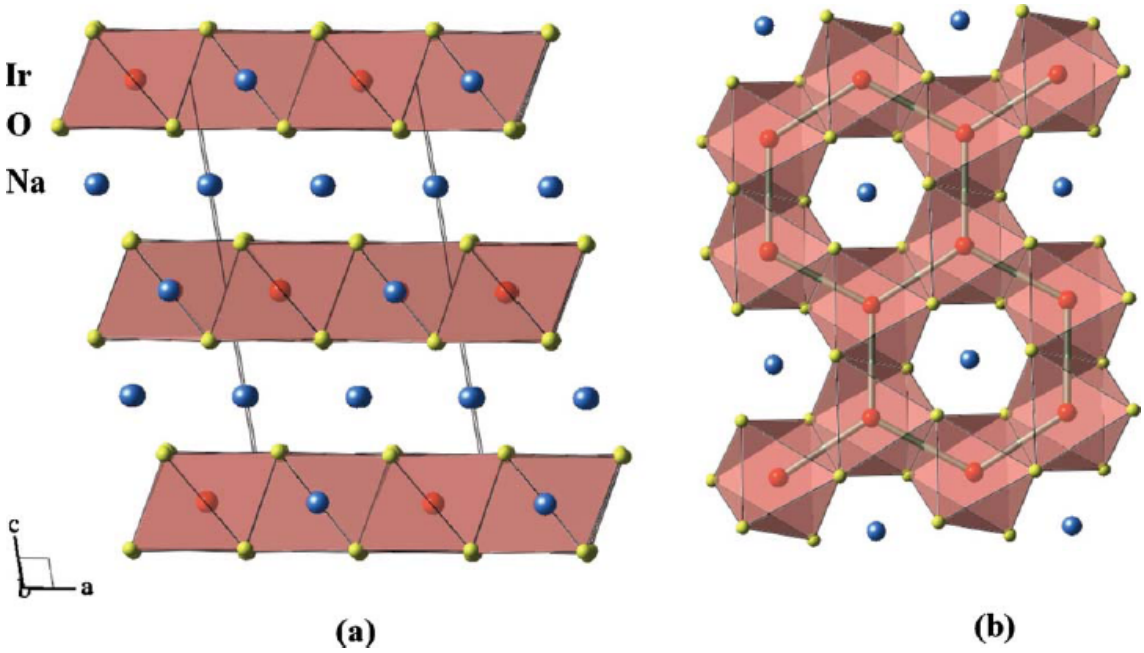

Figure 7.1: The crystallographic structure of Na_2IrO_3 compound. (a) The view perpendicular to the c axis showing the layered structure. (b) One of the $NaIr_2O_6$ slabs viewed down the c axis to highlight the honeycomb lattice of Ir atoms within the layer[9].

studied theoretically and based on the relative strength of the two exchanges three magnetic ground states were envisaged. A simple Neel anti-ferromagnet in the Heisenberg limit, a quantum spin-liquid (QSL) in the Kitaev limit, and an unusual stripy magnetic order where both are present, were predicted [78]. These predictions have led to a flurry of activity on the honeycomb lattice iridates A_2IrO$_3$ (A = Na, Li) [79, 80, 36, 81, 78, 2, 35, 82, 11, 83, 84, 85, 86, 87, 88, 89]. First experiments on single crystals found that Na$_2$IrO$_3$ was indeed a Mott insulator with strong anti-ferromagnetic interactions (Weiss temperature $\theta_{cw} = -120$ K). It also showed long-ranged magnetic order at a much lower temperature $T_N = 15$ K [35]. This magnetic order however, was found to be of the zig-zag kind [80, 36, 81], and not one of the predicted phases of the KH model [78]. Subsequently several attempts were made to modify the nearest-neighbour (NN) KH model to get the experimentally observed zig-zag order. It was found that substantial further neighbour interactions of the Heisenberg type could stabilize the zig-zag order as well as explain the inelastic neutron scattering data [36, 82]. In a more drastic attempt to reconcile experiments with a NN KH model the signs of H- and K-interactions were reversed from anti-ferromagnetic and ferromagnetic to ferromagnetic and anti-ferromagnetic, respectively [11]. This also led to the zig-zag order being stabilized in some part of parameter space. New quantum chemistry calculations have concluded that the Kitaev term is large ($\approx$ 17 meV) and ferromagnetic and additionally, bond-dependent anisotropic exchanges are also present[86]. Presence of such anisotropic bond-dependent NN exchanges has also been found in recent exact diagonalization calculations [87]. Another recent study has proposed a model with both Heisenberg and Kitaev interactions which exist beyond nearest-neighbor spins [90]. Thus the minimal model for these materials and in particular, how close the real materials are to the SL state in the dominant Kitaev limit is still unclear.

The first direct evidence of dominant bond-dependent magnetic interactions has been found very recently using diffuse RIXS measurements on Na_2IrO_3 [91]. Additionally, this study showed that short ranged zig-zag correlations which are present above T_N = 15 K do not change as the temperature is lowered into the magnetically ordered state suggesting that fluctuating moments survive deep into the ordered state [91]. This indicates that only that a small fraction of the magnetic moment orders while a large fraction is still dynamically fluctuating down to the lowest temperatures. This study therefore suggests that Na_2IrO_3 maybe close to the SL state predicted in the strong Kitaev limit [91].

A novel prediction has recently been made for observing the signatures of the Kitaev QSL in Raman scattering on Na_2IrO_3 in the form of a polarization-independent broad band response centred at $6J_K$ (J_K is the Kitaev interaction strength) [12]. In these calculations the Heisenberg interaction (J_H) is assumed to be a weak perturbation ($J_H/J_K = 0.1$) so the Raman response from the Heisenberg term will be an order of magnitude smaller with a band maximum at much lower frequency than the Kitaev part. Predictions of a broad continuous polarization independent Raman band seems to be a generic feature of spin-liquids with similar broad bands being predicted for the Kagome lattice material Herbertsmithite $ZnCu_3(OH)_6Cl_2$ [92, 93]. Recently, an experimental Raman study on Herbertsmithite has shown a quasi-elastic signal at high temperature and a broad maximum ~ 250 cm^{-1} at low temperature. These features have been associated with the excitation of a gapless spin liquid ground state [94]. Thus Raman scattering seems to be a new tool to look for signatures of QSL's [92, 93, 12]. Recent Raman scattering measurements on the honeycomb lattice Ruthenate α-$RuCl_3$, another material proposed for realization of KH physics, has also revealed a broad continuum of excitations which was interpreted as resulting from proximity to the QSL phase in the strong Kitaev limit [95].

We present here a comprehensive study of Raman scattering from the honeycomb lattice iridates Na_2IrO_3. These materials have previously been reported to have zigzag magnetic long range order for $T_N \approx 15$ K, 10 K, and 6 K, respectively [80, 96, 97]. We use a Kitaev-Heisenberg spin Hamiltonian model treated in a generalized mean field theory that even in the zigzag magnetically long range ordered state close to the SL phase boundary, the predicted Raman excitation has a broad Kitaev SL like spectrum quite similar to what is observed [98]. We believe that this demonstrates both the applicability of a Kitaev-Heisenberg Hamiltonian to the honeycomb iridates, and also the survival of Kitaev like spin correlations in such systems in spite of long range magnetic order. Some implications of this discovery are that some of the quantum entanglement and coherence manifest in Kitaev spin liquid systems could survive recognizably and usefully in real systems with magnetic long range order with possible applications, and also that there is hope for finding realistic materials which have Kitaev spin liquid like ground states whose exact solubility lays bare the nature of low lying excitations (Majorana fermions) and quantum coherence.

7.2 The Ir_3O_8-type iridates

Recently, $Na_4Ir_3O_8$ compound has been proposed as one of the candidates for hosting Mott insulating spin liquid phase in three-dimension [10, 99, 100, 101, 102, 103, 104, 105, 106, 107]. The structure of the material is shown in Fig:(7.2) which is derived from those of spinel oxides AB_2O_4 which can be obtained by rewriting the chemical formula for the compound as $(Na_{1.5})_1(Ir_{3/4}Na_{1/4})_2O_4$. In $Na_4Ir_3O_8$, each tetrahedron in the B sub-lattice of the spinel structure is occupied by three Ir atoms and one Na atom. Therefore, Ir sites form a geometrically frustrated hyper-kagome lattice which is a three-dimensional network of corner-sharing triangles[10]. Temperature dependent susceptibility, χ, measurement shows that spin $1/2$ Ir atoms interact anti-ferromagnetically with a large Curie-Weiss constant $\theta_w \approx -650K$ and moment $p_{eff} = 1.96\mu_B$ [10]. However no anomaly is present in the magnetic susceptibility down to $2K$, indicating no long range ordering in $Na_4Ir_3O_8$, which is further supported by NMR Knight shift measurement [101]. Later on, it was shown that the spin-orbit coupling SOC that breaks the $SU(2)$ spin-rotation symmetry induces anisotropic exchange interactions. These interactions relieve frustration and may give rise to magnetic ordering at low temperatures [99]. The magnetic susceptibility saturates to a fi-

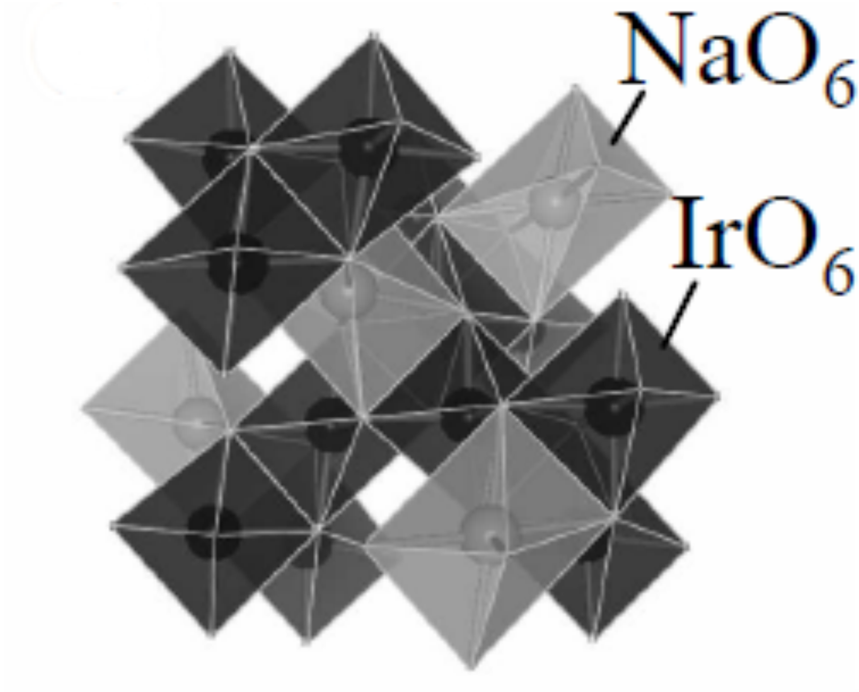

Figure 7.2: The crystallographic structure of $Na_4Ir_3O_8$ compound. Black and gray octahedra represent IrO_6 and NaO_6 respectively. The spheres inside the octahedra represent Ir and Na atoms and oxygens occupy all the corners [10].

nite value as temperature approaches to zero while heat capacity C_V follow linear temperature dependence with a rather small coefficient γ where $\gamma = \frac{C_V}{T}$. This gives the Wilson ratio [101], defined by $R_W = \frac{\pi^2 k_B \chi}{3\gamma}$ to be 35 at low temperature which is much higher than other promising quantum spin liquid candidates where R_W is of the order of unity. This anomalously large Wilson ratio is explained by using extended Hubbard model on hyper-kagome lattice that includes spin-orbit coupling and multi-orbital interactions [101]. The charge gap of $Na_4Ir_3O_8$ is reported to be $500K$, which is comparable to Curie-Weiss temperature, suggesting that the compound is near the Mott transition [10]. Application of moderate hydrostatic pressure or relatively small concentration of dopants turn $Na_4Ir_3O_8$ in to metallic state from Mott insulator [100]. The influence of electron-phonon interaction on these electronic properties and phase behaviour has not yet been addressed despite its prominent role in $3D$ transition metal oxides. Recently, Raman studies on this compound (to be published soon) also show a broad Raman band similar to the Na_2IrO_3 compound. We use a Kitaev-Heisenberg spin Hamiltonian model treated in a generalized mean field theory to show that in the spin liquid phase, the predicted Raman excitation has a broad spectrum quite similar to what is observed.

Chapter 8

A Brief History of Raman Spectroscopy

Give light, and the darkness will disappear of itself.

Desiderius Erasmus

A large fraction of light scattered from a target material occurs via elastic scattering. Raman scattering is an example of the rarer inelastic light scattering, and occurs when light interacts with electric dipoles of the material. As such, Raman scattering is also a useful tool for probing the polarizability of the material. The energy shifts required for Raman scattering do not require a large transfer of momentum and thus can be generated from any type of excitation. Optical phonons occurring near the center of the Brillouin zone appear as sharp peaks in the Raman spectrum. Two-magnon scattering is an excitation typical of cuprates that produces an exchange between a pair of neighbouring spins on the anti-ferromagnetically ordered copper sub-lattice. In the context of the topics discussed in this thesis, Raman scattering has recently emerged as a powerful tool in detecting quantum spin liquids [92, 93, 108, 12]. For instance, the Raman cross-section acquires a characteristic polarization dependence in the broken symmetry phase, but loses the same in the spin liquid phase, thus revealing the presence—or absence—of the latter.

Beginning with the Peierls coupling and proceeding along the lines of the Loudon-Fleury approach [109, 110], it is possible to derive the general expression for the Raman scattering intensity. We summarize here briefly the method for the derivation. Shastry *et al.*[109] start with a one band Hubbard model given by

$$H = H_t + H_U \tag{8.1}$$

where H_t is the nearest neighbour hopping Hamiltonian, H_U is the onsite interaction, to describe the system. This Hamiltonian is now coupled to external electromagnetic field with vector potential in real space $\mathbf{A}$, done by replacing the hopping matrix element $t \rightarrow te^{i\mathbf{A}\cdot\mathbf{x}}$. The Hamiltonian can now be written as

$$H = H_t + H_U + H_\gamma + H_C \tag{8.2}$$

and

$$H_C = -\sum_{\langle ij\rangle} t c_i^\dagger c_j \left\{ \frac{ie}{\hbar c}\mathbf{A}\cdot(\mathbf{x}_i - \mathbf{x}_j) - \frac{e^2}{\hbar^2 c^2}\left[\mathbf{A}\cdot(\mathbf{x}_i - \mathbf{x}_j)\right]^2 + \cdots \right\} + h.c. \tag{8.3}$$

$$H_\gamma = \sum_q \omega_q a_q^{\alpha\dagger} a_q^\alpha \tag{8.4}$$

where a_q^α denotes the annihilation of a photon at momentum q and polarization α and $\cdots$ represents higher order terms of $\mathbf{A}$. H_C is treated as a time-dependant perturbation and the basic Raman scattering cross section is given by the Fermi-

Golden rule

$$R = 2\pi|\langle f|M|i\rangle|^2\delta(E_f - E_i) \tag{8.5}$$

where M is the effective scattering operator causing a scattering between the initial state $|i\rangle$ and the final state $|f\rangle$ with the corresponding energies E_i and E_f. Let ω_{in}, $\mathbf{k}_{in}$ and $\boldsymbol{\epsilon}_{in}$ be the frequency, momentum and polarization of the incoming photon with $in \rightarrow out$ representing the corresponding physical quantities for the outgoing photon. Let $\mathbf{A} = g_{in}\boldsymbol{\epsilon}_{in}a_{\mathbf{k}_{in}} + g_{out}\boldsymbol{\epsilon}_{out}a^{\dagger}_{\mathbf{k}_{out}}$ where g_{in}, g_{out} are laser coupling constants and we have assumed that the photon momenta is much smaller than the lattice spacing. Keeping terms of only zeroth order in t/U and assuming that the system is at half filling and near resonance, M can be expressed in terms of spin-operators. The final Raman operator for the model can be computed to be

$$R = \sum_{\langle ij\rangle\alpha}(\boldsymbol{\epsilon}_{in}.\boldsymbol{d}^{\alpha})(\boldsymbol{\epsilon}_{out}.\mathbf{d}^{\alpha})K_1\mathbf{S}_i\cdot\mathbf{S}_j. \tag{8.6}$$

Similar expression can be obtained for the Kitaev-Heisenberg model starting from say a one band Hubbard model like say the Kitaev-Hubbard model Eq:(3.1) which is given by [12]

$$R = \sum_{\langle ij\rangle\alpha}(\boldsymbol{\epsilon}_{in}.\boldsymbol{d}^{\alpha})(\boldsymbol{\epsilon}_{out}.\mathbf{d}^{\alpha})(KS_i^{\alpha}S_j^{\alpha} + K_1\mathbf{S}_i\cdot\mathbf{S}_j) \tag{8.7}$$

where constants $K \propto J_K$ and $K_1 \propto J_H$. The expression for the Raman response is written in the Heisenberg picture, where $\boldsymbol{\epsilon}_{in}$ and $\boldsymbol{\epsilon}_{out}$ correspond to the incoming and outgoing polarization directions of light. The most commonly used experimental configuration with scattering of linearly polarized light $(A'_{1g}, B_{1g}, B_{2g})$ and of left circularly polarized light into left or right polarization denoted by LL and

LR respectively is given below.

$$\begin{array}{|c|c|c|c|} \hline & & \boldsymbol{\epsilon}_{in} & \boldsymbol{\epsilon}_{out} \\ \hline I & A'_{1g} & \frac{\mathbf{x}+\mathbf{y}}{2} & \frac{\mathbf{x}+\mathbf{y}}{2} \\ II & B_{1g} & \frac{\mathbf{x}+\mathbf{y}}{2} & \frac{\mathbf{x}-\mathbf{y}}{2} \\ III & B_{2g} & \mathbf{x} & \mathbf{y} \\ IV & LR & \frac{\mathbf{x}+i\mathbf{y}}{2} & \frac{\mathbf{x}-i\mathbf{y}}{2} \\ V & LL & \frac{\mathbf{x}+i\mathbf{y}}{2} & \frac{\mathbf{x}+i\mathbf{y}}{2} \\ \hline \end{array}. \tag{8.8}$$

The Raman intensity is therefore computed as

$$I(\omega) = \int dt\, e^{i\omega t}\, iF(t) \tag{8.9}$$

$$iF(t) = \langle GS|R(t)R(0)|GS\rangle \tag{8.10}$$

where $|GS\rangle$ is the ground state of the model.

It is possible to detect, based on the symmetries of the underlying lattice, if a particular mode is active in the Raman way. The symmetry groups for the square lattice, honeycomb lattice and hyper-kagome lattice are $C4v$, $C6v$ and a very complicated $P4332$ respectively. The Raman intensity in each of the experimental configurations can be represented in terms of the linear combinations of the one dimensional irreducible representations of these groups. For example the square lattice $C4v$ has four of them : A_1, A_2, B_1,B_2. The relations between the Raman intensity for these and the experimental configurations has been discussed by Shastry *et al.*. [109].

The computation of the ground state provides another challenge in the computation of the Raman intensity of any spin model. As our discussions earlier in the thesis reveals, while the ground state for the Kitaev model is well known, it is imperative that Majorana mean field theory is used for the Kitaev-Heisenberg model. In the next two chapters we compute the Raman intensity for the Kitaev-Heisenberg model for honeycomb and hyper-kagome lattices which are, respectively, models for the materials Na_2IrO_3 and $Na_4Ir_3O_8$ compounds.

Chapter 9

Raman Response for Honeycomb Sodium Iridate

Expectation is the root of all heartache.

William Shakespeare

It is still unclear what a minimal model for the $A_2\mathrm{IrO}_3$ materials is and how strong the Kitaev interactions are in these materials. There are quantum chemical calculations [111, 112] of the actual iridate systems, with a view to finding the appropriate model Hamiltonians and their interaction parameters. Iridium has an atomic number 77 with the electronic configuration $[Xe]4f^{14}5d^{7}6s^{2}$ with 7 electrons in the outermost $5d$ shell. In Iridate compounds, the Ir^{4+} ions have a hole which can lie in any one of the t_{2g} orbitals of xy, yz or xz. A local effective Hamiltonian for the holes can be written based on the spin-orbit coupling parameter λ and tetragonal t_{2g} level splitting parameter Δ[33]. This gives us an low energy effective two level system in which the spin and the orbital degrees of freedom are coupled represented by a pseudo-spin $1/2$ at each Ir site. An interacting fermion model for these pseudospins on the honeycomb lattice can be written. In terms of these degrees of freedom, the tight binding Hamiltonian H can be formally written as the sum of two terms H_{Kitaev} (H_K) and $H_{Heisenberg}$ (H_H), where H_K couples the spins of the nearest neighbours in the bond direction, and H_H is the conventional Heisenberg spin Hamiltonian. A very attractive two parameter Hamiltonian is due to Chaloupka *et al.*[11]

$$H = A\cos\phi \sum \mathbf{S}_i \cdot \mathbf{S}_j + 2A\sin\phi \sum S_i^a S_j^a \tag{9.1}$$

where S_i^a is the a component of the spin half operator at site i; i and j are nearest neighbours. The two parameters are the overall magnitude A of the coupling as well as the relative weight and sign of the Kitaev ($J_K = 2A\sin\phi$) as well as Heisenberg ($J_H = A\cos\phi$) parts of the Hamiltonian described by the angle ϕ. Chaloupka *et al.*. [11] have shown from exact diagonalization that there is a zigzag magnetically long range ordered phase for $\phi > 92.2^o$. See Fig:(9.1)

Rau et al. [87] on the other hand have worked on a Kitaev-Heisenberg model with off-diagonal bond direction-type interactions Γ,

$$\mathcal{H} = \sum_{\langle ij\rangle^a} \left[J_H \mathbf{S}_i \cdot \mathbf{S}_j + J_K S_i^a S_j^a + \Gamma(S_i^b S_j^c + S_i^c S_j^b) \right] \tag{9.2}$$

and have found, using exact diagonalization, a spin-liquid–zig-zag transition. Though most of our discussions pertain to the model of Eq.(9.1), we have also done calculations with Eq.(9.2).

Knolle *et al.*[12] considered the spin liquid phase of Eq.(9.1) with $J_K = -1, J_H = 0.1$ with $\phi = -78.7^o$. Since the phase is still spin liquid, the Heisenberg term can

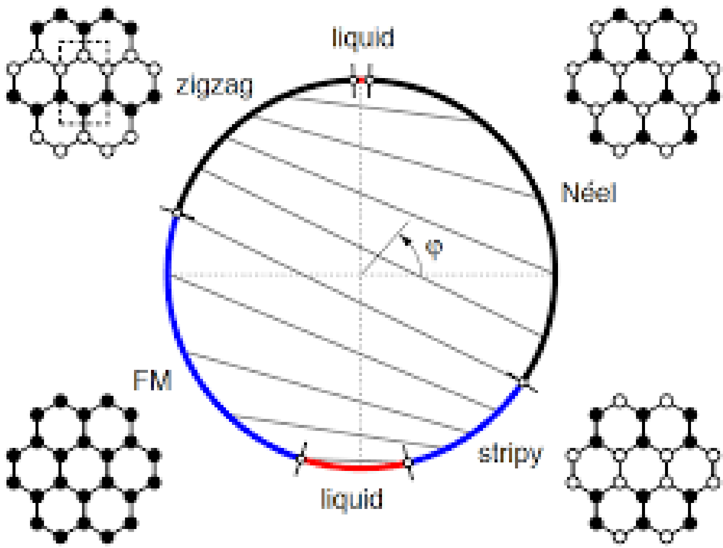

Figure 9.1: The phase diagram of the Kitaev Heisenberg model Eq:(9.1) computed using exact diagonalization[11] showing the location of various magnetic and spin liquid phases.

be considered as a perturbation with the Kitaev as the unperturbed Hamiltonian. The Raman response is computed numerically upto second order of perturbation with respect to the Kitaev ground state which contains decoupled contributions from the Kitaev part and the Heisenberg parts of the Raman response. We discuss the calculations and results in brief.

The ground state of the Kitaev model, with decoupled matter and conserved gauge sectors is given as

$$|GS\rangle = |GS_k\rangle = |M\rangle|G\rangle \tag{9.3}$$

with the action of the Kitaev model on the ground state to be

$$H_k|M\rangle|G\rangle = E_0|M\rangle|G\rangle. \tag{9.4}$$

The Raman response operator given in Eq:(10.24) is now written in interaction picture where the Heisenberg term is considered as a perturbation turned on at $-\infty$. Thus we get

$$iF(t) = \langle GS_k|S^\dagger(t,-\infty)R(t)S(t,0)R(0)S(0,-\infty)|GS_k\rangle \tag{9.5}$$

which when expanded to leading order of $S(t,t')$ which is 1 and rewriting $R = R_k + \gamma R_h$, $\gamma = \frac{J_1}{J_k}$ defines the amount of perturbation, we get

$$\begin{aligned} iF(t) &\approx \langle GS_k|R(t)R(0)|GS_k\rangle && (9.6)\\ &= \langle GS_k|(R_k(t)+\gamma R_h(t))(R_k(0)+\gamma R_h(0))|GS_k\rangle && (9.7)\\ &= \langle GS_k|R_k(t)R_k(0)|GS_k\rangle + \gamma^2\langle GS_k|R_h(t)R_h(0)|GS_k\rangle. && (9.8)\end{aligned}$$

The operators are now in interaction picture. The first term of the above expression can be calculated easily. For the second term we have

$$\begin{aligned} \langle GS_k|R_h(t)R_h(0))|GS_k\rangle &= \langle M|\langle G|R_h(t)R_h(0)|M\rangle|G\rangle && (9.9)\\ &= \langle M|\langle G|e^{-iH_kt}R_he^{iH_kt}R_h|M\rangle|G\rangle. && (9.10)\end{aligned}$$

Contribution from each of the Raman operator terms can be computed qualitatively as

$$\begin{aligned} \langle GS_k|R_h(t)R_h(0))|GS_k\rangle &\approx \langle M|\langle G|e^{-iH_kt}cbcbe^{iH_kt}cbcb|M\rangle|G\rangle && (9.11)\\ &= \langle M|\langle G|e^{-iH_kt}cce^{i(H_k+V_0)t}bbccbb|M\rangle|G\rangle && (9.12)\\ &= \langle M|e^{-iH_kt}cce^{i(H_k+V_0)t}cc|M\rangle\langle G|bbbb|G\rangle && (9.13)\\ &\approx \langle M|e^{-iH_kt}cc\sum_\lambda|\lambda\rangle\langle\lambda|e^{i(H_k+V_0)t}cc|M\rangle && (9.14)\end{aligned}$$

such that $(H_k + V_0)|\lambda\rangle = E_\lambda$ thereby giving us

$$\langle GS_k|R_h(t)R_h(0))|GS_k\rangle \approx \sum_\lambda e^{-i(E_0-E_\lambda)t}\langle M|cc|\lambda\rangle\langle\lambda|cc|M\rangle. \tag{9.15}$$

Knolle *et al.*[12] numerically studied the system upto 62x62 unit cells and the results can be seen in Fig:(9.2).

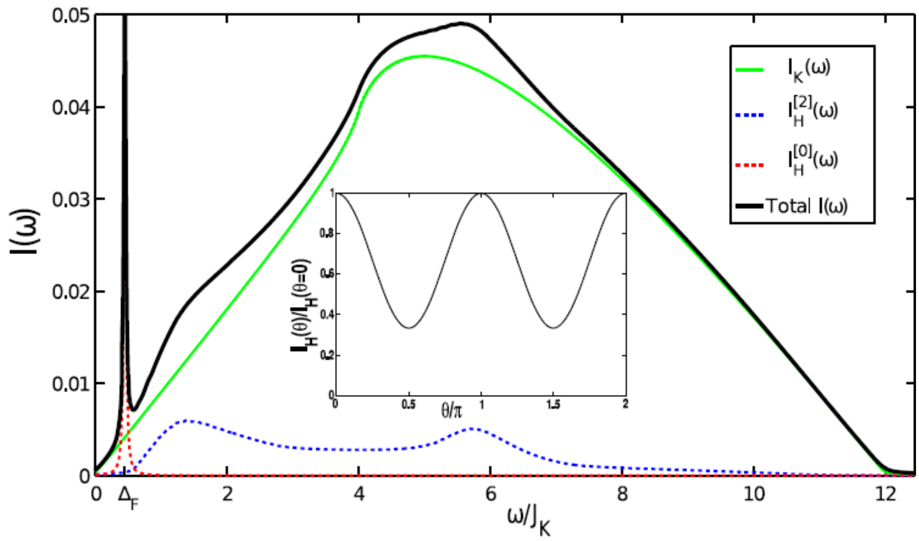

Figure 9.2: The Raman Intensity $I(\omega)$ (black curve) computed for the spin liquid using Heisenberg perturbation [12].

9.1 Mean Field Theory of the KH model

We use a mean field theory because of its versatility and because of its giving the observed phases through the actual critical values of the self consistent coupling constants separating the phases. They are different from that obtained in finite-size exact diagonalization calculations. We write the Kitaev-Heisenberg

Hamiltonian in terms of the Majorana fermions

$$\mathcal{H} = J_K \sum_{\langle ij\rangle^\alpha} ic_i b_i^\alpha ic_j b_j^\alpha + J_H \sum_{\langle ij\rangle} \sum_\alpha ic_i b_i^\alpha ic_j b_j^\alpha. \tag{9.16}$$

To solve the model we perform a mean field decoupling of the Majorana fermions to include the possibility of both spin liquid and magnetic phases, since the material actually shows magnetic order at low temperatures, as

$$\begin{aligned}\sigma_i^\alpha \sigma_j^\beta = -ic_i c_j \; ib_i^\alpha b_j^\beta \approx -ic_i c_j B_{ij}^{\alpha\beta} - iC_{ij} b_i^\alpha b_j^\beta + C_{ij} B_{ij}^{\alpha\beta} \\ + ic_i b_i^\alpha M_j^\beta + ic_j b_j^\beta M_i^\alpha - M_i^\alpha M_j^\beta.\end{aligned} \tag{9.17}$$

The self-consistency equations are

$$B_{\langle ij\rangle^\gamma}^{\alpha\beta} \equiv \langle ib_i^\alpha b_{j^\gamma}^\beta\rangle, \;\; C_{\langle ij\rangle^\gamma} \equiv \langle ic_i c_{j^\gamma}\rangle, \;\; M_i^\alpha \equiv \langle ic_i b_i^\alpha\rangle. \tag{9.18}$$

Here B_{ij} and C_{ij} represent nearest neighbour correlations and M_i the magnetic order parameter. When $M_i = 0$, the phase is a spin liquid phase where the c and the b fermion Hamiltonians decouple. The c fermions modify the hopping of the b fermions and vice-versa. When $M_i \neq 0$, the phase is a magnetic phase and the type of order is determined by its variation throughout the lattice.

In the Hamiltonian Eq.(9.1), we analyze the spin-liquid–zigzag regime of Fig:(9.1). We see a spin liquid to zigzag transition at $\phi = 101.4^o$ using Majorana mean field decoupling discussed above and comparing the free energy of the system. We show this in Fig:(9.3) where we plot a few of the mean field parameters as a function of ϕ. The phase transition is first order due to the underlying symmetry of the phases. Close to the boundary, Kitaev-like spin correlations exist and beyond $\phi = 110^o$ they die. We expect that the Na_2IrO_3 compound lies in this zigzag phase with short range correlations. We proceed now to compute the Raman Response of the the model and compare with experiments.

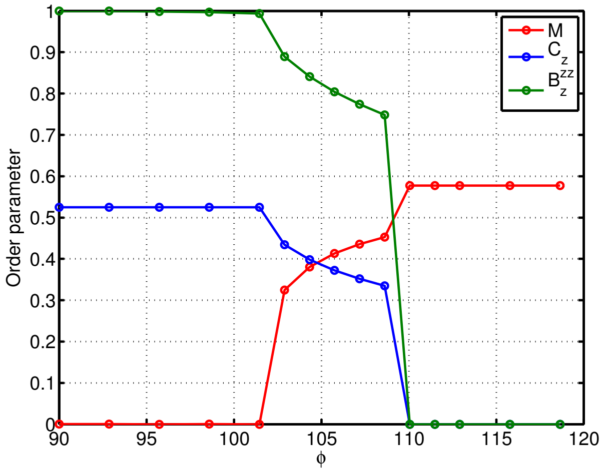

Figure 9.3: The mean field parameters around the spin liquid at $\phi = \frac{\pi}{2}$.

For the spin-liquid phase of the KH model some level of analytical treatment for the mean field decoupling of the gauge and the spinon sector and the Raman Response can be done. The Hamiltonian for the spinon sector c with $\eta = B^{\alpha}_{\alpha\alpha}$ is given as

$$
\begin{aligned}
\mathcal{H}_c &= \frac{-(3J_1 + J_k)\eta}{4} \sum_k \begin{pmatrix} f_k^\dagger & f_{-k} \end{pmatrix} \begin{pmatrix} 1 + \cos k_1 + \cos k_2 & -i(\sin k_1 - \sin k_2) \\ i(\sin k_1 - \sin k_2) & -(1 + \cos k_1 + \cos k_2) \end{pmatrix} \begin{pmatrix} f_k \\ f_{-k}^\dagger \end{pmatrix} \\
&= \sum_k \begin{pmatrix} f_k^\dagger & f_{-k} \end{pmatrix} \begin{pmatrix} \epsilon_k & -i\delta_k \\ i\delta_k & -\epsilon_k \end{pmatrix} \begin{pmatrix} f_k \\ f_{-k}^\dagger \end{pmatrix} \\
&= \sum_k E_k \begin{pmatrix} f_k^\dagger & f_{-k} \end{pmatrix} \begin{pmatrix} \cos 2\theta & -i \sin 2\theta \\ i \sin 2\theta & -\cos 2\theta \end{pmatrix} \begin{pmatrix} f_k \\ f_{-k}^\dagger \end{pmatrix}.
\end{aligned}
$$

The diagonalization of the Hamiltonian can be done using the following expressions

$$\begin{aligned}
&\epsilon_k = \frac{-(3J_1+J_k)\eta}{4}(1+\cos k_1+\cos k_2) \quad \delta_k = \frac{-(3J_1+J_k)\eta}{4}(\sin k_1 - \sin k_2)\\
&\sin 2\theta = \frac{\delta_k}{E_k} \quad \cos 2\theta = \frac{\epsilon_k}{E_k}\\
&\begin{pmatrix} \alpha_k \\ \beta_k \end{pmatrix} = \begin{pmatrix} \cos\theta & -i\sin\theta \\ -i\sin\theta & \cos\theta \end{pmatrix}\begin{pmatrix} f_k \\ f_{-k}^\dagger \end{pmatrix} \quad e^{2i\theta_k} = \frac{-s_k}{|s_k|}\\
&E_k = \frac{(3J_1+J_k)\eta}{4}|1+e^{ik_1}+e^{-ik_2}| = \frac{(3J_1+J_k)}{4}|s_k|
\end{aligned}$$

by which we get

$$\mathcal{H}_c = \sum_k E_k \begin{pmatrix} \alpha_k^\dagger & \beta_k^\dagger \end{pmatrix}\begin{pmatrix} 1 & 0 \\ 0 & -1 \end{pmatrix}\begin{pmatrix} \alpha_k \\ \beta_k \end{pmatrix}. \tag{9.19}$$

So finally if we put $\beta_k = \alpha_{-k}^\dagger$

$$\mathcal{H}_c = \sum_k E_k(\alpha_k^\dagger \alpha_k - \beta_k^\dagger \beta_k) = \sum_k E_k(2\alpha_k^\dagger \alpha_k - 1). \tag{9.20}$$

Similarly for the gauge sector with $C^\alpha = \epsilon'$, we have $g_k = \left(g_k^{x\dagger}, g_{-k}^x, g_k^{y\dagger}, g_{-k}^y, g_k^{z\dagger}, g_{-k}^z\right)^T$

$$\mathcal{H}_b = \frac{-\epsilon'}{4}\sum_k g_k^\dagger \begin{pmatrix} G_x^b & 0 & 0 \\ 0 & G_y^b & 0 \\ 0 & 0 & G_z^b \end{pmatrix} g_k \tag{9.21}$$

with

$$G_b^x = \begin{pmatrix} J_1(1+\cos k_1+\cos k_2)+J_k\cos k_1 & -iJ_1(\sin k_1-\sin k_2)-iJ_k\sin k_1 \\ iJ_1(\sin k_1-\sin k_2)+iJ_k\sin k_1 & -J_1(1+\cos k_1+\cos k_2)-J_k\cos k_1 \end{pmatrix} \tag{9.22}$$

$$G_b^y = \begin{pmatrix} J_1(1+\cos k_1+\cos k_2)+J_k\cos k_2 & -iJ_1(\sin k_1-\sin k_2)+iJ_k\sin k_2 \\ iJ_1(\sin k_1-\sin k_2)-iJ_k\sin k_2 & -J_1(1+\cos k_1+\cos k_2)-J_k\cos k_2 \end{pmatrix} \tag{9.23}$$

$$G_b^z = \begin{pmatrix} J_1(1+\cos k_1+\cos k_2)+J_k & -iJ_1(\sin k_1-\sin k_2) \\ iJ_1(\sin k_1-\sin k_2) & -J_1(1+\cos k_1+\cos k_2)-J_k \end{pmatrix}. \tag{9.24}$$

Now we can easily diagonalize the above Hamiltonian using

$$\begin{pmatrix} \alpha_k^x \\ \beta_k^x \end{pmatrix} = \begin{pmatrix} \cos\phi^x & -i\sin\phi^x \\ -i\sin\phi^x & \cos\phi^x \end{pmatrix}\begin{pmatrix} g_k^x \\ g_{-k}^{x\dagger} \end{pmatrix}$$

$$e^{2i\phi_k^x} = \frac{-(J_1 s_k + J_k e^{ik_1})}{4E_k^x} \qquad E_k^x = \frac{|J_1 s_k + J_k e^{ik_1}|\epsilon}{4}$$

$$\begin{pmatrix} \alpha_k^y \\ \beta_k^y \end{pmatrix} = \begin{pmatrix} \cos\phi^y & -i\sin\phi^y \\ -i\sin\phi^y & \cos\phi^y \end{pmatrix}\begin{pmatrix} g_k^y \\ g_{-k}^{y\dagger} \end{pmatrix}$$

$$e^{2i\phi_k^y} = \frac{-(J_1 s_k + J_k e^{-ik_2})}{4E_k^y} \qquad E_k^y = \frac{|J_1 s_k + J_k e^{-ik_2}|\epsilon}{4}$$

$$\begin{pmatrix} \alpha_k^z \\ \beta_k^z \end{pmatrix} = \begin{pmatrix} \cos\phi^z & -i\sin\phi^z \\ -i\sin\phi^z & \cos\phi^z \end{pmatrix}\begin{pmatrix} g_k^z \\ g_{-k}^{z\dagger} \end{pmatrix}$$

$$e^{2i\phi_k^z} = \frac{-(J_1 s_k + J_k)}{4E_k^x} \qquad E_k^x = \frac{|J_1 s_k + J_k|\epsilon}{4}$$

and hence

$$\mathcal{H}_b^x = \sum_k \left(\begin{array}{cc} \alpha_k^{x\dagger} & \beta_k^{x\dagger} \end{array} \right) \left(\begin{array}{cc} E_k^x & 0 \\ 0 & -E_k^x \end{array} \right) \left(\begin{array}{c} \alpha_k^x \\ \beta_k^{x\dagger} \end{array} \right) \tag{9.25}$$

$$= \sum_k E_k^x (2\alpha_k^{x\dagger}\alpha_k^x - 1) \tag{9.26}$$

$$\mathcal{H}_b^y = \sum_k \left(\begin{array}{cc} \alpha_k^{y\dagger} & \beta_k^{y\dagger} \end{array} \right) \left(\begin{array}{cc} E_k^y & 0 \\ 0 & -E_k^y \end{array} \right) \left(\begin{array}{c} \alpha_k^y \\ \beta_k^{y\dagger} \end{array} \right) \tag{9.27}$$

$$= \sum_k E_k^y (2\alpha_k^{y\dagger}\alpha_k^y - 1) \tag{9.28}$$

$$\mathcal{H}_b^z = \sum_k \left(\begin{array}{cc} \alpha_k^{z\dagger} & \beta_k^{z\dagger} \end{array} \right) \left(\begin{array}{cc} E_k^z & 0 \\ 0 & -E_k^z \end{array} \right) \left(\begin{array}{c} \alpha_k^z \\ \beta_k^{z\dagger} \end{array} \right) \tag{9.29}$$

$$= \sum_k E_k^z (2\alpha_k^{z\dagger}\alpha_k^z - 1) \tag{9.30}$$

with

$$\alpha_k^a(t) = \alpha_k^a(0)e^{-2iE_k^a t}; \quad \alpha_k^{a\dagger}(t) = \alpha_k^{a\dagger}(0)e^{2iE_k^a t}. \tag{9.31}$$

We digress the Raman operator as

$$iF(t) = \langle R(t)R(0)\rangle \tag{9.32}$$

$$= \sum_{i,l} \epsilon^{'2}\eta^2 \sum_{\alpha,\beta} m_\alpha m_\beta + \eta^2\langle R_c(t)R_c(0)\rangle + \epsilon^{'2}\langle R_b(t)R_b(0)\rangle$$

$$+ C_{xx}B_{xx} + C_{yy}B_{yy} + C_{zz}B_{zz}. \tag{9.33}$$

The first term is a constant and we just neglect that. The Raman operator R_c has the following contributions

$$R_c = R_c^k + R_c^h \tag{9.34}$$

The Kitaev contribution can be written as

$$R_c^k = -K \sum_{i_1,i_2} im_z c_{i_1,i_2,A} c_{i_1,i_2,B} + im_x c_{i_1,i_2,A} c_{i_1+1,i_2,B} + im_y c_{i_1,i_2,A} c_{i_1,i_2-1,B} \tag{9.35}$$

$$= -K \sum_k \begin{pmatrix} f_k^\dagger & f_{-k} \end{pmatrix} \begin{pmatrix} m_z + m_x \cos k_1 + m_y \cos k_2 & -i(m_x \sin k_1 - m_y \sin k_2) \\ i(m_x \sin k_1 - m_y \sin k_2) & -(m_z + m_x \cos k_1 + m_y \cos k_2) \end{pmatrix} \begin{pmatrix} f_k \\ f_{-k}^\dagger \end{pmatrix} \tag{9.36}$$

with $m_\alpha = (\boldsymbol{\epsilon}_{in} \cdot \mathbf{d}_\alpha)(\boldsymbol{\epsilon}_{out} \cdot \mathbf{d}_\alpha)$. Defining

$$m_1 = \mathrm{Re}\left(m_z + m_x e^{ik_1} + m_y e^{-ik_2}\right) = m_z + m_x \cos k_1 + m_y \cos k_2 \tag{9.37}$$

$$m_2 = \mathrm{Im}\left(m_z + m_x e^{ik_1} + m_y e^{-ik_2}\right) = (m_x \sin k_1 - m_y \sin k_2) \tag{9.38}$$

and since m_a is real, the Raman operator takes the form

$$R_c^k = -K \sum_k \begin{pmatrix} f_k^\dagger & f_{-k} \end{pmatrix} \begin{pmatrix} m_1 & -im_2 \\ im_2 & -m_1 \end{pmatrix} \begin{pmatrix} f_k \\ f_{-k}^\dagger \end{pmatrix} \tag{9.39}$$

$$= -K \sum_k \begin{pmatrix} \alpha_k^\dagger & \alpha_{-k} \end{pmatrix} \begin{pmatrix} \cos\theta & -i\sin\theta \\ -i\sin\theta & \cos\theta \end{pmatrix} \begin{pmatrix} m_1 & -im_2 \\ im_2 & -m_1 \end{pmatrix} \begin{pmatrix} \cos\theta & i\sin\theta \\ i\sin\theta & \cos\theta \end{pmatrix} \begin{pmatrix} \alpha_k \\ \alpha_{-k}^\dagger \end{pmatrix} \tag{9.40}$$

$$= -K \sum_k \begin{pmatrix} \alpha_k^\dagger & \alpha_{-k} \end{pmatrix} \begin{pmatrix} m_1 \cos 2\theta + m_2 \sin 2\theta & i(m_1 \sin 2\theta - m_2 \cos 2\theta) \\ -i(m_1 \sin 2\theta - m_2 \cos 2\theta) & -(m_1 \cos 2\theta + m_2 \sin 2\theta) \end{pmatrix} \begin{pmatrix} \alpha_k \\ \alpha_{-k}^\dagger \end{pmatrix} \tag{9.41}$$

which gives the full Raman operator to be

$$
\begin{aligned}
R_c^k(0) = -K \sum_q \Big\{&(m_1 \cos(2\theta_q) + m_2 \sin(2\theta_q))\alpha_q^\dagger(0)\alpha_q(0) + i(m_1 \sin(2\theta_q) \\
&-m_2 \cos(2\theta_q))\alpha_q^\dagger(0)\alpha_{-q}^\dagger(0) - i(m_1 \sin(2\theta_q) - m_2 \cos(2\theta_q))\alpha_{-q}(0)\alpha_q(0) \\
&-(m_1 \cos(2\theta_q) + m_2 \sin(2\theta_q))\alpha_{-q}(0)\alpha_{-q}^\dagger(0)\Big\} \qquad (9.42) \\
R_c^k(t) = -K \sum_q \Big\{&(m_1 \cos(2\theta_q) + m_2 \sin(2\theta_q))\alpha_q^\dagger(t)\alpha_q(t) + i(m_1 \sin(2\theta_q) \\
&-m_2 \cos(2\theta_q))\alpha_q^\dagger(t)\alpha_{-q}^\dagger(t) - i(m_1 \sin(2\theta_q) - m_2 \cos(2\theta_q))\alpha_{-q}(t)\alpha_q(t) \\
&-(m_1 \cos(2\theta_q) + m_2 \sin(2\theta_q))\alpha_{-q}(t)\alpha_{-q}^\dagger(t)\Big\}. \qquad (9.43)
\end{aligned}
$$

The terms that contribute to the Response function are

$$
\begin{aligned}
\langle \alpha_{-k}(t)\alpha_k(t)\alpha_q^\dagger(0)\alpha_{-q}^\dagger(0)\rangle &= e^{-4iE_k t}(-\delta_{k,-q} + \delta_{k,q}) \qquad (9.44) \\
\langle \alpha_{-k}(t)\alpha_{-k}^\dagger(t)\alpha_{-q}(0)\alpha_{-q}^\dagger(0)\rangle &= 1. \qquad (9.45)
\end{aligned}
$$

The second term gives a contribution that is independent of time and hence we shall neglect it thereby giving the final expression for the Raman response as

$$
\begin{aligned}
iF(t) = K^2 &\sum_{k,q} (m_{k1} \sin(2\theta_k) - m_{k2} \cos(2\theta_k))(m_{q1} \sin(2\theta_q) - m_{q2} \cos(2\theta_q)) \\
&\langle a_{-k}(t)a_k(t)a_q^\dagger(t)a_{-q}^\dagger(t)\rangle \qquad (9.46) \\
= K^2 &\sum_{k,q} (m_{k1} \sin(2\theta_k) - m_{k2} \cos(2\theta_k))(m_{q1} \sin(2\theta_q) - m_{q2} \cos(2\theta_q)) \\
&e^{-4iE_k t}(-\delta_{k,-q} + \delta_{k,q}) \qquad (9.47) \\
= 2K^2 &\sum_k (m_{k1} \sin(2\theta_k) - m_{k2} \cos(2\theta_k))^2 e^{-4iE_k t}. \qquad (9.48)
\end{aligned}
$$

Thus we get an analytical expression

$$iF(t) = 2\sum_k \left[\mathrm{Im}\left(-\sum_\alpha m_\alpha e^{ik.e_\alpha} e^{-2i\theta_k}\right)\right]^2 e^{-4iE_k t}. \tag{9.49}$$

The intensity contribution due to the above response is given as

$$\begin{aligned} I(\omega) &= \int dt e^{i\omega t} iF(t) &(9.50)\\ &= \int dt e^{i\omega t} 2\sum_k \left[\mathrm{Im}\left(-\sum_\alpha m_\alpha e^{ik.e_\alpha} e^{-2i\theta_k}\right)\right]^2 e^{-4iE_k t} &(9.51)\\ &= 2\sum_k \delta(\omega - 4E_k)\left[\mathrm{Im}\left(-\sum_\alpha m_\alpha e^{ik.e_\alpha} e^{-2i\theta_k}\right)\right]^2. &(9.52)\end{aligned}$$

One can compute in the similar fashion, the contribution to the Heisenberg term and the mixed Kitaev-Heisenberg type of terms as

$$\begin{aligned} I_c^h(\omega) &= 18K_1^2 \sum_k \delta(\omega - 4E_k)\left[\mathrm{Im}\left(-\sum_\alpha m_\alpha e^{ik.e_\alpha} e^{-2i\theta_k}\right)\right]^2 &(9.53)\\ I_c^{kh}(\omega) &= 6KK_1 \sum_k \delta(\omega - 4E_k)\left[\mathrm{Im}\left(-\sum_\alpha m_\alpha e^{ik.e_\alpha} e^{-2i\theta_k}\right)\right]^2 &(9.54)\\ I_c^{hk}(\omega) &= 6KK_1 \sum_k \delta(\omega - 4E_k)\left[\mathrm{Im}\left(-\sum_\alpha m_\alpha e^{ik.e_\alpha} e^{-2i\theta_k}\right)\right]^2. &(9.55)\end{aligned}$$

For the gauge sector on the other hand we get the following expressions:

$$I_b^k(\omega) = 2K^2 \sum_{k\alpha} \delta(\omega - 4E_k^\alpha) \left[\mathrm{Im}\left(-m_\alpha e^{ik.e_\alpha} e^{-2i\phi_k^\alpha}\right)\right]^2 \tag{9.56}$$

$$I_b^h(\omega) = 2K_1^2 \sum_{k\beta} \delta(\omega - 4E_k^\beta) \left[\mathrm{Im}\left(-\sum_\alpha m_\alpha e^{ik.e_\alpha} e^{-2i\phi_k^\beta}\right)\right]^2 \tag{9.57}$$

$$I_b^{kh}(\omega) = 2KK_1 \sum_{k\beta} \delta(\omega - 4E_k^\beta) \mathrm{Im}\left(-\sum_\alpha m_\alpha e^{ik.e_\alpha} e^{-2i\phi_k^\beta}\right) \mathrm{Im}\left(-n_\beta e^{ik.e_\beta} e^{-2i\phi_k^\beta}\right) \tag{9.58}$$

$$I_b^{hk}(\omega) = I_b^{kh}. \tag{9.59}$$

Finally we come to the non trivial contributions which lead to three $2D$ momentum summations.

$$\begin{aligned}
\sum_\alpha C_{\alpha\alpha} B_{\alpha\alpha} = &\sum_\alpha K^2 m_\alpha^2 \sum_{k,q,p,n} e^{-2iE_k t - 2iE_q t - 2iE_p^\alpha t - 2iE_n^\alpha t} \delta^2(k+q+p+n) \\
&(1 - e^{i(k_\alpha - q_\alpha)} e^{-2i\theta_k} e^{2i\theta_q})(1 - e^{i(p_\alpha - n_\alpha)} e^{-2i\phi_p^\alpha} e^{2i\phi_n^\alpha}) \\
&+ K_1^2 m_\alpha^2 \sum_{k,q,p,n} \delta^2(k+q+p+n)(1 - e^{i(k_\alpha - q_\alpha)} e^{-2i\theta_k} e^{2i\theta_q}) \\
&\left[e^{-2iE_k t - 2iE_q t - 2iE_p^x t - 2iE_n^x t}(1 - e^{i(p_\alpha - n_\alpha)} e^{-2i\phi_p^x} e^{2i\phi_n^x}) \right. \\
&+ e^{-2iE_k t - 2iE_q t - 2iE_p^y t - 2iE_n^y t}(1 - e^{i(p_\alpha - n_\alpha)} e^{-2i\phi_p^y} e^{2i\phi_n^y}) \\
&\left. + e^{-2iE_k t - 2iE_q t - 2iE_p^z t - 2iE_n^z t}(1 - e^{i(p_\alpha - n_\alpha)} e^{-2i\phi_p^z} e^{2i\phi_n^z})\right] \\
&+ KK_1 m_\alpha^2 \sum_{k,q,p,n} e^{-2iE_k t - 2iE_q t - 2iE_p t - 2iE_n t} \delta^2(k+q+p+n) \\
&(1 - e^{i(k_\alpha - q_\alpha)} e^{-2i\theta_k} e^{2i\theta_q})(1 - e^{i(p_\alpha - m_\alpha)} e^{-2i\phi_p^\alpha} e^{2i\phi_n^\alpha}).
\end{aligned} \tag{9.60}$$

There is still a time integration that needs to be done to get the intensity. These terms are orders of magnitude smaller when compared to the individual spinon and gauge contributions. Therefore to compute the Raman Intensity for the zigzag phase with short range correlations we neglect these and follow the algorithm.

1. Solve the mean field Hamiltonian and generate the parameters self consistently.

2. The dominant contribution to the Raman response comes from decoupled momentum k terms.

3. The Raman vertex for each k with the appropriate mean field parameters and the corresponding delta function for the frequency is generated and summed to obtain the dominant Raman Intensity.

9.2 Raman Response for the pure Kitaev Model

For $\phi = \frac{\pi}{2}$ and $\frac{3\pi}{2}$, that is at the pure Kitaev limit Eq:(9.1) the only term that contributes is $I_c^k(\omega)$. In Fig:(9.4), we plot the Raman intensity for the pure Kitaev model when the light is polarized along the A_{1g} direction. The broad Raman band signifies the presence of the spin liquid phase. The Raman intensity also shows a weak polarization dependence which occurs due to the fact that the ground state is a spin liquid. These are thus the key points that one must look for to detect the presence of spin liquids in experiments. The band width of the Raman intensity is proportional to the band width of the c sector density of states. At low energies around $\omega = 0$, the Raman intensity shows a linear behaviour which is a signature of the Dirac point. A dip is found at $\omega = 4J_k$ corresponding to the van-hove singularity point in the density of states of the c fermions.

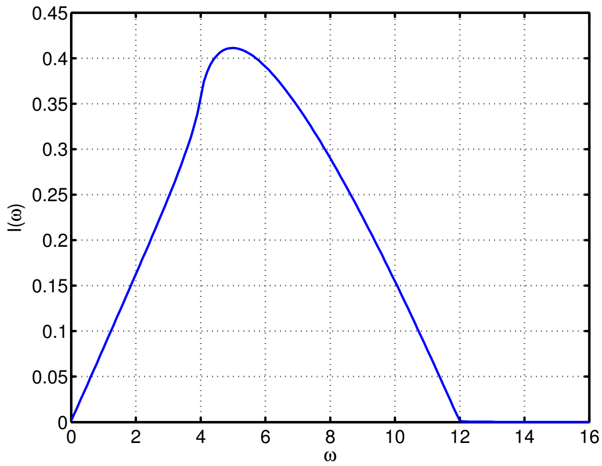

Figure 9.4: The Raman Intensity for the the ground state configuration of the pure Kitaev Model. The broad Raman band is a signature of the spin liquid phase.

9.3 Raman Intensity for the Kitaev-Heisenberg model

For the spin liquid state of Eq:(9.1) we find a broad polarization independent Raman spectrum qualitatively similar to that found in [12]. See Fig:(9.5). In this regime since the c and b fermions decouple, the band edge of the Raman intensity still depends on the c energy spectra. The b fermions are no longer static as in the case for the pure Kitaev model and the peak around $2J_k$ occurs due to the gap in the b spectra. Knolle *et al.*[12] find a delta function peak using perturbation theory at $\omega = 0.46J_k$. The width of our peak corresponds to the width of the b spectra. This peak feature comes from the Heisenberg contribution to the Raman operator and is hence proportional to $K_1/K-$ with no peak at $K_1 = 0$. The van-hove singularity dip point still persists but is shifted to $\omega = 3.7J_k$.

Fig.9.6 shows the Raman spectrum for $A = 1$ and $\phi = 101.5^o$, values which give zigzag phase close to spin liquid-zigzag boundary where Kitaev like spin correlations exist. We note that the broad Raman mode seen for the SL survives in the magnetic state as well. This explains the observation of the BRB below

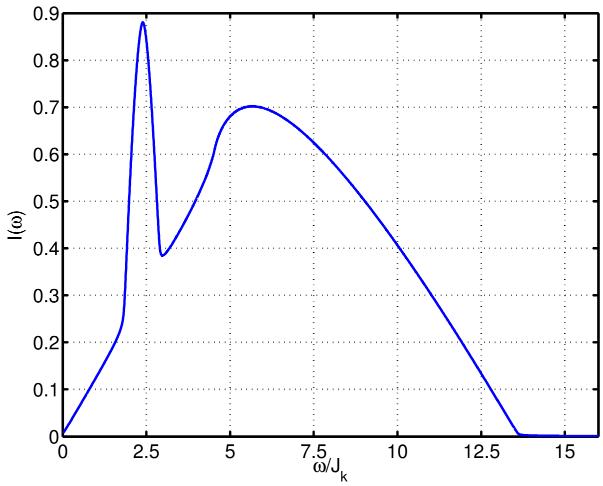

Figure 9.5: The Raman intensity in the spin liquid regime at $\phi = 101.4°$.

T$_N$ in the experiments [98]. It is worth mentioning that the experimental BRB looks more like the Raman response for the SL state than the Raman response for the magnetic state which shows some additional structure around 3.75 ω/J_K and 9 ω/J_K. The peak at 3.75 ω/J_K corresponds to the van Hove singularity point. We have also found that the Raman response does not change much even if an off-diagonal bond directional term ($\Gamma \approx 0.01$) is added like in Eq.(9.2). Thus the BRB survives in the magnetic state and in the presence of other small terms apart from the Kitaev term. An estimate for the strength of the Kitaev coupling can be found using the band centering of the experiments $2750cm^{-1}$, and the peak center from our theoretical calculations $6.1J_k$ to be $J_k \approx 57meV$. This estimate is much larger than the values estimated before in literature, $J_k = -2meV$ to $J_k = -17meV$ [80, 11, 36, 86]. However, it is consistent with the experimentally observed Weiss temperature.

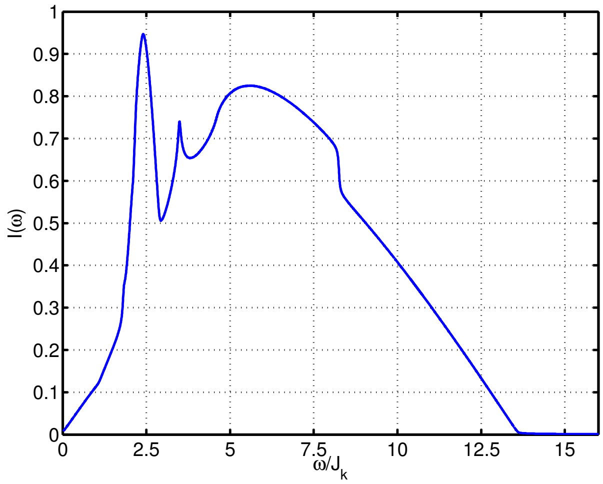

Figure 9.6: The Raman intensity in the zigzag phase with short range correlations close to the spin liquid boundary at $\phi = 101.5°$.

9.4 Summary and Discussion

Experiments[98] have shown the existence of a broad, polarization independent Raman band at high energies for single crystals of Na_2IrO_3. Similar observations have recently been made on another candidate Kitaev material α-$RuCl_3$. The observation of the BRB in that material was interpreted as resulting from proximity to the QSL phase in the strong Kitaev limit [95]. However, the real materials (both the iridates and the above ruthenate) are all magnetically ordered at low temperatures. Thus it was unclear whether this broad continuum, predicted for the SL state, would survive in the magnetically ordered state. We have shown using mean field calculations that the BRB, predicted for the SL state survives in the magnetically ordered state at least near the zigzag-SL phase boundary where the Na_2IrO_3 material is most likely situated [91]. The BRB predicted for the magnetic state acquires more structure compared to the BRB in the SL state. Our observed BRB resembles that predicted for the SL state more than it does for the magnetic phase. This suggests that Na_2IrO_3 is close to the QSL state and strong Kitaev correlations are present. From the position of the peak of the band, we make a first direct experimental estimate of the Kitaev interaction strength to be $J_K = 57$ meV. The fact that we observe the BRB well into the magnetically ordered state is consistent with recent diffuse RIXS observations which indicate that dynamical fluctuations, present above T_N, survive almost unchanged into the magnetic phase [91]. Finally, this suggests that these materials and their doped analog maybe better avenues to search for further proof for dominant Kitaev physics.

This concludes our work on the honeycomb sodium iridates. We now move on to the hyper-kagome sodium iridates which presents a different scenario altogether.

Chapter 10

Raman Response for the Hyperkagome Sodium Iridate

The moment you are ready to quit
is usually the moment right before
the miracle happens.

Unknown

There have been several attempts to arrive at a minimal spin model that would best describe $Na_4Ir_3O_8$ [113, 102, 103, 99, 114]. The search is still on. Hopkinson [113] worked on the nearest neighbour Heisenberg model, used large-N mean field theory and carried out Monte Carlo simulations on the $O(N)$ classical spin model. Hopkinson predicted a coplanar spin configuration to be the ground state at low temperatures. Lawler *et al.*(2008) [102] solved the same model numerically using large N $Sp(N)$ methods. Chen [99] suggested that the the anisotropic heisenberg model should be used when the iridate shows strong SO coupling and, alternatively, when the SO coupling is weak, the isotropic heisenberg model with DM interactions should be used. In most of these works predominantly the Heisenberg model on the hyper-kagome lattice has been explored. A recent study has explored the Kitaev-Heisenberg model on various lattices with edge shared octahedra including the hyperkagome lattice relevant for $Na_4Ir_3O_8$ [7]. This work is based on the Kitaev-Heisenberg model that seemed to work well on the honeycomb lattice Na_2IrO_3 compound. It is found that while the Kitaev spin-liquid exact solution doesn't generalize to the hyper-kagome lattice, a quantum phase with extensive degeneracy is found in both limits of strong Kitaev or strong Heisenberg, with a 3D stripy order in between [7]. The stripy magnetic order has clearly not been found in experiments on $Na_4Ir_3O_8$. However, most thermodynamic measurements suggest proximity to a spin liquid state. Which limit (Kitaev or Heisenberg) is more appropriate for the real material is thus still an open question. Experimentally, this compound has presented a huge challenge. Various groups have been working on obtaining a crystalline form of this compound as it quickly destabilizes and forms the more stable Na_2IrO_3 honeycomb compound. Therefore there is scope for exploring both the theoretical and experimental directions for $Na_4Ir_3O_8$ material.

In this chapter, we start by describing the hyper-kagome lattice. Drawing from the success of our previous work on the Kitaev-Heisenberg model on the honeycomb lattice, we study and compare the Kitaev model on the hyper-kagome with the honeycomb lattices. Finally, we analyse the Kitaev-Heisenberg model on the hyperkagome lattice, compute the Raman intensity in the spin liquid phase of the model and compare it with experiments.

10.1 The hyper-kagome lattice

The hyper-kagome lattice is a lattice in three dimensions which can be generated from the pyrochlore structure. A pyrochlore lattice is composed of tetrahedrons with a basis of four sites, and in a cube we have four such distinct tetrahedrons. Each site is connected to two tetrahedrons giving it a coordination number of six. One way to generate a hyper-kagome lattice is to keep removing lattice sites from the pyrochlore lattice. One atom from each of the tetrahedrons is removed in a consistent fashion so that each atom has four nearest neighbours. The lattice thus formed has a larger unit cell comprising of 12 sites, and forms corner-sharing equilateral triangles. This is the desired hyperkagome. Figure:(10.1) compares the hyperkagome and the pyrochlore lattices. A_i, B_i and C_i, $i = 1, 2, 3, 4$ represent the 12 distinct basis for the hyper-kagome lattice and A, B, C, D represent the basis sites for the pyrochlore lattice. The blue lines represent the connections of the triangles and the tetrahedrons for the hyper-kagome and pyrochlore lattices respectively. The red lines, on the other hand represent the connections arising from repeating the cell structure in all the dimensions.

10.2 Kitaev model on the hyper-kagome lattice

The general Kitaev model on the hyper-kagome lattice [7] is plotted in Fig:(10.2) with the colours indicating the three types of links x, y and z.

The honeycomb and the hyper-kagome lattices are quite different, and the differences manifest itself in areas beyond dimensional considerations. For example, the former has only 3 nearest neighbours while the latter has 4. The Kitaev model is exactly solvable on the honeycomb lattice but is not so on the hyper-

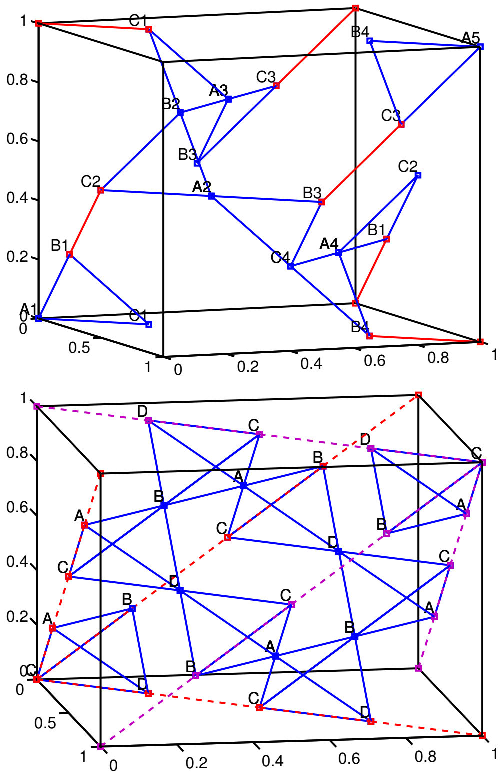

Figure 10.1: The hyper-kagome and pyrochlore lattices showing the unit cell and the location of the basis atoms.

kagome. Switching off all but one of the Kitaev links—this amounts to setting $J_x = J_y = 0$—the honeycomb becomes a disconnected set of 2 line segments while the hyper-kagome is such a set of 3 line segments. The electron hopping spectra for the honeycomb lattice is similar to c fermions hopping but the electron hopping for the hyper-kagome is rather different from the c fermion hopping spectra. In particular, electron hopping is not particle hole symmetric, whereas c fermion hopping is for the hyper-kagome.

The Kitaev spin Hamiltonian on the hyper-kagome lattice is given as:

$$
\begin{aligned}
\mathcal{H} = J_{kx} \sum_i \Big[& S^x_{R_i,A_1} S^x_{R_i+\frac{x+z}{4},B_1} + S^x_{R_i+\frac{x+z}{4},B_1} S^x_{R_i+\frac{x+z}{2},C_2} + S^x_{R_i+\frac{x+y}{4},C_1} S^x_{R_{i-1}+x+y+\frac{2x+y+3z}{4},B_2} \\
& + S^x_{R_i+\frac{3x+y+2z}{4},A_2} S^x_{R_i+\frac{2x+y+3z}{4},B_2} + S^x_{R_i+\frac{x+2y+3z}{4},A_3} S^x_{R_i+\frac{2y+2z}{4},B_3} + S^x_{R_i+\frac{2y+2z}{4},B_3} S^x_{R_{i-1}+y+z+\frac{3x+2y+z}{4},C_4} \\
& + S^x_{R_i+\frac{3y+3z}{4},C_3} S^x_{R_{i-1}+y+z+\frac{3x+3y+4z}{4},B_4} + S^x_{R_i+\frac{2x+3y+z}{4},A_4} S^x_{R_i+\frac{3x+3y}{4},B_4} \Big] \\
+ J_{ky} \sum_i \Big[& S^y_{R_i,A_1} S^y_{R_i+\frac{x+y}{4},C_1} + S^y_{R_i,A_1} S^y_{R_{i-1}+\frac{3x+3y+4z}{4},B_4} + S^y_{R_i+\frac{x+z}{4},B_1} S^y_{R_{i-1}+x+z+\frac{2x+3y+z}{4},A_4} \\
& + S^y_{R_i+\frac{3x+y+2z}{4},A_2} S^y_{R_i+\frac{2x+2z}{4},C_2} + S^y_{R_i+\frac{3x+y+2z}{4},A_2} S^y_{R_i+\frac{4x+2y+2z}{4},B_3} + S^y_{R_i+\frac{2x+y+3z}{4},B_2} S^y_{R_i+\frac{x+2y+3z}{4},A_3} \\
& + S^y_{R_i+\frac{x+2y+3z}{4},A_3} S^y_{R_i+\frac{3y+3z}{4},C_3} + S^y_{R_i+\frac{2x+3y+z}{4},A_4} S^y_{R_i+\frac{3x+2y+z}{4},C_4} \Big] \\
+ J_{kz} \sum_i \Big[& S^z_{R_i,A_1} S^z_{R_{i-1}+\frac{4x+3y+3z}{4},C_3} + S^z_{R_i+\frac{x+z}{4},B_1} S^z_{R_i+\frac{x+y}{4},C_1} + S^z_{R_i+\frac{x+y}{4},C_1} S^z_{R_{i-1}+x+y+\frac{x+2y+3z}{4},A_3} \\
& + S^z_{R_i+\frac{3x+y+2z}{4},A_2} S^z_{R_i+\frac{3x+2y+z}{4},C_4} + S^z_{R_i+\frac{2x+y+3z}{4},B_2} S^z_{R_i+\frac{2x+2z}{4},C_2} + S^z_{R_i+\frac{2x+2z}{4},C_2} S^z_{R_{i-1}+x+z+\frac{2x+3y+z}{4},A_4} \\
& + S^z_{R_i+\frac{2y+2z}{4},B_3} S^z_{R_i+\frac{3y+3z}{4},C_3} + S^z_{R_i+\frac{3x+3y}{4},B_4} S^z_{R_i+\frac{3x+2y+z}{4},C_4} \Big].
\end{aligned}
$$

from which the location of the basis sites can be extracted. With this prescription

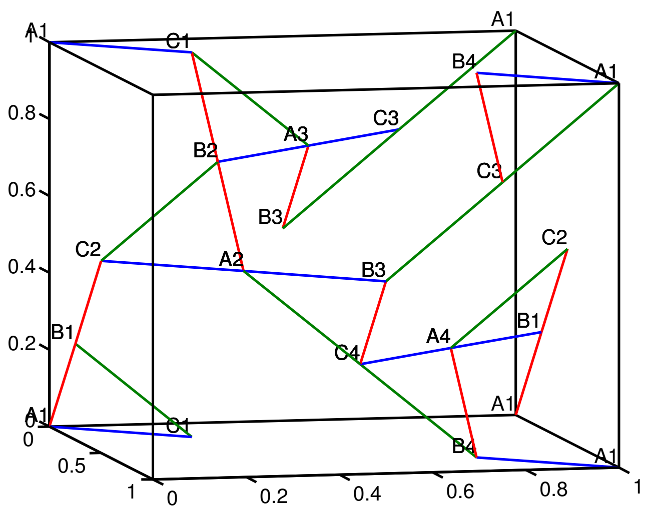

Figure 10.2: The Kitaev model on the hyper-kagome lattice

one can write the Kitaev-Heisenberg model on the hyper-kagome lattice to be

$$\mathcal{H} = \sum_{\langle ij \rangle^{\alpha}} J_{k\alpha} S_i^{\alpha} S_j^{\alpha} + J_1 \mathbf{S}_i \cdot \mathbf{S}_j. \tag{10.1}$$

Even though the Kitaev model is not exactly solvable on the hyper-kagome lattice, we can still resort to the Majorana fermion language discussed earlier in order to solve the model. At the Kitaev point the ground state is known to have high quantum degeneracy [7]. The mean field decoupling involves the nearest neighbour Majorana correlations alone

$$\sigma_i^{\alpha}\sigma_j^{\beta} = -ic_i c_j \; ib_i^{\alpha} b_j^{\beta} \approx -ic_i c_j B_{ij}^{\alpha\beta} - iC_{ij} b_i^{\alpha} b_j^{\beta} + C_{ij} B_{ij}^{\alpha\beta} \tag{10.2}$$

since this compound has not shown any order till date. For the self-consistency equations we have

$$B_{\langle ij \rangle^{\gamma}}^{\alpha\beta} \equiv \langle i b_i^{\alpha} b_{j^{\gamma}}^{\beta} \rangle \qquad\qquad C_{\langle ij \rangle^{\gamma}} \equiv \langle i c_i c_{j^{\gamma}} \rangle. \tag{10.3}$$

Fourier transforming the operators we get the effective decoupled Hamiltonian of the system to be

$$H_{MF} = H_{MF}^{b} + H_{MF}^{c} = \frac{1}{4} \sum_{k \in HBZ, \gamma} b_{\mathbf{k}\gamma}^{\alpha\dagger} h_{\mathbf{k}}^{b} b_{\mathbf{k}\gamma}^{\alpha} + c_{\mathbf{k}\gamma}^{\dagger} h_{\mathbf{k}}^{c} c_{\mathbf{k}\gamma}. \tag{10.4}$$

γ represents the sub-lattice indices. We define s_x, s_y and s_z matrices whose non-zero elements are:

```
sx = zeros(12);
sx(1,2) = iexp(i(kx+kz)); sx(2,6) = iexp(i(kx+kz));
sx(3,5) = iexp(i(kx-kz)); sx(4,5) = iexp(i(-kx+kz));
```

```
sx(7,8) = iexp(-i(kx+kz)); sx(8,12) = iexp(-i(kx+kz));
sx(9,11) = iexp(-i(kx-kz)); sx(10,11) = iexp(i(kx-kz));

sy = zeros(12);
sy(1,3) = iexp(i(kx+ky)); sy(1,11) = iexp(-i(kx+ky));
sy(2,10) = iexp(i(kx-ky)); sy(4,6) = iexp(-i(kx+ky));
sy(4,8) = iexp(i(kx+ky)); sy(5,7) = iexp(i(-kx+ky));
sy(7,9) = iexp(i(-kx+ky)); sy(10,12) = iexp(i(kx-ky));

sz = zeros(12);
sz(1,9) = iexp(-i(ky+kz)); sz(2,3) = iexp(i(ky-kz));
sz(3,7) = iexp(i(ky-kz)); sz(4,12) = iexp(i(ky-kz));
sz(5,6) = iexp(-i(ky+kz)); sz(6,10) = iexp(-i(ky+kz));
sz(8,9) = iexp(i(ky+kz)); sz(11,12) = iexp(-i(ky-kz));
```

with the matrices

$$h_{\mathbf{k}}^{c} = \sum_{\gamma}\left(B_{\gamma\gamma}J_{k\gamma} + \sum_{\delta} B_{\gamma\delta}J_1\right)s_{\gamma} + h.c. \tag{10.5}$$

$$h_{\mathbf{k}\gamma}^{b} = \left[(J_{k\gamma} + J_1)C_{\gamma}s_{\gamma} + \sum_{\gamma\neq\delta} J_1 C_{\delta}s_{\delta}\right] + h.c. \tag{10.6}$$

$k_i = \mathbf{k}\cdot\mathbf{e}_i$, $\mathbf{e}_i$ represents $\hat{x}$, $\hat{y}$ and $\hat{z}$ directions.

Consider the limit $J_1 = 0, J_{ky} = J_{kz} = 0$ and $J_{kx} = 1$. At this point we have disconnected line segments. One line segment is formed by A_1, B_1, C_2. The matrix structure of the c and b^x fermionic hamiltonians are the same and are given by

$$\mathcal{H}_c = J_{kx}B_{xx}\begin{pmatrix} 0 & ie^{i(k_x+k_z)} & 0 \\ -ie^{-i(k_x+k_z)} & 0 & ie^{i(k_x+k_z)} \\ 0 & -ie^{-i(k_x+k_z)} & 0 \end{pmatrix} \tag{10.7}$$

$$\mathcal{H}_{bx} = J_{kx}C_x\begin{pmatrix} 0 & ie^{i(k_x+k_z)} & 0 \\ -ie^{-i(k_x+k_z)} & 0 & ie^{i(k_x+k_z)} \\ 0 & -ie^{-i(k_x+k_z)} & 0 \end{pmatrix} \tag{10.8}$$

The eigenvalues are $-\sqrt{2}J_{kx}B_{xx}, 0, \sqrt{2}J_{kx}B_{xx}$ and $-\sqrt{2}J_{kx}C_x, 0, \sqrt{2}J_{kx}C_x$. The eigenvectors are actually independent of the mean field parameters and is given as

$$V = \begin{pmatrix} -\frac{1}{2}e^{2i(k_x+k_z)} & \frac{1}{\sqrt{2}}e^{2i(k_x+k_z)} & -\frac{1}{2}e^{2i(k_x+k_z)} \\ \frac{1}{\sqrt{2}}ie^{i(k_x+k_z)} & 0 & -\frac{1}{\sqrt{2}}ie^{i(k_x+k_z)} \\ \frac{1}{2} & \frac{1}{\sqrt{2}} & \frac{1}{2} \end{pmatrix} \tag{10.9}$$

The correlation function $C_x = \langle c_1 c_2 \rangle$ and $B_{xx} = \langle b_1^x b_2^x \rangle$ for which we get

$$C_x = i\sum_j \frac{e^{i(k_x+k_z)}V^\dagger_{j,1}V_{2,j} - e^{-i(k_x+k_z)}V^\dagger_{j,2}V_{1,j}}{e^{\beta E^c_j}+1} \tag{10.10}$$

For large $\beta = \frac{1}{T}$, i.e. small T, the state with positive energy will not contribute. The state with zero energy will not contribute as $V_{2,2} = 0$. The only contribution coming from the negative energy state is

$$C_x = i\left(e^{i(k_x+k_z)}V^{\dagger}_{1,1}V_{2,1} - e^{-i(k_x+k_z)}V^{\dagger}_{1,2}V_{1,1}\right) \tag{10.11}$$

$$= i\left(e^{i(k_x+k_z)}(-)\frac{1}{2}e^{-2i(k_x+k_z)}\frac{1}{\sqrt{2}}ie^{i(k_x+k_z)} - e^{-i(k_x+k_z)}(-)\frac{1}{\sqrt{2}}ie^{-i(k_x+k_z)}(-)\frac{1}{2}e^{2i(k_x+k_z)}\right) \tag{10.12}$$

$$= i\left(-\frac{1}{2\sqrt{2}}i - \frac{1}{2\sqrt{2}}i\right) = \frac{1}{\sqrt{2}} \tag{10.13}$$

which is independent of the momentum values. One can follow similar calculations and obtain the self consistent solutions: $C_z = B_{zz} = \pm\frac{1}{\sqrt{2}}$ with all other parameters zero. In the honeycomb scenario we get $C_z = B_{zz} = \pm 1$. This fact also indicates that the gauge sector, b, is not conserved for the hyper-kagome lattice.

Consider the isotropic Kitaev limit, $J_{kx} = 1, J_{ky} = 1, J_{kz} = 1$ with $J_1 = 0$, in which numerically we get the following mean field parameters

$$C_\alpha = 0.43, \qquad B^{\alpha}_{\alpha\alpha} = \frac{1}{\sqrt{2}}. \tag{10.14}$$

depicting that the c fermions are no longer static and develop a density of states. The density of states for the c fermions, spinons, on the hyper-kagome lattice is non-zero at half filling or at $\omega = 0$, meaning it has a fermi-surface compared to the linear density of states around the $\omega = 0$ due to the existence of Dirac points in the honeycomb lattice case. The spectra for the b sectors has three flat bands. In Fig:(10.3) we have plotted the density of states for the c sector alone. We have also plotted the electron hopping on the hyper-kagome lattice for comparison. The band width of both the density of states are different too. For the b sector we know that the density of states will be Dirac-δ peaks at the energies $-\sqrt{2}J_{kx}C_\alpha, 0, \sqrt{2}J_{k\alpha}C_\alpha$. The Kitaev-Heisenberg model on the hyperkagome lattice can be written as in Eq:(10.1) with an isotropic Kitaev model where $J_k = J_{kx} = J_{ky} = J_{kz} = 2A\sin\phi$ and $J_1 = A\cos\phi$. ϕ represents the ratio of the strengths of the Kitaev to Heisenberg coupling. In the presence of the Heisenberg term, the b spectra is no longer flat and gains a dispersion as expected. On the other hand the c density of states change slightly.

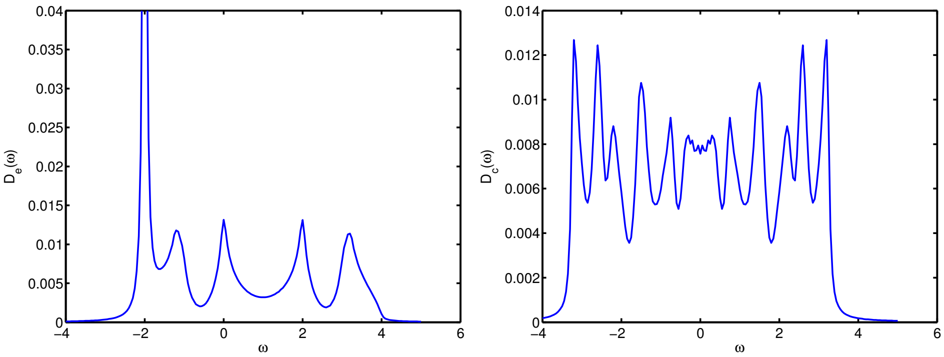

Figure 10.3: Density of states for nearest neighbour hopping for the electron and the c fermion on the hyper-kagome lattice (The c fermion corresponds to the pure Kitaev Model). The curves are not-normalized

The general mean field Hamiltonian written in momentum basis μ_k and ν_k^α becomes

$$H_{MF} = H_c + H_b + \sum_{\langle ij\rangle^\alpha}\left[J_k C_\alpha B_\alpha^{\alpha\alpha} + J_1\sum_\beta C_\alpha B_\alpha^{\beta\beta}\right] \tag{10.15}$$

$$H_c = \sum_{\langle ij\rangle^\alpha}\left[J_k\left[-ic_ic_jB_\alpha^{\alpha\alpha}\right] + J_1\sum_\beta\left[-ic_ic_jB_\alpha^{\beta\beta}\right]\right] = \sum_k \mu_k^\dagger\, h_k^c\, \mu_k \tag{10.16}$$

$$H_b = \sum_{\langle ij\rangle^\alpha}\left[J_k\left[-iC_\alpha b_i^\alpha b_j^\alpha\right] + J_1\sum_\beta\left[-iC_\alpha b_i^\beta b_j^\beta\right]\right] = \sum_{k\alpha} \nu_k^{\alpha\dagger}\, h_k^{b^\alpha}\, \nu_k^\alpha \tag{10.17}$$

Let M_k and N_k^α represent the unitary matrices that diagonalize h_k^c and $h_k^{b^\alpha}$ respectively giving the simplified hamiltonians

$$\mathcal{H}_c = \sum_k \mu_k^\dagger M_k \, (M_k^\dagger h_k^c M_k) \, M_k^\dagger \mu_k = \sum_k \left(f_k^\dagger, \; f_{-k}\right) \begin{pmatrix} E_k & 0 \\ 0 & -E_k \end{pmatrix} \begin{pmatrix} f_k \\ f_{-k}^\dagger \end{pmatrix} \tag{10.18}$$

$$= \sum_k E_k^a (2 f_k^{a\dagger} f_k^a - 1) \tag{10.19}$$

$$\mathcal{H}_b = \sum_{k\alpha} v_k^{\alpha\dagger} N_k^\alpha \, (N_k^{\alpha\dagger} h_k^{b\alpha} N_k^\alpha) \, N_k^{\alpha\dagger} v_k^\alpha = \sum_k \left(g_k^{\alpha\dagger}, \; g_{-k}^\alpha\right) \begin{pmatrix} E_k^\alpha & 0 \\ 0 & -E_k^\alpha \end{pmatrix} \begin{pmatrix} g_k^\alpha \\ g_{-k}^{\alpha\dagger} \end{pmatrix} \tag{10.20}$$

$$= \sum_{k\alpha} E_k^{a\alpha} (2 g_k^{a\alpha\dagger} g_k^{a\alpha} - 1) \tag{10.21}$$

where $a = 1, 2, \cdots 6$ and $\alpha = x, y, z$. The diagonal operators f_k and g_k^α and the eigenvalues E_k, E_k^α can be computed numerically. The single particle density of states for the spinons as shown in Fig.10.4(a) has a lot of features. On the other hand, the vison density of states as shown in Fig.10.4(b) has two peaks one centered around $\omega_{p1} = 0$ and the other around $\omega_{p2} = 1.5 J_k$. The ground state is $|GS\rangle = \Pi_{k,a,b,\alpha} f^a(\mathbf{k}) g^{b\alpha}(\mathbf{k}) |0\rangle$. These peaks play an important role in the Raman response of the system. The operators evolve as

$$f_k^a(t) = f_k^a(0) e^{-2iE_k^a t}; \qquad f_k^{a\dagger}(t) = f_k^{a\dagger}(0) e^{2iE_k^a t} \tag{10.22}$$

$$g_k^{a\alpha}(t) = g_k^{a\alpha}(0) e^{-2iE_k^{a\alpha} t}; \qquad g_k^{a\alpha\dagger}(t) = g_k^{a\alpha\dagger}(0) e^{2iE_k^{a\alpha} t} \tag{10.23}$$

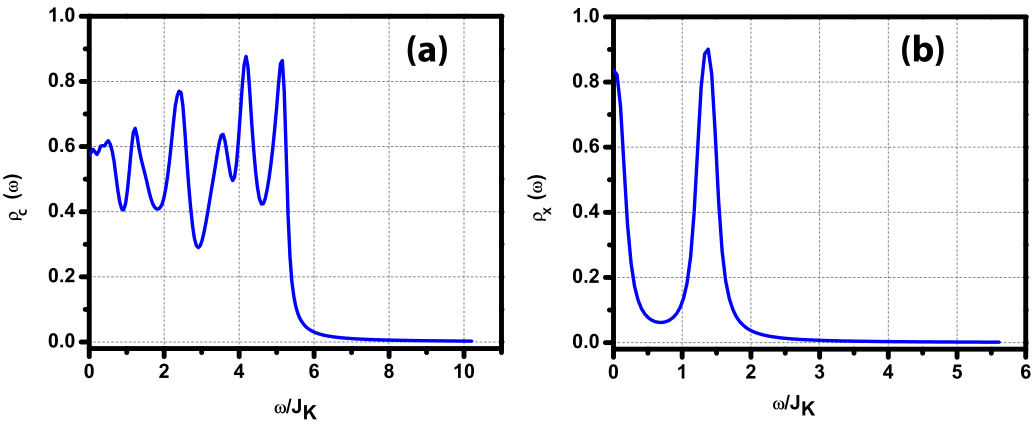

Figure 10.4: Density of states for the Spinon and Visons for the Kitaev model with small Heisenberg interaction $J_k = 1.96$, $J_1 = 0.2$ with $J_1/J_k \sim 0.1$. The curves have been normalized.

10.3 Raman Intensity calculations

Our focus is to understand the material based on Raman Intensity experiments. For the mean field ground state, the Raman Intensity is computed [98]

$$I(\omega) = \int dt\, e^{i\omega t}\, iF(t) = \int dt\, e^{i\omega t}\, \langle GS|R(t)R(0)|GS\rangle \tag{10.24}$$

where the Raman operator is given by[12]

$$R = \sum_{\langle ij\rangle\alpha} (\boldsymbol{\epsilon}_{in} \cdot \boldsymbol{d}^{\alpha})(\boldsymbol{\epsilon}_{out} \cdot \boldsymbol{d}^{\alpha})(KS_i^{\alpha}S_j^{\alpha} + K_1\mathbf{S}_i \cdot \mathbf{S}_j) = \sum_{\langle ij\rangle\alpha} m_{\alpha}(KS_i^{\alpha}S_j^{\alpha} + K_1\mathbf{S}_i \cdot \mathbf{S}_j) \tag{10.25}$$

$K \propto J_K$, $K_1 \propto J_H$, $\boldsymbol{\epsilon}_{in/out}$ correspond to the incoming and outgoing polarization directions respectively and $\boldsymbol{d}^{\alpha}$ the nearest neighbour bond vectors. The calculation for the response is illustrated for the pure Kitaev model as

$$iF(t) = K^2 \sum_{\langle ij\rangle\alpha} \sum_{\langle kl\rangle\beta} m_\alpha m_\beta \langle ic_i(t)c_j(t)ib_i^\alpha(t)b_j^\alpha(t)ic_k(0)c_l(0)ib_k^\beta(0)b_l^\beta(0)\rangle \tag{10.26}$$

$$= K^2 \sum_{\langle ij\rangle\alpha} \sum_{\langle kl\rangle\beta} m_\alpha m_\beta \langle ic_i(t)c_j(t)ic_k(0)c_l(0)\rangle\langle ib_i^\alpha(t)b_j^\alpha(t)ib_k^\beta(0)b_l^\beta(0)\rangle \tag{10.27}$$

In the spinon sector a correlation function can be expanded

$$\begin{aligned}\langle ic_i(t)c_j(t)ic_k(0)c_l(0)\rangle &= \langle ic_i(t)c_j(t)\rangle\langle ic_k(0)c_l(0)\rangle - \langle ic_i(t)c_k(0)\rangle\langle ic_j(t)c_l(0)\rangle \\ &+ \langle ic_i(t)c_l(0)\rangle\langle ic_j(t)c_k(0)\rangle\end{aligned} \tag{10.28}$$

From Eq:(10.3) the first term becomes a constant

$$\langle ic_i(t)c_j(t)\rangle = C_\gamma; \qquad \langle ic_k(0)c_l(0)\rangle = C_{\gamma'}. \tag{10.29}$$

Similar expressions for the vison sector can be obtained. Considering only the dominant time dependant contribution to the Raman intensity, the Raman operator becomes

$$\begin{aligned}iF(t) \approx\ & K^2 \sum_{\langle ij\rangle\alpha} \sum_{\langle kl\rangle\beta} m_\alpha m_\beta \langle ic_i(t)c_j(t)ic_k(0)c_l(0)\rangle B_\alpha^{\alpha\alpha} B_\beta^{\beta\beta} \\ &+ K^2 \sum_{\langle ij\rangle\alpha} \sum_{\langle kl\rangle\beta} m_\alpha m_\beta C_\alpha C_\beta \langle ib_i^\alpha(t)b_j^\alpha(t)ib_k^\beta(0)b_l^\beta(0)\rangle \qquad (10.30) \\ &= \langle R_c(t)R_c(0)\rangle + \langle R_b(t)R_b(0)\rangle \qquad (10.31)\end{aligned}$$

where R_c and R_b are the Raman operators in the spinons and visons alone and rewritten in the diagonal operators $f(\mathbf{k}), g^{\alpha}(\mathbf{k})$ as

$$R_c = K\sum_{\langle ij\rangle\alpha} m_\alpha i c_i c_j B^{\alpha\alpha}_{\alpha} = \sum_k \mu_k^\dagger \tilde{h}_k \mu_k = \sum_k \mu_k^\dagger M_k (M_k^\dagger \tilde{h}_k M_k) M_k^\dagger \mu_k \tag{10.32}$$

$$= \sum_k \left(f_k^\dagger,\ f_{-k}\right)\begin{pmatrix} F_1(\mathbf{k}) & F_2(\mathbf{k}) \\ F_2^\dagger(\mathbf{k}) & -F_1(\mathbf{k})\end{pmatrix}\begin{pmatrix} f_k \\ f_{-k}^\dagger\end{pmatrix} \tag{10.33}$$

$$= \sum_k F_1^{ab}(\mathbf{k}) f_k^{a\dagger} f_k^b + F_2^{ab}(\mathbf{k}) f_k^{a\dagger} f_{-k}^{b\dagger} + h.c. \tag{10.34}$$

$$R_b = K\sum_{\langle ij\rangle\alpha} m_\alpha C_\alpha i b_i^\alpha b_j^\alpha = \sum_{k\alpha} \nu_k^{\alpha\dagger} \tilde{h}_k^\alpha \nu_k^\alpha = \sum_{k\alpha} \nu_k^{\alpha\dagger} N_k^\alpha (N_k^{\alpha\dagger} \tilde{h}_k^\alpha N_k^\alpha) N_k^{\alpha\dagger} \nu_k^\alpha \tag{10.35}$$

$$= \sum_{k\alpha} \left(g_k^{\alpha\dagger},\ g_{-k}^\alpha\right)\begin{pmatrix} G_1^\alpha(\mathbf{k}) & G_2^\alpha(\mathbf{k}) \\ G_2^{\alpha\dagger}(\mathbf{k}) & -G_1^\alpha(\mathbf{k})\end{pmatrix}\begin{pmatrix} g_k^\alpha \\ g_{-k}^{\alpha\dagger}\end{pmatrix} \tag{10.36}$$

$$= \sum_{k\alpha} G_1^{ab\alpha}(\mathbf{k}) g_k^{a\alpha\dagger} g_k^{b\alpha} + G_2^{ab\alpha}(\mathbf{k}) g_k^{a\alpha\dagger} g_{-k}^{b\alpha\dagger} + h.c. \tag{10.37}$$

with the time evolution Eq:(10.22),(10.23). Therefore the dominant contribution to the intensity can be written as

$$I(\omega) \approx 2\pi \sum_{\mathbf{k},a,b} \delta(\omega - 2E^a(\mathbf{k}) - 2E^b(\mathbf{k}))\, |F_2^{ab}(\mathbf{k})|^2$$
$$+ 2\pi \sum_{\mathbf{k},a,b,\alpha} \delta(\omega - 2E^{a\alpha}(\mathbf{k}) - 2E^{b\alpha}(\mathbf{k}))\, |G_2^{ab\alpha}(\mathbf{k})|^2 \tag{10.38}$$
$$= -2Im\left[\sum_{\mathbf{k},a,b} \frac{1}{\omega - 2E^a(\mathbf{k}) - 2E^b(\mathbf{k}) + i\epsilon}\, |F_2^{ab}(\mathbf{k})|^2\right]$$
$$- 2Im\left[\sum_{\mathbf{k},a,b,\alpha} \frac{1}{\omega - 2E^{a\alpha}(\mathbf{k}) - 2E^{b\alpha}(\mathbf{k}) + i\epsilon}\, |G_2^{ab\alpha}(\mathbf{k})|^2\right] \tag{10.39}$$

where ϵ is the broadening parameter. The calculation can be easily extended to the Kitaev-Heisenberg model.

The Raman scattering experiments of $Na_4Ir_3O_8$ compound have been done using a powdered sample. It has been a difficult task to obtain a crystalline sample for this compound which would give information regarding the polarization dependence of the Raman scattering. We have the liberty to probe the polarization directions in our theoretical calculations, and have found weak polarization dependence. In Fig:(10.5) we plot the Raman Intensity for the pure Kitaev model with anti-ferromagnetic coupling corresponding to the A_{1g} and B_{1g} polarization directions for the broadening parameter $\epsilon = 0.1J_k$. The intensities of few of the frequency modes have been enhanced/diminished keeping the overall feature intact. Since the compound has a 3 dimensional structure, we test the true polarization independence by changing the planes of the incoming and outgoing photon from $X-Y$ to $X-Z$ and $Y-Z$. We find that the results do not change.

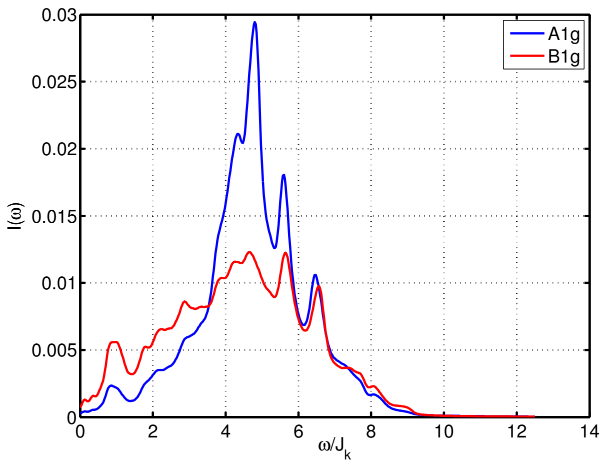

Figure 10.5: Comparison of the Raman Intensity for $\phi = 90^o$, the pure Kitaev model, along the A_{1g} and B_{1g} polarization directions for the broadening parameter $\epsilon = 0.1J_k$.

A broad Raman band, a feature of the quantum spin liquid, can be seen similar to the honeycomb lattice case. It increases as a function of ϕ. The Raman intensity is non-zero at $\omega = 0$ corresponding to the Fermi surface that exists in the spinon spectra of this system. In the honeycomb case, the Raman Intensity close to $\omega = 0$ goes linearly in ω due to the Dirac point structure.

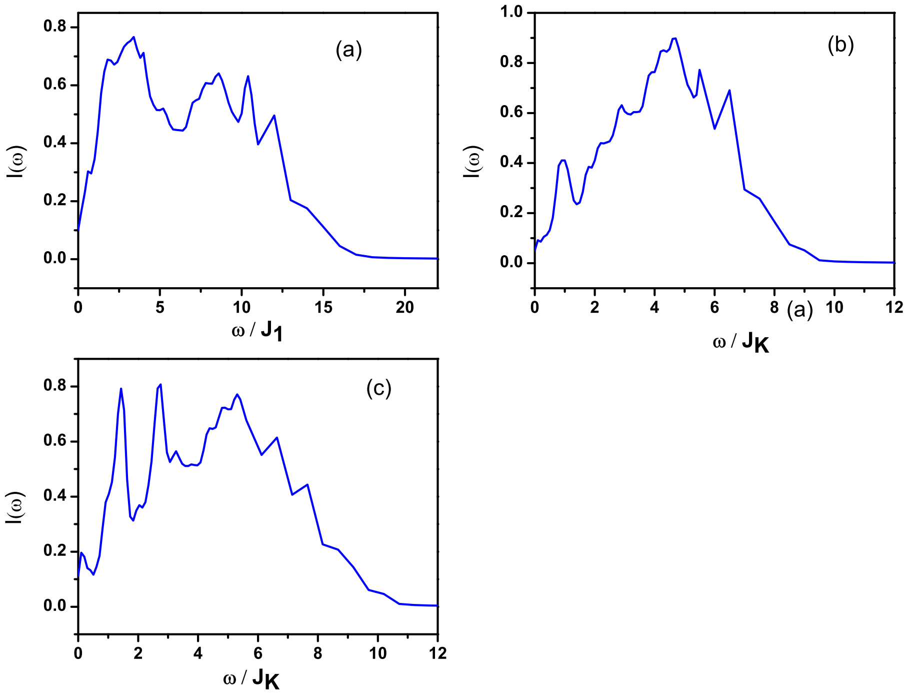

Figure 10.6: Theoretical curves: a) Pure Heisenberg model, b) Pure Kitaev model and c) Kitaev model with small Heisenberg interaction $J_k = 1.96$, $J_1 = 0.2$ with $J_1/J_k \sim 0.1$. The broadening used in (a) is $\epsilon = 0.2J_1$ while in (b) and (c), it is $\epsilon = 0.1J_K$.

We have studied both the extreme limits of purely Heisenberg exchange (no Kitaev) and purely Kitaev exchange. We have also studied the effect on the Raman response in these two limits of adding small perturbations of the other kind.

For broadening $\epsilon = 0.2J_1$ for pure Heisenberg , $\epsilon = 0.1J_K$ for pure Kitaev and both Kitaev and Heisenberg, the computed Raman response is given in Fig.10.6. The wiggles in the Raman response at lower broadening stems from those present in the spinon density of states shown in Fig.10.4(a). The two sharp peaks in Fig.10.6(c) occuring around $\omega = 1.5J_k$ and $\omega = 2.7J_k$, arises from the peaks in the vison density of states: around ω_{p2} and $2\omega_{p2}$.

Fig:(10.8) shows the experimentally obtained Raman Intensity curve. To match

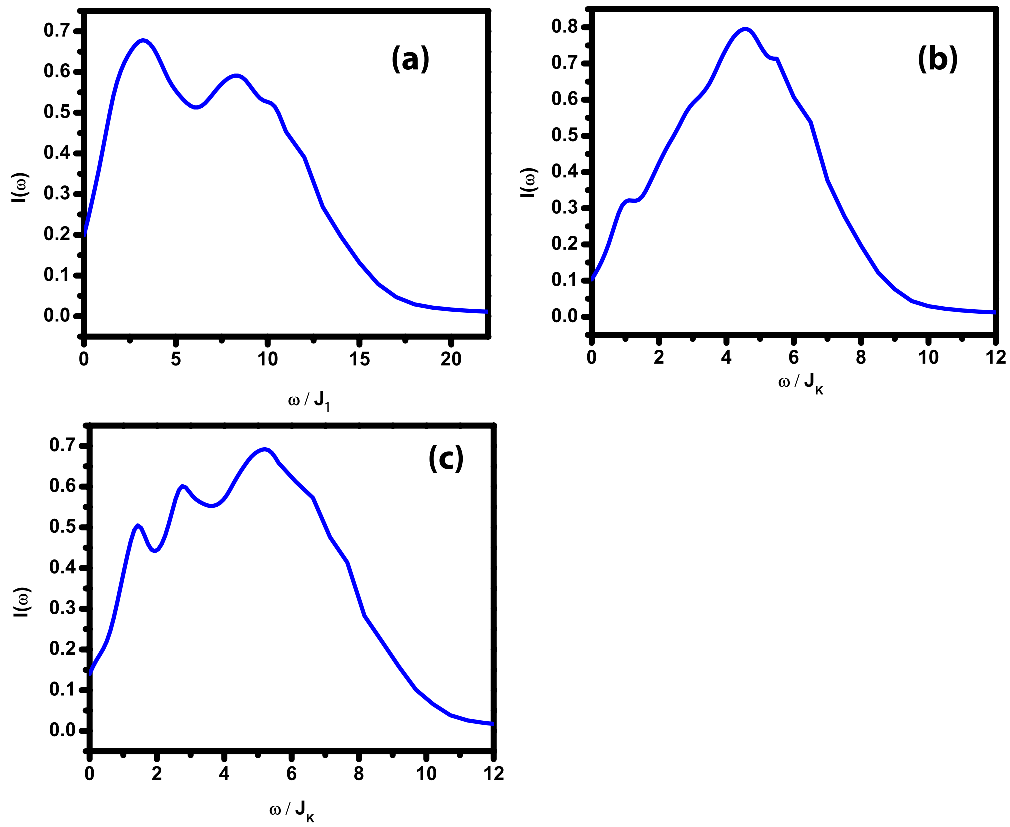

Figure 10.7: (Color online) Theoretical curves: a) Pure Heisenberg model, b) Pure Kitaev model and c) Kitaev model with small Heisenberg interaction $J_k = 1.96$, $J_1 = 0.2$ with $J_1/J_k \sim 0.1$. The broadening used is $\epsilon = 0.8$.

our theoretical curves better with the experiments, we increase the broadening parameter. The Raman response obtained from our theoretical calculations for the broadening parameter $\epsilon = 0.8J_1$ for pure Heisenberg , $\epsilon = 0.4J_K$ for pure Kitaev and both Kitaev and Heisenberg are shown in Fig. 10.7. We have studied both Heisenberg and Kitaev limits assuming a spin liquid ground state. The calculated Raman response for these two cases are shown in Figs. 10.7 (a) and (b). The Raman response of the pure (antiferomagnetic) Heisenberg limit shows a two peak structure arising due to the spinon and gauge sectors, with the lower energy peak being more intense, very different from the experimentally observed BRB in Fig. 10.8. On introducing small Kitaev perturbations the curves (not shown) do not vary. The calculated Raman response of the pure Kitaev model reveals a broad band similar to the experiments, but there are additional peaks (M4 and M5 modes) in the experimental data which need to be explained. On the addition of a small Heisenberg term ($J_1/J_K \sim 0.1$) as a perturbation to the Kitaev term we obtain a response shown in Fig. 10.7 (c) which looks a better match to the experimentally observed BRB. The calculated BRB is broad and has additional weak features at lower energies. It is thus clear that the Raman response calculated for the pure Heisenberg limit is inconsistent with our observed BRB while the strong Kitaev limit with small Heisenberg term gives results consistent with experiments. Comparing the experimental BRB with the theoretical results of Fig. 10.7 (c) we make an estimate of the strength of the Kitaev interactions to be $J_K \sim 75$ meV. This value is quite large but is consistent with the very large Weiss temperature of −650 K obtained from magnetic measurements [10, 115]. Taking $J_K = 75$ meV, the two additional weak features at $1.5J_K$ and $2.7J_K$ in the calculated BRB correspond to 920 cm^{-1} and 1650 cm^{-1} respectively which are close to the experimentally observed M4 (1395 cm^{-1}) and M5 (1580 cm^{-1}) modes (see Fig. 10.8).

10.4 Summary and Discussion

Raman response of high quality polycrystalline pellet samples of $Na_4Ir_3O_8$ were measured [13] and shown in Fig:(10.8). First order phonons are observed and a broad band with a maximum at ~ 3500 cm^{-1} and a band-width ~ 1700 cm^{-1}. The broad band has some additional structure in contrast to the featureless response found earlier for Na_2IrO_3 [98]. To understand these observations and to try to throw light on whether Heisenberg or Kitaev like interactions are dominant

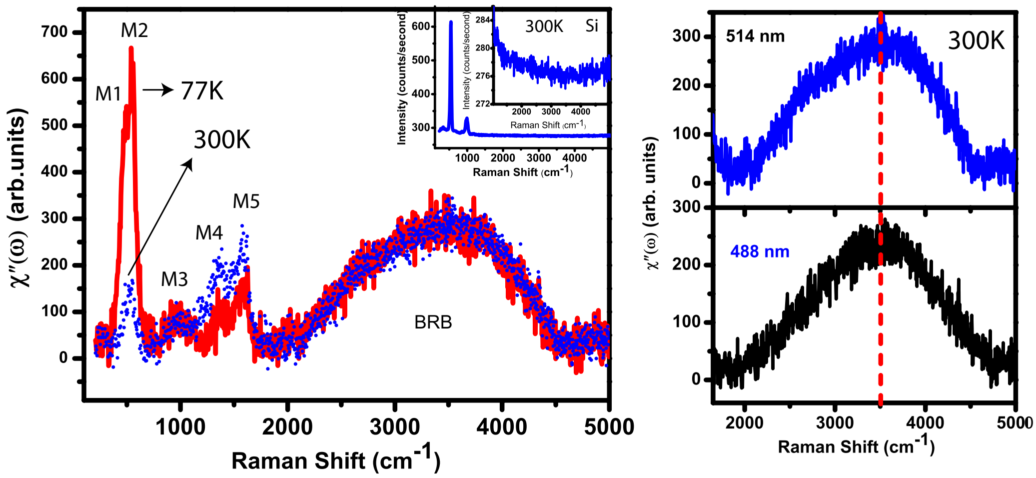

Figure 10.8: (a) Raman spectra of $Na_4Ir_3O_8$ measured at T = 77K (red line) and 300K (blue circles) in the spectral range 100 to 5000 cm^{-1} using excitation laser wavelength of 514.5 nm. Inset: Raman spectra of silicon at 300K. The sharp lines near 520 cm^{-1} and 1040 cm^{-1} are first and second order Raman modes of Si respectively. The magnified Si spectra from 1000 to 5000 cm^{-1} is shown in the inset. (b) Raman spectra recorded with two different laser excitation lines 514.5 and 488 nm. The vertical dashed line shows the center of the BRB[13].

in $Na_4Ir_3O_8$, we have computed the Raman response for the nearest-neighbour Kitaev-Heisenberg model in both the strong Heisenberg and Kitaev limits. The Raman response was calculated using the Majorana mean field framework assuming a spin liquid ground state for both limits. For the Heisenberg limit we find two peaks which do not match the experimentally observed Raman response. Even on introducing small Kitaev terms as perturbation doesn't give results which match experiments. For the pure Kitaev limit we obtain a broad band response. There are however, additional features in the experiments which suggest the presence of other terms. Hence we finally added small Heisenberg terms ($J_1/J_K \sim 0.1$) and find that additional peaks which develop, match the experimental observations. Although the Kitaev limit is not exactly solvable for the hyperkagome lattice we find a spin-liquid state for the parameters used to calculate the Raman response which match the experiments. These results strongly indicate that $Na_4Ir_3O_8$ is a spin liquid driven by strong Kitaev interactions but with Heisenberg coupling present.

Chapter 11

Conclusion

It always seems impossible until it's done.

Nelson Mandela

In the first part of the thesis we have mainly concentrated on understanding a Hubbard model that has spin-dependent hopping on a honeycomb lattice; we call this the Kitaev-Hubbard model. This model in general does not preserve time-reversal symmetry, and was initially introduced in order to realize the Kitaev model in optical lattice systems. The non-interacting limit of the Kitaev-Hubbard model shows interesting merging and emerging Dirac point physics. This signals a topological Lifshitz transition due to the change in the Fermi surface topology. The density of states shows a sharp behavioural change at these transition points. We carried out numerical simulations for Bloch-Zener oscillations of the model which probe the Dirac points. We numerically computed properties such as the Pancharatnam-Berry curvature.

Another highlight of the model is a stable algebraic spin liquid (ASL) phase. We established its “algebraic nature” by showing that the spin-spin correlation decays as a power law. Since spin liquids are generally susceptible to perturbations, their stability needs to be ensured. In our model, time-reversal symmetry for the Mott phase is sufficient for stability. Using perturbative canonical unitary transformations (PCUT) we computed the effective spin model in the large U limit for 14 site cluster (from 2-14 sites compatible with honeycomb lattice) and found that it contains an even number of spin operators. Based on this, and using the charge conjugation operator, we proved that the effective spin model will be time reversal symmetric for all orders of perturbation theory. We also performed a Majorana mean field calculation to eliminate the possibility of spontaneous time reversal symmetry breaking which leads to chiral spin liquid phase.

In the second part of the thesis we have worked on the Kitaev-Heisenberg model which has been a strong contender for studying the properties of iridate materials, especially Na_2IrO_3 and $Na_4Ir_3O_8$, the former having a honeycomb lattice and the latter a hyper-kagome lattice. Na_2IrO_3 compounds are known to be magnetically ordered and show residual spin liquid behaviour at high temperatures whereas no order has been seen yet in $Na_4Ir_3O_8$. The effectiveness of the Kitaev-Heisenberg in describing iridates has been questioned in recent times, and evidence has emerged that indicate that the presence of additional bond-directional terms is essential.

Our work on Majorana mean-field decoupling of the honeycomb lattice Iridate model has uncovered a transition between a spin liquid phase and a zigzag phase. In the zigzag phase, a region exists where short-range Majorana correlations exist. It was in this regime, close to the spin liquid boundary, that we computed the Raman Response for the model at zero temperature and found a broad band which is a signature of short range correlations. For the hyper-kagome lattice on the other hand, we studied the Raman Response in the spin liquid regime of the Kitaev-Heisenberg model and find a polarization independent broad band. We also estimated the strength of the Kitaev term J_k using the Raman response. We found our results to be in good agreement with the experiments.

11.1 Future Work

Our calculations on the Kitaev-Hubbard model showed that there is a topological transition from an anti-ferromagnetic insulator to an algebraic spin liquid phase in this model. The nature of the underlying collective excitations in the spin liquid phase (spinons) is very different compared to the magnetic phases (magnons). To understand the nature of the quasi-particles, we would first write down a topological field theory for the Kitaev-Hubbard model in the path-integral notation and compute the saddle point mean-field solution for this system. This would help us in deriving an effective field theory for the low energy modes of the model in the large U limit. We would then introduce slowly varying fields close to the saddle point solution, that is the mean-field solution so that the study of the effects of quantum fluctuations becomes viable. This formalism would result in the non-linear σ model for the quantum fluctuations of the Néel anti-ferromagnetic phase. We would finally compute the theory for the algebraic spin liquid phase and would expect to see a Hopf term in the non-linear σ model due to the breaking of time-reversal symmetry.

We have worked on computing the Raman response for iridate compounds. Two important aspects we have not probed at all – one is the finite temperature effects and the second is *Li* doping effects. We would like to study these and uncover the true nature of the Raman response and compare them with experimental results.

We would also like to extend our calculations to include the effect of fluctuations to achieve results comparable with previous attempts.

Appendices

Appendix A

Appendix

A.1 PCUT: Second Order Calculations

Now that we have the definitions let us first compute the second order spin Hamiltonian for the z link. We have the following expressions

$$-T^{\dagger}T|\uparrow,\downarrow\rangle = -T^{\dagger}\frac{1}{2}(t+t_z)|0,\uparrow\downarrow\rangle - T^{\dagger}\frac{1}{2}(t-t_z)|\uparrow\downarrow,0\rangle \tag{A.1}$$

$$= -\frac{1}{2}(t+t_z)T^{\dagger}|0,\uparrow\downarrow\rangle - \frac{1}{2}(t-t_z)T^{\dagger}|\uparrow\downarrow,0\rangle \tag{A.2}$$

$$= -\frac{1}{2}(t+t_z)(\frac{1}{2}(t+t_z)|\uparrow,\downarrow\rangle - \frac{1}{2}(t-t_z)|\downarrow,\uparrow\rangle) \tag{A.3}$$

$$-\frac{1}{2}(t-t_z)(\frac{1}{2}(t-t_z)|\uparrow,\downarrow\rangle - \frac{1}{2}(t+t_z)|\downarrow,\uparrow\rangle) \tag{A.4}$$

$$= -\frac{1}{4}((t+t_z)^2 + (t-t_z)^2)|\uparrow,\downarrow\rangle + \frac{1}{2}(t^2 - t_z^2)|\downarrow,\uparrow\rangle \tag{A.5}$$

$$= -\frac{1}{2}(t^2 + t_z^2)|\uparrow,\downarrow\rangle + \frac{1}{2}(t^2 - t_z^2)|\downarrow,\uparrow\rangle \tag{A.6}$$

Similarly we can write

$$-T^{\dagger}T|\downarrow,\uparrow\rangle = \frac{1}{2}(t^2 - t_z^2)|\uparrow,\downarrow\rangle - \frac{1}{2}(t^2 + t_z^2)|\downarrow,\uparrow\rangle \tag{A.7}$$

A.2 PCUT: Fourth order

Consider a three site open chain where 1 and 2 are connected by the z link and 2 and 3 by x link. See Fig:(A.1). Three sites of this form and the symmetry of the Hamiltonian is enough to determine the effective Hamiltonian for the full lattice. The expression for the fourth order effective Hamiltonian as computed before is given as

$$H^{(4)} = \frac{1}{U^3}(T^{\dagger}TT^{\dagger}T - T^{\dagger}T_0T_0T - \frac{1}{2}T^{\dagger}T^{\dagger}TT) \tag{A.8}$$

The last term of the above expression does not contribute to the three site case

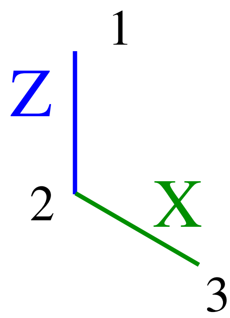

Figure A.1: Three site cluster for PCUT.

that we have started with. This is because three site half filled case has three fermions whereas the last term minimally requires four fermions. We need to compute the first two expressions part by part so let us start with

$$
\begin{aligned}
T^{\dagger}_{12}T_{12}T^{\dagger}_{12}T_{12} = &\left[-\frac{1}{4}(t^2+t_z^2)\sigma_1^0\sigma_2^0+\frac{1}{4}(t^2+t_z^2)\sigma_1^z\sigma_2^z+\frac{1}{4}(t^2-t_z^2)\sigma_1^x\sigma_2^x+\frac{1}{4}(t^2-t_z^2)\sigma_1^y\sigma_2^y\right]\\
&\left[-\frac{1}{4}(t^2+t_z^2)\sigma_1^0\sigma_2^0+\frac{1}{4}(t^2+t_z^2)\sigma_1^z\sigma_2^z+\frac{1}{4}(t^2-t_z^2)\sigma_1^x\sigma_2^x+\frac{1}{4}(t^2-t_z^2)\sigma_1^y\sigma_2^y\right]\\
&= -\frac{1}{8}((t^2+t_z^2)^2+(t^2-t_z^2)^2)\sigma_1^z\sigma_2^z-\frac{1}{4}(t^4-t_z^4)\sigma_1^x\sigma_2^x-\frac{1}{4}(t^4-t_z^4)\sigma_1^y\sigma_2^y\\
&= -(t^4+t_z^4)S_1^zS_2^z-(t^4-t_z^4)S_1^xS_2^x-(t^4-t_z^4)S_1^yS_2^y
\end{aligned}
$$

Similarly we get

$$
T^{\dagger}_{23}T_{23}T^{\dagger}_{23}T_{23} = -(t^4+t_x^4)S_2^xS_3^x-(t^4-t_x^4)S_2^yS_3^y-(t^4-t_x^4)S_2^zS_3^z
$$

Now there are two more terms in this type

$$
\begin{aligned}
T^{\dagger}_{12}T_{12}T^{\dagger}_{23}T_{23} = &\left[-\frac{1}{4}(t^2+t_z^2)\sigma_1^0\sigma_2^0+\frac{1}{4}(t^2+t_z^2)\sigma_1^z\sigma_2^z+\frac{1}{4}(t^2-t_z^2)\sigma_1^x\sigma_2^x+\frac{1}{4}(t^2-t_z^2)\sigma_1^y\sigma_2^y\right]\\
&\left[-\frac{1}{4}(t^2+t_x^2)\sigma_2^0\sigma_3^0+\frac{1}{4}(t^2+t_x^2)\sigma_2^x\sigma_3^x+\frac{1}{4}(t^2-t_x^2)\sigma_2^y\sigma_3^y+\frac{1}{4}(t^2-t_x^2)\sigma_2^z\sigma_3^z\right]\\
&= -\frac{1}{16}(t^2+t_z^2)(t^2+t_x^2)\sigma_1^z\sigma_2^z-\frac{1}{16}(t^2-t_z^2)(t^2+t_x^2)\sigma_1^x\sigma_2^x-\frac{1}{16}(t^2-t_z^2)(t^2+t_x^2)\sigma_1^y\sigma_2^y\\
&-\frac{1}{16}(t^2+t_x^2)(t^2+t_z^2)\sigma_2^x\sigma_3^x-\frac{1}{16}(t^2-t_x^2)(t^2+t_z^2)\sigma_2^y\sigma_3^y-\frac{1}{16}(t^2-t_x^2)(t^2+t_z^2)\sigma_2^z\sigma_3^z\\
&+\frac{1}{16}(t^2-t_z^2)(t^2+t_x^2)\sigma_1^x\sigma_3^x+\frac{1}{16}(t^2+t_z^2)(t^2-t_x^2)\sigma_1^z\sigma_3^z+\frac{1}{16}(t^2-t_z^2)(t^2-t_x^2)\sigma_1^y\sigma_3^y\\
&= -\frac{1}{4}(t^2+t_z^2)(t^2+t_x^2)S_1^zS_2^z-\frac{1}{4}(t^2-t_z^2)(t^2+t_x^2)S_1^xS_2^x-\frac{1}{4}(t^2-t_z^2)(t^2+t_x^2)S_1^yS_2^y\\
&-\frac{1}{4}(t^2+t_x^2)(t^2+t_z^2)S_2^xS_3^x-\frac{1}{4}(t^2-t_x^2)(t^2+t_z^2)S_2^yS_3^y-\frac{1}{4}(t^2-t_x^2)(t^2+t_z^2)S_2^zS_3^z\\
&+\frac{1}{4}(t^2-t_z^2)(t^2+t_x^2)S_1^xS_3^x+\frac{1}{4}(t^2+t_z^2)(t^2-t_x^2)S_1^zS_3^z+\frac{1}{4}(t^2-t_z^2)(t^2-t_x^2)S_1^yS_3^y
\end{aligned}
$$

In the above expression some three spin terms are generated which get cancelled when combined with the hermitian partner of the above term $T^{\dagger}_{23}T_{23}T^{\dagger}_{12}T_{12}$ and hence we dont write the three spin terms. Now for the hermitian conjugate term we have

$$T^{\dagger}_{23}T_{23}T^{\dagger}_{12}T_{12} = -\frac{1}{4}(t^2+t_z^2)(t^2+t_x^2)S^z_1S^z_2 - \frac{1}{4}(t^2-t_z^2)(t^2+t_x^2)S^x_1S^x_2 - \frac{1}{4}(t^2-t_z^2)(t^2+t_x^2)S^y_1S^y_2$$
$$- \frac{1}{4}(t^2+t_x^2)(t^2+t_z^2)S^x_2S^x_3 - \frac{1}{4}(t^2-t_x^2)(t^2+t_z^2)S^y_2S^y_3 - \frac{1}{4}(t^2-t_x^2)(t^2+t_z^2)S^z_2S^z_3$$
$$+ \frac{1}{4}(t^2-t_z^2)(t^2+t_x^2)S^x_1S^x_3 + \frac{1}{4}(t^2+t_z^2)(t^2-t_x^2)S^z_1S^z_3 + \frac{1}{4}(t^2-t_z^2)(t^2-t_x^2)S^y_1S^y_3$$

This completes the calculation of the effective Hamiltonian of the first term. For the next term the final operation

$$-T^{\dagger}_{12}T^0_{23}T^0_{23}T_{12}|\uparrow,\downarrow,\uparrow\rangle = -\frac{(t^2+t_x^2)}{8}(t^2+t_z^2)|\uparrow,\downarrow,\uparrow\rangle + \frac{(t^2+t_x^2)}{8}(t^2-t_z^2)|\downarrow,\uparrow,\uparrow\rangle + \frac{t^2t_xt_z}{2}|\uparrow,\downarrow,\downarrow\rangle$$
$$-T^{\dagger}_{12}T^0_{23}T^0_{23}T_{12}|\uparrow,\downarrow,\downarrow\rangle = \frac{t^2t_xt_z}{2}|\uparrow,\downarrow,\uparrow\rangle - \frac{(t^2+t_x^2)}{8}(t^2+t_z^2)|\uparrow,\downarrow,\downarrow\rangle + \frac{(t^2+t_x^2)}{8}(t^2-t_z^2)|\downarrow,\uparrow,\downarrow\rangle$$
$$-T^{\dagger}_{12}T^0_{23}T^0_{23}T_{12}|\downarrow,\uparrow,\uparrow\rangle = -\frac{1}{8}(t^2+t_x^2)(t^2+t_z^2)|\downarrow,\uparrow,\uparrow\rangle - \frac{t^2t_xt_z}{2}|\downarrow,\uparrow,\downarrow\rangle + \frac{1}{8}(t^2+t_x^2)(t^2-t_z^2)|\uparrow,\downarrow,\uparrow\rangle$$
$$-T^{\dagger}_{12}T^0_{23}T^0_{23}T_{12}|\downarrow,\uparrow,\downarrow\rangle = -\frac{t^2t_zt_x}{2}|\downarrow,\uparrow,\uparrow\rangle + \frac{t^2+t_x^2}{8}(t^2-t_z^2)|\uparrow,\downarrow,\downarrow\rangle - \frac{t^2+t_x^2}{8}(t^2+t_z^2)|\downarrow,\uparrow,\downarrow\rangle$$

which when converted to spin basis is given as

$$H^{(4)} = -\frac{(t^4+t_z^4)}{4}\sigma^z_1\sigma^z_2 - \frac{(t^4+t_x^4)}{4}\sigma^x_2\sigma^x_3 + \frac{3t^2t_xt_z}{4}\sigma^z_1\sigma^x_3$$
$$- \frac{(t^2-t_z^4)}{4}(\sigma^x_1\sigma^x_2+\sigma^y_1\sigma^y_2) - \frac{(t^2-t_x^4)}{4}(\sigma^y_2\sigma^y_3+\sigma^z_2\sigma^z_3)$$
$$- \frac{t^2t_xt_z}{2}(\sigma^z_1\sigma^x_2+\sigma^z_2\sigma^x_3) + \frac{(t^2-t_z^2)(t^2-t_x^2)}{16}\sigma^y_1\sigma^y_3$$
$$+ \frac{(t^2-t_z^2)(t^2+t_x^2)}{16}\sigma^x_1\sigma^x_3 + \frac{(t^2+t_z^2)(t^2-t_x^2)}{16}\sigma^z_1\sigma^z_3$$

which finally gives the effective fourth order spin Hamiltonian.

A.3 PCUT: Numerical 6th order

For a six site plaquette with periodic boundary as shown in Fig:(A.2) on the honeycomb lattice we compute the sixth order effective Hamiltonian.

$$\mathcal{H}^6 =$$

$$(t/U)^6\Big[-20.95 + 23.94S_1^xS_2^x + 13.19S_1^yS_2^x + 11.44S_1^zS_2^x + 13.19S_1^xS_2^y + 23.94S_1^yS_2^y$$

$$+ 11.44S_1^zS_2^y + 11.44S_1^xS_2^z + 11.44S_1^yS_2^z + 21.31S_1^zS_2^z - 12.44S_1^xS_3^x - 11.81S_1^yS_3^x$$

$$- 13.56S_1^zS_3^x + 21.31S_2^xS_3^x + 11.44S_2^yS_3^x + 11.44S_2^zS_3^x - 13.56S_1^xS_3^y - 12.44S_1^yS_3^y$$

$$- 11.81S_1^zS_3^y + 11.44S_2^xS_3^y + 23.94S_2^yS_3^y + 13.19S_2^zS_3^y - 11.81S_1^xS_3^z - 13.56S_1^yS_3^z$$

$$- 12.44S_1^zS_3^z + 11.44S_2^xS_3^z + 13.19S_2^yS_3^z + 23.94S_2^zS_3^z + 21.31S_1^xS_4^x + 11.44S_1^yS_4^x$$

$$+ 11.44S_1^zS_4^x - 12.44S_2^xS_4^x - 11.81S_2^yS_4^x - 13.56S_2^zS_4^x + 23.94S_3^xS_4^x - 39.25S_1^xS_2^xS_3^xS_4^x$$

$$- 14.25S_1^yS_2^xS_3^xS_4^x - 43.25S_1^zS_2^xS_3^xS_4^x - 14.25S_1^xS_2^yS_3^xS_4^x$$

$$- 32.25S_1^yS_2^yS_3^xS_4^x - 14.75S_1^zS_2^yS_3^xS_4^x - 43.25S_1^xS_2^zS_3^xS_4^x$$

$$- 14.75S_1^yS_2^zS_3^xS_4^x - 83.75S_1^zS_2^zS_3^xS_4^x + 11.44S_3^yS_4^x - 43.25S_1^xS_2^xS_3^yS_4^x - 9.25S_1^yS_2^xS_3^yS_4^x$$

$$- 25.75S_1^zS_2^xS_3^yS_4^x - 24.75S_1^xS_2^yS_3^yS_4^x - 36.25S_1^yS_2^yS_3^yS_4^x - 23.25S_1^zS_2^yS_3^yS_4^x$$

$$- 76.75S_1^xS_2^zS_3^yS_4^x - 21.25S_1^yS_2^zS_3^yS_4^x - 39.75S_1^zS_2^zS_3^yS_4^x$$

$$+ 13.19S_3^zS_4^x - 14.25S_1^xS_2^xS_3^zS_4^x - 31.25S_1^yS_2^xS_3^zS_4^x - 9.25S_1^zS_2^xS_3^zS_4^x + 46.25S_1^xS_2^yS_3^zS_4^x$$

$$- 19.25S_1^yS_2^yS_3^zS_4^x + 32.75S_1^zS_2^yS_3^zS_4^x - 24.75S_1^xS_2^zS_3^zS_4^x - 38.25S_1^yS_2^zS_3^zS_4^x$$

$$- 21.25S_1^zS_2^zS_3^zS_4^x + 11.44S_1^xS_4^y + 23.94S_1^yS_4^y + 13.19S_1^zS_4^y - 13.56S_2^xS_4^y - 12.44S_2^yS_4^y$$

$$- 11.81S_2^zS_4^y + 11.44S_3^xS_4^y - 43.25S_1^xS_2^xS_3^xS_4^y - 24.75S_1^yS_2^xS_3^xS_4^y - 76.75S_1^zS_2^xS_3^xS_4^y$$

$$- 9.25S_1^xS_2^yS_3^xS_4^y - 36.25S_1^yS_2^yS_3^xS_4^y - 21.25S_1^zS_2^yS_3^xS_4^y - 25.75S_1^xS_2^zS_3^xS_4^y - 23.25S_1^yS_2^zS_3^xS_4^y$$

$$- 39.75S_1^zS_2^zS_3^xS_4^y + 21.31S_3^yS_4^y - 83.75S_1^xS_2^xS_3^yS_4^y - 21.25S_1^yS_2^xS_3^yS_4^y - 39.75S_1^zS_2^xS_3^yS_4^y$$

$$- 21.25S_1^xS_2^yS_3^yS_4^y - 56.75S_1^yS_2^yS_3^yS_4^y - 28.25S_1^zS_2^yS_3^yS_4^y - 39.75S_1^xS_2^zS_3^yS_4^y - 28.25S_1^yS_2^zS_3^yS_4^y$$

$$- 39.25S_1^zS_2^zS_3^yS_4^y + 11.44S_3^zS_4^y - 14.75S_1^xS_2^xS_3^zS_4^y - 38.25S_1^yS_2^xS_3^zS_4^y$$

$$+ 23.94S_1^zS_4^z - 11.81S_2^xS_4^z - 13.56S_2^yS_4^z - 12.44S_2^zS_4^z + 13.19S_3^xS_4^z - 14.25S_1^xS_2^xS_3^xS_4^z$$

$$+ 46.25S_1^yS_2^xS_3^xS_4^z - 24.75S_1^zS_2^xS_3^xS_4^z - 31.25S_1^xS_2^yS_3^xS_4^z - 19.25S_1^yS_2^yS_3^xS_4^z - 38.25S_1^zS_2^yS_3^xS_4^z$$

$$- 9.25S_1^xS_2^zS_3^xS_4^z + 32.75S_1^yS_2^zS_3^xS_4^z - 21.25S_1^zS_2^zS_3^xS_4^z + 11.44S_3^yS_4^z$$

$$- 14.75S_1^xS_2^xS_3^yS_4^z + 32.75S_1^yS_2^xS_3^yS_4^z - 23.25S_1^zS_2^xS_3^yS_4^z - 38.25S_1^xS_2^yS_3^yS_4^z$$

$$- 12.75S_1^yS_2^yS_3^yS_4^z - 41.75S_1^zS_2^yS_3^yS_4^z - 21.25S_1^xS_2^zS_3^yS_4^z + 28.75S_1^yS_2^zS_3^yS_4^z - 28.25S_1^zS_2^zS_3^yS_4^z$$

$$+ 23.94S_3^zS_4^z - 32.25S_1^xS_2^xS_3^zS_4^z - 19.25S_1^yS_2^xS_3^zS_4^z - 36.25S_1^zS_2^xS_3^zS_4^z - 19.25S_1^xS_2^yS_3^zS_4^z$$

$$- 39.25S_1^yS_2^yS_3^zS_4^z - 12.75S_1^zS_2^yS_3^zS_4^z - 36.25S_1^xS_2^zS_3^zS_4^z - 12.75S_1^yS_2^zS_3^zS_4^z - 13.56S_1^yS_5^x$$

$$- 56.75S_1^zS_2^zS_3^zS_4^z - 12.44S_1^xS_5^x - 11.81S_1^zS_5^x + 23.94S_2^xS_5^x + 11.44S_2^yS_5^x$$

$$+ 13.19S_2^zS_5^x - 12.44S_3^xS_5^x - 9.25S_1^xS_2^xS_3^xS_5^x + 44.25S_1^yS_2^xS_3^xS_5^x + 7.25S_1^zS_2^xS_3^xS_5^x$$

$$- 23.25S_1^xS_2^yS_3^xS_5^x + 8.75S_1^yS_2^yS_3^xS_5^x - 10.75S_1^zS_2^yS_3^xS_5^x - 23.25S_1^xS_2^zS_3^xS_5^x$$

$$+ 15.75S_1^yS_2^zS_3^xS_5^x + 21.25S_1^zS_2^zS_3^xS_5^x - 11.81S_3^yS_5^x + 45.75S_1^xS_2^xS_3^yS_5^x + 3.25S_1^yS_2^xS_3^yS_5^x$$

$$+ 16.25S_1^zS_2^xS_3^yS_5^x + 3.25S_1^xS_2^yS_3^yS_5^x + 45.75S_1^yS_2^yS_3^yS_5^x + 16.25S_1^zS_2^yS_3^yS_5^x$$

$$- 3.25S_1^xS_2^zS_3^yS_5^x - 3.25S_1^yS_2^zS_3^yS_5^x + 2.25S_1^zS_2^zS_3^yS_5^x - 13.56S_3^zS_5^x + 45.75S_1^xS_2^xS_3^zS_5^x$$

$$+ 45.75S_1^yS_2^xS_3^zS_5^x + 8.75S_1^zS_2^xS_3^zS_5^x - 3.25S_1^xS_2^yS_3^zS_5^x + 45.75S_1^yS_2^yS_3^zS_5^x$$

$$+ 15.75S_1^zS_2^yS_3^zS_5^x + 3.25S_1^xS_2^zS_3^zS_5^x + 45.75S_1^yS_2^zS_3^zS_5^x + 44.25S_1^zS_2^zS_3^zS_5^x + 23.94S_4^xS_5^x$$

$$- 56.75S_1^xS_2^xS_4^xS_5^x - 12.75S_1^yS_2^xS_4^xS_5^x - 36.25S_1^zS_2^xS_4^xS_5^x - 28.25S_1^xS_2^yS_4^xS_5^x$$

$$- 41.75S_1^yS_2^yS_4^xS_5^x - 23.25S_1^zS_2^yS_4^xS_5^x - 21.25S_1^xS_2^zS_4^xS_5^x - 38.25S_1^yS_2^zS_4^xS_5^x$$

$$- 24.75S_1^zS_2^zS_4^xS_5^x - 9.25S_1^xS_3^xS_4^xS_5^x + 45.75S_1^yS_3^xS_4^xS_5^x + 45.75S_1^zS_3^xS_4^xS_5^x - 56.75S_2^xS_3^xS_4^xS_5^x$$

$$- 36.25S_2^yS_3^xS_4^xS_5^x - 12.75S_2^zS_3^xS_4^xS_5^x + 7.25S_1^xS_3^yS_4^xS_5^x + 8.75S_1^yS_3^yS_4^xS_5^x + 16.25S_1^zS_3^yS_4^xS_5^x$$

$$- 36.25S_2^xS_3^yS_4^xS_5^x - 32.25S_2^yS_3^yS_4^xS_5^x - 19.25S_2^zS_3^yS_4^xS_5^x + 44.25S_1^xS_3^zS_4^xS_5^x$$

$$+ 45.75S_1^yS_3^zS_4^xS_5^x + 3.25S_1^zS_3^zS_4^xS_5^x - 12.75S_2^xS_3^zS_4^xS_5^x - 19.25S_2^yS_3^zS_4^xS_5^x - 39.25S_2^zS_3^zS_4^xS_5^x$$

$$+ 13.19S_4^yS_5^x - 12.75S_1^xS_2^xS_4^yS_5^x - 39.25S_1^yS_2^xS_4^yS_5^x - 19.25S_1^zS_2^xS_4^yS_5^x$$

$$+ 28.75S_1^xS_2^yS_4^yS_5^x - 12.75S_1^yS_2^yS_4^yS_5^x + 32.75S_1^zS_2^yS_4^yS_5^x + 32.75S_1^xS_2^zS_4^yS_5^x$$

$$- 19.25S_1^yS_2^zS_4^yS_5^x + 46.25S_1^zS_2^zS_4^yS_5^x - 23.25S_1^xS_3^xS_4^yS_5^x + 3.25S_1^yS_3^xS_4^yS_5^x - 3.25S_1^zS_3^xS_4^yS_5^x$$

$$+ 15.75S_1^xS_3^zS_4^yS_5^x + 45.75S_1^yS_3^zS_4^yS_5^x - 3.25S_1^zS_3^zS_4^yS_5^x - 38.25S_2^xS_3^zS_4^yS_5^x - 31.25S_2^yS_3^zS_4^yS_5^x$$

$$- 19.25S_2^zS_3^zS_4^yS_5^x + 11.44S_4^zS_5^x - 36.25S_1^xS_2^xS_4^zS_5^x - 19.25S_1^yS_2^xS_4^zS_5^x$$

$$- 32.25S_1^zS_2^xS_4^zS_5^x - 21.25S_1^xS_2^yS_4^zS_5^x - 38.25S_1^yS_2^yS_4^zS_5^x - 14.75S_1^zS_2^yS_4^zS_5^x - 9.25S_1^xS_2^zS_4^zS_5^x$$

$$- 31.25S_1^yS_2^zS_4^zS_5^x - 14.25S_1^zS_2^zS_4^zS_5^x - 23.25S_1^xS_3^xS_4^zS_5^x - 3.25S_1^yS_3^xS_4^zS_5^x$$

$$+ 3.25S_1^zS_3^xS_4^zS_5^x - 28.25S_2^xS_3^xS_4^zS_5^x - 21.25S_2^yS_3^xS_4^zS_5^x + 28.75S_2^zS_3^xS_4^zS_5^x - 10.75S_1^xS_3^yS_4^zS_5^x$$

$$+ 15.75S_1^yS_3^yS_4^zS_5^x + 16.25S_1^zS_3^yS_4^zS_5^x - 23.25S_2^xS_3^yS_4^zS_5^x - 14.75S_2^yS_3^yS_4^zS_5^x$$

$$+ 32.75S_2^zS_3^yS_4^zS_5^x + 8.75S_1^xS_3^zS_4^zS_5^x + 45.75S_1^yS_3^zS_4^zS_5^x + 45.75S_1^zS_3^zS_4^zS_5^x - 41.75S_2^xS_3^zS_4^zS_5^x$$

$$- 38.25S_2^yS_3^zS_4^zS_5^x - 12.75S_2^zS_3^zS_4^zS_5^x - 11.81S_1^xS_5^y - 12.44S_1^yS_5^y$$

$$- 13.56S_1^zS_5^y + 11.44S_2^xS_5^y + 21.31S_2^yS_5^y + 11.44S_2^zS_5^y - 13.56S_3^xS_5^y + 7.25S_1^xS_2^xS_3^xS_5^y$$

$$+ 21.25S_1^yS_2^xS_3^xS_5^y - 1.75S_1^zS_2^xS_3^xS_5^y + 21.25S_1^xS_2^yS_3^xS_5^y + 7.25S_1^yS_2^yS_3^xS_5^y - 1.75S_1^zS_2^yS_3^xS_5^y$$

$$- 10.75S_1^xS_2^zS_3^xS_5^y - 10.75S_1^yS_2^zS_3^xS_5^y - 1.75S_1^zS_2^zS_3^xS_5^y - 12.44S_3^yS_5^y$$

$$+ 8.75S_1^xS_2^xS_3^yS_5^y - 23.25S_1^yS_2^xS_3^yS_5^y - 10.75S_1^zS_2^xS_3^yS_5^y + 44.25S_1^xS_2^yS_3^yS_5^y - 9.25S_1^yS_2^yS_3^yS_5^y$$

$$+ 7.25S_1^zS_2^yS_3^yS_5^y + 15.75S_1^xS_2^zS_3^yS_5^y - 23.25S_1^yS_2^zS_3^yS_5^y + 21.25S_1^zS_2^zS_3^yS_5^y$$

$$- 11.81S_3^zS_5^y + 16.25S_1^xS_2^xS_3^zS_5^y + 15.75S_1^yS_2^xS_3^zS_5^y - 10.75S_1^zS_2^xS_3^zS_5^y + 2.25S_1^xS_2^yS_3^zS_5^y$$

$$+ 44.25S_1^yS_2^yS_3^zS_5^y + 21.25S_1^zS_2^yS_3^zS_5^y + 16.25S_1^xS_2^zS_3^zS_5^y + 8.75S_1^yS_2^zS_3^zS_5^y$$

$$+ 7.25S_1^zS_2^zS_3^zS_5^y + 13.19S_4^xS_5^y - 28.25S_1^xS_2^xS_4^xS_5^y + 28.75S_1^yS_2^xS_4^xS_5^y - 21.25S_1^zS_2^xS_4^xS_5^y$$

$$- 39.25S_1^xS_2^yS_4^xS_5^y - 28.25S_1^yS_2^yS_4^xS_5^y - 39.75S_1^zS_2^yS_4^xS_5^y - 39.75S_1^xS_2^zS_4^xS_5^y$$

$$- 21.25S_1^yS_2^zS_4^xS_5^y - 76.75S_1^zS_2^zS_4^xS_5^y + 44.25S_1^xS_3^xS_4^xS_5^y + 3.25S_1^yS_3^xS_4^xS_5^y + 45.75S_1^zS_3^xS_4^xS_5^y$$

$$- 21.25S_2^xS_3^xS_4^xS_5^y - 24.75S_2^yS_3^xS_4^xS_5^y - 38.25S_2^zS_3^xS_4^xS_5^y + 21.25S_1^xS_3^yS_4^xS_5^y$$

$$- 23.25S_1^yS_3^yS_4^xS_5^y + 15.75S_1^zS_3^yS_4^xS_5^y - 9.25S_2^xS_3^yS_4^xS_5^y - 14.25S_2^yS_3^yS_4^xS_5^y - 31.25S_2^zS_3^yS_4^xS_5^y$$

$$+ 2.25S_1^xS_3^zS_4^xS_5^y - 3.25S_1^yS_3^zS_4^xS_5^y - 3.25S_1^zS_3^zS_4^xS_5^y + 32.75S_2^xS_3^zS_4^xS_5^y$$

$$+ 46.25S_2^yS_3^zS_4^xS_5^y - 19.25S_2^zS_3^zS_4^xS_5^y + 23.94S_4^yS_5^y - 41.75S_1^xS_2^xS_4^yS_5^y$$

$$- 12.75S_1^yS_2^xS_4^yS_5^y - 38.25S_1^zS_2^xS_4^yS_5^y - 28.25S_1^xS_2^yS_4^yS_5^y - 56.75S_1^yS_2^yS_4^yS_5^y$$

$$- 21.25S_1^zS_2^yS_4^yS_5^y - 23.25S_1^xS_2^zS_4^yS_5^y - 36.25S_1^yS_2^zS_4^yS_5^y - 24.75S_1^zS_2^zS_4^yS_5^y$$

$$- 43.25S_2^yS_3^xS_4^yS_5^y - 14.75S_2^zS_3^xS_4^yS_5^y + 7.25S_1^xS_3^yS_4^yS_5^y - 9.25S_1^yS_3^yS_4^yS_5^y + 44.25S_1^zS_3^yS_4^yS_5^y$$

$$- 43.25S_2^xS_3^yS_4^yS_5^y - 39.25S_2^yS_3^yS_4^yS_5^y - 14.25S_2^zS_3^yS_4^yS_5^y + 16.25S_1^xS_3^zS_4^yS_5^y$$

$$+ 45.75S_1^yS_3^zS_4^yS_5^y + 3.25S_1^zS_3^zS_4^yS_5^y - 14.75S_2^xS_3^zS_4^yS_5^y - 14.25S_2^yS_3^zS_4^yS_5^y$$

$$- 32.25S_2^zS_3^zS_4^yS_5^y + 11.44S_4^zS_5^y - 23.25S_1^xS_2^xS_4^zS_5^y + 32.75S_1^yS_2^xS_4^zS_5^y$$

$$- 14.75S_1^zS_2^xS_4^zS_5^y - 39.75S_1^xS_2^yS_4^zS_5^y - 21.25S_1^yS_2^yS_4^zS_5^y - 83.75S_1^zS_2^yS_4^zS_5^y$$

$$- 25.75S_1^xS_2^zS_4^zS_5^y - 9.25S_1^yS_2^zS_4^zS_5^y - 43.25S_1^zS_2^zS_4^zS_5^y + 15.75S_1^xS_3^xS_4^zS_5^y - 3.25S_1^yS_3^xS_4^zS_5^y$$

$$+ 45.75S_1^zS_3^xS_4^zS_5^y - 39.75S_2^xS_3^xS_4^zS_5^y - 76.75S_2^yS_3^xS_4^zS_5^y - 21.25S_2^zS_3^xS_4^zS_5^y - 10.75S_1^xS_3^yS_4^zS_5^y$$

$$- 23.25S_1^yS_3^yS_4^zS_5^y + 8.75S_1^zS_3^yS_4^zS_5^y - 25.75S_2^xS_3^yS_4^zS_5^y - 43.25S_2^yS_3^yS_4^zS_5^y$$

$$- 9.25S_2^zS_3^yS_4^zS_5^y + 16.25S_1^xS_3^zS_4^zS_5^y + 3.25S_1^yS_3^zS_4^zS_5^y + 45.75S_1^zS_3^zS_4^zS_5^y - 23.25S_2^xS_3^zS_4^zS_5^y$$

$$- 24.75S_2^yS_3^zS_4^zS_5^y - 36.25S_2^zS_3^zS_4^zS_5^y - 13.56S_1^xS_5^z - 11.81S_1^yS_5^z$$

$$- 12.44S_1^zS_5^z + 13.19S_2^xS_5^z + 11.44S_2^yS_5^z + 23.94S_2^zS_5^z - 11.81S_3^xS_5^z + 44.25S_1^xS_2^xS_3^xS_5^z$$

$$+ 2.25S_1^yS_2^xS_3^xS_5^z + 21.25S_1^zS_2^xS_3^xS_5^z + 15.75S_1^xS_2^yS_3^xS_5^z + 16.25S_1^yS_2^yS_3^xS_5^z - 10.75S_1^zS_2^yS_3^xS_5^z$$

$$+ 8.75S_1^xS_2^zS_3^xS_5^z + 16.25S_1^yS_2^zS_3^xS_5^z + 7.25S_1^zS_2^zS_3^xS_5^z - 13.56S_3^yS_5^z$$

$$+ 45.75S_1^xS_2^xS_3^yS_5^z - 3.25S_1^yS_2^xS_3^yS_5^z + 15.75S_1^zS_2^xS_3^yS_5^z + 45.75S_1^xS_2^yS_3^yS_5^z$$

$$+ 45.75S_1^yS_2^yS_3^yS_5^z + 8.75S_1^zS_2^yS_3^yS_5^z + 45.75S_1^xS_2^zS_3^yS_5^z + 3.25S_1^yS_2^zS_3^yS_5^z + 44.25S_1^zS_2^zS_3^yS_5^z$$

$$- 12.44S_3^zS_5^z + 3.25S_1^xS_2^xS_3^zS_5^z - 3.25S_1^yS_2^xS_3^zS_5^z - 23.25S_1^zS_2^xS_3^zS_5^z - 3.25S_1^xS_2^yS_3^zS_5^z$$

$$+ 3.25S_1^yS_2^yS_3^zS_5^z - 23.25S_1^zS_2^yS_3^zS_5^z + 45.75S_1^xS_2^zS_3^zS_5^z + 45.75S_1^yS_2^zS_3^zS_5^z$$

$$- 9.25S_1^zS_2^zS_3^zS_5^z + 11.44S_4^xS_5^z - 21.25S_1^xS_2^xS_4^xS_5^z + 32.75S_1^yS_2^xS_4^xS_5^z$$

$$- 9.25S_1^zS_2^xS_4^xS_5^z - 39.75S_1^xS_2^yS_4^xS_5^z - 23.25S_1^yS_2^yS_4^xS_5^z - 25.75S_1^zS_2^yS_4^xS_5^z - 83.75S_1^xS_2^zS_4^xS_5^z$$

$$- 14.75S_1^yS_2^zS_4^xS_5^z - 43.25S_1^zS_2^zS_4^xS_5^z + 7.25S_1^xS_3^xS_4^xS_5^z + 16.25S_1^yS_3^xS_4^xS_5^z$$

$$+ 8.75S_1^zS_3^xS_4^xS_5^z - 28.25S_2^xS_3^xS_4^xS_5^z - 23.25S_2^yS_3^xS_4^xS_5^z - 41.75S_2^zS_3^xS_4^xS_5^z - 1.75S_1^xS_3^yS_4^xS_5^z$$

$$- 10.75S_1^yS_3^yS_4^xS_5^z - 10.75S_1^zS_3^yS_4^xS_5^z - 21.25S_2^xS_3^yS_4^xS_5^z - 14.75S_2^yS_3^yS_4^xS_5^z$$

$$- 38.25S_2^zS_3^yS_4^xS_5^z + 21.25S_1^xS_3^zS_4^xS_5^z + 15.75S_1^yS_3^zS_4^xS_5^z - 23.25S_1^zS_3^zS_4^xS_5^z + 28.75S_2^xS_3^zS_4^xS_5^z$$

$$+ 32.75S_2^yS_3^zS_4^xS_5^z - 12.75S_2^zS_3^zS_4^xS_5^z + 11.44S_4^yS_5^z - 38.25S_1^xS_2^xS_4^yS_5^z$$

$$- 14.75S_1^xS_2^zS_4^yS_5^z - 32.25S_1^yS_2^zS_4^yS_5^z - 14.25S_1^zS_2^zS_4^yS_5^z - 10.75S_1^xS_3^xS_4^yS_5^z$$

$$+ 16.25S_1^yS_3^xS_4^yS_5^z + 15.75S_1^zS_3^xS_4^yS_5^z - 39.75S_2^xS_3^xS_4^yS_5^z - 25.75S_2^yS_3^xS_4^yS_5^z - 23.25S_2^zS_3^xS_4^yS_5^z$$

$$- 1.75S_1^xS_3^yS_4^yS_5^z + 7.25S_1^yS_3^yS_4^yS_5^z + 21.25S_1^zS_3^yS_4^yS_5^z - 76.75S_2^xS_3^yS_4^yS_5^z$$

$$- 43.25S_2^yS_3^yS_4^yS_5^z - 24.75S_2^zS_3^yS_4^yS_5^z - 10.75S_1^xS_3^zS_4^yS_5^z + 8.75S_1^yS_3^zS_4^yS_5^z - 23.25S_1^zS_3^zS_4^yS_5^z$$

$$- 21.25S_2^xS_3^zS_4^yS_5^z - 9.25S_2^yS_3^zS_4^yS_5^z - 36.25S_2^zS_3^zS_4^yS_5^z + 21.31S_4^zS_5^z$$

$$- 24.75S_1^xS_2^xS_4^zS_5^z + 46.25S_1^yS_2^xS_4^zS_5^z - 14.25S_1^zS_2^xS_4^zS_5^z - 76.75S_1^xS_2^yS_4^zS_5^z - 24.75S_1^yS_2^yS_4^zS_5^z$$

$$- 14.25S_1^yS_2^zS_4^zS_5^z - 39.25S_1^zS_2^zS_4^zS_5^z + 21.25S_1^xS_3^xS_4^zS_5^z + 2.25S_1^yS_3^xS_4^zS_5^z$$

$$+ 44.25S_1^zS_3^xS_4^zS_5^z - 39.25S_2^xS_3^xS_4^zS_5^z - 39.75S_2^yS_3^xS_4^zS_5^z - 28.25S_2^zS_3^xS_4^zS_5^z$$

$$- 1.75S_1^xS_3^yS_4^zS_5^z + 21.25S_1^yS_3^yS_4^zS_5^z + 7.25S_1^zS_3^yS_4^zS_5^z - 39.75S_2^xS_3^yS_4^zS_5^z - 83.75S_2^yS_3^yS_4^zS_5^z$$

$$- 21.25S_2^zS_3^yS_4^zS_5^z + 7.25S_1^xS_3^zS_4^zS_5^z + 44.25S_1^yS_3^zS_4^zS_5^z - 9.25S_1^zS_3^zS_4^zS_5^z - 28.25S_2^xS_3^zS_4^zS_5^z$$

$$- 21.25S_2^yS_3^zS_4^zS_5^z - 56.75S_2^zS_3^zS_4^zS_5^z + 23.94S_1^xS_6^x + 11.44S_1^yS_6^x$$

$$- 11.81S_2^zS_6^x + 23.94S_3^xS_6^x - 56.75S_1^xS_2^xS_3^xS_6^x - 43.25S_1^zS_2^yS_4^zS_5^z - 43.25S_1^xS_2^zS_4^zS_5^z$$

$$+ 13.19S_1^zS_6^x - 12.44S_2^xS_6^x - 13.56S_2^yS_6^x - 28.25S_1^yS_2^xS_3^xS_6^x - 21.25S_1^zS_2^xS_3^xS_6^x - 12.75S_1^xS_2^yS_3^xS_6^x$$

$$- 41.75S_1^yS_2^yS_3^xS_6^x - 38.25S_1^zS_2^yS_3^xS_6^x - 36.25S_1^xS_2^zS_3^xS_6^x - 23.25S_1^yS_2^zS_3^xS_6^x$$

$$- 24.75S_1^zS_2^zS_3^xS_6^x + 13.19S_3^yS_6^x - 12.75S_1^xS_2^xS_3^yS_6^x + 28.75S_1^yS_2^xS_3^yS_6^x + 32.75S_1^zS_2^xS_3^yS_6^x$$

$$- 39.25S_1^xS_2^yS_3^yS_6^x - 12.75S_1^yS_2^yS_3^yS_6^x - 19.25S_1^zS_2^yS_3^yS_6^x - 19.25S_1^xS_2^zS_3^yS_6^x$$

$$+ 32.75S_1^yS_2^zS_3^yS_6^x + 46.25S_1^zS_2^zS_3^yS_6^x + 11.44S_3^zS_6^x - 36.25S_1^xS_2^xS_3^zS_6^x - 21.25S_1^yS_2^xS_3^zS_6^x$$

$$- 9.25S_1^zS_2^xS_3^zS_6^x - 19.25S_1^xS_2^yS_3^zS_6^x - 38.25S_1^yS_2^yS_3^zS_6^x - 31.25S_1^zS_2^yS_3^zS_6^x$$

$$- 32.25S_1^xS_2^zS_3^zS_6^x - 14.75S_1^yS_2^zS_3^zS_6^x - 14.25S_1^zS_2^zS_3^zS_6^x - 12.44S_4^xS_6^x - 9.25S_1^xS_2^xS_4^xS_6^x$$

$$- 23.25S_1^yS_2^xS_4^xS_6^x - 23.25S_1^zS_2^xS_4^xS_6^x + 44.25S_1^xS_2^yS_4^xS_6^x + 8.75S_1^yS_2^yS_4^xS_6^x$$

$$+ 15.75S_1^zS_2^yS_4^xS_6^x + 7.25S_1^xS_2^zS_4^xS_6^x - 10.75S_1^yS_2^zS_4^xS_6^x + 21.25S_1^zS_2^zS_4^xS_6^x - 56.75S_1^xS_3^xS_4^xS_6^x$$

$$- 36.25S_1^yS_3^xS_4^xS_6^x - 12.75S_1^zS_3^xS_4^xS_6^x - 9.25S_2^xS_3^xS_4^xS_6^x + 45.75S_2^yS_3^xS_4^xS_6^x$$

$$+ 45.75S_2^zS_3^xS_4^xS_6^x - 21.25S_1^xS_3^yS_4^xS_6^x - 9.25S_1^yS_3^yS_4^xS_6^x + 32.75S_1^zS_3^yS_4^xS_6^x - 23.25S_2^xS_3^yS_4^xS_6^x$$

$$+ 3.25S_2^yS_3^yS_4^xS_6^x - 3.25S_2^zS_3^yS_4^xS_6^x - 28.25S_1^xS_3^zS_4^xS_6^x - 21.25S_1^yS_3^zS_4^xS_6^x$$

$$+ 45.75S_1^xS_2^xS_4^yS_6^x + 3.25S_1^yS_2^xS_4^yS_6^x - 3.25S_1^zS_2^xS_4^yS_6^x + 3.25S_1^xS_2^yS_4^yS_6^x$$

$$+ 45.75S_1^yS_2^yS_4^yS_6^x - 3.25S_1^zS_2^yS_4^yS_6^x + 16.25S_1^xS_2^zS_4^yS_6^x + 16.25S_1^yS_2^zS_4^yS_6^x + 2.25S_1^zS_2^zS_4^yS_6^x$$

$$- 36.25S_1^xS_3^xS_4^yS_6^x - 32.25S_1^yS_3^xS_4^yS_6^x - 19.25S_1^zS_3^xS_4^yS_6^x + 7.25S_2^xS_3^xS_4^yS_6^x + 8.75S_2^yS_3^xS_4^yS_6^x$$

$$+ 16.25S_2^zS_3^xS_4^yS_6^x - 24.75S_1^xS_3^yS_4^yS_6^x - 14.25S_1^yS_3^yS_4^yS_6^x + 46.25S_1^zS_3^yS_4^yS_6^x$$

$$+ 21.25S_2^xS_3^yS_4^yS_6^x + 44.25S_2^yS_3^yS_4^yS_6^x + 2.25S_2^zS_3^yS_4^yS_6^x - 23.25S_1^xS_3^zS_4^yS_6^x$$

$$- 14.75S_1^yS_3^zS_4^yS_6^x + 32.75S_1^zS_3^zS_4^yS_6^x - 10.75S_2^xS_3^zS_4^yS_6^x + 15.75S_2^yS_3^zS_4^yS_6^x + 16.25S_2^zS_3^zS_4^yS_6^x$$

$$- 13.56S_4^zS_6^x + 45.75S_1^xS_2^xS_4^zS_6^x - 3.25S_1^yS_2^xS_4^zS_6^x + 3.25S_1^zS_2^xS_4^zS_6^x + 45.75S_1^xS_2^yS_4^zS_6^x$$

$$+ 45.75S_1^yS_2^yS_4^zS_6^x + 45.75S_1^zS_2^yS_4^zS_6^x + 8.75S_1^xS_2^zS_4^zS_6^x + 15.75S_1^yS_2^zS_4^zS_6^x$$

$$+ 44.25S_1^zS_2^zS_4^zS_6^x - 12.75S_1^xS_3^xS_4^zS_6^x - 19.25S_1^yS_3^xS_4^zS_6^x - 39.25S_1^zS_3^xS_4^zS_6^x + 44.25S_2^xS_3^xS_4^zS_6^x$$

$$+ 45.75S_2^yS_3^xS_4^zS_6^x + 3.25S_2^zS_3^xS_4^zS_6^x - 38.25S_1^xS_3^yS_4^zS_6^x - 31.25S_1^yS_3^yS_4^zS_6^x$$

$$- 19.25S_1^zS_3^yS_4^zS_6^x + 15.75S_2^xS_3^yS_4^zS_6^x + 45.75S_2^yS_3^yS_4^zS_6^x - 3.25S_2^zS_3^yS_4^zS_6^x$$

$$- 41.75S_1^xS_3^zS_4^zS_6^x - 38.25S_1^yS_3^zS_4^zS_6^x - 12.75S_1^zS_3^zS_4^zS_6^x + 8.75S_2^xS_3^zS_4^zS_6^x + 45.75S_2^yS_3^zS_4^zS_6^x$$

$$+ 45.75S_2^zS_3^zS_4^zS_6^x + 21.31S_5^xS_6^x - 56.75S_1^xS_2^xS_5^xS_6^x - 21.25S_1^yS_2^xS_5^xS_6^x$$

$$- 28.25S_1^zS_2^xS_5^xS_6^x - 21.25S_1^xS_2^yS_5^xS_6^x - 83.75S_1^yS_2^yS_5^xS_6^x - 39.75S_1^zS_2^yS_5^xS_6^x - 28.25S_1^xS_2^zS_5^xS_6^x$$

$$- 39.75S_1^yS_2^zS_5^xS_6^x - 39.25S_1^zS_2^zS_5^xS_6^x - 9.25S_1^xS_3^xS_5^xS_6^x + 7.25S_1^yS_3^xS_5^xS_6^x$$

$$+ 44.25S_1^zS_3^xS_5^xS_6^x - 39.25S_2^xS_3^xS_5^xS_6^x - 43.25S_2^yS_3^xS_5^xS_6^x - 14.25S_2^zS_3^xS_5^xS_6^x + 44.25S_1^xS_3^yS_5^xS_6^x$$

$$+ 21.25S_1^yS_3^yS_5^xS_6^x + 2.25S_1^zS_3^yS_5^xS_6^x - 14.25S_2^xS_3^yS_5^xS_6^x - 24.75S_2^yS_3^yS_5^xS_6^x$$

$$+ 46.25S_2^zS_3^yS_5^xS_6^x + 7.25S_1^xS_3^zS_5^xS_6^x - 1.75S_1^yS_3^zS_5^xS_6^x + 21.25S_1^zS_3^zS_5^xS_6^x - 43.25S_2^xS_3^zS_5^xS_6^x$$

$$- 76.75S_2^yS_3^zS_5^xS_6^x - 24.75S_2^zS_3^zS_5^xS_6^x - 39.25S_1^xS_4^xS_5^xS_6^x - 43.25S_1^yS_4^xS_5^xS_6^x$$

$$- 14.25S_1^zS_4^xS_5^xS_6^x - 9.25S_2^xS_4^xS_5^xS_6^x + 7.25S_2^yS_4^xS_5^xS_6^x + 44.25S_2^zS_4^xS_5^xS_6^x - 56.75S_3^xS_4^xS_5^xS_6^x$$

$$+ 189S_1^xS_2^xS_3^xS_4^xS_5^xS_6^x + 63S_1^yS_2^xS_3^xS_4^xS_5^xS_6^x + 63S_1^zS_2^xS_3^xS_4^xS_5^xS_6^x + 63S_1^xS_2^yS_3^xS_4^xS_5^xS_6^x$$

$$+ 189S_1^yS_2^yS_3^xS_4^xS_5^xS_6^x + 63S_1^zS_2^yS_3^xS_4^xS_5^xS_6^x + 63S_1^xS_2^zS_3^xS_4^xS_5^xS_6^x + 63S_1^yS_2^zS_3^xS_4^xS_5^xS_6^x$$

$$+ 315S_1^zS_2^zS_3^xS_4^xS_5^xS_6^x - 28.25S_3^yS_4^xS_5^xS_6^x + 63S_1^xS_2^xS_3^yS_4^xS_5^xS_6^x - 63S_1^yS_2^xS_3^yS_4^xS_5^xS_6^x$$

$$+ 63S_1^zS_2^xS_3^yS_4^xS_5^xS_6^x + 63S_1^xS_2^yS_3^yS_4^xS_5^xS_6^x + 63S_1^yS_2^yS_3^yS_4^xS_5^xS_6^x + 63S_1^zS_2^yS_3^yS_4^xS_5^xS_6^x$$

$$- 21.25S_3^zS_4^xS_5^xS_6^x + 63S_1^xS_2^xS_3^zS_4^xS_5^xS_6^x - 63S_1^yS_2^xS_3^zS_4^xS_5^xS_6^x - 63S_1^zS_2^xS_3^zS_4^xS_5^xS_6^x$$

$$+ 63S_1^xS_2^yS_3^zS_4^xS_5^xS_6^x + 63S_1^yS_2^yS_3^zS_4^xS_5^xS_6^x - 189S_1^zS_2^yS_3^zS_4^xS_5^xS_6^x + 63S_1^xS_2^zS_3^zS_4^xS_5^xS_6^x$$

$$+ 63S_1^yS_2^zS_3^zS_4^xS_5^xS_6^x + 63S_1^zS_2^zS_3^zS_4^xS_5^xS_6^x - 14.25S_1^xS_4^yS_5^xS_6^x - 24.75S_1^yS_4^yS_5^xS_6^x + 46.25S_1^zS_4^yS_5^xS_6^x$$

$$+ 44.25S_2^xS_4^yS_5^xS_6^x + 21.25S_2^yS_4^yS_5^xS_6^x + 2.25S_2^zS_4^yS_5^xS_6^x - 28.25S_3^xS_4^yS_5^xS_6^x$$

$$+ 63S_1^xS_2^xS_3^xS_4^yS_5^xS_6^x + 63S_1^yS_2^xS_3^xS_4^yS_5^xS_6^x + 63S_1^zS_2^xS_3^xS_4^yS_5^xS_6^x - 63S_1^xS_2^yS_3^xS_4^yS_5^xS_6^x$$

$$+ 63S_1^yS_2^yS_3^xS_4^yS_5^xS_6^x + 63S_1^zS_2^yS_3^xS_4^yS_5^xS_6^x + 63S_1^xS_2^zS_3^xS_4^yS_5^xS_6^x$$

$$+ 63S_1^yS_2^zS_3^xS_4^yS_5^xS_6^x + 189S_1^zS_2^zS_3^xS_4^yS_5^xS_6^x - 39.25S_3^yS_4^yS_5^xS_6^x + 315S_1^xS_2^xS_3^yS_4^yS_5^xS_6^x$$

$$+ 63S_1^yS_2^xS_3^yS_4^yS_5^xS_6^x + 189S_1^zS_2^xS_3^yS_4^yS_5^xS_6^x + 63S_1^xS_2^yS_3^yS_4^yS_5^xS_6^x + 315S_1^yS_2^yS_3^yS_4^yS_5^xS_6^x$$

$$+ 189S_1^zS_2^yS_3^yS_4^yS_5^xS_6^x + 189S_1^xS_2^zS_3^yS_4^yS_5^xS_6^x + 189S_1^yS_2^zS_3^yS_4^yS_5^xS_6^x + 189S_1^zS_2^zS_3^yS_4^yS_5^xS_6^x$$

$$- 39.75S_3^zS_4^yS_5^xS_6^x + 63S_1^xS_2^xS_3^zS_4^yS_5^xS_6^x + 63S_1^yS_2^xS_3^zS_4^yS_5^xS_6^x + 63S_1^zS_2^xS_3^zS_4^yS_5^xS_6^x$$

$$- 189S_1^xS_2^yS_3^zS_4^yS_5^xS_6^x + 63S_1^yS_2^yS_3^zS_4^yS_5^xS_6^x - 63S_1^zS_2^yS_3^zS_4^yS_5^xS_6^x + 63S_1^xS_2^zS_3^zS_4^yS_5^xS_6^x$$

$$+ 315S_1^yS_2^zS_3^zS_4^yS_5^xS_6^x + 189S_1^zS_2^zS_3^zS_4^yS_5^xS_6^x - 43.25S_1^xS_4^zS_5^xS_6^x - 76.75S_1^yS_4^zS_5^xS_6^x$$

$$- 24.75S_1^zS_4^zS_5^xS_6^x + 7.25S_2^xS_4^zS_5^xS_6^x - 1.75S_2^yS_4^zS_5^xS_6^x + 21.25S_2^zS_4^zS_5^xS_6^x - 21.25S_3^xS_4^zS_5^xS_6^x$$

$$+ 63S_1^xS_2^xS_3^xS_4^zS_5^xS_6^x + 63S_1^yS_2^xS_3^xS_4^zS_5^xS_6^x + 63S_1^zS_2^xS_3^xS_4^zS_5^xS_6^x - 63S_1^xS_2^yS_3^xS_4^zS_5^xS_6^x$$

$$+ 63S_1^zS_2^yS_3^xS_4^zS_5^xS_6^x - 63S_1^xS_2^zS_3^xS_4^zS_5^xS_6^x - 189S_1^yS_2^zS_3^xS_4^zS_5^xS_6^x + 63S_1^zS_2^zS_3^xS_4^zS_5^xS_6^x$$

$$- 39.75S_3^yS_4^zS_5^xS_6^x + 63S_1^xS_2^xS_3^yS_4^zS_5^xS_6^x - 189S_1^yS_2^xS_3^yS_4^zS_5^xS_6^x + 63S_1^yS_2^yS_3^xS_4^zS_5^xS_6^x$$

$$+ 63S_1^xS_2^yS_3^yS_4^zS_5^xS_6^x + 63S_1^yS_2^yS_3^yS_4^zS_5^xS_6^x + 315S_1^zS_2^yS_3^yS_4^zS_5^xS_6^x + 63S_1^xS_2^zS_3^yS_4^zS_5^xS_6^x$$

$$- 63S_1^yS_2^zS_3^yS_4^zS_5^xS_6^x + 63S_1^zS_2^xS_3^yS_4^zS_5^xS_6^x + 189S_1^zS_2^zS_3^yS_4^zS_5^xS_6^x - 83.75S_3^zS_4^zS_5^xS_6^x$$

$$+ 189S_1^xS_2^xS_3^zS_4^zS_5^xS_6^x + 63S_1^yS_2^xS_3^zS_4^zS_5^xS_6^x + 63S_1^zS_2^xS_3^zS_4^zS_5^xS_6^x + 63S_1^xS_2^yS_3^zS_4^zS_5^xS_6^x$$

$$+ 189S_1^yS_2^yS_3^zS_4^zS_5^xS_6^x + 63S_1^zS_2^yS_3^zS_4^zS_5^xS_6^x + 63S_1^xS_2^zS_3^zS_4^zS_5^xS_6^x + 63S_1^yS_2^zS_3^zS_4^zS_5^xS_6^x$$

$$+ 315S_1^zS_2^zS_3^zS_4^zS_5^xS_6^x + 11.44S_5^yS_6^x - 36.25S_1^xS_2^xS_5^yS_6^x - 9.25S_1^yS_2^xS_5^yS_6^x - 21.25S_1^zS_2^xS_5^yS_6^x$$

$$- 24.75S_1^xS_2^yS_5^yS_6^x - 43.25S_1^yS_2^yS_5^yS_6^x - 76.75S_1^zS_2^yS_5^yS_6^x - 23.25S_1^xS_2^zS_5^yS_6^x - 25.75S_1^yS_2^zS_5^yS_6^x$$

$$- 39.75S_1^zS_2^zS_5^yS_6^x + 45.75S_1^xS_3^xS_5^yS_6^x + 8.75S_1^yS_3^xS_5^yS_6^x + 45.75S_1^zS_3^xS_5^yS_6^x$$

$$- 43.25S_2^xS_3^xS_5^yS_6^x - 83.75S_2^yS_3^xS_5^yS_6^x - 14.75S_2^zS_3^xS_5^yS_6^x + 3.25S_1^xS_3^yS_5^yS_6^x$$

$$+ 16.25S_1^xS_3^zS_5^yS_6^x - 10.75S_1^yS_3^zS_5^yS_6^x + 15.75S_1^zS_3^zS_5^yS_6^x - 25.75S_2^xS_3^zS_5^yS_6^x - 39.75S_2^yS_3^zS_5^yS_6^x$$

$$- 23.25S_2^zS_3^zS_5^yS_6^x - 14.25S_1^xS_4^xS_5^yS_6^x - 9.25S_1^yS_4^xS_5^yS_6^x - 31.25S_1^zS_4^xS_5^yS_6^x$$

$$- 23.25S_2^xS_4^xS_5^yS_6^x + 21.25S_2^yS_4^xS_5^yS_6^x + 15.75S_2^zS_4^xS_5^yS_6^x - 12.75S_3^xS_4^xS_5^yS_6^x$$

$$+ 63S_1^xS_2^xS_3^xS_4^xS_5^yS_6^x - 63S_1^yS_2^xS_3^xS_4^xS_5^yS_6^x - 63S_1^zS_2^xS_3^xS_4^xS_5^yS_6^x + 315S_1^xS_2^yS_3^xS_4^xS_5^yS_6^x$$

$$+ 63S_1^yS_2^yS_3^xS_4^xS_5^yS_6^x + 63S_1^zS_2^yS_3^xS_4^xS_5^yS_6^x + 63S_1^xS_2^zS_3^xS_4^xS_5^yS_6^x - 63S_1^yS_2^zS_3^xS_4^xS_5^yS_6^x$$

$$+ 63S_1^zS_2^zS_3^xS_4^xS_5^yS_6^x + 28.75S_3^yS_4^xS_5^yS_6^x - 63S_1^xS_2^xS_3^yS_4^xS_5^yS_6^x + 63S_1^yS_2^xS_3^yS_4^xS_5^yS_6^x$$

$$- 63S_1^zS_2^xS_3^yS_4^xS_5^yS_6^x + 63S_1^xS_2^yS_3^yS_4^xS_5^yS_6^x - 63S_1^yS_2^yS_3^yS_4^xS_5^yS_6^x - 189S_1^zS_2^yS_3^yS_4^xS_5^yS_6^x$$

$$- 189S_1^xS_2^zS_3^yS_4^xS_5^yS_6^x - 63S_1^yS_2^zS_3^yS_4^xS_5^yS_6^x - 63S_1^zS_2^zS_3^yS_4^xS_5^yS_6^x + 32.75S_3^zS_4^xS_5^yS_6^x$$

$$+ 63S_1^xS_2^xS_3^zS_4^xS_5^yS_6^x - 63S_1^yS_2^xS_3^zS_4^xS_5^yS_6^x - 63S_1^zS_2^xS_3^zS_4^xS_5^yS_6^x + 189S_1^xS_2^yS_3^zS_4^xS_5^yS_6^x$$

$$+ 63S_1^yS_2^yS_3^zS_4^xS_5^yS_6^x - 63S_1^zS_2^yS_3^zS_4^xS_5^yS_6^x + 63S_1^xS_2^zS_3^zS_4^xS_5^yS_6^x - 63S_1^yS_2^zS_3^zS_4^xS_5^yS_6^x$$

$$- 189S_1^zS_2^zS_3^zS_4^xS_5^yS_6^x - 32.25S_1^xS_4^yS_5^yS_6^x - 36.25S_1^yS_4^yS_5^yS_6^x - 19.25S_1^zS_4^yS_5^yS_6^x$$

$$+ 8.75S_2^xS_4^yS_5^yS_6^x + 7.25S_2^yS_4^yS_5^yS_6^x + 16.25S_2^zS_4^yS_5^yS_6^x - 41.75S_3^xS_4^yS_5^yS_6^x$$

$$+ 189S_1^xS_2^xS_3^xS_4^yS_5^yS_6^x + 63S_1^yS_2^xS_3^xS_4^yS_5^yS_6^x + 63S_1^zS_2^xS_3^xS_4^yS_5^yS_6^x + 63S_1^xS_2^yS_3^xS_4^yS_5^yS_6^x$$

$$+ 189S_1^yS_2^yS_3^xS_4^yS_5^yS_6^x + 63S_1^zS_2^yS_3^xS_4^yS_5^yS_6^x + 63S_1^xS_2^zS_3^xS_4^yS_5^yS_6^x + 63S_1^yS_2^zS_3^xS_4^yS_5^yS_6^x$$

$$+ 315S_1^zS_2^zS_3^xS_4^yS_5^yS_6^x - 28.25S_3^yS_4^yS_5^yS_6^x + 63S_1^xS_2^xS_3^yS_4^yS_5^yS_6^x - 63S_1^yS_2^xS_3^yS_4^yS_5^yS_6^x$$

$$+ 63S_1^zS_2^xS_3^yS_4^yS_5^yS_6^x + 63S_1^xS_2^yS_3^yS_4^yS_5^yS_6^x + 63S_1^yS_2^yS_3^yS_4^yS_5^yS_6^x + 63S_1^zS_2^yS_3^yS_4^yS_5^yS_6^x$$

$$+ 63S_1^xS_2^zS_3^yS_4^yS_5^yS_6^x + 63S_1^yS_2^zS_3^yS_4^yS_5^yS_6^x + 189S_1^zS_2^zS_3^yS_4^yS_5^yS_6^x - 23.25S_3^zS_4^yS_5^yS_6^x$$

$$+ 63S_1^xS_2^xS_3^zS_4^yS_5^yS_6^x - 63S_1^yS_2^xS_3^zS_4^yS_5^yS_6^x - 63S_1^zS_2^xS_3^zS_4^yS_5^yS_6^x + 63S_1^xS_2^yS_3^zS_4^yS_5^yS_6^x$$

$$+ 63S_1^yS_2^yS_3^zS_4^yS_5^yS_6^x - 189S_1^zS_2^yS_3^zS_4^yS_5^yS_6^x + 63S_1^xS_2^zS_3^zS_4^yS_5^yS_6^x + 63S_1^yS_2^zS_3^zS_4^yS_5^yS_6^x$$

$$+ 63S_1^zS_2^zS_3^zS_4^yS_5^yS_6^x - 14.75S_1^xS_4^zS_5^yS_6^x - 21.25S_1^yS_4^zS_5^yS_6^x - 38.25S_1^zS_4^zS_5^yS_6^x$$

$$- 10.75S_2^xS_4^zS_5^yS_6^x - 1.75S_2^yS_4^zS_5^yS_6^x - 10.75S_2^zS_4^zS_5^yS_6^x - 38.25S_3^xS_4^zS_5^yS_6^x$$

$$+ 63S_1^xS_2^xS_3^xS_4^zS_5^yS_6^x + 63S_1^yS_2^xS_3^xS_4^zS_5^yS_6^x + 63S_1^zS_2^xS_3^xS_4^zS_5^yS_6^x + 63S_1^xS_2^yS_3^xS_4^zS_5^yS_6^x$$

$$+ 63S_1^yS_2^yS_3^xS_4^zS_5^yS_6^x + 189S_1^zS_2^yS_3^xS_4^zS_5^yS_6^x - 63S_1^xS_2^zS_3^xS_4^zS_5^yS_6^x$$

$$- 63S_1^yS_2^zS_3^yS_4^zS_5^yS_6^x + 63S_1^zS_2^zS_3^yS_4^zS_5^yS_6^x - 14.75S_3^zS_4^zS_5^yS_6^x + 63S_1^xS_2^xS_3^zS_4^zS_5^yS_6^x$$

$$- 63S_1^zS_2^xS_3^zS_4^zS_5^yS_6^x + 315S_1^xS_2^yS_3^zS_4^zS_5^yS_6^x + 63S_1^yS_2^yS_3^zS_4^zS_5^yS_6^x + 63S_1^zS_2^yS_3^zS_4^zS_5^yS_6^x$$

$$+ 63S_1^xS_2^zS_3^zS_4^zS_5^yS_6^x - 63S_1^yS_2^zS_3^zS_4^zS_5^yS_6^x + 63S_1^zS_2^zS_3^zS_4^zS_5^yS_6^x - 63S_1^yS_2^xS_3^zS_4^zS_5^yS_6^x$$

$$+ 11.44S_5^zS_6^x - 12.75S_1^xS_2^xS_5^zS_6^x + 32.75S_1^yS_2^xS_5^zS_6^x + 28.75S_1^zS_2^xS_5^zS_6^x - 38.25S_1^xS_2^yS_5^zS_6^x$$

$$- 14.75S_1^yS_2^yS_5^zS_6^x - 21.25S_1^zS_2^yS_5^zS_6^x - 41.75S_1^xS_2^zS_5^zS_6^x - 23.25S_1^yS_2^zS_5^zS_6^x$$

$$- 28.25S_1^zS_2^zS_5^zS_6^x + 45.75S_1^xS_3^xS_5^zS_6^x + 16.25S_1^yS_3^xS_5^zS_6^x + 3.25S_1^zS_3^xS_5^zS_6^x$$

$$- 14.25S_2^xS_3^xS_5^zS_6^x - 14.75S_2^yS_3^xS_5^zS_6^x - 32.25S_2^zS_3^xS_5^zS_6^x + 45.75S_1^xS_3^yS_5^zS_6^x + 15.75S_1^yS_3^yS_5^zS_6^x$$

$$- 3.25S_1^zS_3^yS_5^zS_6^x - 31.25S_2^xS_3^yS_5^zS_6^x - 38.25S_2^yS_3^yS_5^zS_6^x - 19.25S_2^zS_3^yS_5^zS_6^x + 8.75S_1^xS_3^zS_5^zS_6^x$$

$$- 10.75S_1^yS_3^zS_5^zS_6^x - 23.25S_1^zS_3^zS_5^zS_6^x - 9.25S_2^xS_3^zS_5^zS_6^x - 21.25S_2^yS_3^zS_5^zS_6^x$$

$$- 36.25S_2^zS_3^zS_5^zS_6^x - 43.25S_1^xS_4^xS_5^zS_6^x - 25.75S_1^yS_4^xS_5^zS_6^x - 9.25S_1^zS_4^xS_5^zS_6^x - 23.25S_2^xS_4^xS_5^zS_6^x$$

$$- 10.75S_2^yS_4^xS_5^zS_6^x + 8.75S_2^zS_4^xS_5^zS_6^x - 36.25S_3^xS_4^xS_5^zS_6^x + 63S_1^xS_2^xS_3^xS_4^xS_5^zS_6^x$$

$$+ 63S_1^yS_2^xS_3^xS_4^xS_5^zS_6^x - 63S_1^zS_2^xS_3^xS_4^xS_5^zS_6^x + 63S_1^xS_2^yS_3^xS_4^xS_5^zS_6^x + 63S_1^yS_2^yS_3^xS_4^xS_5^zS_6^x$$

$$+ 189S_1^xS_2^zS_3^xS_4^xS_5^zS_6^x + 63S_1^yS_2^zS_3^xS_4^xS_5^zS_6^x + 63S_1^zS_2^zS_3^xS_4^xS_5^zS_6^x - 21.25S_3^yS_4^xS_5^zS_6^x$$

$$- 63S_1^xS_2^xS_3^yS_4^xS_5^zS_6^x - 63S_1^yS_2^xS_3^yS_4^xS_5^zS_6^x - 63S_1^zS_2^xS_3^yS_4^xS_5^zS_6^x - 63S_1^zS_2^yS_3^xS_4^xS_5^zS_6^x$$

$$+ 63S_1^xS_2^yS_3^yS_4^xS_5^zS_6^x - 63S_1^yS_2^yS_3^yS_4^xS_5^zS_6^x - 63S_1^zS_2^yS_3^yS_4^xS_5^zS_6^x + 63S_1^xS_2^zS_3^yS_4^xS_5^zS_6^x$$

$$- 63S_1^yS_2^zS_3^yS_4^xS_5^zS_6^x + 63S_1^zS_2^zS_3^yS_4^xS_5^zS_6^x - 9.25S_3^zS_4^xS_5^zS_6^x - 63S_1^xS_2^xS_3^zS_4^xS_5^zS_6^x$$

$$- 63S_1^yS_2^xS_3^zS_4^xS_5^zS_6^x + 63S_1^zS_2^xS_3^zS_4^xS_5^zS_6^x + 63S_1^xS_2^yS_3^zS_4^xS_5^zS_6^x - 63S_1^yS_2^yS_3^zS_4^xS_5^zS_6^x$$

$$- 63S_1^zS_2^yS_3^zS_4^xS_5^zS_6^x + 63S_1^xS_2^zS_3^zS_4^xS_5^zS_6^x - 63S_1^yS_2^zS_3^zS_4^xS_5^zS_6^x - 63S_1^zS_2^zS_3^zS_4^xS_5^zS_6^x$$

$$- 14.75S_1^xS_4^yS_5^zS_6^x - 23.25S_1^yS_4^yS_5^zS_6^x + 32.75S_1^zS_4^yS_5^zS_6^x + 15.75S_2^xS_4^yS_5^zS_6^x - 10.75S_2^yS_4^yS_5^zS_6^x$$

$$+ 16.25S_2^zS_4^yS_5^zS_6^x - 23.25S_3^xS_4^yS_5^zS_6^x + 63S_1^xS_2^xS_3^xS_4^yS_5^zS_6^x + 63S_1^yS_2^xS_3^xS_4^yS_5^zS_6^x$$

$$- 63S_1^xS_2^yS_3^xS_4^yS_5^zS_6^x + 63S_1^yS_2^yS_3^xS_4^yS_5^zS_6^x - 63S_1^zS_2^yS_3^xS_4^yS_5^zS_6^x + 63S_1^xS_2^zS_3^xS_4^yS_5^zS_6^x$$

$$+ 63S_1^yS_2^zS_3^xS_4^yS_5^zS_6^x + 63S_1^zS_2^zS_3^xS_4^yS_5^zS_6^x - 39.75S_3^yS_4^yS_5^zS_6^x + 63S_1^xS_2^xS_3^yS_4^yS_5^zS_6^x$$

$$- 63S_1^zS_2^xS_3^yS_4^yS_5^zS_6^x + 63S_1^xS_2^yS_3^yS_4^yS_5^zS_6^x + 63S_1^yS_2^yS_3^yS_4^yS_5^zS_6^x + 63S_1^zS_2^yS_3^yS_4^yS_5^zS_6^x$$

$$+ 315S_1^xS_2^zS_3^yS_4^yS_5^zS_6^x + 63S_1^yS_2^zS_3^yS_4^yS_5^zS_6^x + 189S_1^zS_2^zS_3^yS_4^yS_5^zS_6^x - 189S_1^zS_2^xS_3^xS_4^yS_5^zS_6^x$$

$$- 63S_1^zS_2^xS_3^zS_4^yS_5^zS_6^x - 63S_1^xS_2^yS_3^zS_4^yS_5^zS_6^x - 63S_1^yS_2^yS_3^zS_4^yS_5^zS_6^x - 63S_1^zS_2^yS_3^zS_4^yS_5^zS_6^x$$

$$+ 63S_1^xS_2^zS_3^zS_4^yS_5^zS_6^x + 63S_1^yS_2^zS_3^zS_4^yS_5^zS_6^x + 63S_1^zS_2^zS_3^zS_4^yS_5^zS_6^x - 83.75S_1^xS_4^zS_5^zS_6^x$$

$$- 39.75S_1^yS_4^zS_5^zS_6^x - 21.25S_1^zS_4^zS_5^zS_6^x + 21.25S_2^xS_4^zS_5^zS_6^x - 1.75S_2^yS_4^zS_5^zS_6^x$$

$$+ 7.25S_2^zS_4^zS_5^zS_6^x - 24.75S_3^xS_4^zS_5^zS_6^x + 315S_1^xS_2^xS_3^xS_4^zS_5^zS_6^x + 189S_1^yS_2^xS_3^xS_4^zS_5^zS_6^x$$

$$+ 63S_1^zS_2^xS_3^xS_4^zS_5^zS_6^x + 63S_1^xS_2^yS_3^xS_4^zS_5^zS_6^x + 315S_1^yS_2^yS_3^xS_4^zS_5^zS_6^x + 63S_1^zS_2^yS_3^xS_4^zS_5^zS_6^x$$

$$+ 63S_1^xS_2^zS_3^xS_4^zS_5^zS_6^x + 63S_1^yS_2^zS_3^xS_4^zS_5^zS_6^x + 63S_1^zS_2^zS_3^xS_4^zS_5^zS_6^x - 76.75S_3^yS_4^zS_5^zS_6^x$$

$$+ 63S_1^xS_2^xS_3^yS_4^zS_5^zS_6^x - 63S_1^yS_2^xS_3^yS_4^zS_5^zS_6^x - 189S_1^zS_2^xS_3^yS_4^zS_5^zS_6^x + 189S_1^xS_2^yS_3^yS_4^zS_5^zS_6^x$$

$$+ 63S_1^yS_2^yS_3^yS_4^zS_5^zS_6^x + 63S_1^zS_2^yS_3^yS_4^zS_5^zS_6^x + 63S_1^xS_2^zS_3^yS_4^zS_5^zS_6^x - 189S_1^yS_2^zS_3^yS_4^zS_5^zS_6^x$$

$$+ 63S_1^zS_2^zS_3^yS_4^zS_5^zS_6^x - 43.25S_3^zS_4^zS_5^zS_6^x + 63S_1^xS_2^xS_3^zS_4^zS_5^zS_6^x + 63S_1^yS_2^xS_3^zS_4^zS_5^zS_6^x$$

$$- 63S_1^zS_2^xS_3^zS_4^zS_5^zS_6^x + 63S_1^xS_2^yS_3^zS_4^zS_5^zS_6^x + 63S_1^yS_2^yS_3^zS_4^zS_5^zS_6^x - 63S_1^zS_2^yS_3^zS_4^zS_5^zS_6^x$$

$$+ 189S_1^xS_2^zS_3^zS_4^zS_5^zS_6^x + 63S_1^yS_2^zS_3^zS_4^zS_5^zS_6^x + 63S_1^zS_2^zS_3^zS_4^zS_5^zS_6^x + 11.44S_1^xS_6^y$$

$$+ 21.31S_1^yS_6^y + 11.44S_1^zS_6^y - 11.81S_2^xS_6^y - 12.44S_2^yS_6^y - 13.56S_2^zS_6^y + 13.19S_3^xS_6^y$$

$$- 28.25S_1^xS_2^xS_3^xS_6^y - 39.25S_1^yS_2^xS_3^xS_6^y - 39.75S_1^zS_2^xS_3^xS_6^y + 28.75S_1^xS_2^yS_3^xS_6^y$$

$$- 28.25S_1^yS_2^yS_3^xS_6^y - 21.25S_1^zS_2^yS_3^xS_6^y - 21.25S_1^xS_2^zS_3^xS_6^y - 39.75S_1^yS_2^zS_3^xS_6^y$$

$$- 76.75S_1^zS_2^zS_3^xS_6^y + 23.94S_3^yS_6^y - 41.75S_1^xS_2^xS_3^yS_6^y - 28.25S_1^yS_2^xS_3^yS_6^y - 23.25S_1^zS_2^xS_3^yS_6^y$$

$$- 12.75S_1^xS_2^yS_3^yS_6^y - 56.75S_1^yS_2^yS_3^yS_6^y - 36.25S_1^zS_2^yS_3^yS_6^y - 38.25S_1^xS_2^zS_3^yS_6^y$$

$$- 21.25S_1^yS_2^zS_3^yS_6^y - 24.75S_1^zS_2^zS_3^yS_6^y + 11.44S_3^zS_6^y - 23.25S_1^xS_2^xS_3^zS_6^y - 39.75S_1^yS_2^xS_3^zS_6^y$$

$$- 25.75S_1^zS_2^xS_3^zS_6^y + 32.75S_1^xS_2^yS_3^zS_6^y - 21.25S_1^yS_2^yS_3^zS_6^y - 9.25S_1^zS_2^yS_3^zS_6^y - 14.75S_1^xS_2^zS_3^zS_6^y$$

$$- 83.75S_1^yS_2^zS_3^zS_6^y - 43.25S_1^zS_2^zS_3^zS_6^y - 13.56S_4^xS_6^y + 7.25S_1^xS_2^xS_4^xS_6^y$$

$$+ 21.25S_1^yS_2^xS_4^xS_6^y - 10.75S_1^zS_2^xS_4^xS_6^y + 21.25S_1^xS_2^yS_4^xS_6^y + 7.25S_1^yS_2^yS_4^xS_6^y$$

$$- 10.75S_1^zS_2^yS_4^xS_6^y - 1.75S_1^xS_2^zS_4^xS_6^y - 1.75S_1^yS_2^zS_4^xS_6^y - 1.75S_1^zS_2^zS_4^xS_6^y - 21.25S_1^xS_3^xS_4^xS_6^y$$

$$- 24.75S_1^yS_3^xS_4^xS_6^y - 38.25S_1^zS_3^xS_4^xS_6^y + 44.25S_2^xS_3^xS_4^xS_6^y + 3.25S_2^yS_3^xS_4^xS_6^y$$

$$+ 45.75S_2^zS_3^xS_4^xS_6^y - 83.75S_1^xS_3^yS_4^xS_6^y - 43.25S_1^yS_3^yS_4^xS_6^y - 14.75S_1^zS_3^yS_4^xS_6^y + 8.75S_2^xS_3^yS_4^xS_6^y$$

$$+ 45.75S_2^yS_3^yS_4^xS_6^y + 45.75S_2^zS_3^yS_4^xS_6^y - 39.75S_1^xS_3^zS_4^xS_6^y - 76.75S_1^yS_3^zS_4^xS_6^y$$

$$+ 8.75S_1^xS_2^xS_4^yS_6^y + 44.25S_1^yS_2^xS_4^yS_6^y + 15.75S_1^zS_2^xS_4^yS_6^y - 23.25S_1^xS_2^yS_4^yS_6^y$$

$$- 9.25S_1^yS_2^yS_4^yS_6^y - 23.25S_1^zS_2^yS_4^yS_6^y - 10.75S_1^xS_2^zS_4^yS_6^y + 7.25S_1^yS_2^zS_4^yS_6^y + 21.25S_1^zS_2^zS_4^yS_6^y$$

$$- 9.25S_1^xS_3^xS_4^yS_6^y - 14.25S_1^yS_3^xS_4^yS_6^y - 31.25S_1^zS_3^xS_4^yS_6^y + 21.25S_2^xS_3^xS_4^yS_6^y$$

$$- 23.25S_2^yS_3^xS_4^yS_6^y + 15.75S_2^zS_3^xS_4^yS_6^y - 43.25S_1^xS_3^yS_4^yS_6^y - 39.25S_1^yS_3^yS_4^yS_6^y$$

$$- 14.25S_1^zS_3^yS_4^yS_6^y + 7.25S_2^xS_3^yS_4^yS_6^y - 9.25S_2^yS_3^yS_4^yS_6^y + 44.25S_2^zS_3^yS_4^yS_6^y$$

$$- 25.75S_1^xS_3^zS_4^yS_6^y - 43.25S_1^yS_3^zS_4^yS_6^y - 9.25S_1^zS_3^zS_4^yS_6^y - 10.75S_2^xS_3^zS_4^yS_6^y$$

$$- 23.25S_2^yS_3^zS_4^yS_6^y + 8.75S_2^zS_3^zS_4^yS_6^y - 11.81S_4^zS_6^y + 16.25S_1^xS_2^xS_4^zS_6^y + 2.25S_1^yS_2^xS_4^zS_6^y$$

$$+ 16.25S_1^zS_2^xS_4^zS_6^y + 15.75S_1^xS_2^yS_4^zS_6^y + 44.25S_1^yS_2^yS_4^zS_6^y + 8.75S_1^zS_2^yS_4^zS_6^y$$

$$- 10.75S_1^xS_2^zS_4^zS_6^y + 21.25S_1^yS_2^zS_4^zS_6^y + 7.25S_1^zS_2^zS_4^zS_6^y + 32.75S_1^xS_3^xS_4^zS_6^y + 46.25S_1^yS_3^xS_4^zS_6^y$$

$$- 3.25S_2^yS_3^xS_4^zS_6^y - 3.25S_2^zS_3^xS_4^zS_6^y - 14.75S_1^xS_3^yS_4^zS_6^y - 14.25S_1^yS_3^yS_4^zS_6^y$$

$$- 32.25S_1^zS_3^yS_4^zS_6^y + 16.25S_2^xS_3^yS_4^zS_6^y + 45.75S_2^yS_3^yS_4^zS_6^y + 3.25S_2^zS_3^yS_4^zS_6^y$$

$$- 23.25S_1^xS_3^zS_4^zS_6^y - 24.75S_1^yS_3^zS_4^zS_6^y - 36.25S_1^zS_3^zS_4^zS_6^y + 16.25S_2^xS_3^zS_4^zS_6^y + 3.25S_2^yS_3^zS_4^zS_6^y$$

$$+ 45.75S_2^zS_3^zS_4^zS_6^y + 11.44S_5^xS_6^y - 36.25S_1^xS_2^xS_5^xS_6^y - 19.25S_1^zS_3^xS_4^zS_6^y + 2.25S_2^xS_3^xS_4^zS_6^y$$

$$- 24.75S_1^yS_2^xS_5^xS_6^y - 23.25S_1^zS_2^xS_5^xS_6^y - 9.25S_1^xS_2^yS_5^xS_6^y - 43.25S_1^yS_2^yS_5^xS_6^y$$

$$- 25.75S_1^zS_2^yS_5^xS_6^y - 21.25S_1^xS_2^zS_5^xS_6^y - 76.75S_1^yS_2^zS_5^xS_6^y - 39.75S_1^zS_2^zS_5^xS_6^y - 23.25S_1^xS_3^xS_5^xS_6^y$$

$$+ 21.25S_1^yS_3^xS_5^xS_6^y + 15.75S_1^zS_3^xS_5^xS_6^y - 14.25S_2^xS_3^xS_5^xS_6^y - 9.25S_2^yS_3^xS_5^xS_6^y$$

$$- 31.25S_2^zS_3^xS_5^xS_6^y + 8.75S_1^xS_3^yS_5^xS_6^y + 7.25S_1^yS_3^yS_5^xS_6^y + 16.25S_1^zS_3^yS_5^xS_6^y - 32.25S_2^xS_3^yS_5^xS_6^y$$

$$- 36.25S_2^yS_3^yS_5^xS_6^y - 19.25S_2^zS_3^yS_5^xS_6^y - 10.75S_1^xS_3^zS_5^xS_6^y - 1.75S_1^yS_3^zS_5^xS_6^y$$

$$- 10.75S_1^zS_3^zS_5^xS_6^y - 14.75S_2^xS_3^zS_5^xS_6^y - 21.25S_2^yS_3^zS_5^xS_6^y - 38.25S_2^zS_3^zS_5^xS_6^y - 43.25S_1^xS_4^xS_5^xS_6^y$$

$$- 83.75S_1^yS_4^xS_5^xS_6^y - 14.75S_1^zS_4^xS_5^xS_6^y + 45.75S_2^xS_4^xS_5^xS_6^y + 8.75S_2^yS_4^xS_5^xS_6^y$$

$$+ 45.75S_2^zS_4^xS_5^xS_6^y - 12.75S_3^xS_4^xS_5^xS_6^y + 63S_1^xS_2^xS_3^xS_4^xS_5^xS_6^y + 315S_1^yS_2^xS_3^xS_4^xS_5^xS_6^y$$

$$+ 63S_1^zS_2^xS_3^xS_4^xS_5^xS_6^y - 63S_1^xS_2^yS_3^xS_4^xS_5^xS_6^y + 63S_1^yS_2^yS_3^xS_4^xS_5^xS_6^y - 63S_1^zS_2^yS_3^xS_4^xS_5^xS_6^y$$

$$- 63S_1^xS_2^zS_3^xS_4^xS_5^xS_6^y + 63S_1^yS_2^zS_3^xS_4^xS_5^xS_6^y + 63S_1^zS_2^zS_3^xS_4^xS_5^xS_6^y - 41.75S_3^yS_4^xS_5^xS_6^y$$

$$+ 189S_1^xS_2^xS_3^yS_4^xS_5^xS_6^y + 63S_1^yS_2^xS_3^yS_4^xS_5^xS_6^y + 63S_1^zS_2^xS_3^yS_4^xS_5^xS_6^y + 63S_1^xS_2^yS_3^yS_4^xS_5^xS_6^y$$

$$+ 315S_1^zS_2^zS_3^yS_4^xS_5^xS_6^y - 38.25S_3^zS_4^xS_5^xS_6^y + 63S_1^xS_2^xS_3^zS_4^xS_5^xS_6^y + 63S_1^yS_2^xS_3^zS_4^xS_5^xS_6^y$$

$$- 63S_1^zS_2^xS_3^zS_4^xS_5^xS_6^y + 63S_1^xS_2^yS_3^zS_4^xS_5^xS_6^y + 63S_1^yS_2^yS_3^zS_4^xS_5^xS_6^y - 63S_1^zS_2^yS_3^zS_4^xS_5^xS_6^y$$

$$+ 63S_1^xS_2^zS_3^zS_4^xS_5^xS_6^y + 189S_1^yS_2^zS_3^zS_4^xS_5^xS_6^y + 63S_1^zS_2^zS_3^zS_4^xS_5^xS_6^y - 9.25S_1^xS_4^yS_5^xS_6^y$$

$$- 21.25S_1^yS_4^yS_5^xS_6^y + 32.75S_1^zS_4^yS_5^xS_6^y + 3.25S_2^xS_4^yS_5^xS_6^y - 23.25S_2^yS_4^yS_5^xS_6^y$$

$$- 3.25S_2^zS_4^yS_5^xS_6^y + 28.75S_3^xS_4^yS_5^xS_6^y - 63S_1^xS_2^xS_3^xS_4^yS_5^xS_6^y + 63S_1^yS_2^xS_3^xS_4^yS_5^xS_6^y$$

$$- 189S_1^zS_2^xS_3^xS_4^yS_5^xS_6^y + 63S_1^xS_2^yS_3^xS_4^yS_5^xS_6^y - 63S_1^yS_2^yS_3^xS_4^yS_5^xS_6^y - 63S_1^zS_2^yS_3^xS_4^yS_5^xS_6^y$$

$$- 63S_1^xS_2^zS_3^xS_4^yS_5^xS_6^y - 189S_1^yS_2^zS_3^xS_4^yS_5^xS_6^y - 63S_1^zS_2^zS_3^xS_4^yS_5^xS_6^y - 28.25S_3^yS_4^yS_5^xS_6^y$$

$$+ 63S_1^xS_2^xS_3^yS_4^yS_5^xS_6^y + 63S_1^yS_2^xS_3^yS_4^yS_5^xS_6^y + 63S_1^zS_2^xS_3^yS_4^yS_5^xS_6^y - 63S_1^xS_2^yS_3^yS_4^yS_5^xS_6^y$$

$$+ 63S_1^yS_2^yS_3^yS_4^yS_5^xS_6^y + 63S_1^zS_2^yS_3^yS_4^yS_5^xS_6^y + 63S_1^xS_2^zS_3^yS_4^yS_5^xS_6^y + 63S_1^yS_2^zS_3^yS_4^yS_5^xS_6^y$$

$$- 21.25S_3^zS_4^yS_5^xS_6^y - 63S_1^xS_2^xS_3^zS_4^yS_5^xS_6^y + 63S_1^yS_2^xS_3^zS_4^yS_5^xS_6^y - 63S_1^zS_2^xS_3^zS_4^yS_5^xS_6^y$$

$$- 63S_1^xS_2^yS_3^zS_4^yS_5^xS_6^y - 63S_1^yS_2^yS_3^zS_4^yS_5^xS_6^y - 63S_1^zS_2^yS_3^zS_4^yS_5^xS_6^y - 63S_1^xS_2^zS_3^zS_4^yS_5^xS_6^y$$

$$+ 63S_1^yS_2^zS_3^zS_4^yS_5^xS_6^y + 63S_1^zS_2^zS_3^zS_4^yS_5^xS_6^y - 25.75S_1^xS_4^zS_5^xS_6^y + 189S_1^zS_2^zS_3^yS_4^yS_5^xS_6^y$$

$$- 39.75S_1^yS_4^zS_5^xS_6^y - 23.25S_1^zS_4^zS_5^xS_6^y + 16.25S_2^xS_4^zS_5^xS_6^y - 10.75S_2^yS_4^zS_5^xS_6^y$$

$$+ 15.75S_2^zS_4^zS_5^xS_6^y + 32.75S_3^xS_4^zS_5^xS_6^y + 63S_1^xS_2^xS_3^xS_4^zS_5^xS_6^y + 189S_1^yS_2^xS_3^xS_4^zS_5^xS_6^y$$

$$+ 63S_1^zS_2^xS_3^xS_4^zS_5^xS_6^y - 63S_1^xS_2^yS_3^xS_4^zS_5^xS_6^y + 63S_1^yS_2^yS_3^xS_4^zS_5^xS_6^y - 63S_1^zS_2^yS_3^xS_4^zS_5^xS_6^y$$

$$- 63S_1^yS_2^zS_3^xS_4^zS_5^xS_6^y - 189S_1^zS_2^zS_3^xS_4^zS_5^xS_6^y - 23.25S_3^yS_4^zS_5^xS_6^y + 63S_1^xS_2^xS_3^yS_4^zS_5^xS_6^y$$

$$+ 63S_1^yS_2^xS_3^yS_4^zS_5^xS_6^y + 63S_1^zS_2^xS_3^yS_4^zS_5^xS_6^y - 63S_1^xS_2^yS_3^yS_4^zS_5^xS_6^y + 63S_1^yS_2^yS_3^yS_4^zS_5^xS_6^y$$

$$+ 63S_1^zS_2^yS_3^yS_4^zS_5^xS_6^y - 63S_1^xS_2^zS_3^yS_4^zS_5^xS_6^y - 189S_1^yS_2^zS_3^yS_4^zS_5^xS_6^y - 63S_1^xS_2^zS_3^xS_4^zS_5^xS_6^y$$

$$+ 63S_1^zS_2^zS_3^yS_4^zS_5^xS_6^y - 14.75S_3^zS_4^zS_5^xS_6^y + 63S_1^xS_2^xS_3^zS_4^zS_5^xS_6^y + 315S_1^yS_2^xS_3^zS_4^zS_5^xS_6^y$$

$$+ 63S_1^zS_2^xS_3^zS_4^zS_5^xS_6^y - 63S_1^xS_2^yS_3^zS_4^zS_5^xS_6^y + 63S_1^yS_2^yS_3^zS_4^zS_5^xS_6^y - 63S_1^zS_2^yS_3^zS_4^zS_5^xS_6^y$$

$$- 63S_1^xS_2^zS_3^zS_4^zS_5^xS_6^y + 63S_1^yS_2^zS_3^zS_4^zS_5^xS_6^y + 63S_1^zS_2^zS_3^zS_4^zS_5^xS_6^y + 23.94S_5^yS_6^y$$

$$- 32.25S_1^xS_2^xS_5^yS_6^y - 14.25S_1^yS_2^xS_5^yS_6^y - 14.75S_1^zS_2^xS_5^yS_6^y - 14.25S_1^xS_2^yS_5^yS_6^y$$

$$- 39.25S_1^yS_2^yS_5^yS_6^y - 43.25S_1^zS_2^yS_5^yS_6^y - 14.75S_1^xS_2^zS_5^yS_6^y - 43.25S_1^yS_2^zS_5^yS_6^y - 83.75S_1^zS_2^zS_5^yS_6^y$$

$$+ 3.25S_1^xS_3^xS_5^yS_6^y + 44.25S_1^yS_3^xS_5^yS_6^y + 45.75S_1^zS_3^xS_5^yS_6^y - 24.75S_2^xS_3^xS_5^yS_6^y$$

$$+ 16.25S_1^xS_3^zS_5^yS_6^y + 7.25S_1^yS_3^zS_5^yS_6^y + 8.75S_1^zS_3^zS_5^yS_6^y - 23.25S_2^xS_3^zS_5^yS_6^y$$

$$- 28.25S_2^yS_3^zS_5^yS_6^y - 41.75S_2^zS_3^zS_5^yS_6^y - 24.75S_1^xS_4^xS_5^yS_6^y - 21.25S_1^yS_4^xS_5^yS_6^y$$

$$- 38.25S_1^zS_4^xS_5^yS_6^y + 3.25S_2^xS_4^xS_5^yS_6^y + 44.25S_2^yS_4^xS_5^yS_6^y + 45.75S_2^zS_4^xS_5^yS_6^y$$

$$- 39.25S_3^xS_4^xS_5^yS_6^y + 63S_1^xS_2^xS_3^xS_4^xS_5^yS_6^y + 63S_1^yS_2^xS_3^xS_4^xS_5^yS_6^y + 63S_1^zS_2^xS_3^xS_4^xS_5^yS_6^y$$

$$+ 63S_1^xS_2^yS_3^xS_4^xS_5^yS_6^y + 63S_1^yS_2^yS_3^xS_4^xS_5^yS_6^y + 63S_1^zS_2^yS_3^xS_4^xS_5^yS_6^y + 63S_1^xS_2^zS_3^xS_4^xS_5^yS_6^y$$

$$+ 63S_1^yS_2^zS_3^xS_4^xS_5^yS_6^y + 189S_1^zS_2^zS_3^xS_4^xS_5^yS_6^y - 12.75S_3^yS_4^xS_5^yS_6^y + 63S_1^xS_2^xS_3^yS_4^xS_5^yS_6^y$$

$$- 63S_1^yS_2^xS_3^yS_4^xS_5^yS_6^y - 63S_1^zS_2^xS_3^yS_4^xS_5^yS_6^y + 315S_1^xS_2^yS_3^yS_4^xS_5^yS_6^y + 63S_1^yS_2^yS_3^yS_4^xS_5^yS_6^y$$

$$+ 63S_1^zS_2^yS_3^yS_4^xS_5^yS_6^y + 63S_1^xS_2^zS_3^yS_4^xS_5^yS_6^y - 63S_1^yS_2^zS_3^yS_4^xS_5^yS_6^y + 63S_1^zS_2^zS_3^yS_4^xS_5^yS_6^y$$

$$- 19.25S_3^zS_4^xS_5^yS_6^y + 63S_1^xS_2^xS_3^zS_4^xS_5^yS_6^y - 189S_1^yS_2^xS_3^zS_4^xS_5^yS_6^y - 63S_1^zS_2^xS_3^zS_4^xS_5^yS_6^y$$

$$+ 189S_1^xS_2^yS_3^zS_4^xS_5^yS_6^y + 63S_1^yS_2^yS_3^zS_4^xS_5^yS_6^y + 63S_1^zS_2^yS_3^zS_4^xS_5^yS_6^y + 315S_1^xS_2^zS_3^zS_4^xS_5^yS_6^y$$

$$+ 63S_1^yS_2^zS_3^zS_4^xS_5^yS_6^y + 63S_1^zS_2^zS_3^zS_4^xS_5^yS_6^y - 36.25S_1^xS_4^yS_5^yS_6^y - 56.75S_1^yS_4^yS_5^yS_6^y$$

$$- 12.75S_1^zS_4^yS_5^yS_6^y + 45.75S_2^xS_4^yS_5^yS_6^y - 9.25S_2^yS_4^yS_5^yS_6^y + 45.75S_2^zS_4^yS_5^yS_6^y$$

$$- 12.75S_3^xS_4^yS_5^yS_6^y + 63S_1^xS_2^xS_3^xS_4^yS_5^yS_6^y + 315S_1^yS_2^xS_3^xS_4^yS_5^yS_6^y + 63S_1^zS_2^xS_3^xS_4^yS_5^yS_6^y$$

$$- 63S_1^xS_2^yS_3^xS_4^yS_5^yS_6^y + 63S_1^yS_2^yS_3^xS_4^yS_5^yS_6^y - 63S_1^zS_2^yS_3^xS_4^yS_5^yS_6^y - 63S_1^xS_2^zS_3^xS_4^yS_5^yS_6^y$$

$$+ 63S_1^yS_2^zS_3^xS_4^yS_5^yS_6^y + 63S_1^zS_2^zS_3^xS_4^yS_5^yS_6^y - 56.75S_3^yS_4^yS_5^yS_6^y + 189S_1^xS_2^xS_3^yS_4^yS_5^yS_6^y$$

$$+ 63S_1^yS_2^xS_3^yS_4^yS_5^yS_6^y + 63S_1^zS_2^xS_3^yS_4^yS_5^yS_6^y + 63S_1^xS_2^yS_3^yS_4^yS_5^yS_6^y + 189S_1^yS_2^yS_3^yS_4^yS_5^yS_6^y$$

$$+ 63S_1^zS_2^yS_3^yS_4^yS_5^yS_6^y + 63S_1^xS_2^zS_3^yS_4^yS_5^yS_6^y + 63S_1^yS_2^zS_3^yS_4^yS_5^yS_6^y + 315S_1^zS_2^zS_3^yS_4^yS_5^yS_6^y$$

$$- 36.25S_3^zS_4^yS_5^yS_6^y + 63S_1^xS_2^xS_3^zS_4^yS_5^yS_6^y + 63S_1^yS_2^xS_3^zS_4^yS_5^yS_6^y - 63S_1^zS_2^xS_3^zS_4^yS_5^yS_6^y$$

$$+ 63S_1^xS_2^yS_3^zS_4^yS_5^yS_6^y + 63S_1^yS_2^yS_3^zS_4^yS_5^yS_6^y - 63S_1^zS_2^yS_3^zS_4^yS_5^yS_6^y + 63S_1^xS_2^zS_3^zS_4^yS_5^yS_6^y$$

$$+ 189S_1^yS_2^zS_3^zS_4^yS_5^yS_6^y + 63S_1^zS_2^zS_3^zS_4^yS_5^yS_6^y - 23.25S_1^xS_4^zS_5^yS_6^y - 28.25S_1^yS_4^zS_5^yS_6^y$$

$$- 41.75S_1^zS_4^zS_5^yS_6^y + 16.25S_2^xS_4^zS_5^yS_6^y + 7.25S_2^yS_4^zS_5^yS_6^y + 8.75S_2^zS_4^zS_5^yS_6^y$$

$$- 19.25S_3^xS_4^zS_5^yS_6^y + 63S_1^xS_2^xS_3^xS_4^zS_5^yS_6^y + 189S_1^yS_2^xS_3^xS_4^zS_5^yS_6^y$$

$$+ 315S_1^zS_2^xS_3^xS_4^zS_5^yS_6^y - 189S_1^xS_2^yS_3^xS_4^zS_5^yS_6^y + 63S_1^yS_2^yS_3^xS_4^zS_5^yS_6^y$$

$$+ 63S_1^zS_2^yS_3^xS_4^zS_5^yS_6^y - 63S_1^xS_2^zS_3^xS_4^zS_5^yS_6^y + 63S_1^yS_2^zS_3^xS_4^zS_5^yS_6^y$$

$$+ 63S_1^yS_2^yS_3^yS_4^zS_5^yS_6^y + 189S_1^zS_2^yS_3^yS_4^zS_5^yS_6^y - 63S_1^xS_2^zS_3^yS_4^zS_5^yS_6^y$$

$$- 63S_1^yS_2^zS_3^yS_4^zS_5^yS_6^y + 63S_1^zS_2^zS_3^yS_4^zS_5^yS_6^y - 32.25S_3^zS_4^zS_5^yS_6^y$$

$$+ 63S_1^xS_2^xS_3^zS_4^zS_5^yS_6^y + 63S_1^yS_2^xS_3^zS_4^zS_5^yS_6^y + 63S_1^zS_2^xS_3^zS_4^zS_5^yS_6^y$$

$$+ 63S_1^xS_2^yS_3^zS_4^zS_5^yS_6^y + 63S_1^yS_2^yS_3^zS_4^zS_5^yS_6^y + 63S_1^zS_2^yS_3^zS_4^zS_5^yS_6^y$$

$$+ 63S_1^xS_2^zS_3^zS_4^zS_5^yS_6^y + 63S_1^yS_2^zS_3^zS_4^zS_5^yS_6^y + 189S_1^zS_2^zS_3^zS_4^zS_5^yS_6^y$$

$$+ 13.19S_5^zS_6^y - 19.25S_1^xS_2^xS_5^zS_6^y + 46.25S_1^yS_2^xS_5^zS_6^y$$

$$+ 32.75S_1^zS_2^xS_5^zS_6^y - 31.25S_1^xS_2^yS_5^zS_6^y - 14.25S_1^yS_2^yS_5^zS_6^y$$

$$- 9.25S_1^zS_2^yS_5^zS_6^y - 38.25S_1^xS_2^zS_5^zS_6^y - 24.75S_1^yS_2^zS_5^zS_6^y$$

$$- 21.25S_1^zS_2^zS_5^zS_6^y - 3.25S_1^xS_3^xS_5^zS_6^y + 2.25S_1^yS_3^xS_5^zS_6^y$$

$$- 3.25S_1^zS_3^xS_5^zS_6^y + 46.25S_2^xS_3^xS_5^zS_6^y + 32.75S_2^yS_3^xS_5^zS_6^y$$

$$- 19.25S_2^zS_3^xS_5^zS_6^y + 45.75S_1^xS_3^yS_5^zS_6^y + 44.25S_1^yS_3^yS_5^zS_6^y$$

$$+ 3.25S_1^zS_3^yS_5^zS_6^y - 19.25S_2^xS_3^yS_5^zS_6^y - 12.75S_2^yS_3^yS_5^zS_6^y$$

$$- 39.25S_2^zS_3^yS_5^zS_6^y + 15.75S_1^xS_3^zS_5^zS_6^y + 21.25S_1^yS_3^zS_5^zS_6^y$$

$$- 23.25S_1^zS_3^zS_5^zS_6^y + 32.75S_2^xS_3^zS_5^zS_6^y + 28.75S_2^yS_3^zS_5^zS_6^y$$

$$- 12.75S_2^zS_3^zS_5^zS_6^y - 76.75S_1^xS_4^xS_5^zS_6^y - 39.75S_1^yS_4^xS_5^zS_6^y$$

$$- 21.25S_1^zS_4^xS_5^zS_6^y - 3.25S_2^xS_4^xS_5^zS_6^y + 15.75S_2^yS_4^xS_5^zS_6^y$$

$$+ 45.75S_2^zS_4^xS_5^zS_6^y - 19.25S_3^xS_4^xS_5^zS_6^y + 63S_1^xS_2^xS_3^xS_4^xS_5^zS_6^y$$

$$+ 189S_1^yS_2^xS_3^xS_4^xS_5^zS_6^y + 63S_1^zS_2^xS_3^xS_4^xS_5^zS_6^y - 189S_1^xS_2^yS_3^xS_4^xS_5^zS_6^y$$

$$+ 63S_1^yS_2^yS_3^xS_4^xS_5^zS_6^y - 63S_1^zS_2^yS_3^xS_4^xS_5^zS_6^y + 63S_1^xS_2^zS_3^xS_4^xS_5^zS_6^y$$

$$+ 315S_1^yS_2^zS_3^xS_4^xS_5^zS_6^y + 63S_1^zS_2^zS_3^xS_4^xS_5^zS_6^y - 38.25S_3^yS_4^xS_5^zS_6^y$$

$$+ 63S_1^xS_2^xS_3^yS_4^xS_5^zS_6^y + 63S_1^yS_2^xS_3^yS_4^xS_5^zS_6^y - 63S_1^zS_2^xS_3^yS_4^xS_5^zS_6^y$$

$$+ 63S_1^xS_2^yS_3^yS_4^xS_5^zS_6^y + 63S_1^yS_2^yS_3^yS_4^xS_5^zS_6^y - 63S_1^zS_2^yS_3^yS_4^xS_5^zS_6^y$$

$$+ 189S_1^xS_2^zS_3^yS_4^xS_5^zS_6^y + 63S_1^yS_2^zS_3^yS_4^xS_5^zS_6^y + 63S_1^zS_2^zS_3^yS_4^xS_5^zS_6^y$$

$$- 31.25S_3^zS_4^xS_5^zS_6^y - 189S_1^xS_2^xS_3^zS_4^xS_5^zS_6^y - 63S_1^yS_2^xS_3^zS_4^xS_5^zS_6^y$$

$$- 63S_1^zS_2^yS_3^zS_4^xS_5^zS_6^y + 63S_1^xS_2^zS_3^zS_4^xS_5^zS_6^y + 63S_1^yS_2^zS_3^zS_4^xS_5^zS_6^y$$

$$- 63S_1^zS_2^zS_3^zS_4^xS_5^zS_6^y - 21.25S_1^xS_4^yS_5^zS_6^y - 28.25S_1^yS_4^yS_5^zS_6^y$$

$$+ 28.75S_1^zS_4^yS_5^zS_6^y - 3.25S_2^xS_4^yS_5^zS_6^y - 23.25S_2^yS_4^yS_5^zS_6^y$$

$$+ 3.25S_2^zS_4^yS_5^zS_6^y + 32.75S_3^xS_4^yS_5^zS_6^y + 63S_1^xS_2^xS_3^xS_4^yS_5^zS_6^y$$

$$+ 189S_1^yS_2^xS_3^xS_4^yS_5^zS_6^y - 63S_1^zS_2^xS_3^xS_4^yS_5^zS_6^y - 63S_1^xS_2^yS_3^xS_4^yS_5^zS_6^y$$

$$+ 63S_1^yS_2^yS_3^xS_4^yS_5^zS_6^y - 63S_1^zS_2^yS_3^xS_4^yS_5^zS_6^y - 63S_1^xS_2^zS_3^xS_4^yS_5^zS_6^y$$

$$+ 63S_1^yS_2^zS_3^xS_4^yS_5^zS_6^y - 189S_1^zS_2^zS_3^xS_4^yS_5^zS_6^y - 21.25S_3^yS_4^yS_5^zS_6^y$$

$$+ 63S_1^xS_2^xS_3^yS_4^yS_5^zS_6^y + 63S_1^yS_2^xS_3^yS_4^yS_5^zS_6^y - 189S_1^zS_2^xS_3^yS_4^yS_5^zS_6^y$$

$$- 63S_1^xS_2^yS_3^yS_4^yS_5^zS_6^y + 63S_1^yS_2^yS_3^yS_4^yS_5^zS_6^y - 63S_1^zS_2^yS_3^yS_4^yS_5^zS_6^y$$

$$+ 63S_1^xS_2^zS_3^yS_4^yS_5^zS_6^y + 63S_1^yS_2^zS_3^yS_4^yS_5^zS_6^y + 63S_1^zS_2^zS_3^yS_4^yS_5^zS_6^y$$

$$- 9.25S_3^zS_4^yS_5^zS_6^y - 63S_1^xS_2^xS_3^zS_4^yS_5^zS_6^y + 63S_1^yS_2^xS_3^zS_4^yS_5^zS_6^y$$

$$- 63S_1^zS_2^xS_3^zS_4^yS_5^zS_6^y - 63S_1^xS_2^yS_3^zS_4^yS_5^zS_6^y - 63S_1^yS_2^yS_3^zS_4^yS_5^zS_6^y$$

$$+ 63S_1^zS_2^yS_3^zS_4^yS_5^zS_6^y - 63S_1^xS_2^zS_3^zS_4^yS_5^zS_6^y + 63S_1^yS_2^zS_3^zS_4^yS_5^zS_6^y$$

$$- 63S_1^zS_2^zS_3^zS_4^yS_5^zS_6^y - 39.75S_1^xS_4^zS_5^zS_6^y - 39.25S_1^yS_4^zS_5^zS_6^y$$

$$- 28.25S_1^zS_4^zS_5^zS_6^y + 2.25S_2^xS_4^zS_5^zS_6^y + 21.25S_2^yS_4^zS_5^zS_6^y$$

$$+ 44.25S_2^zS_4^zS_5^zS_6^y + 46.25S_3^xS_4^zS_5^zS_6^y + 189S_1^xS_2^xS_3^xS_4^zS_5^zS_6^y$$

$$+ 189S_1^yS_2^xS_3^xS_4^zS_5^zS_6^y + 189S_1^zS_2^xS_3^xS_4^zS_5^zS_6^y - 63S_1^xS_2^yS_3^xS_4^zS_5^zS_6^y$$

$$+ 189S_1^yS_2^yS_3^xS_4^zS_5^zS_6^y + 63S_1^zS_2^yS_3^xS_4^zS_5^zS_6^y + 63S_1^xS_2^zS_3^xS_4^zS_5^zS_6^y$$

$$+ 189S_1^yS_2^zS_3^xS_4^zS_5^zS_6^y + 63S_1^zS_2^zS_3^xS_4^zS_5^zS_6^y - 24.75S_3^yS_4^zS_5^zS_6^y$$

$$+ 315S_1^xS_2^xS_3^yS_4^zS_5^zS_6^y + 189S_1^yS_2^xS_3^yS_4^zS_5^zS_6^y + 63S_1^zS_2^xS_3^yS_4^zS_5^zS_6^y$$

$$+ 63S_1^xS_2^yS_3^yS_4^zS_5^zS_6^y + 315S_1^yS_2^yS_3^yS_4^zS_5^zS_6^y + 63S_1^zS_2^yS_3^yS_4^zS_5^zS_6^y$$

$$+ 63S_1^xS_2^zS_3^yS_4^zS_5^zS_6^y + 63S_1^yS_2^zS_3^yS_4^zS_5^zS_6^y + 63S_1^zS_2^zS_3^yS_4^zS_5^zS_6^y$$

$$- 14.25S_3^zS_4^zS_5^zS_6^y + 63S_1^xS_2^xS_3^zS_4^zS_5^zS_6^y + 189S_1^yS_2^xS_3^zS_4^zS_5^zS_6^y$$

$$+ 63S_1^zS_2^xS_3^zS_4^zS_5^zS_6^y - 189S_1^xS_2^yS_3^zS_4^zS_5^zS_6^y + 63S_1^yS_2^yS_3^zS_4^zS_5^zS_6^y$$

$$- 63S_1^zS_2^yS_3^zS_4^zS_5^zS_6^y + 63S_1^xS_2^zS_3^zS_4^zS_5^zS_6^y + 315S_1^yS_2^zS_3^zS_4^zS_5^zS_6^y$$

$$+ 63S_1^zS_2^zS_3^zS_4^zS_5^zS_6^y + 13.19S_1^xS_6^z + 11.44S_1^yS_6^z$$

$$+ 23.94S_1^zS_6^z - 13.56S_2^xS_6^z - 11.81S_2^yS_6^z$$

$$- 12.44S_2^zS_6^z + 11.44S_3^xS_6^z - 21.25S_1^xS_2^xS_3^xS_6^z$$

$$- 39.75S_1^yS_2^xS_3^xS_6^z - 83.75S_1^zS_2^xS_3^xS_6^z + 32.75S_1^xS_2^yS_3^xS_6^z$$

$$- 23.25S_1^yS_2^yS_3^xS_6^z - 14.75S_1^zS_2^yS_3^xS_6^z - 9.25S_1^xS_2^zS_3^xS_6^z$$

$$- 25.75S_1^yS_2^zS_3^xS_6^z - 43.25S_1^zS_2^zS_3^xS_6^z + 11.44S_3^yS_6^z$$

$$- 38.25S_1^xS_2^xS_3^yS_6^z - 21.25S_1^yS_2^xS_3^yS_6^z - 14.75S_1^zS_2^xS_3^yS_6^z$$

$$- 19.25S_1^xS_2^yS_3^yS_6^z - 36.25S_1^yS_2^yS_3^yS_6^z - 32.25S_1^zS_2^yS_3^yS_6^z$$

$$- 31.25S_1^xS_2^zS_3^yS_6^z - 9.25S_1^yS_2^zS_3^yS_6^z - 14.25S_1^zS_2^zS_3^yS_6^z$$

$$+ 21.31S_3^zS_6^z - 24.75S_1^xS_2^xS_3^zS_6^z - 76.75S_1^yS_2^xS_3^zS_6^z$$

$$- 43.25S_1^zS_2^xS_3^zS_6^z + 46.25S_1^xS_2^yS_3^zS_6^z - 24.75S_1^yS_2^yS_3^zS_6^z$$

$$- 14.25S_1^zS_2^yS_3^zS_6^z - 14.25S_1^xS_2^zS_3^zS_6^z - 43.25S_1^yS_2^zS_3^zS_6^z$$

$$- 39.25S_1^zS_2^zS_3^zS_6^z - 11.81S_4^xS_6^z + 44.25S_1^xS_2^xS_4^xS_6^z$$

$$+ 15.75S_1^yS_2^xS_4^xS_6^z + 8.75S_1^zS_2^xS_4^xS_6^z + 2.25S_1^xS_2^yS_4^xS_6^z$$

$$+ 16.25S_1^yS_2^yS_4^xS_6^z + 16.25S_1^zS_2^yS_4^xS_6^z + 21.25S_1^xS_2^zS_4^xS_6^z$$

$$- 10.75S_1^yS_2^zS_4^xS_6^z + 7.25S_1^zS_2^zS_4^xS_6^z - 28.25S_1^xS_3^xS_4^xS_6^z$$

$$- 23.25S_1^yS_3^xS_4^xS_6^z - 41.75S_1^zS_3^xS_4^xS_6^z + 7.25S_2^xS_3^xS_4^xS_6^z$$

$$+ 16.25S_2^yS_3^xS_4^xS_6^z + 8.75S_2^zS_3^xS_4^xS_6^z - 39.75S_1^xS_3^yS_4^xS_6^z$$

$$- 25.75S_1^yS_3^yS_4^xS_6^z - 23.25S_1^zS_3^yS_4^xS_6^z - 10.75S_2^xS_3^yS_4^xS_6^z$$

$$+ 16.25S_2^yS_3^yS_4^xS_6^z + 15.75S_2^zS_3^yS_4^xS_6^z - 39.25S_1^xS_3^zS_4^xS_6^z$$

$$- 39.75S_1^yS_3^zS_4^xS_6^z - 28.25S_1^zS_3^zS_4^xS_6^z + 21.25S_2^xS_3^zS_4^xS_6^z$$

$$+ 2.25S_2^yS_3^zS_4^xS_6^z + 44.25S_2^zS_3^zS_4^xS_6^z - 13.56S_4^yS_6^z$$

$$+ 45.75S_1^xS_2^xS_4^yS_6^z + 45.75S_1^yS_2^xS_4^yS_6^z + 45.75S_1^zS_2^xS_4^yS_6^z$$

$$+ 15.75S_1^xS_2^zS_4^yS_6^z + 8.75S_1^yS_2^zS_4^yS_6^z + 44.25S_1^zS_2^zS_4^yS_6^z$$

$$- 21.25S_1^xS_3^xS_4^yS_6^z - 14.75S_1^yS_3^xS_4^yS_6^z - 38.25S_1^zS_3^xS_4^yS_6^z$$

$$- 1.75S_2^xS_3^xS_4^yS_6^z - 10.75S_2^yS_3^xS_4^yS_6^z - 10.75S_2^zS_3^xS_4^yS_6^z$$

$$- 76.75S_1^xS_3^yS_4^yS_6^z - 43.25S_1^yS_3^yS_4^yS_6^z - 24.75S_1^zS_3^yS_4^yS_6^z$$

$$- 1.75S_2^xS_3^yS_4^yS_6^z + 7.25S_2^yS_3^yS_4^yS_6^z + 21.25S_2^zS_3^yS_4^yS_6^z$$

$$- 39.75S_1^xS_3^zS_4^yS_6^z - 83.75S_1^yS_3^zS_4^yS_6^z - 21.25S_1^zS_3^zS_4^yS_6^z$$

$$- 1.75S_2^xS_3^zS_4^yS_6^z + 21.25S_2^yS_3^zS_4^yS_6^z + 7.25S_2^zS_3^zS_4^yS_6^z$$

$$- 12.44S_4^zS_6^z + 3.25S_1^xS_2^xS_4^zS_6^z - 3.25S_1^yS_2^xS_4^zS_6^z$$

$$+ 45.75S_1^zS_2^xS_4^zS_6^z - 3.25S_1^xS_2^yS_4^zS_6^z + 3.25S_1^yS_2^yS_4^zS_6^z$$

$$+ 45.75S_1^zS_2^yS_4^zS_6^z - 23.25S_1^xS_2^zS_4^zS_6^z - 23.25S_1^yS_2^zS_4^zS_6^z$$

$$- 9.25S_1^zS_2^zS_4^zS_6^z + 28.75S_1^xS_3^xS_4^zS_6^z + 32.75S_1^yS_3^xS_4^zS_6^z$$

$$- 12.75S_1^zS_3^xS_4^zS_6^z + 21.25S_2^xS_3^xS_4^zS_6^z + 15.75S_2^yS_3^xS_4^zS_6^z$$

$$- 23.25S_2^zS_3^xS_4^zS_6^z - 21.25S_1^xS_3^yS_4^zS_6^z - 9.25S_1^yS_3^yS_4^zS_6^z$$

$$- 36.25S_1^zS_3^yS_4^zS_6^z - 10.75S_2^xS_3^yS_4^zS_6^z + 8.75S_2^yS_3^yS_4^zS_6^z$$

$$- 23.25S_2^zS_3^yS_4^zS_6^z - 28.25S_1^xS_3^zS_4^zS_6^z - 21.25S_1^yS_3^zS_4^zS_6^z$$

$$- 56.75S_1^zS_3^zS_4^zS_6^z + 7.25S_2^xS_3^zS_4^zS_6^z + 44.25S_2^yS_3^zS_4^zS_6^z$$

$$- 9.25S_2^zS_3^zS_4^zS_6^z + 11.44S_5^xS_6^z - 12.75S_1^xS_2^xS_5^xS_6^z$$

$$- 38.25S_1^yS_2^xS_5^xS_6^z - 41.75S_1^zS_2^xS_5^xS_6^z + 32.75S_1^xS_2^yS_5^xS_6^z$$

$$- 14.75S_1^yS_2^yS_5^xS_6^z - 23.25S_1^zS_2^yS_5^xS_6^z + 28.75S_1^xS_2^zS_5^xS_6^z$$

$$- 21.25S_1^yS_2^zS_5^xS_6^z - 28.25S_1^zS_2^zS_5^xS_6^z - 23.25S_1^xS_3^xS_5^xS_6^z$$

$$- 10.75S_1^yS_3^xS_5^xS_6^z + 8.75S_1^zS_3^xS_5^xS_6^z - 43.25S_2^xS_3^xS_5^xS_6^z$$

$$- 25.75S_2^yS_3^xS_5^xS_6^z - 9.25S_2^zS_3^xS_5^xS_6^z + 15.75S_1^xS_3^yS_5^xS_6^z$$

$$- 10.75S_1^yS_3^yS_5^xS_6^z + 16.25S_1^zS_3^yS_5^xS_6^z - 14.75S_2^xS_3^yS_5^xS_6^z$$

$$- 23.25S_2^yS_3^yS_5^xS_6^z + 32.75S_2^zS_3^yS_5^xS_6^z + 21.25S_1^xS_3^zS_5^xS_6^z$$

$$- 39.75S_2^yS_3^zS_5^xS_6^z - 21.25S_2^zS_3^zS_5^xS_6^z - 14.25S_1^xS_4^xS_5^xS_6^z$$

$$- 14.75S_1^yS_4^xS_5^xS_6^z - 32.25S_1^zS_4^xS_5^xS_6^z + 45.75S_2^xS_4^xS_5^xS_6^z$$

$$+ 16.25S_2^yS_4^xS_5^xS_6^z + 3.25S_2^zS_4^xS_5^xS_6^z - 36.25S_3^xS_4^xS_5^xS_6^z$$

$$+ 63S_1^xS_2^xS_3^xS_4^xS_5^xS_6^z + 63S_1^yS_2^xS_3^xS_4^xS_5^xS_6^z + 189S_1^zS_2^xS_3^xS_4^xS_5^xS_6^z$$

$$+ 63S_1^xS_2^yS_3^xS_4^xS_5^xS_6^z + 63S_1^yS_2^yS_3^xS_4^xS_5^xS_6^z + 63S_1^zS_2^yS_3^xS_4^xS_5^xS_6^z$$

$$- 63S_1^xS_2^zS_3^xS_4^xS_5^xS_6^z - 63S_1^yS_2^zS_3^xS_4^xS_5^xS_6^z + 63S_1^zS_2^zS_3^xS_4^xS_5^xS_6^z$$

$$- 23.25S_3^yS_4^xS_5^xS_6^z + 63S_1^xS_2^xS_3^yS_4^xS_5^xS_6^z - 63S_1^yS_2^xS_3^yS_4^xS_5^xS_6^z$$

$$+ 63S_1^zS_2^xS_3^yS_4^xS_5^xS_6^z + 63S_1^xS_2^yS_3^yS_4^xS_5^xS_6^z + 63S_1^yS_2^yS_3^yS_4^xS_5^xS_6^z$$

$$+ 63S_1^zS_2^yS_3^yS_4^xS_5^xS_6^z - 189S_1^xS_2^zS_3^yS_4^xS_5^xS_6^z - 63S_1^yS_2^zS_3^yS_4^xS_5^xS_6^z$$

$$+ 63S_1^zS_2^zS_3^yS_4^xS_5^xS_6^z - 24.75S_3^zS_4^xS_5^xS_6^z + 315S_1^xS_2^xS_3^zS_4^xS_5^xS_6^z$$

$$+ 63S_1^yS_2^xS_3^zS_4^xS_5^xS_6^z + 63S_1^zS_2^xS_3^zS_4^xS_5^xS_6^z + 189S_1^xS_2^yS_3^zS_4^xS_5^xS_6^z$$

$$+ 315S_1^yS_2^yS_3^zS_4^xS_5^xS_6^z + 63S_1^zS_2^yS_3^zS_4^xS_5^xS_6^z + 63S_1^xS_2^zS_3^zS_4^xS_5^xS_6^z$$

$$+ 63S_1^yS_2^zS_3^zS_4^xS_5^xS_6^z + 63S_1^zS_2^zS_3^zS_4^xS_5^xS_6^z - 31.25S_1^xS_4^yS_5^xS_6^z$$

$$- 38.25S_1^yS_4^yS_5^xS_6^z - 19.25S_1^zS_4^yS_5^xS_6^z + 45.75S_2^xS_4^yS_5^xS_6^z$$

$$+ 15.75S_2^yS_4^yS_5^xS_6^z - 3.25S_2^zS_4^yS_5^xS_6^z - 21.25S_3^xS_4^yS_5^xS_6^z$$

$$- 63S_1^xS_2^xS_3^xS_4^yS_5^xS_6^z + 63S_1^yS_2^xS_3^xS_4^yS_5^xS_6^z + 63S_1^zS_2^xS_3^xS_4^yS_5^xS_6^z$$

$$- 63S_1^xS_2^yS_3^xS_4^yS_5^xS_6^z - 63S_1^yS_2^yS_3^xS_4^yS_5^xS_6^z - 63S_1^zS_2^yS_3^xS_4^yS_5^xS_6^z$$

$$- 63S_1^xS_2^zS_3^xS_4^yS_5^xS_6^z - 63S_1^yS_2^zS_3^xS_4^yS_5^xS_6^z + 63S_1^zS_2^zS_3^xS_4^yS_5^xS_6^z$$

$$- 39.75S_3^yS_4^yS_5^xS_6^z + 63S_1^xS_2^xS_3^yS_4^yS_5^xS_6^z + 63S_1^yS_2^xS_3^yS_4^yS_5^xS_6^z$$

$$+ 315S_1^zS_2^xS_3^yS_4^yS_5^xS_6^z - 189S_1^xS_2^yS_3^yS_4^yS_5^xS_6^z + 63S_1^yS_2^yS_3^yS_4^yS_5^xS_6^z$$

$$+ 63S_1^zS_2^yS_3^yS_4^yS_5^xS_6^z - 63S_1^xS_2^zS_3^yS_4^yS_5^xS_6^z + 63S_1^yS_2^zS_3^yS_4^yS_5^xS_6^z$$

$$+ 189S_1^zS_2^zS_3^yS_4^yS_5^xS_6^z - 76.75S_3^zS_4^yS_5^xS_6^z + 63S_1^xS_2^xS_3^zS_4^yS_5^xS_6^z$$

$$+ 189S_1^yS_2^xS_3^zS_4^yS_5^xS_6^z + 63S_1^zS_2^xS_3^zS_4^yS_5^xS_6^z - 63S_1^xS_2^yS_3^zS_4^yS_5^xS_6^z$$

$$+ 63S_1^yS_2^yS_3^zS_4^yS_5^xS_6^z - 189S_1^zS_2^yS_3^zS_4^yS_5^xS_6^z - 189S_1^xS_2^zS_3^zS_4^yS_5^xS_6^z$$

$$- 21.25S_1^yS_4^zS_5^xS_6^z - 36.25S_1^zS_4^zS_5^xS_6^z + 8.75S_2^xS_4^zS_5^xS_6^z$$

$$- 10.75S_2^yS_4^zS_5^xS_6^z - 23.25S_2^zS_4^zS_5^xS_6^z - 9.25S_3^xS_4^zS_5^xS_6^z$$

$$- 63S_1^xS_2^xS_3^xS_4^zS_5^xS_6^z + 63S_1^yS_2^xS_3^xS_4^zS_5^xS_6^z + 63S_1^zS_2^xS_3^xS_4^zS_5^xS_6^z$$

$$- 63S_1^xS_2^yS_3^xS_4^zS_5^xS_6^z - 63S_1^yS_2^yS_3^xS_4^zS_5^xS_6^z - 63S_1^zS_2^yS_3^xS_4^zS_5^xS_6^z$$

$$+ 63S_1^xS_2^zS_3^xS_4^zS_5^xS_6^z - 63S_1^yS_2^zS_3^xS_4^zS_5^xS_6^z - 63S_1^zS_2^zS_3^xS_4^zS_5^xS_6^z$$

$$- 25.75S_3^yS_4^zS_5^xS_6^z - 63S_1^xS_2^xS_3^yS_4^zS_5^xS_6^z - 63S_1^yS_2^xS_3^yS_4^zS_5^xS_6^z$$

$$+ 63S_1^zS_2^xS_3^yS_4^zS_5^xS_6^z - 63S_1^xS_2^yS_3^yS_4^zS_5^xS_6^z - 63S_1^yS_2^yS_3^yS_4^zS_5^xS_6^z$$

$$+ 63S_1^zS_2^yS_3^yS_4^zS_5^xS_6^z - 63S_1^xS_2^zS_3^yS_4^zS_5^xS_6^z - 63S_1^yS_2^zS_3^yS_4^zS_5^xS_6^z$$

$$+ 63S_1^zS_2^zS_3^yS_4^zS_5^xS_6^z - 43.25S_3^zS_4^zS_5^xS_6^z + 63S_1^xS_2^xS_3^zS_4^zS_5^xS_6^z$$

$$+ 63S_1^yS_2^xS_3^zS_4^zS_5^xS_6^z + 189S_1^zS_2^xS_3^zS_4^zS_5^xS_6^z + 63S_1^xS_2^yS_3^zS_4^zS_5^xS_6^z$$

$$+ 63S_1^yS_2^yS_3^zS_4^zS_5^xS_6^z + 63S_1^zS_2^yS_3^zS_4^zS_5^xS_6^z - 63S_1^xS_2^zS_3^zS_4^zS_5^xS_6^z$$

$$- 63S_1^yS_2^zS_3^zS_4^zS_5^xS_6^z + 63S_1^zS_2^zS_3^zS_4^zS_5^xS_6^z + 13.19S_5^yS_6^z$$

$$- 19.25S_1^xS_2^xS_5^yS_6^z - 31.25S_1^yS_2^xS_5^yS_6^z - 38.25S_1^zS_2^xS_5^yS_6^z$$

$$+ 46.25S_1^xS_2^yS_5^yS_6^z - 14.25S_1^yS_2^yS_5^yS_6^z - 24.75S_1^zS_2^yS_5^yS_6^z$$

$$+ 32.75S_1^xS_2^zS_5^yS_6^z - 9.25S_1^yS_2^zS_5^yS_6^z - 21.25S_1^zS_2^zS_5^yS_6^z$$

$$- 3.25S_1^xS_3^xS_5^yS_6^z + 15.75S_1^yS_3^xS_5^yS_6^z + 45.75S_1^zS_3^xS_5^yS_6^z$$

$$- 76.75S_2^xS_3^xS_5^yS_6^z - 39.75S_2^yS_3^xS_5^yS_6^z - 21.25S_2^zS_3^xS_5^yS_6^z$$

$$- 3.25S_1^xS_3^yS_5^yS_6^z - 23.25S_1^yS_3^yS_5^yS_6^z + 3.25S_1^zS_3^yS_5^yS_6^z$$

$$- 21.25S_2^xS_3^yS_5^yS_6^z - 28.25S_2^yS_3^yS_5^yS_6^z + 28.75S_2^zS_3^yS_5^yS_6^z$$

$$+ 2.25S_1^xS_3^zS_5^yS_6^z + 21.25S_1^yS_3^zS_5^yS_6^z + 44.25S_1^zS_3^zS_5^yS_6^z$$

$$- 39.75S_2^xS_3^zS_5^yS_6^z - 39.25S_2^yS_3^zS_5^yS_6^z - 28.25S_2^zS_3^zS_5^yS_6^z$$

$$+ 46.25S_1^xS_4^xS_5^yS_6^z + 32.75S_1^yS_4^xS_5^yS_6^z - 19.25S_1^zS_4^xS_5^yS_6^z$$

$$- 3.25S_2^xS_4^xS_5^yS_6^z + 2.25S_2^yS_4^xS_5^yS_6^z - 3.25S_2^zS_4^xS_5^yS_6^z$$

$$- 19.25S_3^xS_4^xS_5^yS_6^z + 63S_1^xS_2^xS_3^xS_4^xS_5^yS_6^z - 189S_1^yS_2^xS_3^xS_4^xS_5^yS_6^z$$

$$+ 63S_1^zS_2^xS_3^xS_4^xS_5^yS_6^z + 189S_1^xS_2^yS_3^xS_4^xS_5^yS_6^z + 63S_1^yS_2^yS_3^xS_4^xS_5^yS_6^z$$

$$+ 315S_1^zS_2^yS_3^xS_4^xS_5^yS_6^z + 63S_1^xS_2^zS_3^xS_4^xS_5^yS_6^z - 63S_1^yS_2^zS_3^xS_4^xS_5^yS_6^z$$

$$+ 63S_1^zS_2^zS_3^xS_4^xS_5^yS_6^z + 32.75S_3^yS_4^xS_5^yS_6^z + 63S_1^xS_2^xS_3^yS_4^xS_5^yS_6^z$$

$$- 63S_1^yS_2^xS_3^yS_4^xS_5^yS_6^z - 63S_1^zS_2^xS_3^yS_4^xS_5^yS_6^z + 189S_1^xS_2^yS_3^yS_4^xS_5^yS_6^z$$

$$+ 63S_1^yS_2^yS_3^yS_4^xS_5^yS_6^z + 63S_1^zS_2^yS_3^yS_4^xS_5^yS_6^z - 63S_1^xS_2^zS_3^yS_4^xS_5^yS_6^z$$

$$- 63S_1^yS_2^zS_3^yS_4^xS_5^yS_6^z - 189S_1^zS_2^zS_3^yS_4^xS_5^yS_6^z + 46.25S_3^zS_4^xS_5^yS_6^z$$

$$+ 189S_1^xS_2^xS_3^zS_4^xS_5^yS_6^z - 63S_1^yS_2^xS_3^zS_4^xS_5^yS_6^z + 63S_1^zS_2^xS_3^zS_4^xS_5^yS_6^z$$

$$+ 189S_1^xS_2^yS_3^zS_4^xS_5^yS_6^z + 189S_1^yS_2^yS_3^zS_4^xS_5^yS_6^z + 189S_1^zS_2^yS_3^zS_4^xS_5^yS_6^z$$

$$+ 189S_1^xS_2^zS_3^zS_4^xS_5^yS_6^z + 63S_1^yS_2^zS_3^zS_4^xS_5^yS_6^z + 63S_1^zS_2^zS_3^zS_4^xS_5^yS_6^z$$

$$- 19.25S_1^xS_4^yS_5^yS_6^z - 12.75S_1^yS_4^yS_5^yS_6^z - 39.25S_1^zS_4^yS_5^yS_6^z$$

$$+ 45.75S_2^xS_4^yS_5^yS_6^z + 44.25S_2^yS_4^yS_5^yS_6^z + 3.25S_2^zS_4^yS_5^yS_6^z$$

$$- 38.25S_3^xS_4^yS_5^yS_6^z + 63S_1^xS_2^xS_3^xS_4^yS_5^yS_6^z + 63S_1^yS_2^xS_3^xS_4^yS_5^yS_6^z$$

$$+ 189S_1^zS_2^xS_3^xS_4^yS_5^yS_6^z + 63S_1^xS_2^yS_3^xS_4^yS_5^yS_6^z + 63S_1^yS_2^yS_3^xS_4^yS_5^yS_6^z$$

$$+ 63S_1^zS_2^yS_3^xS_4^yS_5^yS_6^z - 63S_1^xS_2^zS_3^xS_4^yS_5^yS_6^z - 63S_1^yS_2^zS_3^xS_4^yS_5^yS_6^z$$

$$+ 63S_1^zS_2^zS_3^xS_4^yS_5^yS_6^z - 21.25S_3^yS_4^yS_5^yS_6^z + 63S_1^xS_2^xS_3^yS_4^yS_5^yS_6^z$$

$$- 63S_1^yS_2^xS_3^yS_4^yS_5^yS_6^z + 63S_1^zS_2^xS_3^yS_4^yS_5^yS_6^z + 63S_1^xS_2^yS_3^yS_4^yS_5^yS_6^z$$

$$+ 63S_1^yS_2^yS_3^yS_4^yS_5^yS_6^z + 63S_1^zS_2^yS_3^yS_4^yS_5^yS_6^z - 189S_1^xS_2^zS_3^yS_4^yS_5^yS_6^z$$

$$- 63S_1^yS_2^zS_3^yS_4^yS_5^yS_6^z + 63S_1^zS_2^zS_3^yS_4^yS_5^yS_6^z - 24.75S_3^zS_4^yS_5^yS_6^z$$

$$+ 315S_1^xS_2^xS_3^zS_4^yS_5^yS_6^z + 63S_1^yS_2^xS_3^zS_4^yS_5^yS_6^z + 63S_1^zS_2^xS_3^zS_4^yS_5^yS_6^z$$

$$+ 189S_1^xS_2^yS_3^zS_4^yS_5^yS_6^z + 315S_1^yS_2^yS_3^zS_4^yS_5^yS_6^z + 63S_1^zS_2^yS_3^zS_4^yS_5^yS_6^z$$

$$+ 63S_1^xS_2^zS_3^zS_4^yS_5^yS_6^z + 63S_1^yS_2^zS_3^zS_4^yS_5^yS_6^z + 63S_1^zS_2^zS_3^zS_4^yS_5^yS_6^z$$

$$+ 32.75S_1^xS_4^zS_5^yS_6^z + 28.75S_1^yS_4^zS_5^yS_6^z - 12.75S_1^zS_4^zS_5^yS_6^z$$

$$+ 15.75S_2^xS_4^zS_5^yS_6^z + 21.25S_2^yS_4^zS_5^yS_6^z - 23.25S_2^zS_4^zS_5^yS_6^z$$

$$- 31.25S_3^xS_4^zS_5^yS_6^z - 189S_1^xS_2^xS_3^xS_4^zS_5^yS_6^z - 63S_1^yS_2^xS_3^xS_4^zS_5^yS_6^z$$

$$+ 63S_1^zS_2^yS_3^xS_4^zS_5^yS_6^z - 63S_1^xS_2^zS_3^xS_4^zS_5^yS_6^z - 63S_1^yS_2^zS_3^xS_4^zS_5^yS_6^z$$

$$- 63S_1^zS_2^zS_3^xS_4^zS_5^yS_6^z - 9.25S_3^yS_4^zS_5^yS_6^z - 63S_1^xS_2^xS_3^yS_4^zS_5^yS_6^z$$

$$- 63S_1^yS_2^xS_3^yS_4^zS_5^yS_6^z - 63S_1^zS_2^xS_3^yS_4^zS_5^yS_6^z + 63S_1^xS_2^yS_3^yS_4^zS_5^yS_6^z$$

$$- 63S_1^yS_2^yS_3^yS_4^zS_5^yS_6^z + 63S_1^zS_2^yS_3^yS_4^zS_5^yS_6^z - 63S_1^xS_2^zS_3^yS_4^zS_5^yS_6^z$$

$$+ 63S_1^yS_2^zS_3^yS_4^zS_5^yS_6^z - 63S_1^zS_2^zS_3^yS_4^zS_5^yS_6^z - 14.25S_3^zS_4^zS_5^yS_6^z$$

$$+ 63S_1^xS_2^xS_3^zS_4^zS_5^yS_6^z - 189S_1^yS_2^xS_3^zS_4^zS_5^yS_6^z + 63S_1^zS_2^xS_3^zS_4^zS_5^yS_6^z$$

$$+ 189S_1^xS_2^yS_3^zS_4^zS_5^yS_6^z + 63S_1^yS_2^yS_3^zS_4^zS_5^yS_6^z + 315S_1^zS_2^yS_3^zS_4^zS_5^yS_6^z$$

$$+ 63S_1^xS_2^zS_3^zS_4^zS_5^yS_6^z - 63S_1^yS_2^zS_3^zS_4^zS_5^yS_6^z + 63S_1^zS_2^zS_3^zS_4^zS_5^yS_6^z$$

$$+ 23.94S_5^zS_6^z - 39.25S_1^xS_2^xS_5^zS_6^z - 19.25S_1^yS_2^xS_5^zS_6^z$$

$$- 12.75S_1^zS_2^xS_5^zS_6^z - 19.25S_1^xS_2^yS_5^zS_6^z - 32.25S_1^yS_2^yS_5^zS_6^z$$

$$- 36.25S_1^zS_2^yS_5^zS_6^z - 12.75S_1^xS_2^zS_5^zS_6^z - 36.25S_1^yS_2^zS_5^zS_6^z$$

$$- 56.75S_1^zS_2^zS_5^zS_6^z + 3.25S_1^xS_3^xS_5^zS_6^z + 16.25S_1^yS_3^xS_5^zS_6^z$$

$$+ 45.75S_1^zS_3^xS_5^zS_6^z - 24.75S_2^xS_3^xS_5^zS_6^z - 23.25S_2^yS_3^xS_5^zS_6^z$$

$$- 36.25S_2^zS_3^xS_5^zS_6^z + 45.75S_1^xS_3^yS_5^zS_6^z + 8.75S_1^yS_3^yS_5^zS_6^z$$

$$+ 45.75S_1^zS_3^yS_5^zS_6^z - 38.25S_2^xS_3^yS_5^zS_6^z - 41.75S_2^yS_3^yS_5^zS_6^z$$

$$- 12.75S_2^zS_3^yS_5^zS_6^z + 44.25S_1^xS_3^zS_5^zS_6^z + 7.25S_1^yS_3^zS_5^zS_6^z$$

$$- 9.25S_1^zS_3^zS_5^zS_6^z - 21.25S_2^xS_3^zS_5^zS_6^z - 28.25S_2^yS_3^zS_5^zS_6^z$$

$$- 56.75S_2^zS_3^zS_5^zS_6^z - 24.75S_1^xS_4^xS_5^zS_6^z - 23.25S_1^yS_4^xS_5^zS_6^z$$

$$- 36.25S_1^zS_4^xS_5^zS_6^z + 3.25S_2^xS_4^xS_5^zS_6^z + 16.25S_2^yS_4^xS_5^zS_6^z$$

$$+ 45.75S_2^zS_4^xS_5^zS_6^z - 32.25S_3^xS_4^xS_5^zS_6^z + 63S_1^xS_2^xS_3^xS_4^xS_5^zS_6^z$$

$$+ 63S_1^yS_2^xS_3^xS_4^xS_5^zS_6^z + 63S_1^zS_2^xS_3^xS_4^xS_5^zS_6^z + 63S_1^xS_2^yS_3^xS_4^xS_5^zS_6^z$$

$$+ 63S_1^yS_2^yS_3^xS_4^xS_5^zS_6^z + 63S_1^zS_2^yS_3^xS_4^xS_5^zS_6^z + 63S_1^xS_2^zS_3^xS_4^xS_5^zS_6^z$$

$$+ 63S_1^yS_2^zS_3^xS_4^xS_5^zS_6^z + 189S_1^zS_2^zS_3^xS_4^xS_5^zS_6^z - 14.75S_3^yS_4^xS_5^zS_6^z$$

$$+ 63S_1^xS_2^xS_3^yS_4^xS_5^zS_6^z - 63S_1^yS_2^xS_3^yS_4^xS_5^zS_6^z - 63S_1^zS_2^xS_3^yS_4^xS_5^zS_6^z$$

$$+ 315S_1^xS_2^yS_3^yS_4^xS_5^zS_6^z + 63S_1^yS_2^yS_3^yS_4^xS_5^zS_6^z + 63S_1^zS_2^yS_3^yS_4^xS_5^zS_6^z$$

$$+ 63S_1^xS_2^zS_3^yS_4^xS_5^zS_6^z - 63S_1^yS_2^zS_3^yS_4^xS_5^zS_6^z + 63S_1^zS_2^zS_3^yS_4^xS_5^zS_6^z$$

$$- 14.25S_3^zS_4^xS_5^zS_6^z + 63S_1^xS_2^xS_3^zS_4^xS_5^zS_6^z - 189S_1^yS_2^xS_3^zS_4^xS_5^zS_6^z$$

$$- 63S_1^zS_2^xS_3^zS_4^xS_5^zS_6^z + 189S_1^xS_2^yS_3^zS_4^xS_5^zS_6^z + 63S_1^yS_2^yS_3^zS_4^xS_5^zS_6^z$$

$$+ 63S_1^zS_2^yS_3^zS_4^xS_5^zS_6^z + 315S_1^xS_2^zS_3^zS_4^xS_5^zS_6^z + 63S_1^yS_2^zS_3^zS_4^xS_5^zS_6^z$$

$$+ 63S_1^zS_2^zS_3^zS_4^xS_5^zS_6^z - 38.25S_1^xS_4^yS_5^zS_6^z - 41.75S_1^yS_4^yS_5^zS_6^z$$

$$- 12.75S_1^zS_4^yS_5^zS_6^z + 45.75S_2^xS_4^yS_5^zS_6^z + 8.75S_2^yS_4^yS_5^zS_6^z$$

$$+ 45.75S_2^zS_4^yS_5^zS_6^z - 14.75S_3^xS_4^yS_5^zS_6^z + 63S_1^xS_2^xS_3^xS_4^yS_5^zS_6^z$$

$$+ 315S_1^yS_2^xS_3^xS_4^yS_5^zS_6^z + 63S_1^zS_2^xS_3^xS_4^yS_5^zS_6^z - 63S_1^xS_2^yS_3^xS_4^yS_5^zS_6^z$$

$$+ 63S_1^yS_2^yS_3^xS_4^yS_5^zS_6^z - 63S_1^zS_2^yS_3^xS_4^yS_5^zS_6^z - 63S_1^xS_2^zS_3^xS_4^yS_5^zS_6^z$$

$$+ 63S_1^yS_2^zS_3^xS_4^yS_5^zS_6^z + 63S_1^zS_2^zS_3^xS_4^yS_5^zS_6^z - 83.75S_3^yS_4^yS_5^zS_6^z$$

$$+ 189S_1^xS_2^xS_3^yS_4^yS_5^zS_6^z + 63S_1^yS_2^xS_3^yS_4^yS_5^zS_6^z + 63S_1^zS_2^xS_3^yS_4^yS_5^zS_6^z$$

$$+ 63S_1^xS_2^yS_3^yS_4^yS_5^zS_6^z + 189S_1^yS_2^yS_3^yS_4^yS_5^zS_6^z + 63S_1^zS_2^yS_3^yS_4^yS_5^zS_6^z$$

$$+ 63S_1^xS_2^zS_3^yS_4^yS_5^zS_6^z + 63S_1^yS_2^zS_3^yS_4^yS_5^zS_6^z + 315S_1^zS_2^zS_3^yS_4^yS_5^zS_6^z$$

$$- 43.25S_3^zS_4^yS_5^zS_6^z + 63S_1^xS_2^xS_3^zS_4^yS_5^zS_6^z + 63S_1^yS_2^xS_3^zS_4^yS_5^zS_6^z$$

$$- 63S_1^zS_2^xS_3^zS_4^yS_5^zS_6^z + 63S_1^xS_2^yS_3^zS_4^yS_5^zS_6^z + 63S_1^yS_2^yS_3^zS_4^yS_5^zS_6^z$$

$$- 63S_1^zS_2^yS_3^zS_4^yS_5^zS_6^z + 63S_1^xS_2^zS_3^zS_4^yS_5^zS_6^z + 189S_1^yS_2^zS_3^zS_4^yS_5^zS_6^z$$

$$+ 63S_1^zS_2^zS_3^zS_4^yS_5^zS_6^z - 21.25S_1^xS_4^zS_5^zS_6^z - 28.25S_1^yS_4^zS_5^zS_6^z$$

$$- 56.75S_1^zS_4^zS_5^zS_6^z + 44.25S_2^xS_4^zS_5^zS_6^z + 7.25S_2^yS_4^zS_5^zS_6^z$$

$$- 9.25S_2^zS_4^zS_5^zS_6^z - 14.25S_3^xS_4^zS_5^zS_6^z + 63S_1^xS_2^xS_3^xS_4^zS_5^zS_6^z$$

$$+ 189S_1^yS_2^xS_3^xS_4^zS_5^zS_6^z + 315S_1^zS_2^xS_3^xS_4^zS_5^zS_6^z - 189S_1^xS_2^yS_3^xS_4^zS_5^zS_6^z$$

$$+ 63S_1^yS_2^yS_3^xS_4^zS_5^zS_6^z + 63S_1^zS_2^yS_3^xS_4^zS_5^zS_6^z - 63S_1^xS_2^zS_3^xS_4^zS_5^zS_6^z$$

$$+ 63S_1^yS_2^zS_3^xS_4^zS_5^zS_6^z + 63S_1^zS_2^zS_3^xS_4^zS_5^zS_6^z - 43.25S_3^yS_4^zS_5^zS_6^z$$

$$+ 63S_1^xS_2^xS_3^yS_4^zS_5^zS_6^z + 63S_1^yS_2^xS_3^yS_4^zS_5^zS_6^z + 63S_1^zS_2^xS_3^yS_4^zS_5^zS_6^z$$

$$- 63S_1^xS_2^zS_3^yS_4^zS_5^zS_6^z - 63S_1^yS_2^zS_3^yS_4^zS_5^zS_6^z + 63S_1^zS_2^zS_3^yS_4^zS_5^zS_6^z$$

$$- 39.25S_3^zS_4^zS_5^zS_6^z + 63S_1^xS_2^xS_3^zS_4^zS_5^zS_6^z + 63S_1^yS_2^xS_3^zS_4^zS_5^zS_6^z$$

$$+ 63S_1^zS_2^xS_3^zS_4^zS_5^zS_6^z + 63S_1^xS_2^yS_3^zS_4^zS_5^zS_6^z + 63S_1^yS_2^yS_3^zS_4^zS_5^zS_6^z$$

$$+ 63S_1^zS_2^yS_3^zS_4^zS_5^zS_6^z + 63S_1^xS_2^zS_3^zS_4^zS_5^zS_6^z + 63S_1^yS_2^zS_3^zS_4^zS_5^zS_6^z$$

$$- 41.75S_1^yS_2^zS_3^zS_4^y - 28.25S_1^zS_2^zS_3^zS_4^y + 11.44S_1^xS_4^z + 13.19S_1^yS_4^z$$

$$- 21.25S_1^zS_2^xS_3^zS_4^y + 32.75S_1^xS_2^yS_3^zS_4^y - 12.75S_1^yS_2^yS_3^zS_4^y + 28.75S_1^zS_2^yS_3^zS_4^y - 23.25S_1^xS_2^zS_3^zS_4^y$$

$$- 21.25S_2^xS_3^xS_4^yS_5^x - 9.25S_2^yS_3^xS_4^yS_5^x + 32.75S_2^zS_3^xS_4^yS_5^x + 21.25S_1^xS_3^yS_4^yS_5^x + 44.25S_1^yS_3^yS_4^yS_5^x$$

$$+ 2.25S_1^zS_3^yS_4^yS_5^x - 24.75S_2^xS_3^yS_4^yS_5^x - 14.25S_2^yS_3^yS_4^yS_5^x + 46.25S_2^zS_3^yS_4^yS_5^x$$

$$+ 8.75S_1^xS_3^xS_4^yS_5^y + 45.75S_1^yS_3^xS_4^yS_5^y + 45.75S_1^zS_3^xS_4^yS_5^y - 83.75S_2^xS_3^xS_4^yS_5^y$$

$$- 19.25S_1^yS_2^xS_4^yS_5^z - 31.25S_1^zS_2^xS_4^yS_5^z - 21.25S_1^xS_2^yS_4^yS_5^z - 36.25S_1^yS_2^yS_4^yS_5^z - 9.25S_1^zS_2^yS_4^yS_5^z$$

$$+ 28.75S_1^zS_3^zS_4^xS_6^x - 23.25S_2^xS_3^zS_4^xS_6^x - 3.25S_2^yS_3^zS_4^xS_6^x + 3.25S_2^zS_3^zS_4^xS_6^x - 11.81S_4^yS_6^x$$

$$+ 63S_1^xS_2^zS_3^yS_4^xS_5^xS_6^x + 63S_1^yS_2^zS_3^yS_4^xS_5^xS_6^x + 189S_1^zS_2^zS_3^yS_4^xS_5^xS_6^x$$

$$- 23.25S_1^yS_3^yS_5^yS_6^x - 3.25S_1^zS_3^yS_5^yS_6^x - 9.25S_2^xS_3^yS_5^yS_6^x - 21.25S_2^yS_3^yS_5^yS_6^x + 32.75S_2^zS_3^yS_5^yS_6^x$$

$$- 63S_1^yS_2^zS_3^xS_4^zS_5^yS_6^x - 63S_1^zS_2^xS_3^yS_4^zS_5^yS_6^x$$

$$+ 63S_1^zS_2^zS_3^xS_4^zS_5^yS_6^x - 21.25S_3^yS_4^zS_5^yS_6^x - 63S_1^xS_2^xS_3^yS_4^zS_5^yS_6^x - 63S_1^yS_2^xS_3^yS_4^zS_5^yS_6^x$$

$$+ 63S_1^xS_2^yS_3^yS_4^zS_5^yS_6^x - 63S_1^yS_2^yS_3^yS_4^zS_5^yS_6^x + 63S_1^zS_2^yS_3^yS_4^zS_5^yS_6^x - 63S_1^xS_2^zS_3^yS_4^zS_5^yS_6^x$$

$$- 25.75S_3^zS_4^yS_5^zS_6^x - 63S_1^xS_2^xS_3^zS_4^yS_5^zS_6^x - 63S_1^yS_2^xS_3^zS_4^yS_5^zS_6^x - 189S_1^yS_2^xS_3^yS_4^yS_5^zS_6^x$$

$$- 21.25S_1^zS_3^zS_4^xS_6^y + 15.75S_2^xS_3^zS_4^xS_6^y - 3.25S_2^yS_3^zS_4^xS_6^y + 45.75S_2^zS_3^zS_4^xS_6^y - 12.44S_4^yS_6^y$$

$$+ 189S_1^yS_2^yS_3^yS_4^xS_5^xS_6^y + 63S_1^zS_2^yS_3^yS_4^xS_5^xS_6^y + 63S_1^xS_2^zS_3^yS_4^xS_5^xS_6^y + 63S_1^yS_2^zS_3^yS_4^xS_5^xS_6^y$$

$$- 21.25S_2^yS_3^xS_5^yS_6^y - 38.25S_2^zS_3^xS_5^yS_6^y + 45.75S_1^xS_3^yS_5^yS_6^y - 9.25S_1^yS_3^yS_5^yS_6^y$$

$$+ 45.75S_1^zS_3^yS_5^yS_6^y - 36.25S_2^xS_3^yS_5^yS_6^y - 56.75S_2^yS_3^yS_5^yS_6^y - 12.75S_2^zS_3^yS_5^yS_6^y$$

$$+ 63S_1^zS_2^zS_3^xS_4^zS_5^yS_6^y - 36.25S_3^yS_4^zS_5^yS_6^y + 63S_1^xS_2^xS_3^yS_4^zS_5^yS_6^y$$

$$+ 63S_1^yS_2^xS_3^yS_4^zS_5^yS_6^y + 63S_1^zS_2^xS_3^yS_4^zS_5^yS_6^y + 63S_1^xS_2^yS_3^yS_4^zS_5^yS_6^y$$

$$- 63S_1^zS_2^xS_3^zS_4^xS_5^zS_6^y - 63S_1^xS_2^yS_3^zS_4^xS_5^zS_6^y - 189S_1^yS_2^yS_3^zS_4^xS_5^zS_6^y$$

$$
\begin{aligned}
&- 3.25S_1^xS_2^yS_4^yS_6^z + 45.75S_1^yS_2^yS_4^yS_6^z + 3.25S_1^zS_2^yS_4^yS_6^z \\
&- 1.75S_1^yS_3^zS_5^xS_6^z + 7.25S_1^zS_3^zS_5^xS_6^z - 83.75S_2^xS_3^zS_5^xS_6^z \\
&+ 63S_1^yS_2^zS_3^zS_4^yS_5^xS_6^z + 63S_1^zS_2^zS_3^zS_4^yS_5^xS_6^z - 9.25S_1^xS_4^zS_5^xS_6^z \\
&+ 63S_1^zS_2^xS_3^xS_4^zS_5^yS_6^z - 63S_1^xS_2^yS_3^xS_4^zS_5^yS_6^z - 189S_1^yS_2^yS_3^xS_4^zS_5^yS_6^z \\
&+ 63S_1^xS_2^yS_3^yS_4^zS_5^zS_6^z + 63S_1^yS_2^yS_3^yS_4^zS_5^zS_6^z + 189S_1^zS_2^yS_3^yS_4^zS_5^zS_6^z \\
&+ 189S_1^zS_2^zS_3^zS_4^zS_5^zS_6^z\Big]
\end{aligned}
$$

which has no odd spin terms as can be seen.

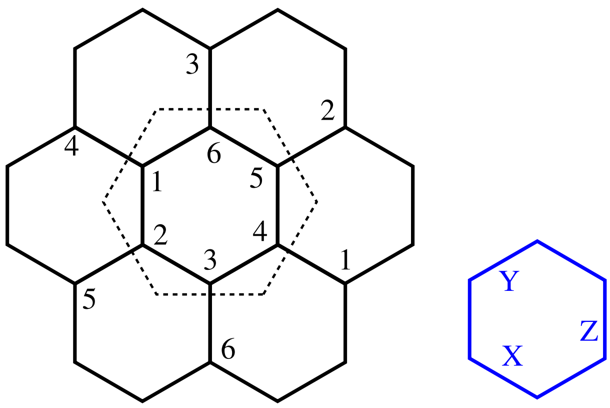

Figure A.2: Six site plaquette cluster with pbc for computing the effective Hamiltonian using PCUT

Bibliography

[1] X.-G. Wen, "Quantum orders and symmetric spin liquids," *Phys. Rev. B*, vol. 65, p. 165113, Apr 2002.

[2] A. Kitaev, "Anyons in an exactly solved model and beyond," *Annals of Physics*, vol. 321, no. 1, pp. 2–111, 2006.

[3] K. S. Tikhonov, M. V. Feigel'man, and A. Y. Kitaev, "Power-law spin correlations in a perturbed spin model on a honeycomb lattice," *Phys. Rev. Lett.*, vol. 106, p. 067203, Feb 2011.

[4] S. Mandal, S. Bhattacharjee, K. Sengupta, R. Shankar, and G. Baskaran, "Confinement-deconfinement transition and spin correlations in a generalized kitaev model," *Phys. Rev. B*, vol. 84, p. 155121, Oct 2011.

[5] L. M. Duan, E. Demler, and M. D. Lukin, "Controlling spin exchange interactions of ultracold atoms in optical lattices," *Phys. Rev. Lett.*, vol. 91, no. 9, p. 090402, 2003.

[6] J. Chaloupka, G. Jackeli, and G. Khaliullin, "Kitaev-heisenberg model on a honeycomb lattice: Possible exotic phases in iridium oxides A_2iro_3," *Phys. Rev. Lett.*, vol. 105, p. 027204, Jul 2010.

[7] I. Kimchi and A. Vishwanath, "Kitaev-heisenberg models for iridates on the triangular, hyperkagome, kagome, fcc, and pyrochlore lattices," *Phys. Rev. B*, vol. 89, p. 014414, Jan 2014.

[8] L. J. LeBlanc, "The hyperfine structure of potassium-40," tech. rep., Technical report, University of Toronto, Canada, 2006.

[9] Y. Singh and P. Gegenwart, "Antiferromagnetic mott insulating state in single crystals of the honeycomb lattice material na_2iro_3," *Phys. Rev. B*, vol. 82, p. 064412, Aug 2010.

[10] Y. Okamoto, M. Nohara, H. Aruga-Katori, and H. Takagi, "Spin-liquid state in the $s = 1/2$ hyperkagome antiferromagnet $na_4ir_3o_8$," *Phys. Rev. Lett.*, vol. 99, p. 137207, Sep 2007.

[11] J. Chaloupka, G. Jackeli, and G. Khaliullin, "Zigzag magnetic order in the iridium oxide na 2 iro 3," *Phys. Rev. Lett.*, vol. 110, no. 9, p. 097204, 2013.

[12] J. Knolle, G.-W. Chern, D. L. Kovrizhin, R. Moessner, and N. B. Perkins, "Raman scattering signatures of kitaev spin liquids in A_2iro_3 iridates with a = Na or li," *Phys. Rev. Lett.*, vol. 113, p. 187201, Oct 2014.

[13] S. Nath Gupta, P. V. Sriluckshmy, A. Balodhi, D. V. S. Muthu, S. R. Hassan, Y. Singh, T. V. Ramakrishnan, and A. K. Sood, "Spin liquid like Raman signatures in hyperkagome iridate Na_4Ir_3O_8," *ArXiv e-prints*, June 2016.

[14] L. Landau and E. Lifshitz, *Statistical Physics*. No. v. 5, Elsevier Science, 2013.

[15] P. Fazekas and P. Anderson, "On the ground state properties of the anisotropic triangular antiferromagnet," *Philosophical Magazine*, vol. 30, no. 2, pp. 423–440, 1974.

[16] P. Anderson, "The resonating valence bond state in La_2CuO_4 and superconductivity," *Science*, vol. 235, pp. 1196 – 8, 1987.

[17] G. Baskaran and P. W. Anderson, "Gauge theory of high-temperature superconductors and strongly correlated fermi systems," *Phys. Rev. B*, vol. 37, pp. 580–583, Jan 1988.

[18] T. Senthil and M. Fisher, "Z_{2} gauge theory of electron fractionalization in strongly correlated systems," *Physical Review B*, vol. 62, no. 12, p. 7850, 2000.

[19] Y. Shimizu, K. Miyagawa, K. Kanoda, M. Maesato, and G. Saito, "Spin liquid state in an organic mott insulator with a triangular lattice," *Phys. Rev. Lett.*, vol. 91, p. 107001, Sep 2003.

[20] T.-H. Han, J. S. Helton, S. Chu, D. G. Nocera, J. A. Rodriguez-Rivera, C. Broholm, and Y. S. Lee, "Fractionalized excitations in the spin-liquid state of a kagome-lattice antiferromagnet," *Nature*, vol. 492, no. 7429, pp. 406–410, 2012.

[21] H. D. Zhou, E. S. Choi, G. Li, L. Balicas, C. R. Wiebe, Y. Qiu, J. R. D. Copley, and J. S. Gardner, "Spin liquid state in the $s = 1/2$ triangular lattice $ba_3cusb_2o_9$," *Phys. Rev. Lett.*, vol. 106, p. 147204, Apr 2011.

[22] Y. Okamoto, H. Yoshida, and Z. Hiroi, "Vesignieite $bacu_3v_2o_8(oh)_2$ as a candidate spin-1/2 kagome antiferromagnet," *Journal of the Physical Society of Japan*, vol. 78, no. 3, p. 033701, 2009.

[23] A. Kitaev, "Anyons in an exactly solved model and beyond," *Annals of Physics*, vol. 321, no. 1, pp. 2 – 111, 2006.

[24] G. Baskaran, S. Mandal, and R. Shankar, "Exact results for spin dynamics and fractionalization in the kitaev model," *Phys. Rev. Lett.*, vol. 98, p. 247201, Jun 2007.

[25] S. Mandal, S. Bhattacharjee, K. Sengupta, R. Shankar, and G. Baskaran, "Confinement-deconfinement transition and spin correlations in a generalized kitaev model," *Phys. Rev. B*, vol. 84, p. 155121, Oct 2011.

[26] J. Chaloupka, G. Jackeli, and G. Khaliullin, "Kitaev-heisenberg model on a honeycomb lattice: Possible exotic phases in iridium oxides A_2IrO_3.," *Physical review letters*, vol. 105, no. 2, p. 27204, 2010.

[27] R. Schaffer, S. Bhattacharjee, and Y. Kim, "Quantum phase transition in heisenberg-kitaev model," *arXiv preprint arXiv:1206.5814*, 2012.

[28] I. Affleck and J. B. Marston, "Large- n limit of the heisenberg-hubbard model: Implications for high-T_c superconductors," *Phys. Rev. B*, vol. 37, pp. 3774–3777, Mar 1988.

[29] W. Rantner and X.-G. Wen, "Electron spectral function and algebraic spin liquid for the normal state of underdoped high T_c superconductors," *Phys. Rev. Lett.*, vol. 86, pp. 3871–3874, Apr 2001.

[30] T. Senthil and P. A. Lee, "Cuprates as doped $u(1)$ spin liquids," *Phys. Rev. B*, vol. 71, p. 174515, May 2005.

[31] S. R. Hassan, P. V. Srilucksshmy, S. K. Goyal, R. Shankar, and D. Sénéchal, "Stable algebraic spin liquid in a hubbard model," *Phys. Rev. Lett.*, vol. 110, no. 3, p. 037201, 2013.

[32] H. Yao, S.-C. Zhang, and S. A. Kivelson, "Algebraic spin liquid in an exactly solvable spin model," *Phys. Rev. Lett.*, vol. 102, p. 217202, May 2009.

[33] G. Jackeli and G. Khaliullin, "Mott insulators in the strong spin-orbit coupling limit: From heisenberg to a quantum compass and kitaev models," *Phys. Rev. Lett.*, vol. 102, p. 017205, Jan 2009.

[34] Z. Alpichshev, F. Mahmood, G. Cao, and N. Gedik, "Confinement-deconfinement transition as an indication of spin-liquid-type behavior in na_2iro_3," *Phys. Rev. Lett.*, vol. 114, p. 017203, Jan 2015.

[35] Y. Singh and P. Gegenwart, "Antiferromagnetic mott insulating state in single crystals of the honeycomb lattice material na 2 iro 3," *Phys. Rev. B*, vol. 82, no. 6, p. 064412, 2010.

[36] S. Choi, R. Coldea, A. Kolmogorov, T. Lancaster, I. Mazin, S. Blundell, P. Radaelli, Y. Singh, P. Gegenwart, K. Choi, *et al.*, "Spin waves and revised crystal structure of honeycomb iridate na 2 iro 3," *Phys. Rev. Lett.*, vol. 108, no. 12, p. 127204, 2012.

[37] K. B. Lyons, P. A. Fleury, J. P. Remeika, A. S. Cooper, and T. J. Negran, "Dynamics of spin fluctuations in lanthanum cuprate," *Phys. Rev. B*, vol. 37, pp. 2353–2356, Feb 1988.

[38] L. K. LOON, *Ultracold fermions in a honeycomb optical lattice*. PhD thesis, National University of Singapore, 2010.

[39] L. Mazza, *Quantum Simulation of Topological States of Matter*. PhD thesis, MuÌĹnchen, Technische UniversitaÌĹt MuÌĹnchen, Diss., 2012, 2012.

[40] Z. Meng, T. Lang, S. Wessel, F. Assaad, and A. Muramatsu, "Quantum spin liquid emerging in two-dimensional correlated dirac fermions," *Nature*, vol. 464, no. 7290, pp. 847–851, 2010.

[41] Y. O. Sandro Sorella and S. Yunoki, "Absence of a spin liquid phase in the hubbard model on the honeycomb lattice," *Arxiv preprint arXiv:1207.1783*, 2012.

[42] J. P. L. Faye, D. Sénéchal, and S. R. Hassan, "Topological phases of the kitaev-hubbard model at half filling," *Phys. Rev. B*, vol. 89, p. 115130, Mar 2014.

[43] L.-M. Duan, E. Demler, and M. D. Lukin, "Controlling spin exchange interactions of ultracold atoms in optical lattices," *Phys. Rev. Lett.*, vol. 91, p. 090402, Aug 2003.

[44] C. Zhang, V. W. Scarola, S. Tewari, and S. Das Sarma, "Anyonic braiding in optical lattices," *Proceedings of the National Academy of Sciences*, vol. 104, no. 47, pp. 18415–18420, 2007.

[45] S. R. Hassan, S. K. Goyal, R. Shankar, and D. Sénéchal, "Quarter-filled kitaev-hubbard model: A quantum hall state in an optical lattice," *Phys Rev B*, vol. 88, no. 045301, p. 045301, 2013.

[46] P. V. Sriluckshmy, A. Mishra, S. R. Hassan, and R. Shankar, "Topological transitions in a model with particle-hole symmetry, pancharatnam-berry curvature, and dirac points," *Phys. Rev. B*, vol. 89, p. 045105, Jan 2014.

[47] A. P. Schnyder, S. Ryu, A. Furusaki, and A. W. W. Ludwig, "Classification of topological insulators and superconductors in three spatial dimensions," *Phys. Rev. B*, vol. 78, no. 19, p. 195125, 2008.

[48] A. Kitaev, "Periodic table for topological insulators and superconductors," *arXiv preprint arXiv:0901.2686*, 2009.

[49] Y.-M. Lu and A. Vishwanath, "Theory and classification of interacting integer topological phases in two dimensions: A chern-simons approach," *Phys. Rev. B*, vol. 86, p. 125119, Sep 2012.

[50] Y. Hatsugai, "Quantized Berry Phases as a Local Order Parameter of a Quantum Liquid," *Journal of the Physical Society of Japan*, vol. 75, p. 123601, dec 2006.

[51] J. Zak, "Berry's phase for energy bands in solids," *Phys. Rev. Lett.*, vol. 62, pp. 2747–2750, Jun 1989.

[52] A. Saket, S. R. Hassan, and R. Shankar, "Topological aspects of an exactly solvable spin chain," *Phys. Rev. B*, vol. 87, p. 174414, May 2013.

[53] P. Delplace, D. Ullmo, and G. Montambaux, "Zak phase and the existence of edge states in graphene," *Phys. Rev. B*, vol. 84, p. 195452, Nov 2011.

[54] "See Supplemental Material at [URL will be inserted by publisher] for the evolution of the Dirac Points as a function of t', and the dynamics of Bloch-Zener oscillations and Rotating Condensates.."

[55] R. de Gail, J.-N. Fuchs, M. Goerbig, F. Piéchon, and G. Montambaux, "Manipulation of dirac points in graphene-like crystals," *Physica B: Condensed Matter*, vol. 407, no. 11, pp. 1948–1952, 2012.

[56] L.-K. Lim, J.-N. Fuchs, and G. Montambaux, "Bloch-zener oscillations across a merging transition of dirac points," *Phys. Rev. Lett.*, vol. 108, no. 17, p. 175303, 2012.

[57] J.-N. Fuchs, L.-K. Lim, and G. Montambaux, "Interband tunneling near the merging transition of dirac cones," *Phys. Rev. A*, vol. 86, no. 6, p. 063613, 2012.

[58] G. Montambaux, F. Piéchon, J. N. Fuchs, and M. O. Goerbig, "Merging of dirac points in a two-dimensional crystal," *Phys. Rev. B*, vol. 80, no. 15, p. 153412, 2009.

[59] B. Wunsch, F. Guinea, and F. Sols, "Dirac-point engineering and topological phase transitions in honeycomb optical lattices," *New Journal of Physics*, vol. 10, no. 10, p. 103027, 2008.

[60] M. Atala, M. Aidelsburger, J. T. Barreiro, D. Abanin, T. Kitagawa, E. Demler, and I. Bloch, "Direct measurement of the zak phase in topological bloch bands," *arXiv preprint arXiv:1212.0572*, 2012.

[61] B. Breid, D. Witthaut, and H. Korsch, "Bloch–zener oscillations," *New Journal of Physics*, vol. 8, no. 7, 2006.

[62] A. R. Kolovsky and H. J. Korsch, "Bloch oscillations of cold atoms in two-dimensional optical lattices," *Phys. Rev. A*, vol. 67, no. 6, p. 063601, 2003.

[63] L. Tarruell, D. Greif, T. Uehlinger, G. Jotzu, and T. Esslinger, "Creating, moving and merging dirac points with a fermi gas in a tunable honeycomb lattice," *Nature*, vol. 483, no. 7389, pp. 302–305, 2012.

[64] T. Uehlinger, D. Greif, G. Jotzu, L. Tarruell, T. Esslinger, L. Wang, and M. Troyer, "Double transfer through dirac points in a tunable honeycomb optical lattice," *The European Physical Journal Special Topics*, vol. 217, no. 1, pp. 121–133, 2013.

[65] M. Potthoff, "Self-energy-functional approach to systems of correlated electrons," *Eur. Phys. J. B*, vol. 32, no. 4, pp. 429 – 36, 2003.

[66] D. Sénéchal, D. Perez, and M. Pioro-Ladrière, "Spectral weight of the hubbard model through cluster perturbation theory," *Phys. Rev. Lett.*, vol. 84, pp. 522–525, 2000.

[67] D. Sénéchal, D. Perez, and D. Plouffe, "Cluster Perturbation Theory for Hubbard models," *Phys. Rev. B*, vol. 66, p. 075129, 2002.

[68] D. Sénéchal, "Cluster perturbation theory," in *Theoretical methods for Strongly Correlated Systems* (A. Avella and F. Mancini, eds.), vol. 171 of *Springer Series in Solid-State Sciences*, ch. 8, pp. 237–269, Springer, 2012.

[69] M. Potthoff, A. Avella, and F. Mancini, "Strongly correlated systems: Theoretical methods," 2012.

[70] M. Potthoff, "Self-energy-functional theory," in *Theoretical methods for Strongly Correlated Systems* (A. Avella and F. Mancini, eds.), vol. 171 of *Springer Series in Solid-State Sciences*, ch. 9, Springer, 2012.

[71] A. L. Chernyshev, D. Galanakis, P. Phillips, A. V. Rozhkov, and A.-M. S. Tremblay, "Higher order corrections to effective low-energy theories for strongly correlated electron systems," *Phys. Rev. B*, vol. 70, p. 235111, Dec 2004.

[72] H.-Y. Yang, A. M. Läuchli, F. Mila, and K. P. Schmidt, "Effective spin model for the spin-liquid phase of the hubbard model on the triangular lattice," *Phys. Rev. Lett.*, vol. 105, p. 267204, Dec 2010.

[73] A. Kitaev, "Anyons in an exactly solved model and beyond," *Annals of Physics*, vol. 321, no. 1, pp. 2 – 111, 2006.

[74] C. Sanner, E. J. Su, A. Keshet, W. Huang, J. Gillen, R. Gommers, and W. Ketterle, "Speckle imaging of spin fluctuations in a strongly interacting fermi gas," *Phys. Rev. Lett.*, vol. 106, p. 010402, Jan 2011.

[75] W. V. Liu, F. Wilczek, and P. Zoller, "Spin-dependent hubbard model and a quantum phase transition in cold atoms," *Phys. Rev. A*, vol. 70, p. 033603, Sep 2004.

[76] L. Tarruell, D. Greif, T. Uehlinger, J. Gregor, and T. Esslinger, "Creating, moving and merging dirac points with a fermi gas in a tunable honeycomb lattice," *Nature*, vol. 483, pp. 302–305, 2012.

[77] X.-G. Wen and P. A. Lee, "Theory of underdoped cuprates," *Phys. Rev. Lett.*, vol. 76, pp. 503–506, Jan 1996.

[78] J. Chaloupka, G. Jackeli, and G. Khaliullin, "Kitaev-heisenberg model on a honeycomb lattice: possible exotic phases in iridium oxides a 2 iro 3," *Phys. Rev. Lett.*, vol. 105, no. 2, p. 027204, 2010.

[79] A. Shitade, H. Katsura, J. Kuneš, X.-L. Qi, S.-C. Zhang, and N. Nagaosa, "Quantum spin hall effect in a transition metal oxide na 2 iro 3," *Phys. Rev. Lett.*, vol. 102, no. 25, p. 256403, 2009.

[80] Y. Singh, S. Manni, J. Reuther, T. Berlijn, R. Thomale, W. Ku, S. Trebst, and P. Gegenwart, "Relevance of the heisenberg-kitaev model for the honeycomb lattice iridates a 2 iro 3," *Phys. Rev. Lett.*, vol. 108, no. 12, p. 127203, 2012.

[81] F. Ye, S. Chi, H. Cao, B. C. Chakoumakos, J. A. Fernandez-Baca, R. Custelcean, T. Qi, O. Korneta, and G. Cao, "Direct evidence of a zigzag spin-chain structure in the honeycomb lattice: A neutron and x-ray diffraction investigation of single-crystal na 2 iro 3," *Phys. Rev. B*, vol. 85, no. 18, p. 180403, 2012.

[82] I. Kimchi and Y.-Z. You, "Kitaev-heisenberg-j 2-j 3 model for the iridates a 2 iro 3," *Phys. Rev. B*, vol. 84, no. 18, p. 180407, 2011.

[83] S. Manni, Y. Tokiwa, and P. Gegenwart, "Effect of nonmagnetic dilution in the honeycomb-lattice iridates na_2iro_3 and li_2iro_3," *Phys. Rev. B*, vol. 89, p. 241102, Jun 2014.

[84] H. Gretarsson, J. Clancy, X. Liu, J. Hill, E. Bozin, Y. Singh, S. Manni, P. Gegenwart, J. Kim, A. Said, *et al.*, "Crystal-field splitting and correlation effect on the electronic structure of a 2 iro 3," *Phys. Rev. Lett.*, vol. 110, no. 7, p. 076402, 2013.

[85] R. Comin, G. Levy, B. Ludbrook, Z.-H. Zhu, C. Veenstra, J. Rosen, Y. Singh, P. Gegenwart, D. Stricker, J. N. Hancock, *et al.*, "Na 2 iro 3 as a novel relativistic mott insulator with a 340-mev gap," *Phys. Rev. Lett.*, vol. 109, no. 26, p. 266406, 2012.

[86] V. M. Katukuri, S. Nishimoto, V. Yushankhai, A. Stoyanova, H. Kandpal, S. Choi, R. Coldea, I. Rousochatzakis, L. Hozoi, and J. van den Brink, "Kitaev interactions between j= 1/2 moments in honeycomb na2iro3 are large and ferromagnetic: insights from ab initio quantum chemistry calculations," *New Journal of Physics*, vol. 16, no. 1, p. 013056, 2014.

[87] J. G. Rau, E. K.-H. Lee, and H.-Y. Kee, "Generic spin model for the honeycomb iridates beyond the kitaev limit," *Phys. Rev. Lett.*, vol. 112, no. 7, p. 077204, 2014.

[88] J. Reuther, R. Thomale, and S. Rachel, "Spiral order in the honeycomb iridate li 2 iro 3," *Phys. Rev. B*, vol. 90, no. 10, p. 100405, 2014.

[89] R. Schaffer, S. Bhattacharjee, and Y. B. Kim, "Quantum phase transition in heisenberg-kitaev model," *Phys. Rev. B*, vol. 86, no. 22, p. 224417, 2012.

[90] Y. Sizyuk, C. Price, P. Wölfle, and N. B. Perkins, "Importance of anisotropic exchange interactions in honeycomb iridates: Minimal model for zigzag antiferromagnetic order in na 2 iro 3," *Phys. Rev. B*, vol. 90, no. 15, p. 155126, 2014.

[91] S. H. Chun, J.-W. Kim, J. Kim, H. Zheng, C. C. Stoumpos, C. Malliakas, J. Mitchell, K. Mehlawat, Y. Singh, Y. Choi, *et al.*, "Direct evidence for dominant bond-directional interactions in a honeycomb lattice iridate na2iro3," *Nature Physics*, 2015.

[92] O. Cépas, J. O. Haerter, and C. Lhuillier, "Detection of weak emergent broken-symmetries of the kagome antiferromagnet by raman spectroscopy," *Phys. Rev. B*, vol. 77, p. 172406, May 2008.

[93] W.-H. Ko, Z.-X. Liu, T.-K. Ng, and P. A. Lee, "Raman signature of the u(1) dirac spin-liquid state in the spin-$\frac{1}{2}$ kagome system," *Phys. Rev. B*, vol. 81, p. 024414, Jan 2010.

[94] D. Wulferding, P. Lemmens, P. Scheib, J. Röder, P. Mendels, S. Chu, T. Han, and Y. S. Lee, "Interplay of thermal and quantum spin fluctuations

in the kagome lattice compound herbertsmithite," *Phys. Rev. B*, vol. 82, p. 144412, Oct 2010.

[95] L. J. Sandilands, Y. Tian, K. W. Plumb, Y.-J. Kim, and K. S. Burch, "Scattering continuum and possible fractionalized excitations in α- rucl 3," *Phys. Rev. Lett.*, vol. 114, no. 14, p. 147201, 2015.

[96] S. Manni, S. Choi, I. Mazin, R. Coldea, M. Altmeyer, H. O. Jeschke, R. Valenti, and P. Gegenwart, "Effect of isoelectronic doping on the honeycomb-lattice iridate a 2 iro 3," *Phys. Rev. B*, vol. 89, no. 24, p. 245113, 2014.

[97] G. Cao, T. F. Qi, L. Li, J. Terzic, V. S. Cao, S. J. Yuan, M. Tovar, G. Murthy, and R. K. Kaul, "Evolution of magnetism in the single-crystal honeycomb iridates $(\mathrm{na}_{1-x}\mathrm{li}_x)_2\mathrm{Iro}_3$," *Phys. Rev. B*, vol. 88, p. 220414, Dec 2013.

[98] S. N. Gupta, P. V. Sriluckshmy, K. Mehlawat, A. Balodhi, D. K. Mishra, S. R. Hassan, T. V. Ramakrishnan, D. V. S. Muthu, Y. Singh, and A. K. Sood, "Raman signatures of strong kitaev exchange correlations in $(\mathrm{na}_{1x}$ $\mathrm{li}_x\,)_2$ iro_3 : Experiments and theory," *EPL (Europhysics Letters)*, vol. 114, no. 4, p. 47004, 2016.

[99] G. Chen and L. Balents, "Spin-orbit effects in $\mathrm{na}_4\mathrm{ir}_3\mathrm{o}_8$: A hyper-kagome lattice antiferromagnet," *Phys. Rev. B*, vol. 78, p. 094403, Sep 2008.

[100] D. Podolsky and Y. B. Kim, "Spin-orbit coupling in the metallic and spin-liquid phases of $\mathrm{na}_4\mathrm{ir}_3\mathrm{o}_8$," *Phys. Rev. B*, vol. 83, p. 054401, Feb 2011.

[101] G. Chen and Y. B. Kim, "Anomalous enhancement of the wilson ratio in a quantum spin liquid: The case of $\mathrm{na}_4\mathrm{ir}_3\mathrm{o}_8$," *Phys. Rev. B*, vol. 87, p. 165120, Apr 2013.

[102] M. J. Lawler, A. Paramekanti, Y. B. Kim, and L. Balents, "Gapless spin liquids on the three-dimensional hyperkagome lattice of $na_4ir_3o_8$," *Phys. Rev. Lett.*, vol. 101, p. 197202, Nov 2008.

[103] Y. Zhou, P. A. Lee, T.-K. Ng, and F.-C. Zhang, "$na_4ir_3o_8$ as a 3d spin liquid with fermionic spinons," *Phys. Rev. Lett.*, vol. 101, p. 197201, Nov 2008.

[104] E. J. Bergholtz, A. M. Lauchli, and R. Moessner, "Symmetry breaking on the three-dimensional hyperkagome lattice of $na_4ir_3o_8$," *Phys. Rev. Lett.*, vol. 105, p. 237202, Dec 2010.

[105] M. R. Norman and T. Micklitz, "Electronic structure of hyper-kagome $na_4ir_3o_8$," *Phys. Rev. B*, vol. 81, p. 024428, Jan 2010.

[106] Y. Singh, Y. Tokiwa, J. Dong, and P. Gegenwart, "Spin liquid close to a quantum critical point in $na_4ir_3o_8$," *Phys. Rev. B*, vol. 88, p. 220413, Dec 2013.

[107] R. Dally, T. Hogan, A. Amato, H. Luetkens, C. Baines, J. Rodriguez-Rivera, M. J. Graf, and S. D. Wilson, "Short-range correlations in the magnetic ground state of $na_4ir_3o_8$," *Phys. Rev. Lett.*, vol. 113, p. 247601, Dec 2014.

[108] M. Sato, H. Katsura, and N. Nagaosa, "Theory of raman scattering in one-dimensional quantum spin-1 2 antiferromagnets," *Physical review letters*, vol. 108, no. 23, p. 237401, 2012.

[109] B. Sriram Shastry and B. I. Shraiman, "Raman scattering in mott-hubbard systems," *Physical review letters*, vol. 65, no. 8, pp. 1068–1071, 1990.

[110] P. Fleury and R. Loudon, "Scattering of light by one-and two-magnon excitations," *Physical Review*, vol. 166, no. 2, p. 514, 1968.

[111] I. I. Mazin, H. O. Jeschke, K. Foyevtsova, R. Valentí, and D. I. Khomskii, “na_2iro_3 as a molecular orbital crystal,” *Phys. Rev. Lett.*, vol. 109, p. 197201, Nov 2012.

[112] K. Foyevtsova, H. O. Jeschke, I. I. Mazin, D. I. Khomskii, and R. Valentí, “*Ab initio* analysis of the tight-binding parameters and magnetic interactions in na_2iro_3,” *Phys. Rev. B*, vol. 88, p. 035107, Jul 2013.

[113] J. M. Hopkinson, S. V. Isakov, H.-Y. Kee, and Y. B. Kim, “Classical antiferromagnet on a hyperkagome lattice,” *Phys. Rev. Lett.*, vol. 99, p. 037201, Jul 2007.

[114] D. Podolsky, A. Paramekanti, Y. B. Kim, and T. Senthil, “Mott transition between a spin-liquid insulator and a metal in three dimensions,” *Phys. Rev. Lett.*, vol. 102, p. 186401, May 2009.

[115] A. Balodhi, A. Thamizhavel, and Y. Singh, “Evolution of magnetic, transport, and thermal properties in $na_{4-x}ir_3o_8$,” *Phys. Rev. B*, vol. 91, p. 224409, Jun 2015.